NUC TP 506

SPACE/TIME RANDOM PROCESSES AND OPTIMUM ARRAY PROCESSING

by

Arthur B. Baggeroer

Associate Professor of Ocean and Electrical Engineering

Massachusetts Institute of Technology

April 1976

NAVAL UNDERSEA CENTER, SAN DIEGO, CA 92132

AN ACTIVITY OF THE NAVAL MATERIAL COMMAND

R. B. GILCHRIST, CAPT, USN
Commander

HOWARD L. BLOOD, PhD
Technical Director

ADMINISTRATIVE INFORMATION

The work in this report was performed by Dr. Arthur B. Baggeroer, Associate Professor of Ocean and Electrical Engineering, of the Massachusetts Institute of Technology while working as a Consultant to the Naval Undersea Center on an intermittent basis beginning in July 1972 with completion in December 1974.

Released by
G S. Colladay, Head
System Analysis Group

ACKNOWLEDGEMENTS

Many people have contributed measurably to the compilation of this report. Professor H. A. Van Trees simulated my initial interest in optimum array processing by his work in this area. Our continued discussions on this topic have been very beneficial and have sharpened my issues Some of this material has been presented in seminars and short summer courses at MIT; the many discussions with students have been quite useful. Mr. C. S. Stradling of the U.S. Navy Undersea Center pointed out the Navy's interest in array processing. He provided much of the motivation and support for this work. The value of his assistance cannot be underestimated. Dr. W. Squire and H. Whitehouse at NUC continued this support and their assistance is also gratefully acknowledged. Two of my graduate students, K. Theriault and J. Moura, proofread the entire manuscript; their comments improved the clarity of it significantly. Finally, the continuing patience, diligence, and assistance of Beatrice Warnshuis of NUC publications is gratefully acknowledged.

UNCLASSIFIED

SECURITY CLASSIFICATION OF THIS PAGE (When Data Entered)

REPORT DOCUMENTATION PAGE		READ INSTRUCTIONS BEFORE COMPLETING FORM
1 REPORT NUMBER TP 506	2 GOVT ACCESSION NO	3 RECIPIENT'S CATALOG NUMBER
4 TITLE (and Subtitle) Space/Time Random Processes and Optimum Array Processing		5 TYPE OF REPORT & PERIOD COVERED 6 PERFORMING ORG. REPORT NUMBER
7 AUTHOR(s) Arthur B Baggeroer, Associate Professor of Ocean and Electrical Engineering, Massachusetts Institute of Technology		8 CONTRACT OR GRANT NUMBER(s)
9 PERFORMING ORGANIZATION NAME AND ADDRESS Naval Undersea Center San Diego, CA 92132		10 PROGRAM ELEMENT PROJECT TASK AREA & WORK UNIT NUMBERS
11 CONTROLLING OFFICE NAME AND ADDRESS Naval Undersea Center San Diego, CA 92132		12 REPORT DATE April 1976 13 NUMBER OF PAGES Unclassified
14 MONITORING AGENCY NAME & ADDRESS(if different from Controlling Office)		15 SECURITY CLASS (of this report) 15a DECLASSIFICATION DOWNGRADING SCHEDULE

16 DISTRIBUTION STATEMENT (of this Report)

Approved for public release, distribution unlimited

17 DISTRIBUTION STATEMENT (of the abstract entered in Block 20 if different from Report)

18 SUPPLEMENTARY NOTES

19 KEY WORDS (Continue on reverse side if necessary and identify by block number)

arrays	beamforming	preformed beams
space/time signals	receiving array	spatial processing
array processing	adaptive arrays	wave vector estimation
adaptive beamforming	spectral estimation	

20 ABSTRACT (Continue on reverse side if necessary and identify by block number)

Representations of space/time signals as stationary, homogeneous random processes are used to formulate the theory of optimum array processing. Generalized Fourier expansions for one, two, and three dimensions are discussed. These representations include directional, isotropic signal fields, as well as all previously published ambient noise models Receiving arrays are modeled in terms of how they observe signal fields with the roles of their geometry and the observation noise analyzed. The design of optimum beamformers is

DD FORM 1 JAN 73 1473 EDITION OF 1 NOV 65 IS OBSOLETE

UNCLASSIFIED

SECURITY CLASSIFICATION OF THIS PAGE (When Data Entered)

20 (Continued)

formulated and coupled to the representation of the signal field and the receiving array The structure of optimum beamforms are analyzed and related to beam displacement, null placement, and superdirective methods Processing performance obtained by exact methods and approximate methods are compared for various signal fields and array geometries The closeness of the results indicate the usefulness of the representations and array analysis in predicting the performance of optimum systems Finally, the structure of preformed beams and clustered receiving arrays are analyzed with these methods.

CONTENTS

PART 1 - CHARACTERIZING SPACE/TIME RANDOM PROCESSES

1. INTRODUCTION

The analysis of arrays of transducers, or antennas, has had such an extensive development by now that one anticipates little which is novel Yet, in spite of the widespread use of statistical methods in communication systems, it is comparitively recent that array, or antenna, processing methods, based on the statistical properties of both the signal and the interfering noise, were introduced However, sufficient time has elapsed such that a rather formidable literature is available

Unfortunately, most contributions to this literature are quite mathematically oriented– usually couched in a maze of covariance matrix manipulations While a certain amount of this may be necessary to formally establish the logic of the approach, the underlying principles of operation are quite intuitive and can be theoretically explained in terms of an appropriate combination of classical antenna theory and some fairly straightforward spatial random processing Development of this intuitive understanding is particularly important since the processing gain, or signal-to-noise ratio, often carries a high premium for normal array processing applications Often, direct implementation of "optimum" processing methods is not possible either from computational or physical considerations Consequently, the typical concern is with suboptimum methods which exploit the essential features of the "optimum" processing to obtain all but "epsilon" of the ultimate performance In addition to understanding how spatial processors obtain their optimum performance, it is important to determine just what this performance is since it sets the standard, or benchmark, against which to compare the performance of any suboptimal, but implementable, system.

The use of an array of transducers, or an antenna, is typically motivated by two reasons, both of which are generally coupled together. First, the particular spatial coherency of a propagating signal is exploited to improve the signal level versus the background noise The dominant features governing the degree of improvement are the array geometry and the spatial structure of the background noise. Sometimes, the signal can be improved with simple statistical smoothing, while at other times the coherence of the background can be used to combat background noise. In the second application, the directional characteristics of the

ambient field of signals must be determined Again, the degree to which a source position can be located is influenced by the same factors which determine its detectability

This report is divided into three parts Part 1 considers the problem of characterizing space/time random processes The study of this problem is fundamental to the analysis of the operation of arrays, or antennas, with random inputs

In Part 2 we describe the response of arrays to various noise fields We consider the optimization and resulting optimum performance of processing methods for signals and noise fields of interest

Part 3 considers a sequence of topics based upon the results developed in Parts 1 and 2 These focus on the intuitive concepts of the processing methods in the context of some selected examples of noise fields and array geometries and on the introduction of some selected suboptimum processing methods

Two comments are appropriate here First, we assume that the reader has a background in temporal random processes and a knowledge of Fourier methods Appropriate references are given by Papoulis [1], Davenport and Root [2], and Van Trees [3] Second, we formulate our arrays in terms of a continuum, or an aperture, and a representation of spatial signals observed across an aperture This leads to a notation which is somewhat more abstract than that which corresponds to discrete element arrays However, it does lead to a more fundamental consideration of the issues in spatial processing and to results which are much more intuitive and uncluttered by the spatial sampling issue introduced by a discrete formulation Once these results are established with a continuous formulation, we consider the issues needed to relate them to discrete arrays In essence, we are asserting that for many situations a continuous analysis is more fundamental and easier, although we recognize that ultimately most arrays of interest here are discrete and our results must be related to them

2. SPACE/TIME RANDOM PROCESSES

In the theory of temporal processes there are several ways to characterize or describe the random processes of interest Ultimately, one would want to have a complete specification of the processes in terms of their probability distribution functions for an arbitrary number of points in the space/time field With the prominent exception of Gaussian and Poisson processes, this information is generally not available and one must settle for a less complete or partial characterization Most analyses involve a second moment characterization

in which one specifies the mean and covariance function for the processes of interest As is well known, this information is also sufficient to provide a complete characterization for Gaussian processes since its probability distribution of arbitrary order can be related to these two moments We pursue an approach that uses the second moment characterization which suffices for most of our applications Further, we assume that the processes are also Gaussian when we ask probability questions, e g , the performance of optimal detectors

A second method of analysis involves a description of how the random processes are generated While this has found extensive use for purely temporal processes, as evidenced by the wealth of material in the literature regarding state variable estimation procedures, it has not, as yet, found extensive use for space/time processes The role of these processes and their relation to distributed systems is clearly an emerging field of interest, however, the analysis of the partial differential equations introduced to date is quite complicated and is not yet particularly fruitful

2.1 SPACE/TIME COVARIANCES AND FREQUENCY WAVE NUMBER FUNCTIONS

Let us assume that we are concerned with a signal $y(t\ \underline{z})$ that is defined over both time and space [1] We model $y(t\ \underline{z})$ as a random process defined over a field with a temporal domain or index set $t \in \{T_o, T_f\}$ and a spatial domain or index set $\underline{z} \in R^N$ with a mean

$$m_y(t\ \underline{z}) = E[y(t,\underline{z})] \tag{2 1}$$

and a space/time covariance

$$K_y(t,\tau,\underline{z},\underline{\zeta}) = E[(y(t\ \underline{z})-m_y(t,\underline{z}))\ (y(\tau\ \underline{\zeta})-m_y(\tau,\underline{\zeta}))^*] \tag{2 2}$$

(we often assume zero mean processes for simplicity)

In this most general case the processes are both temporally non-stationary and spatially non-stationary, or non-homogeneous Analyzing problems that involve this class of covariance functions using a second moment characterization introduces many issues that arise with

---

[1] *We use scalar processes and introduce vector ones only when necessary*

[2] ** → Complex Conjugate We use a complex formulation throughout This is more appropriate for a sonar analysis than it is for seismic data, however, the correspondence for strictly real processes is direct See Ref 3 for a complete development of complex process representation*

problems involving temporally non-stationary processes In general, the analyses complicate the mathematical detail, but the conceptual issues are unchanged

In many practical situations the processes encountered are temporally stationary, at least in a wide sense, such that we have

$$m_y(t,\underline{z}) = m_y(\underline{z}) \tag{2 3}$$

and

$$K_y(t,\tau,\underline{z},\underline{\xi}) = K_y(t-\tau,\underline{z},\underline{\xi}) \tag{2 4}$$

This assumption may not be strictly satisfied over long intervals of time However, when the processing interval is short compared to the time period over which the covariance changes, it is a realistic practical assumption

We also frequently encounter situations in which the space/time processes are homogeneous or spatially stationary The covariance is only a function of the vector difference of the spatial arguments

$$m_y(t,\underline{z}) = m_y(t) \tag{2 5}$$

and

$$K_y(t,\tau,\underline{z},\underline{\xi}) = K_y(t-\tau,\underline{z}-\underline{\xi}) \tag{2 6}$$

Again, this may not be strictly satisfied over large distances, although it is a realistic approximation when the receiving aperture is small compared to the distances over which the covariance is non-homogeneous. We point out, however, that several problems which involve signals in the near field and array shading effects need to be discussed in the context of a non-homogeneous covariance, so the general model is certainly not void of practical interest.

Finally, we have the situation in which a stationary, homogeneous process exists Combining the two above assumptions we have

$$m_y(t,\underline{z}) = m_y \tag{2 7}$$

and

$$K_y(t,\tau,\underline{z},\underline{\zeta}) = K_y(t\text{-}\tau\ \underline{z}\text{-}\underline{\zeta}) \tag{2 8}$$

We direct our attention principally to problems involving processes which fit within this general class of assumption. We also drop the mean from further consideration

In many of our analyses it is useful to consider a spectral decomposition of the random processes of interest. By pursuing an analysis in a frequency domain, either temporal or spatial, we can often obtain a significant amount of insight into the operations of our processors. To do this we define a series of Fourier transform operations The temporal frequency spatial correlation function associated with a stationary process is given by

$$S_y(\omega:\underline{z},\underline{\zeta}) = \int_{-\infty}^{\infty} K_y(\tau\ \underline{z},\underline{\zeta})e^{-j\omega\tau}\,d\tau \tag{2 9}$$

When $\underline{z} = \underline{\zeta}$, this yields the temporal spectrum at a point in space. If we consider sampling at a number of points in space, so as to form a vector process, we can order the points and create a matrix format the spectral covariance of the vector process by sampling $S_y(\omega:\underline{z},\underline{\zeta})$, appropriately.

Similarly, for a homogeneous process, we can define the temporal correlation, spatial wave number function as

$$F_y(t,\tau\ \underline{k}) = \int_{-\infty}^{\infty}\cdot\int_{-\infty}^{\infty} d\underline{z}K_y(t,\tau:\underline{z})e^{j\underline{k}\cdot\underline{z}} \tag{2 10}$$

Note that the integration is performed over the entire spatial domain of the process Consequently, there is a fundamental difference among the transforms over one, two, or three dimensions We do not use this function very frequently because there are better alternate representations for the signal in the temporal frequency domain

For a stationary homogeneous process, the frequency wave number function is defined as

$$P_y(\omega \cdot \underline{k}) = \int_{-\infty}^{\infty} d\tau \int_{-\infty}^{\infty} \cdot \int d\underline{z}\, K_y(\tau \cdot \underline{z}) e^{-j(\omega\tau - \underline{k}\cdot\underline{z})} \tag{2.11}$$

(Note the sign difference with respect to the spatial variable)

This function has a very appealing interpretation When we pursue an analysis similar to that used for the spectral representation theorem for temporal processes, we find that the process $y(t,\underline{z})$ can be represented in a Stieltjes integral form [4] as

$$y(t;\underline{z}) = \int_{-\infty}^{\infty} \int_{-\infty}^{\infty} \cdot \int_{-\infty}^{\infty} e^{j(\omega t - \underline{k}\cdot\underline{z})} dY(\omega.\underline{k}), \tag{2.12}$$

where $\underline{k}$ has dimension N, the dimension of the space over which the process is defined. For the decomposition of $Y(\omega\ \underline{k})$ we have the following properties·

$$E[\,|Y(\omega_2\ \underline{k}_2) - Y(\omega_1 \cdot \underline{k}_1)|^2] = \int_{\omega_1}^{\omega_2} \frac{d\omega}{2\pi} \int_{\underline{k}_1}^{\underline{k}_2} \frac{dk}{(2\pi)^N} P_y(\omega \cdot \underline{k}) \tag{2.13a}$$

or formally $E[|dY(\omega\ \underline{k})|^2] = \dfrac{d\omega}{2\pi} \dfrac{dk}{(2\pi)^N} P_y(\omega;\underline{k})$, (2.13b)

$$E[(Y(\omega_2;\underline{k}_2) - Y(\omega_1 \cdot \underline{k}_1))(Y(\omega_4 \cdot \underline{k}_4) - Y(\omega_3 \cdot \underline{k}_3))^*] = 0, \tag{2.14a}$$

when $((\omega_1,\omega_2) \times (\underline{k}_1,\underline{k}_2)) \cap ((\omega_3,\omega_4) \times (\underline{k}_3,\underline{k}_4)) = 0$, (2.14b)

i.e , disjoint frequency wave number bands are uncorrelated Consequently, we may consider this class of space/time random processes to be composed of a superposition of plane waves of radian frequency ω and wave number $\underline{k}$ This is the spatial generalization of a spectral decomposition of a random process

If, in addition, we impose the condition that the process $y(t\ \underline{z})$ satisfies the homogeneous wave equation, then we have the constraint

$$\frac{\omega}{c} = |\underline{k}| \ , \tag{2.15a}$$

or

$$\frac{2\pi f}{|\underline{k}|} = f\lambda = c \text{ (velocity of propagation)} \tag{2.15b}$$

This defines a structure which signals propagating in a medium must satisfy. Further this implies that at any particular ω the frequency wave number function is nonzero only on a sphere of radius $2\pi/\lambda = |\underline{k}| = \omega/c$. This constraint is not necessary for $y(t\ \underline{z})$ to correspond to a propagating process. For example, one may have propagation in three dimensions and yet consider a representation over a two-dimensional surface since the two-dimensional wave number value corresponds unambiguously to a three-dimensional surface except for its sign.

The inherent advantage of this representation for homogeneous fields is that it allows us to make many statements regarding the processing of our signals which are completely dual to analogous frequency domain operations when processing temporal waveforms. Naturally, there is a close relationship among the various transforms discussed, which are summarized in Figure 2.1. The paper and text by Yaglom [5,6] are particularly appropriate references for the harmonic analysis of space/time processes. With these references the rigor in using the harmonic analysis can be pursued at length. For our purposes the major problem relates to the notation of representing $y(t\ \underline{z})$ in either temporal or spatial frequency domains. This can be quite awkward if pursued too far. We shall use the Stieltjes notation $dY(\omega\ \underline{k})$ when we wish to do this with the important properties of $Y(\omega\ \underline{k})$ summarized in Eqs. 2.13 and 2.14 above.

Often, it is convenient to use different frequency measures. The temporal frequency, f, in cycles per sec, or Hertz, is given by

$$f = \omega/2\pi \tag{2.16}$$

Similarly, the spatial wave vector $\underline{\nu}$, in cycles per unit distance, is given by

$$\underline{\nu} = \underline{k}/2\pi \tag{2.17}$$

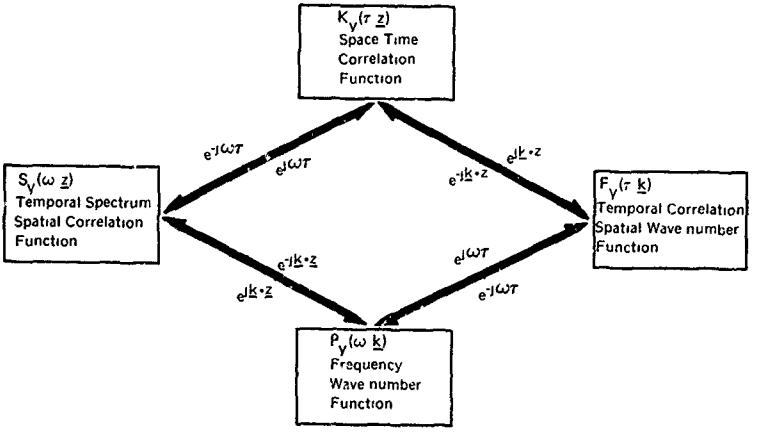

Figure 2-1 Relationship among the various second moment representations for stationary - homogeneous space time random processes

For plane waves

$$|\underline{k}/2\pi| = |\underline{\nu}| = f/c = 1/\lambda \tag{2.18}$$

It is also convenient to define the effective wavelength along each axis in terms of the components of $\underline{\nu}$. In Cartesian coordinates we have

$$\nu_x = 1/\lambda_x \tag{2.19a}$$

$$\nu_y = 1/\lambda_y \tag{2.19b}$$

$$\nu_z = 1/\lambda_z \tag{2.19c}$$

(Note that one does not obtain these effective wavelengths by simply projecting the total wavelength oriented along the propagation direction upon the respective axes)

To illustrate these concepts and to develop some results that we need later, we present some examples First, we shall consider the analysis of some of the various models popularly used in the literature. Next we consider a general discussion of representing space/time processes

Here we also draw upon some results from electromagnetics which apparently have not found their way into the sonar/seismic literature

Generally, it is easiest to discuss these space/time processes in terms of either the temporal frequency spatial correlation or the frequency wave number function. Consequently, many results are specified at a single temporal frequency, or for a narrow frequency band For a broadband analysis, the integration over a specified frequency range is implied.

Example 1 Directional Signal

The simplest signal of interest is a plane wave propagating in a direction with speed c The space/time process has the form

$$y(t,\underline{z}) = y_0[t-(\underline{a}\cdot\underline{z}/c)], \tag{2 20}$$

as illustrated in Figure 2 2

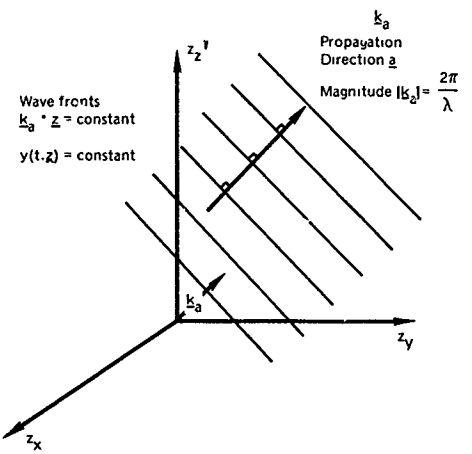

Figure 2-2 Model of plane wave propagation

If we assume that $y_o(t)$ is a stationary random process, then the space time correlation function is given by (assuming zero means)

$$K_y(\Delta\tau\ \Delta\underline{z}) = E[y(t\ \underline{z})\ y^*(t-\Delta\tau\ \underline{z}-\Delta\underline{z})] = E[y_o(t-(\underline{a}\cdot\underline{z}/c))\ y_o^*(t-\Delta\tau-(\underline{a}\cdot(\underline{z}-\Delta\underline{z})/c))]$$

$$= K_{y_o}(\Delta\tau-(\underline{a}\cdot\Delta\underline{z}/c)) \tag{2.21}$$

The temporal frequency spatial correlation function follows the Fourier transform relation of Eq 2 9. We find

$$S_y(\omega.\Delta\underline{z}) = S_{y_o}(\omega)e^{-j(\omega/c)(\underline{a}\cdot\Delta\underline{z})} \tag{2 22}$$

Consequently, we have cross-spectrum of a plane curve at two different locations which is related to the spectrum of the process at a single point by a simple linear phase shift that reflects the propagation phase between the two points. Therefore, the elements of spectral matrices that involve pure plane waves consist of a common amplitude and a set of phase shifts between the various sensors

If we now transform this function with respect to the spatial variable, we obtain the frequency wave number function

$$P_y(\omega:\underline{k}) = \int_{R^N}\int d\underline{z}\ S_y(\omega:z)e^{j\underline{k}\cdot z} = S_{y_o}(\omega)u_o\left(\underline{k}-\frac{\omega}{c}\underline{a}\right) \tag{2 23}$$

where $$u_o\left(\underline{k}-\frac{\omega}{c}\underline{a}\right) = u_o\left(k_x-\frac{\omega}{c}a_x\right)u_o\left(k_y-\frac{\omega}{c}a_y\right)u_o\left(k_z-\frac{\omega}{c}a_z\right) \tag{2 24}$$

is a three-dimensional impulse function (or two-dimensional for a planar analysis), which in Cartesian coordinates can be written as a product of impulse functions of a single variable. (In discussing spatial impulse functions, one needs to be very careful in defining them, especially with regard to the particular coordinate system used The common limiting sequences often yield paradoxical results, and an operational definition that uses generalized functions is appropriate [7].)

We find that a plane wave propagating with speed c and direction $\underline{a}$ has an impulsive frequency wave number spectrum located at

$$\underline{k}_a = \frac{\omega}{c}\,\underline{a} \tag{2 25}$$

in wave number space. (Unless the wave is monochromatic, i e , at a single temporal frequency, the magnitude of the wave number vector changes as a function of the temporal frequency) We again point out that the space over which this transform is taken must be specified Theoretically, in a homogeneous, isotropic medium the magnitude of the wave number $\underline{k}$ at a particular frequency should be a constant, indicating that for three dimensions the function $P_y(\omega\ \underline{k})$ is nonzero only on a sphere, nonzero on a circle in two dimensions, or nonzero at two points opposite in sign in one dimension

However, in many cases one considers representing the waves in a three-dimensional space as projected on a two-dimensional geometry. This leads to an analysis in which the magnitude of the wave number is not a constant at a particular temporal frequency. It should be obvious that any set of statistically independent directional signals propagating as plane waves can be represented with an impulsive frequency wave number function. However, such a representation is not possible if the components are correlated as could possibly be envisioned in some coherent multipath situations The fundamental difficulty stems from the requirement that components from disjoint regions of wave number space must be uncorrelated as specified by Eq. 2 14, therefore such a process would not be homogeneous.

Another commonly used model is isotropic noise. This noise process is commonly advocated for ambient sea noise. It can be viewed as the superposition of plane waves propagating from all directions with a uniform statistical level. This has a spectral covariance structure of the form

$$S_y(\omega\ \underline{z} - \underline{\xi}) = S_o(\omega)\ \mathrm{sinc}\left(\frac{2\pi}{\lambda}|\underline{z} - \underline{\xi}|\right) \tag{2 26}$$[1]

Since this particular process fits within a more general context of a plane wave process, we discuss this more general representation

[1] $\mathrm{sinc}(x) \triangleq \dfrac{\sin(x)}{x}$

2.2 REPRESENTATIONS FOR PROPAGATING SIGNAL PROCESSES

2.2.1 Processes in Three Dimensions

2.2.1.1 Plane Wave. A commonly employed model for the ambient noise background is isotropic or omnidirectional noise We first describe this process and many others in terms of a model for generating its temporal frequency spatial correlation function, after which we find the associated frequency wave number function Later, we specify the frequency wave number function directly. We will find that this is an easier and much more intuitive approach

At a temporal frequency ω, isotropic noise in three dimensions is modeled as a superposition of infinitesimal plane wave processes, all radiating towards a common point [8] These waves may be considered to be generated on the surface of a sphere whose radius is large compared to any geometries or wavelengths of interest Using the integrated transform representation we have

$$dY(\omega_o,\underline{z}) = \int_0^{\pi} d\theta \int_0^{2\pi} \frac{\sin(\theta)\, d\phi}{4\pi}\; dY(\omega_o\ \theta,\phi)e^{-jk_o\underline{a}_r(\theta,\phi)\cdot\underline{z}}, \qquad (2.27a)$$

where

$$y(t,\underline{z}) = \int_{-\infty}^{\infty} dY(\omega\ \underline{z})e^{j\omega t}, \qquad (2.27b)$$

and $k_o = 2\pi/\lambda$ with $\underline{a}_r(\theta,\phi)$ as a unit vector in the radial direction. Consequently, $-k_o\underline{a}_r(\theta,\phi)$ forms a propagation vector $\underline{k}(\theta,\phi)$ at a temporal frequency ω_o radiating towards the center of the sphere, or

$$\underline{k}(\theta,\phi) = -k_o\underline{a}_r(\theta,\phi) = -\frac{2\pi}{\lambda}\,\underline{a}_r(\theta,\phi) = -\frac{\omega_o}{c}\,\underline{a}_r(\theta,\phi) \qquad (2.28)$$

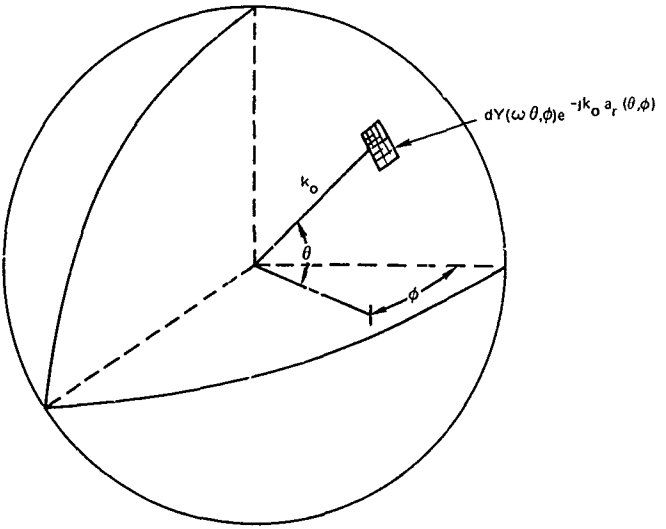

Figure 2-3. Incremental surface area contributing to a plane wave spatial process.

We assume that disjoint regions of the sphere radiate uncorrelated components so that

$$E[dY(\omega_o\ \theta_1,\phi_1)dY^*(\omega_o\ \theta_2,\phi_2)] = S_o(\omega_o,\theta_1,\phi_1)\left(\frac{u_o(\theta_1-\theta_2)u_o(\phi_1-\phi_2)}{(\sin(\theta_1)/4\pi)}\right)\left(\frac{d\omega}{2\pi}\right) \tag{2.29}$$

(The impulse terms should be interpreted formally and should operate simultaneously. The factor of $(4\pi/\sin\theta_1)$ needs to be introduced because of the use of spherical coordinates.) The temporal frequency spatial correlation function is given with some abuse of notation by

$$S_y(\omega_o;\Delta\underline{z}) = E[dY(\omega_o;\underline{z})dY^*(\omega_o\ \underline{z}-\Delta\underline{z})] \tag{2.30}$$

When we use Eq 2 27a, we have

$$S_y(\omega_o\ \Delta\underline{z})$$

$$=\int_0^{\pi} d\,\theta_1 \int_0^{2\pi} \frac{\sin(\theta_1)}{4\pi}\, d\,\phi_1 \int_0^{\pi} d\,\phi_2 \int_0^{2\pi} \frac{\sin(\theta_2)}{4\pi}\ E[dY(\omega_o.\theta_1,\phi_1)dY^*(\omega_1\ \theta_2,\phi_2)]$$

$$\cdot e^{-jk_o\underline{a}_r(\theta_1,\phi_1)\cdot\underline{z}+jk_o\underline{a}_r(\theta_2,\phi_2)\cdot(\underline{z}-\Delta\underline{z})} \qquad (2\ 31)$$

Equation 2 29 implies that disjoint (θ,ϕ) is uncorrelated and yields the desired result

$$S_y(\omega_o\ \Delta\underline{z}) = \int_0^{\pi} d\theta \int_0^{2\pi} \frac{\sin(\theta)}{4\pi}\ d\phi\ S_o(\omega_o\ \theta,\phi)e^{-jk_o\underline{a}_r(\theta,\phi)\cdot\Delta\underline{z}} \qquad (2\ 32)$$

The frequency wave number function follows from the Fourier transform relationship It is useful to define the wave-number $\underline{k}$ in both spherical and Cartesian coordinates

$$\underline{k} = k_x\underline{a}_x + k_y\underline{a}_y + k_z\underline{a}_z = k_r\underline{a}_r\ (\theta_k,\phi_k) \qquad (2\ 33)$$

where $\underline{a}_r\ (\theta_k,\phi_k)$ is a unit radial vector in the same direction as $\underline{k}$ We have

$$P_y(\omega_o\ \underline{k}) = \int\int\int_{-\infty}^{\infty} d\Delta\underline{z}e^{j\underline{k}\cdot\Delta\underline{z}} \int_0^{\pi} d\theta \int_0^{2\pi} \frac{\sin(\theta)}{4\pi}\, d\phi\ S_o(\omega_o.\theta,\phi)e^{-jk_o\underline{a}_r(\theta,\phi)\cdot\Delta\underline{z}}$$

$$=\int_0^{\pi} d\theta \int_0^{2\pi} \frac{\sin(\theta)}{4\pi}\, d\phi\ S_o(\omega_o{:}\theta,\phi) \int\int\int_{-\infty}^{\infty} d\Delta\underline{z}e^{j(k_r\underline{a}_r(\theta_k,\phi_k)-k_o\underline{a}_r(\theta,\phi))\cdot\Delta\underline{z}} \qquad (2\ 34)$$

The evaluation of the last integral leads to an impulse, or delta function, in wave number space, i.e ,

$$\int\int\int_{-\infty}^{\infty} d\Delta\underline{z} e^{j(k_r \underline{a}_r(\theta_k,\phi_k) - k_o \underline{a}_r(\theta,\phi))\cdot\Delta\underline{z}} = (2\pi)^3 \frac{u_o(k_r-k_o)u_o(\theta_k-\theta)u_o(\phi_k-\phi)}{k_o^2 \sin(\theta)} \quad (2\ 35)$$

When we substitute Eq 2 35 into Eq. 2 34, we obtain

$$P_y(\omega_o \underline{k}) = (2\pi)^3 S_o(\omega_o:\theta_k,\phi_k) \frac{u_o(k_r-k_o)}{4\pi k_o^2} \quad (2\ 36)$$

We have the intuitive interpretation that the resulting frequency wave number function has the same distribution as the spectra of the plane waves at the various locations on the sphere. The delta function arises because these waves are modeled as pure plane waves analogous to pure tones temporally. By starting with this specification of the noise field we can model a large number of ambient fields that may be encountered.

2.2.1.2 Series Expansions in Terms of Spherical Harmonics for Space/Time Covariances for Plane Wave Processes. At this point we observe that once $S_o(\omega_o \theta,\phi)$ is specified, $P_y(\omega_o \underline{k})$ follows directly. One can describe the distribution of plane wave power in the signal field quite intuitively in terms of either function. We now demonstrate a series representation for $S_o(\omega_o\ \theta,\phi)$, which enables us to find the temporal frequency spatial correlation function $S_y(\omega \Delta\underline{z})$ quite conveniently Since many of the signal processing techniques involve this function, these results, coupled with a previous analysis of purely directional signals, form a reasonably complete method of analyzing ambient signal fields with a propagating structure. The basic techniques that we employ draw upon some results in spherical expansions which were first used in analyzing similar problems in electromagnetics Our principle reference is Stratton[9].

The expression for the temporal spectrum-spatial covariance function when represented in spherical coordinates is

$$S_y(\omega_o;\underline{z}) = \int_0^{\pi} d\theta \int_0^{2\pi} \frac{\sin\theta}{4\pi}\, d\phi\, S_o(\omega_o\, \theta,\phi)$$

$$\cdot e^{-jk_o r_z[\cos(\theta)\cos(\theta_z)+\sin(\theta)\sin(\theta_z)\,(\sin(\phi)\sin(\phi_z)+\cos(\phi)\cos(\phi_z))]} \qquad (2.37a)$$

where

$$r_z \triangleq |z| \qquad (2\ 37b)$$

Using results for spherical expansions, we can expand $S_o(\omega_o.\theta,\phi)$ in a series of the form [9, Eqs (399)-(420)].

$$S_o(\omega_o.\theta,\phi) = \sum_{n=0}^{\infty} \sum_{m=-n}^{n} S_{nm}(\omega_o)\, P_n^{|m|}(\cos\theta) e^{jm\phi}, \qquad (2.38a)$$

where the coefficient $S_{nm}(\omega_o)$ is given by

$$S_{nm}(\omega_o) = \frac{2n+1}{4\pi}\, \frac{(n-|m|)!}{(n+|m|)!} \int_0^{\pi} d\theta \int_0^{2\pi} \sin\theta d\phi\, S_o(\omega.\theta,\phi)\, P_n^{|m|}(\cos\theta) e^{-jm\phi} \qquad (2\ 38b)$$

and the function $P_n^{|m|}(\cos\theta)$ is a Legendre function of the argument $\cos\theta$. These functions have been tabulated extensively, alternatively one can generate them with the Rodriguez's formula [10]

$$P_n^m(x) = (x^2-1)^{m/2}\, \frac{d^m P_n^o(x)}{dx^m} = \frac{(x^2-1)^{m/2}}{2^n n!}\, \frac{d^{m+n}(x^2-1)^n}{dx^{m+n}} \qquad (2\ 39)$$

Substituting the expansion of Eq 2 38a into the expression for $S_y(\omega_o \underline{z})$ we have, after exchanging the integration and summations,

$$S_y(\omega_o \underline{z}) = \sum_{n=0}^{\infty} \sum_{m=-n}^{m=n} S_{nm}(\omega_o)$$

$$\bullet \int_0^{\pi} d\theta \; \frac{\sin(\theta)}{2} \; P_n^{|m|}(\cos\theta) e^{-jk_o r_z \cos(\theta)\cos(\theta_z)}$$

$$\bullet \; \frac{1}{2\pi} \int_0^{2\pi} d\phi \; e^{j(m\phi - k_o r_z \sin(\theta)\sin(\theta_z)\cos(\phi-\phi_z))} \qquad (2\,40)$$

We now perform the integration with respect to ϕ. We change integration variables first We define

$$\phi' = \phi - \phi_z + \frac{\pi}{2} \qquad (2.41)$$

Substituting this change of variables yields

$$\frac{1}{2\pi} \int_0^{2\pi} d\phi \; e^{j(m\phi - k_o r_z \sin(\theta)\, \sin(\theta_z)\cos(\phi-\phi_z))}$$

$$= \frac{1}{2\pi} \int_0^{2\pi} d\phi' \; e^{jm(\phi_z - \pi/2)} \; e^{j[m\phi' - k_o r_z \sin(\theta)\, \sin(\theta_z)\, \sin(\phi')]}$$

$$= (-j)^m e^{jm\phi_z} \; J_m[\underline{k}_o r_z \sin(\theta)\sin(\theta_z)] \qquad (2\,42)$$

where we have used the tabulated integral[10]

$$J_m(x) = \frac{1}{\pi}\int_0^{\pi} \cos(x\sin(\phi)-m\phi)d\phi = \frac{1}{2\pi}\int_{-\pi}^{\pi} \cos(x\sin(\phi)-m\phi)d\phi$$

$$= \frac{1}{\pi}\int_0^{2\pi} \cos(x\sin(\phi)-m\phi)d\phi = \frac{1}{2\pi}\int_{-\pi}^{\pi} d\phi\, e^{j[m\phi - x\sin(\phi)]} \qquad (2\,43)$$

We substitute this result into Eq 2 40, the expression for $S_y(\omega_o,\underline{z})$, and obtain

$$S_y(\omega_o,\underline{z}) = \sum_{n=o}^{\infty}\sum_{m=-n}^{n} S_{nm}(\omega_o)(-j)^m e^{jm\phi_z}$$

$$\cdot\frac{1}{2}\int_0^{\pi} d\theta\,\sin(\theta)\,P_n^{|m|}(\cos\theta)\,J_m(k_o r_z)\sin(\theta)\sin(\theta_z)e^{-jk_o r_z\cos(\theta)\cos(\theta_z)} \qquad (2.44)$$

To evaluate this integral we use the following addition formulae for spherical harmonics from Stratton [9, p 411 (Eq 2 69a)]:

$$j_n(k_o R)P_n^m(\cos\alpha) = \frac{(-j)^n}{2}\int_0^{\pi} d\theta\, P_n^m(\cos\theta)\,J_m[kR\sin(\alpha)\sin(\theta)]e^{jkR\cos(\alpha)\cos(\theta)}, \qquad (2\,45)$$

where $j_n(x)$ is a spherical Bessel function, which has also been tabulated extensively. We have Rayleigh's formula[11]

$$j_n(x) = x^n\left(\frac{1}{x}\frac{d}{dx}\right)^n \mathrm{sinc}(x) \qquad (2\,46)$$

Making the identification of the respective variables and changing the sign of k_o, we have

$$\int_0^{\pi} \frac{d\theta}{2} \sin(\theta)\, P_n^{|m|}(\cos\theta)\, J_n[k_o r_z \sin(\theta)\sin(\theta_z)]\, e^{-jk_o r_z \cos(\theta)\cos(\theta_z)}$$

$$= (-j)^n J_n(k_o r_z)\, P_n^{|m|}(\cos\theta_z) \qquad (2\,47)$$

In summary, we finally obtain

$$S_y(\omega_o \underline{z}) = \sum_{n=0}^{\infty} \sum_{m=-n}^{m=n} S_{nm}(\omega_o)\,(-j)^{n+m}\, J_n(k_o r_z)\, P_n^{|m|}[\cos(\theta_z)]\, e^{jm\theta_z}\,, \qquad (2\,48)$$

where we have from Eqs 2 28a and 2 28b

$$S_o(\omega_o\, \theta,\phi) = \sum_{n=0}^{\infty} \sum_{m=-n}^{m=n} S_{nm}(\omega_o)\; P_n^{|m|}(\cos\theta) e^{jm\phi} \qquad (2\,49a)$$

and

$$S_{nm}(\omega) = \frac{2n+1}{4\pi} \left(\frac{(n-m)!}{(n+m)!}\right) \int_0^{\pi} d\theta \int_0^{2\pi} d\phi \sin\theta\, S_o(\omega\, \theta,\phi)\, P_n^{|m|}(\cos\theta) e^{jm\phi}$$

(2.49b)

The expressions for finding the Legendre functions $P_n^{|m|}(\cos\theta)$ and the spherical Bessel functions $J_n(|k_o||\underline{z}|)$ are given by, respectively, Eqs. 2.29 and 2 46 We point out that both of these expressions have been tabulated We have confined our attention to plane wave processes that originated on a sphere in wave number space, i e , $|\underline{k}| = 2\pi/\lambda$. Using the references cited, it is straightforward to develop an appropriate theory when we relax this restriction.

Example 2a - Isotropic Noise

The simplest noise field in terms of this representation arises when

$$S_{nm}(\omega) = \begin{cases} S_o(\omega), & n = m = 0 \\ 0, & \text{otherwise} \end{cases} \tag{2.50}$$

We have from Eq. 2.49

$$S_o(\omega:\theta,\phi) = S_o(\omega)\,,\ 0 \leqslant \theta \leqslant \pi,\quad 0 \leqslant \phi < 2\pi \tag{2.51}$$

This is a commonly used model for the ambient noise present in the ocean The temporal frequency spatial correlation function follows directly from Eqs. 2.46 and 2.48

$$S_y(\omega_o\, \underline{z}) = S_o(\omega_o)\, j_o\,(k_o r_z)\, P_o^o\, [\cos(\theta_z)] = S_o(\omega)\, \mathrm{sinc}(k_o r_z) \tag{2.52}$$

This result has been derived in many places, but in a much less general context [8,12]

Example 2b - Surface (or Bottom Noise)

With this noise field we assume that there is a much stronger intensity for the noise field in the vicinity of $\theta = 0$ and that there is an azimutal symmetry To do these we choose

$$S_o(\omega.\theta,\phi) = S_o(\omega)\, [1 + \alpha\cos(\theta)] \tag{2.53}$$

such that the noise level as a function of θ appears as in Figures 2-4 and 2-5. This type of noise can be used to describe a high intensity noise field which is present from the surface (or bottom). We have

$$S_{nm}(\omega_o) = S_o(\omega) \quad \begin{cases} 0, & m \neq 0, \text{ or } n \geqslant 2 \\ 1, & n = 0, \quad m=0 \\ \alpha, & n = 1, \quad m=0 \end{cases} \tag{2.54}$$

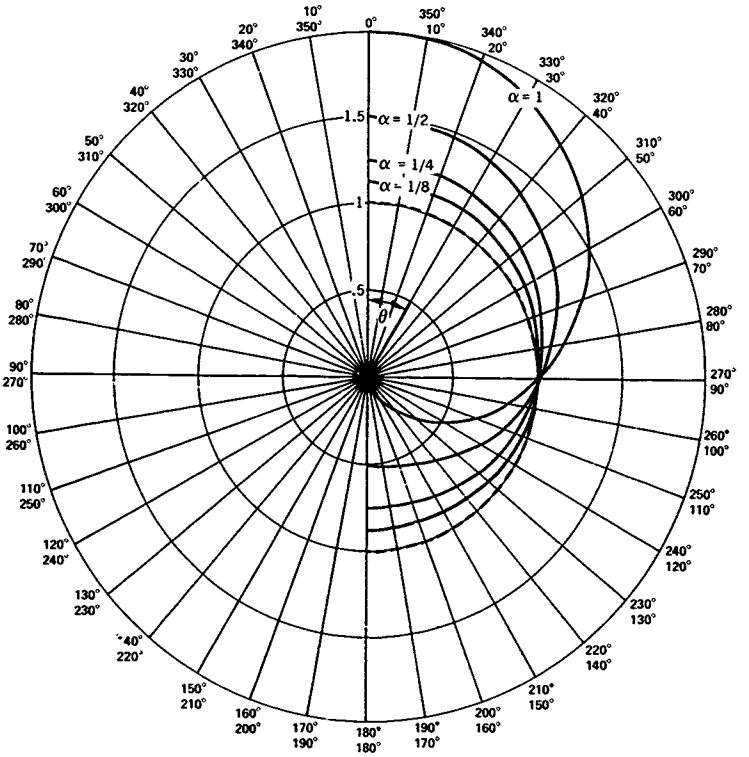

Figure 2-4. Relative intensity of noise power

$$S_o(\omega.\theta,\phi) = 1 + \alpha \cos\theta$$

for a noisy surface.

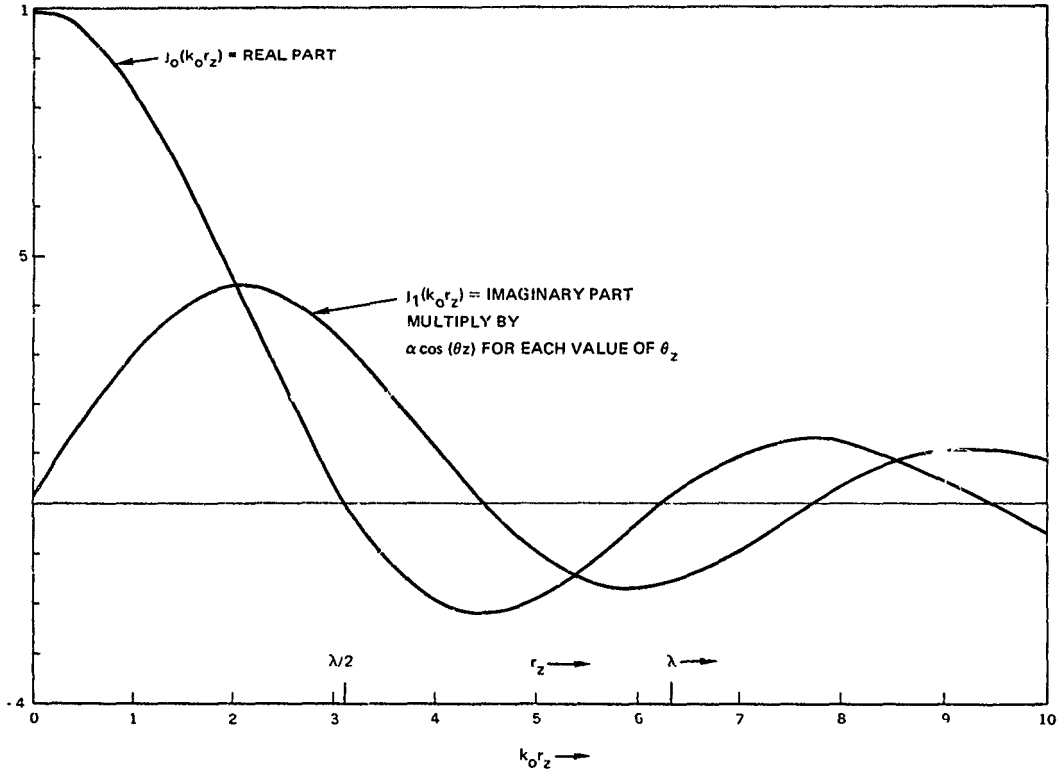

Figure 2-5. Relative real and imaginary parts for the covariance function for noise distribution as shown in Figure 2-4.

Consequently, the temporal frequency spatial correlation function becomes

$$S_y(\omega:\underline{z}) = S_o(\omega)\ j_0(k_o r_z)\, P_0^{(0)}\ [\cos(\theta_z)] + \alpha j_1 (k_o r_z) P_1^{(0)}\ [\cos(\theta_z)]$$

$$= S_o(\omega_o) \left\{ \mathrm{sinc}(k_o r_z) + j\alpha \frac{1}{k_o r_z} [\mathrm{sinc}(k_o r_z) - \cos(k_o r_z)]\ \cos(\theta_z) \right\} \qquad (2.55)$$

Example 2c - Layer Noise

With this model of a noise field we assume that there is a much stronger intensity in the vicinity of $\theta = 90°$, and that there is azimuthal symmetry Specifically, we choose

$$S_o(\omega.\theta,\phi) = S_o(\omega) [1-\alpha P_2(\cos\theta)] = S_o(\omega) \left[1 - \frac{1}{4}\alpha - \frac{3}{4}\alpha \cos(2\theta)\right] \qquad (2.56)$$

The intensity as a function of θ is illustrated in Figures 2-6 and 2-7. We have

$$S_{mn}(\omega_o) = S_o(\omega_o) \begin{cases} 0, & m \neq 0 \\ 1, & n = 0, m = 0 \\ 0, & n = 1, m = 0 \\ -\alpha_2, & n = 2, m = 0 \\ 0 & n \geq 3, m = 0 \end{cases} \qquad (2.57)$$

The temporal frequency spatial correlation function becomes

$$S_y(\omega_o:\underline{z}) = S_o(\omega_o)\ j_0(k_o r_z)\, P_0^{(0)} [\cos(\theta_z)] + \alpha j_2(k_o r_z) P_2^{(0)} [\cos(\theta_z)]$$

$$= S_o(\omega_o) \left\{ \mathrm{sinc}(k_o r_z) + \alpha \left[\left(\frac{3}{(k_o r_z)^2} - 1 \right)\ \mathrm{sinc}(k_o r_z) - \frac{3\cos(k_o r_z)}{(k_o r_z)^2} \right] \left[\frac{3\cos(2\theta_z)+1}{4} \right] \right\} \qquad (2.58)$$

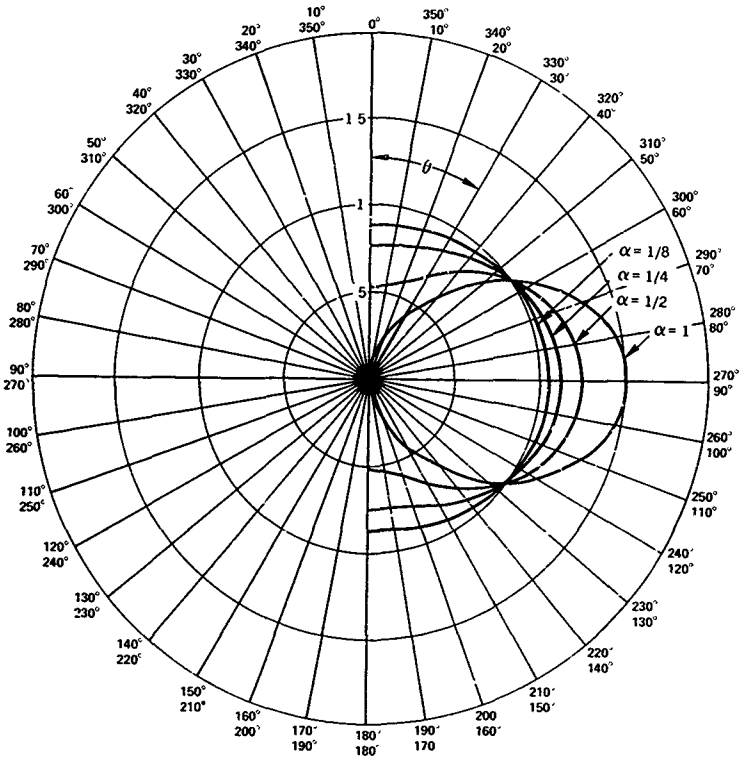

Figure 2-6. Relative intensity of power distribution

$$S_o(\omega_o \cdot \theta, \phi) = 1 - \frac{\alpha}{4} [1 + 3 \cos (2\theta)]$$

for layer noise.

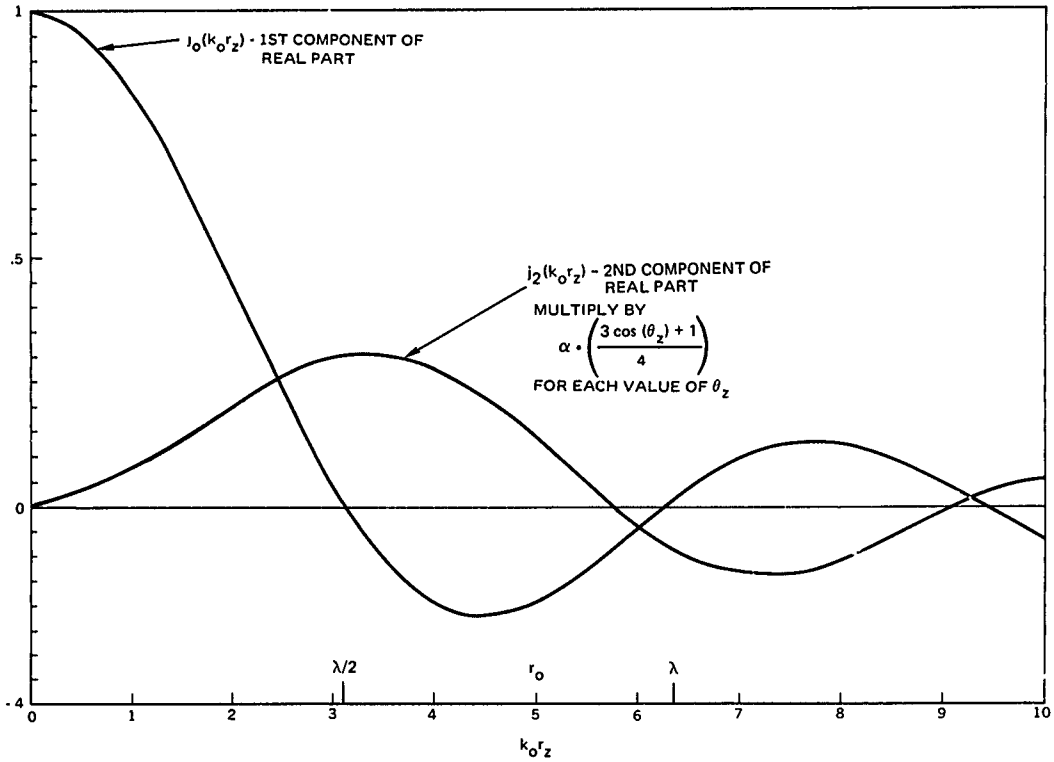

Figure 2-7 Relative parts of real components for the covariance function for noise distribution as shown in Figure 2-6.

It should be clear that we can now model a large class of processes with this method More complex elevation, or θ, dependence can be introduced and sectors of noise in azimuth, or ϕ, can also be incorporated

The model is particularly convenient when there are relatively few significant spherical harmonics. Fortunately, this is a common situation for a typical ambient noise field in many sonar applications.

It is worthwhile to point out that the analysis in terms of spherical harmonics demonstrates that many ambient field models can lead to the similar oscillatory behavior for the temporal frequency spatial covariance function This stems from the ideal bandlimited behavior that the finite velocity of propagation imposes upon the wave number spectrum The oscillatory behavior certainly cannot be interpreted as being particularly unique to an isotropic noise model

2.2.2 Representations for Signal Processes in Two Dimensions

In the discussion of section 2 2 we considered the representation of signals propagating in three dimensions whose wave number was limited in magnitude to $2\pi/\lambda$. In this section we analyze the related problem of the representation of signals on a surface. In many problems, this representation may be more convenient than the one in the previous section Problems in this context may arise in several applications. In many, the medium of interest supports surface waves; for example, seismic Rayleigh and Love waves or internal ocean waves. In other applications, one observes signals which propagate in three dimensions but are observed on a two-dimensional surface

If we confine our attention to plane waves, there is little ambiguity since only two points on the sphere model map to an identical point in the plane. If we assume that this ambiguity can be resolved, possibly via the characteristics of the receivers, the geometry of the model, or its inrelevancy, one can proceed with a two-dimensional analysis which is often considerably simpler than the corresponding three-dimensional one [12, 13, 14][1]. We point out here that in contrast to the previous section, we will not constrain the magnitude of the wave number, although in most applications it will have a finite upper limit

[1] *This model is particularly relevant to processing seismic data for here the signals are all incident from beneath the earth's surface, as partially discussed by Berg, Gaarder, or Capon*

The fundamental relations between the temporal frequency-spatial correlation function and the wave number spectrum remain virtually identical with the exception of the integration region which becomes a plane rather than spherical surface. We have for the frequency wave number function

$$P_y(\omega\ \underline{k}) = \int_{-\infty}^{\infty}\int S_y(\omega\cdot\underline{z})e^{j\underline{k}\cdot\underline{z}}\,d\underline{z} \qquad \text{(Cartesian coordinates)} \qquad (2\ 59a)$$

$$= \int_0^{\infty}\int_0^{2\pi} S_y(\omega.\underline{z})e^{j(k_r r_z)\{\cos(\phi_{\underline{k}})\cos(\phi_z)+\sin(\phi_{\underline{k}})\sin(\phi_z)\}} r_z\,dr_z\,d\phi_{\underline{z}}$$
$$\text{(Polar coordinates)} \qquad (2.59b)$$

Similarly, for the inverse transform we have

$$S_y(\omega\cdot\underline{z}) = \int_{-\infty}^{\infty}\int P_y(\omega\ \underline{k})e^{-j\underline{k}\cdot\underline{z}}\,\frac{d\underline{k}}{(2\pi)^2} \qquad \text{(Cartesian coordinates)} \quad (2\ 60a)$$

$$= \frac{1}{(2\pi)^2}\int_0^{\infty}\int_0^{2\pi} P_y(\omega:\underline{k})e^{-j(k_r r_z)\,[\cos(\phi_{\underline{k}})\cos(\phi_{\underline{z}})+\sin(\phi_{\underline{k}})\sin(\phi_z)]}\,k_r dk_r d\phi_k$$
$$\text{(Polar coordinates)} \qquad (2.60b)$$

We can proceed with an analysis parallel to that which we did for the spherical representation. First, we demonstrate that the analysis of a directional signal remains unchanged, and then we discuss a series representation which leads to a convenient method of analysis.

Example 3 - Directional Signals

One of the principal differences which often arises in a two-dimensional analysis is that the propagation velocity as projected upon the surface need not be a constant unless one confines his attention to surface waves. For a directional signal we have

$$y(t.z) = y_o\,[t-(\underline{\alpha}\cdot\underline{z}/c(\underline{k}_S)] \qquad (2.61)$$

which describes the signal propagation where $c(\underline{k}_s)$ is the propagation velocity as a function of the signal wave number, k_s. This leads to a temporal frequency spatial correlation function of the form

$$S_y(\omega \cdot \underline{z}) = S_o(\omega) e^{-j[\omega/c(\underline{k}_s)]\ \underline{\alpha} \cdot \underline{z}} = S_o(\omega) e^{-j\underline{k}_s \cdot \underline{z}}, \tag{2 62}$$

where we have the relation

$$\underline{k}_s = \frac{\omega}{c(\underline{k}_s)}\ \underline{\alpha} \tag{2 63}$$

The frequency wave number function is still impulsive, or

$$P_y(\omega\ k) = S_o(\omega) u_o(\underline{k}-\underline{k}_s) = S_o(\omega) u_o(k_x - k_{s_x}) u_o(k_y - k_{s_y}) \tag{2.64}$$

To consider an analysis of some more general processes using a series representation, we specify $P_y(\omega.\underline{k})$ in terms of the polar coordinates k_r and $\phi_{\underline{k}}$ We expand the frequency wave number function $P_y(\omega\ \underline{k})$ in the series-integral form

$$P_y(\omega\ \underline{k}) = \sum_{m=-\infty}^{\infty} p_m(\omega : k_r) e^{jm\phi_{\underline{k}}}, \tag{2 65}$$

where

$$p_m(\omega\ k_r) = \frac{1}{2\pi} \int_0^{2\pi} F_y(\omega\ \underline{k}) e^{-jm\phi_{\underline{k}}} d\phi_{k'}, \quad k_r = |\underline{k}| = \text{const} \tag{2 66}$$

This is simply a Fourier series decomposition at a specific k_r

To proceed further, we have the following sequence of Fourier-Bessel or Hankel transforms For any function f(p), $p > 0$ with a bounded first moment, the nth order ($n > -1/2$) Hankel transform is given by

$$F_n(\lambda) = \int_0^\infty f(p) J_n(p\lambda) p dp, \tag{2.67a}$$

while the inverse transform relationship is

$$f(p) = \int_0^\infty F_n(\lambda) J_n(p\lambda) \lambda d\lambda \tag{2.67b}$$

(We note that one can generally use Hankel functions rather than Bessel functions, and, in particular, when $n = 1/2$ one has the common Fourier transform pair [15, Vol 2, p 73])

We define the m^{th} order Fourier-Bessel transform pair for $p_m(\omega\ k_r)$ to be $f_m(\omega:\lambda)$ such that we have

$$f_m(\omega:\lambda) = \frac{1}{2\pi} \int_0^\infty p_m(\omega\ k_r) J_m(\lambda k_r) k_r dk_r \tag{2.68a}$$

and

$$p_m(\omega \cdot k_r) = \int_0^\infty f_m(\omega\ \lambda) J_m(\lambda k_r) \lambda d\lambda \tag{2 68b}$$

(One could choose any order for the Bessel function or transform order, however, it will be convenient to choose it to be m as indicated.) The net result of our decomposition is that we can express $P_y(\omega:\underline{k})$ in the series integral form

$$P_y(\omega:\underline{k}) = \sum_{m=-\infty}^{\infty} \int_0^\infty f_m(\omega:\lambda) J_m(\lambda k_r) \lambda d\lambda\, e^{jm\phi_{\underline{k}}} \tag{2.69}$$

This is simply a Fourier-Bessel representation for a cylindrical coordinate system, and it has been used extensively in the study of electromagnetic fields[9]

The temporal frequency spatial correlation function follows, using this representation We have in polar coordinates from Eq 2 60b

$$S_y(\omega\ \underline{z}) = \frac{1}{(2\pi)^2}\int_0^{\infty} dk_r \int_0^{2\pi} d\phi_{\underline{k}}\, k_r\, P_y(\omega\ \underline{k}) e^{-j(k_r r_{\underline{z}})\cos(\phi_{\underline{k}}-\phi_{\underline{z}})} \qquad (2.70)$$

Substituting Eq 2.65 yields

$$S_y(\omega.z) = \frac{1}{(2\pi)^2}\int_0^{\infty} dk_r \int_0^{2\pi} d\phi_k k_r \sum_{m=-\infty}^{\infty} p_m(\omega\ k_r) e^{j[m\phi_{\underline{k}} - k_r r_{\underline{z}}\cos(\phi_{\underline{k}}-\phi_{\underline{z}})]}$$

$$= \left(\frac{1}{2\pi}\right)\int_0^{\infty} dk_r k_r \sum_{m=-\infty}^{\infty} p_m(\omega.k_r) e^{jm(\phi_{\underline{z}}-\pi/2)} J_m(k_r r_{\underline{z}}) \qquad (2\ 7_1)$$

$$= \sum_{m=-\infty}^{\infty} f_m(\omega{:}r_z) e^{jm(\phi_{\underline{z}}-\pi/2)}$$

In summary, we have the relationships

$$P_y(\omega{:}\underline{k}) = \sum_{m=-\infty}^{\infty} p_m(\omega{:}k_r) e^{jm\phi_k} \qquad (2.72a)$$

and

$$S_y(\omega\ \underline{z}) = \sum_{m=-\infty}^{\infty} f_m(\omega.{}_1 z) e^{jm(\phi_{\underline{z}}-\pi/2)} \qquad (2.72b)$$

where

$$p_m(\omega\ k_r) \leftrightsquigarrow f_m(\omega\ r_z) \tag{2 72c}$$

form an mth order, Fourier–Bessel, or Hankel transform pair

One can use the numerous transform pair relations that have been tabulated by Erdelyi The essential point here is that a large amount of literature and tabulated integrals are available for these transforms [10]

For convenience, we point out a possible, but certainly not exclusive, approach to the analysis of this class of fields Let us assume that the magnitude of the wave number is bounded such that $k_r < k_o$. Just as we did earlier, we can expand either $p_m(\omega\ k_r)$ or $k_r p_m(\omega\ k_r)$ in an orthogonal series of polynominals in the variable k_r/k_o In the following, we consider a Tchebychev expansion of $k_r p_m(\omega\ k_r)$. We have[10]

$$k_r p_m(\omega\ k_r) = \sum_{n=0}^{\infty} \frac{C_{nm}}{(1-(k_r/k_o)^2)^{1/2}}\, T_n\left(\frac{k_r}{k_o}\right), 0 \leq k_r < k_o \text{ ,} \tag{2 73a}$$

where $T_n(x)$ is an nth order Tchebychev polynomial, and

$$C_{nm} = \frac{1}{\pi} \int_0^{k_o} k_r p_m(\omega{:}k_r)\, T_n\left(\frac{k_r}{k_o}\right)\left(\frac{dk_r}{k_o}\right) \text{ , } n\neq 0 \tag{2 73b}$$

$$C_{om} = \frac{2}{\pi} \int_0^{k_o} k_r p_m(\omega\ k_r)\left(\frac{dk_r}{k_o}\right), \text{ n=0} \tag{2 73c}$$

We now have the tabulated integral [15, Vol 2, p 42(I)]

$$\int_0^1 \frac{T_n(p)}{(1-p^2)^{1/2}} J_m(\lambda p)dp = \frac{\pi}{2} J_{(m+2)/2}\left(\frac{\lambda}{2}\right) J_{(m-2)/2}\left(\frac{\lambda}{2}\right) \tag{2 74}$$

Substituting into the transform integral and using Eq 2 74, we obtain

$$f_m(\omega;\underline{z}) = \frac{\pi k_o}{2} \sum_{n=0}^{\infty} C_{nm} J_{(m+n)/2}\left(\frac{k_o r_{\underline{z}}}{2}\right) J_{(m-n)/2}\left(\frac{k_o r_{\underline{z}}}{2}\right) \tag{2.75}$$

such that

$$S_y(\omega,\underline{z}) = \left(\frac{1}{2\pi}\right)\left(\frac{\pi k_o}{2}\right) \sum_{m=-\infty}^{\infty} \sum_{n=0}^{\infty} C_{nm} J_{(m+n)/2}\left(\frac{k_o r_{\underline{z}}}{2}\right) J_{(m-n)/2}\left(\frac{k_o r_{\underline{z}}}{2}\right) e^{jm(\phi_{\underline{z}} - \pi/2)} \tag{2 76}$$

Since the Tchebychev polynominals are orthogonal over (−1,1) we can obtain some degree of freedom since we are interested only in the region (0,1) Consequently, by choosing $p_m(\omega\ k_r)$ appropriately for $k_r < 0$ we can minimize the number of terms needed in a finite term approximation

Alternatively, one could approach the transform using Eq 2 74 by expanding $p_m(\omega\ k_r)$ and using the following recurrence relationship in the transform of Eq 2.72a.

$$xT_n(x) = \frac{T_{n+1}(x) + T_{n-1}(x)}{2} \tag{2.77}$$

Again, the important point is not so much this particular method of expansion, but that there is a wealth of results available using tabulated special functions which can be tailored for an individual application

Example 4 – Circle Noise

A particular noise model often used follows when we choose

$$P_y(\omega\ \underline{k}) = (2\pi)^2 \frac{S_o(\omega) u_o(k_r - k_o)}{2\pi k_o} \quad , \tag{2.78}$$

i.e., this is a ring of plane waves radiating towards the center. We have

$$p_m(\omega:k_r) = \begin{cases} 0, & m\neq 0 \\ 2\pi \dfrac{S_o(\omega)u_o(k_r-k_o)}{k_o}, & m=0 \end{cases} \tag{2.79}$$

When we use the zero order Bessel transform, as indicated by Eq 2 68a, we have

$$f_m(\omega\cdot\underline{z}) = \begin{cases} 0 & m=0 \\ S_o(\omega)J_o(k_o r_{\underline{z}}), & m=0 \end{cases} \tag{2 80}$$

so that the temporal frequency spatial correlation function becomes

$$S_y(\omega\cdot\underline{z}) = S_o(\omega)J_o(k_o r_z) \tag{2 81}$$

Example 5a – Two-dimensional representation for isotropic noise

Let us assume a frequency wave number function of the form

$$P_y(\omega:\underline{k}) = \frac{S_o(\omega)}{2\pi k_o{}^2} \left[1-\left(\frac{k_r}{k_o}\right)^2\right]^{-1/2} \tag{2 82}$$

Due to the angular symmetry, the function $p_m(\omega.k_r)$ is nonzero only for m=0 We have

$$p_m(\omega:k_r) = \begin{cases} 0, & m\neq 0 \\ \dfrac{S_o(\omega)}{2\pi k_o{}^2}\left[1-\left(\dfrac{k_r}{k_o}\right)^2\right]^{-1/2}, & m=0 \end{cases} \tag{2.83}$$

This $P_y(\omega\ \underline{k})$ is shown in Figure 2-8. Using the Tchebychev expansion, as shown in Eq. 2.73a, we find

$$k_r p_m(\omega\ k_r) = \begin{cases} 0, & m \neq 0 \\ S_o(\omega)\ \dfrac{1}{2\pi k_o}\left[1-\left(\dfrac{k_r}{k_o}\right)^2\right]^{-1} T_1\left(\dfrac{k_r}{k_o}\right), & m=0 \end{cases} \tag{2.84}$$

Substituting into Eq. 2.73b we find

$$C_{nm} = \begin{cases} 0, & m \neq 0 \\ 0, & m=0,\ n \neq 1 \\ \dfrac{S_o(\omega)}{2\pi k_o}, & m=0,\ n=1 \end{cases} \tag{2.85}$$

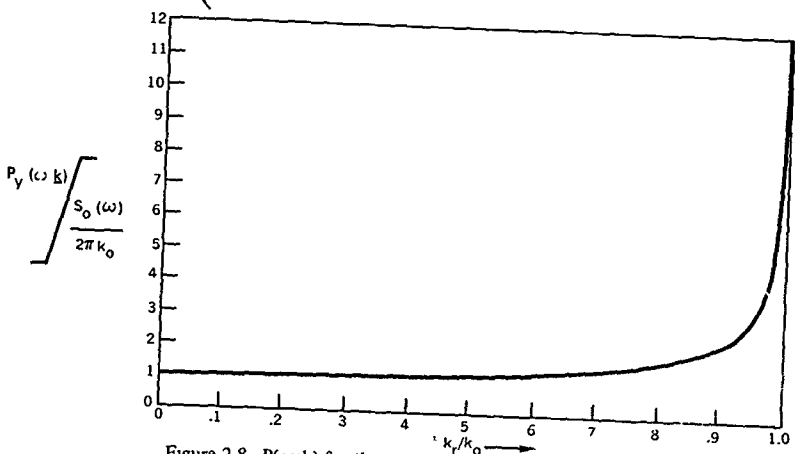

Figure 2-8. $P(\omega:k)$ for three-dimensional isotropic noise projected on a two-dimensional surface

Consequently, we have

$$S_y(\omega\ \underline{z}) = \frac{S_o(\omega)}{2\pi k_o}\ \pi^2 k_o\, J_{1/2}\left(\frac{k_o r_{\underline{z}}}{2}\right)\ J_{-1/2}\left(\frac{k_o r_{\underline{z}}}{2}\right)$$

$$= S_o(\omega)\ \frac{\pi}{2}\left(\frac{4}{\pi k_o r_z}\right)\sin\left(\frac{k_o r_{\underline{z}}}{2}\right)\cos\left(\frac{k_o r_{\underline{z}}}{2}\right) = S_o(\omega)\,\mathrm{sinc}(k_o r_{\underline{z}}) \qquad (2\ 86)$$

We observe that we are led to the same temporal frequency spatial correlation function as with spherically symmetric noise (see Eq 2 52) In a subsequent discussion, we explore the reason for this

Example 5b - Two-dimensional representation for noise with a high concentration of low wave number components

Let us assume that the frequency wave number function $P_y(\omega\ \underline{k})$ has the form

$$P_y(\omega\ \underline{k}) = S_o(\omega)\ \frac{1}{\pi^2 k_o{}^2}\left\{\left(\frac{k_r}{k_o}\right)\left[1-\left(\frac{k_r}{k_o}\right)^2\right]^{1/2}\right\}^{-1} \qquad (2\ 87)$$

This wave number function, shown in Figure 2-9, corresponds to a high intensity source near $k_r = 0$ which may be due to a strong component normal to the surface Pursuing the same analysis we find

$$k_r p_m(\omega{:}k_r) = S_o(\omega)\ \frac{1}{\pi^2 k_o}\left[1-\left(\frac{k_r}{k_o}\right)^2\right]^{-1/2} T_o\left(\frac{k_r}{k_o}\right) \qquad (2.88a)$$

$$C_{nm} = \begin{cases} \dfrac{S_o(\omega)}{\pi^2 k_o}, & n=m=0 \\ 0, & n\neq 0 \text{ or } m\neq 0 \end{cases} \qquad (2\ 88b)$$

Therefore, we have

$$S_y(\omega{:}\underline{z}) = S_o(\omega)\ J_o^2\left(\frac{k_r r_{\underline{z}}}{2}\right) \qquad (2\ 89)$$

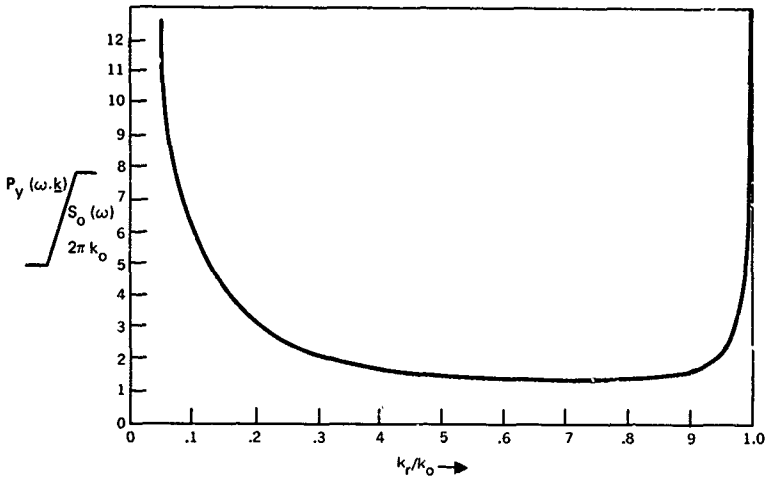

Figure 2-9. Two-dimensional noise with a high concentration of low wave number components

We could pursue examples at length using this procedure, the generality of the approach, however, should now be apparent

2.2.3 Representations for Three-Dimensional Plane Wave Noise Projected on a Two-Dimensional Surface

At this point we investigate the relationship between the three dimensional representation discussed earlier and the two-dimensional one just established, and which is appropriate when three-dimensional noise is observed on a two-dimensional surface. We do this by considering what happens when we confine our attention to a plane in space or, in particular, when $z_z=0$ We define

$$\underline{z}_s = \underline{z}\Big|_{z_z=0} = z_x\underline{a}_x + z_y\underline{a}_y \qquad \underline{k}_s = \underline{k}\Big|_{k_z=0} = k_x\underline{a}_x + k_y\underline{a}_y \tag{2.90}$$

In terms of a three-dimensional wave number function

$$S_y(\omega\ \underline{z}_s) = S_y(\omega\ \underline{z})\Big|_{z_z=0} = \frac{1}{(2\pi)^3} \int\int\int_{-\infty}^{\infty} P_y(\omega\ \underline{k}) e^{-j(k_x z_x + k_y z_y)}\, dk_x dk_y dk_z$$

$$= \int_{-\infty}^{\infty}\int \left[\int_{-\infty}^{\infty} P_y(\omega\ \underline{k}) \frac{dk_z}{2\pi} \right] e^{-jk_z \cdot \underline{z}}\, dk_x dk_y/(2\pi)^2 \qquad (2\ 91)$$

Therefore, the two-dimensional wave number function is given by

$$P_{2y}(\omega\ \underline{k}_s) = \int_{-\infty}^{\infty} P_{3y}(\omega\ \underline{k}) \frac{dk_z}{2\pi} \qquad (2\ 92)$$

We have the two-dimensional Fourier transform pair

$$S_y(\omega.\underline{z}_s) \rightsquigarrow \int_{-\infty}^{\infty} P_{3y}(\omega\ \underline{k}) \frac{dk_z}{2\pi} = P_{2y}(\omega\ \underline{k}_s) \qquad (2.93)$$

Let us now examine what happens when we project our plane wave model on a two-dimensional surface An easy way to do this, which eliminates many of the issues regarding the delta functions in several dimensions, is to establish the Fourier transform of $S_y(\omega\ \underline{z}_s)$ We have from Eq 2 37a with $\theta_z=\pi/2$

$$S_y(\omega\ \underline{z}_s) = \int_0^{\pi} d\theta_{\underline{k}} \int_0^{2\pi} d\phi_{\underline{k}} \frac{\sin(\theta_{\underline{k}})}{4\pi} S_o(\omega \cdot \theta_{\underline{k}}, \phi_{\underline{k}}) e^{-jk_o \sin(\theta_{\underline{k}}) r_{\underline{z}} \cos(\phi_{\underline{z}} - \phi_{\underline{k}})} \qquad (2\ 94)$$

We first perform the integration with respect to θ_k over the regions $[0,\pi/2]$ and $[\pi/2,\pi]$ (This is necessary since two points on the surface of the sphere for the plane wave model project to the same point on the two-dimensional surface) We now change variables in each region Setting

$$\sin(\theta_k) = \frac{k_r}{k_o}, \quad 0 < \theta_k < \pi/2 \tag{2 95a}$$

$$\sin(\pi-\theta_k) = \frac{k_r}{k_o}, \quad \pi/2 < \theta_k < \pi \tag{2.95b}$$

we obtain

$$S(\omega\ \underline{z}_s) = \frac{1}{4\pi k_o^2} \int_0^{k_o} \int_0^{2\pi} \frac{d\phi_{\underline{k}} k_r}{\left[1 - \left(\frac{k_r}{k_o}\right)^2\right]^{1/2}} e^{-jk_r r_{\underline{z}} \cos(\phi_{\underline{z}} - \phi_{\underline{k}})}$$
$$\cdot \left\{ S_o\left[\omega \sin^{-1}\left(\frac{k_r}{k_o}\right), \phi_{\underline{k}}\right] + S_o\left[\omega.\pi - \sin^{-1}\left(\frac{k_r}{k_o}\right), \phi_{\underline{k}}\right] \right\} \tag{2 96}$$

Comparing Eq. 2 96 with our two-dimensional polar coordinate transform (see Eq 2 70), we have

$$P(\omega\ \underline{k}_s) = (2\pi)^2 \frac{S_o\left[\omega \cdot \sin^{-1}\left(\frac{k_r}{k_o}\right), \phi_{\underline{z}}\right] + S_o\left[\omega:\pi - \sin^{-1}\left(\frac{k_r}{k_o}\right), \phi_{\underline{z}}\right]}{4\pi k_o^2 \left[1 - \left(\frac{k_r}{k_o}\right)^2\right]^{1/2}} \tag{2 97}$$

The numerator terms represent those points on the sphere which project to the point on a surface with a two-dimensional wave number k_s, the denominator term is the Jacobian of the transformation Intuitively, the Jacobian plot implies that noise spread over a unit surface area on the sphere leads to a more intense value of the wave number function when it is in the horizontal direction than when in the vertical direction

It should be apparent that we can also go from our surface wave model to a three-dimensional model, with possibly some ambiguity as to which hemisphere We also see that the factor $1/\sqrt{1-(k_r/k_o)^2}$ introduced in our Tchebychev expansion arises quite naturally as a Jacobian in our transformation Consequently, both the expansions in spherical harmonics and in our two-dimensional analysis have many common results

We again point out that while the spherical harmonic expansion is quite natural for our plane wave model, the Tchebychev expansion was only a suggested possible approach For some types of noise fields, another expansion may be much more concise, and one should bring the special function literature, which we have not discussed at all extensively, to bear.

We have discussed the representation of plane wave signals in detail, however, we emphasize the approaches taken, not the specifics of a particular example We now turn our attention to receiver apertures for observing the signal field

PART 2 - RESPONSE OF ARRAYS TO VARIOUS NOISE FIELDS

3. RECEIVING APERTURES

In this chapter we discuss the general properties of receiving apertures, or antennas, with the emphasis on characterizing their response to random excitations Our intent is to understand how knowledge of the statistical characteristics of the ambient noise field can be used to achieve enhanced performance. Toward this goal, classical beamforming theory is quite useful so we introduce results from this literature that are relevant to our analysis.

We first consider describing the aperture response. The development parallels that of Section 2 in that we introduce a temporal-spatial domain description, followed by temporal frequency-spatial domain one, and finally a frequency-wave number one of the response. This is done by discussing several commonly used arrays and analyzing their responses Next we study the role of sensor noise, which is extremely important in the analysis of the statistical characteristics of array processing The noise structure is closely coupled to the array geometry and usually does not lend itself to a separate analysis Finally, we consider the issues separating continuous arrays, i.e., an aperture, and an array of sensors, i e , discrete array We simply state that an array of sensors is the spatial dual to a discrete time, or sampling problem, with some added complexities Since sampling in the time domain tends to obscure the more fundamental issues, we choose not to introduce the corresponding difficulties in the analysis of spatial processing, and, we devote a separate section to the study of the sampling questions introduced by a discrete array.

3.1 ARRAY RESPONSE CHARACTERIZATION

Intuitively, it appears that the description of a receiver aperture should be quite simple. For example, if we have a linear array, as shown in Figure 3-1, which observes a signal field y(t,z) over a specified time duration we would describe our received signal as

$$r(t,\ell) = y(t,\ell \underline{a}_a) \text{ for} \begin{cases} T_o < t < T_f \\ \Omega \quad |\ell| < L/2 \end{cases} \tag{3.1}$$

We see that, just as for a purely temporal process, we need to specify the length of the observation, however, we note that we also need to specify the orientation in space by means of a unit fector $\underline{a}_a$ which is tangent to the array.

As a second example, we have a circular array as illustrated in Figure 3-2. The received signal could be described as

$$r(t,\phi) = y(t \begin{bmatrix} (R(\cos\theta_o \cos\phi_o \cos\phi - \sin\phi_o \sin\phi)\underline{a}_x \\ +(R(\cos\theta_o \sin\phi_o \cos\phi + \sin\phi_o \sin\phi)\underline{a}_y \\ +(R(-\sin\theta_o \cos\phi)\underline{a}_z \end{bmatrix} , 0 < \phi < 2\pi \quad (3\ 2)$$

The formal description of the observation process can be quite tedious As a result, it is usually necessary to keep the geometry simple in order to obtain an intuitive understanding of optimum array processing Similar statements can be made when describing the operation of a discrete array, where one must specify the location of all the individual sensor elements For our purposes we denote the array location by Ω, i e , we consider observation points for $\underline{z} \epsilon \Omega$ In the applications of interest to us, the observed signal is weighted, or shaded, and filtered at each point, and then collected, or summed, together to form an output signal, usually called a beam Figure 3 3 displays this operation graphically while Eq 3 3 expresses it mathematically

$$r_o(t) = \int_{T_o}^{T_f} d\tau \int_{\Omega} dz\, g_i(t,\tau\ \underline{z})\ y(\tau\ \underline{z}) \tag{3 3}$$

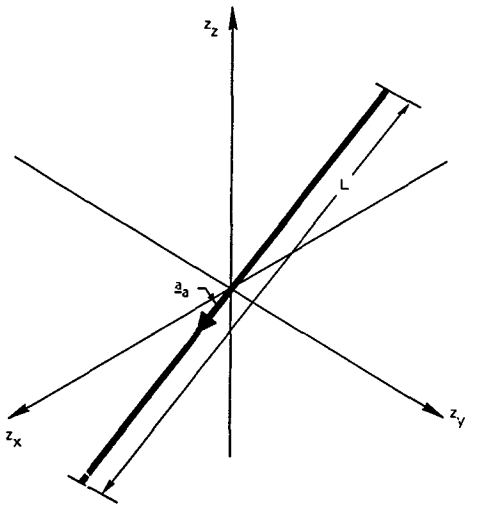

Figure 3-1. Linear array length L, orientation $\underline{a}_a$

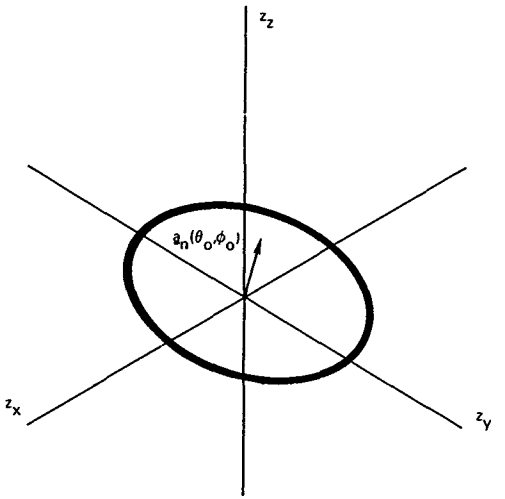

Figure 3-2 Circular array radius R, orientation normal to $a_n(\theta_o,\phi_o)$

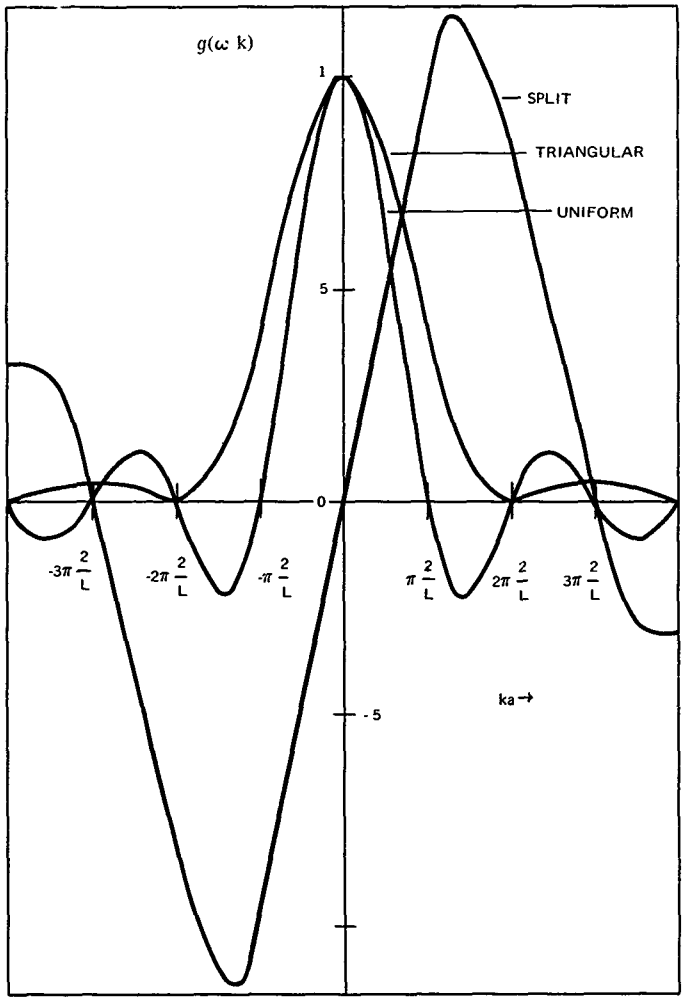

Figure 3-3. Figures of common beam patterns (a) uniform (b) triangular shading (c) split.

This expression has a parallel in classical filtering theory, however, it can be deceptively simple, so a few comments are appropriate

First, one should note that there are two issues in specifying the beam operation the geometry of the array, or aperture, as given by Ω, and the weighting pattern $g(t,\tau\ \underline{z})$ One can consider expressing these in terms of a function with finite limits similar to the analysis of temporal functions Generally, however, it is useful to separate the two The array geometry imposes more fundamental constraints while the shading, or weighting, is adjusted within these constraints In addition, the introduction of geometries of two and three dimensions can lead to some very subtle considerations, especially with regard to spatial impulses, or singularity functions, when one uses a theory dual to the Fourier transform pair relationship between the system impulse response and the transfer function

In this context it is worthwhile to introduce a simple example to illustrate the nature of these subtleties Let us consider a linear array oriented along the z_x axis We represent its response as

$$r(t) = \int_{T_o}^{T_f} d\tau \int_{-L/2}^{L/2} d\ell\ g(t,\tau.\ell)\ y(\tau\ \ell \underline{a}_{z_x}) \tag{3 4}$$

If we want to use infinite limits and specify the array response in terms of a single function, we have

$$r(t) = \int_{-\infty}^{\infty} d\tau \int\int\int_{-\infty}^{\infty} d\underline{z}\ g_{oo}\ (t,\tau\ \underline{z})\ y(\tau\ \underline{z}) \tag{3 5a}$$

where

$$g_{oo}(t,\tau\ \underline{z}) = \begin{cases} g(t,\tau\ z_x)\ u_o(z_y)\ u_o(z_z),\ |z_x| < L,\ T_o \leqslant \tau \leqslant T_f \\ 0,\ |z_x| > L, \text{ or } \tau < T_o \text{ or } \tau > T_f \end{cases} \tag{3 5b}$$

Observe that we incorporate the dependence along the z_y and z_z axes via the use of the impulses While this is a very straightforward example, similar results appear in more complicated contexts, particularly when one uses an analysis via transform methods For simplicity, we use an integral representations as illustrated in Eq. 3 4

One can introduce various formalisms to incorporate these impulse terms, providing one is careful about his description of the aperture and its response

We now develop the concepts of spatial filters in terms of their wave number response This type of approach has many of the same advantages as a frequency domain analysis for purely temporal processes, and the two descriptions complement one another

3.2 FREQUENCY AND WAVE NUMBER DESCRIPTIONS OF ARRAY RESPONSES

Representing signals and filter responses in the frequency domain leads to convenient and intuitive methods of analyses In describing the operation of spatial filters on signals, one can employ a similar analyses with comparable benefits In this section we introduce the necessary tools along lines parallel to those used for space time processes

We assume that at each point $\underline{z}$ on the aperture Ω the filtering operation is time invariant, such that

$$g(t,\tau\ \underline{z}) = g(t-\tau.\underline{z}) = g(\Delta t\ \underline{z}),\ \ \Delta t = t - \tau \tag{3 6}$$

The temporal frequency response at a point on the aperture is given by

$$G(\omega:\underline{z}) = \int_{-\infty}^{\infty} g(\Delta t\ \underline{z})e^{-j\omega\Delta t}\ d(\Delta t) \tag{3 7}$$

(For discrete arrays, $G(\omega\ \underline{z}_i)$ is the transfer function of the i^{th} sensor element)

In most of the analyses that we consider, the spatial operation is of fundamental importance to us, we generally assume that the temporal frequency ω is fixed in that we are concerned with a narrow frequency band If the signals involved are narrowband, this analysis suffices, if they are broadband, one needs to integrate the analysis over the frequency band of interest The most interesting and useful function is the frequency wave number description which characterizes the response of the spatial filter to a plane wave with wave number $\underline{k}$ and temporal frequency ω We define this function to be

$$g(\omega\ \underline{k}) = \int_{-\infty}^{\infty}\int_{\Omega} g(\tau\ \underline{z})e^{-j(\omega\tau-\underline{k}\cdot\underline{z})}\ d\tau d\underline{z} = \int_{\Omega} G(\omega\ \underline{z})e^{j\underline{k}\cdot\underline{z}}\ d\underline{z} \tag{3 8}$$

A beam pattern can be obtained from the wave number response by fixing the magnitude of $\underline{k}$, usually at ω/c, and evaluating as a function of the elevation angle θ and the azimuth ϕ

Since this function is of particular importance in our analyses, we introduce several examples The simplest wave number response is for a linear array with uniform weighting of $\frac{1}{L}$ in magnitude and phasing of $e^{-j\underline{k}_T \cdot \underline{a}_a \ell}$, or

$$g(\omega\ \underline{k}) = \int_{-L/2}^{L/2} \frac{e}{L}^{-j\underline{k}_T \cdot \underline{a}_a \ell}\ e^{j\underline{k} \cdot \underline{a}_a \ell}\, d\ell = \text{sinc}\left[(\underline{k}-\underline{k}_T) \cdot \underline{a}_a \frac{L}{2}\right], \qquad (3\ 9)$$

where k_T is the wave number associated with a particular target direction This wave number response is unity whenever $\underline{k}$ has the same projection in the $\underline{a}_a$ direction as k_T The width of the main lobe along this direction is 1/L between null points

If one introduces a triangular shading with the same phasing

$$g(\tau\ \ell) = \begin{cases} \frac{1}{L} \left\{1 - \frac{2|\ell|}{L}\right\}, & |\ell| < L/2 \\ 0, & |\ell| > L/2 \end{cases} \qquad (3\ 10)$$

$$g(\omega.k) = \int_{-L/2}^{L/2} \frac{1}{L} \left(1 - \frac{2|\ell|}{L}\right) e^{-j\underline{k}_T \cdot \underline{a}_a \ell}\ e^{j\underline{k} \cdot \underline{a}_a \ell} d\ell\,, \qquad (3\ 11)$$

we obtain the wave number response

$$g(\omega\ \underline{k}) = \text{sinc}^2 \left[(\underline{k}-\underline{k}_T) \cdot \underline{a}_a \frac{L}{4}\right] \qquad (3\ 12)$$

This beam pattern has lower sidelobes but twice the main lobe width of the uniformly weighted aperture

If one wants to take the inverse transform of these functions to produce the weighting pattern, one should be careful because of the aforementioned impulse terms For example, assume $\underline{k}_T = \underline{a}_y$ and $\underline{a}_a = \underline{a}_x$ We then have

$$g(\omega.\underline{k}) = \text{sinc}\left[(\underline{k}-\underline{k}_T)\, \underline{a}_x \frac{L}{2}\right] = \text{sinc}\left[k_x \frac{L}{2}\right] \qquad (3.13)$$

The inverse transform is

$$G(\tau\ \underline{z}) = \int_{-\infty}^{\infty} \frac{d\omega}{2\pi} \iiint_{-\infty}^{\infty} \frac{dk}{(2\pi)^3}\ G(\omega\ \underline{k}) e^{j(\omega\tau - \underline{k}\cdot\underline{z})}$$

$$= \begin{cases} \frac{1}{L}\ u_o(z_y)\, u_o(z_x)\, u_o(\tau), & |\ell| < L/2 \\ 0, & |\ell| > L/2 \end{cases} \qquad (3\ 14)$$

Other shadings would lead to a different frequency wave number response Extending the array into the other coordinates just leads to a parallel analysis For example, a disc of radius r_a situated in the x,y plane with a radial shading f(r) and a phasing $e^{-j\underline{k}_T\cdot\underline{z}}$ generates a beam pattern given by

$$g(\omega\ k) = \iint_{\Omega\quad z_x^2 + z_y^2 = R_a^2} f[(z_x^2 + z_y^2)]\, e^{-j\underline{k}_T\cdot\underline{z}}\, e^{j\underline{k}\cdot\underline{z}} dz$$

$$= \int_0^{R_a} dr \int_0^{2\pi} r_d\phi f(r) e^{j(\underline{k}-\underline{k}_T)\cdot r(\cos(\phi)\underline{a}_x + \sin(\phi)\underline{a}_y)} \qquad (3\ 15)$$

$$= \int_0^{R_a} dr \int_0^{2\pi} r d\phi f(r) e^{jr[(k_x - k_{T_x})\cos(\phi) + (k_y - k_{T_y})\sin(\phi)]}$$

$$= 2\pi \int_0^{R_a} f(r)\, J_o[r|\underline{k}-\underline{k}_T|_{xy}]\, r\, dr$$

where

$$|\underline{k}-\underline{k}|_{T_{xy}} = [(k_x - k_{T_x})^2 + (k_y - k_{T_y})^2]^{1/2} \qquad (3\ 16)$$

Consequently, $g(\omega\ k)$ is a zero order Hankel, or Fourier-Bessel transform of f(r) with respect to the term $|\underline{k}-\underline{k}|_{T_{xy}}$ In general, for circular geometries the Fourier-Bessel transforms assume the role of classical Fourier methods for linear arrays In the special case of a ring array

$$f(r) = \frac{1}{2\pi R_a} u_o(r-R_a) \tag{3 17a}$$

the pattern leads to

$$g_(\omega:\underline{k}) = J_o\left[\left|\underline{k}-\underline{k}_T\right|_{xy} R_a\right] \tag{3 17b}$$

If the array forms a disc, then

$$f(r) = \begin{cases} \dfrac{1}{\pi R_a^2}, & r < R_a \\ 0, & r > R_a \end{cases} \tag{3 18}$$

$$g(\omega\ \underline{k}) = \frac{J_1(\left|\underline{k}-\underline{k}_T\right|_{xy} R_a)}{\left|\underline{k}-\underline{k}_T\right|_{xy}\ R_a}$$

(This is the familiar Airy disc response which is quite useful in optical signal processing) Ring and disc arrays can be used in two contexts typically These correspond to

$$\left|\underline{k}-\underline{k}_T\right|_{xy} = (k_x^2 + k_y^2)^{1/2} \tag{3 19a}$$

when the target is normal to the array front, or

$$\left|\underline{k}-\underline{k}_T\right|_{xy} = \left[\left(k_x - \frac{2\pi}{\lambda}\cos\phi_T\right)^2 + \left(k_y - \frac{2\pi}{\lambda}\sin\phi_T\right)^2\right]^{1/2} \tag{3 19b}$$

when the target propagation direction is parallel to the array surface

We now investigate how we can describe the array response in terms of $g(\omega\ \underline{k})$. Consider an arbitrary signal field $y(t\ \underline{z})$. We can represent this function in terms of a frequency wave number transform

$$y(t\cdot\underline{z}) = \int_{-\infty}^{\infty}\int Y(\omega:\underline{k})e^{j(\omega t-\underline{k}\cdot\underline{z})}\ \frac{d\omega}{2\pi}\ \frac{dk}{(2\pi)^N} \tag{3 20a}$$

where

$$Y(\omega\ \underline{k}) = \int_{-\infty}^{\infty}\int y(t\ \underline{z})e^{-j(\omega t-\underline{k}\cdot\underline{z})}\ dt\ d\underline{z} \tag{3 20b}$$

The response of the spatial processor becomes

$$r_o(t) = \int_{\Omega} \int_{-\infty}^{\infty} \left(\iiint_{-\infty}^{\infty} Y(\omega\ \underline{k}) e^{j(\omega\tau - \underline{k}\cdot\underline{z})} \frac{d\omega}{2\pi} \frac{dk}{(2\pi)^N} \right) g(t-\tau\ \underline{z})\, d\tau dz$$

$$\simeq \int_{-\infty}^{\infty} \left(\int_{-\infty}^{\infty} \cdots \int g(\omega.\underline{k})\, Y(\omega\ \underline{k}) \frac{dk}{(2\pi)^N} \right) e^{j\omega t} \frac{d\omega}{2\pi} \tag{3 21}$$

or in the frequency domain

$$R_o(\omega) = \int_{-\infty}^{\infty} \cdots \int g(\omega\ \underline{k})\ Y(\omega\ \underline{k}) \frac{dk}{(2\pi)^N} \tag{3 22}$$

We see that the aperture collimates the signal according to its wave number with a weighting $g(\omega\ \underline{k})$ Equivalently, we may consider that when we have a pure plane wave with frequency ω_T and wave number $\underline{k}_T$; i e ,

$$Y(\omega\ \underline{k}) = u_o(\omega-\omega_T)\ u_o(\underline{k}-k_T)\ (2\pi)^{N+1} \tag{3.23}$$

we are observing it through a window; $g(\omega\ \underline{k})$ such that we have

$$R_o(\omega) = u_o(\omega-\omega_T)\ g(\omega_T\ \underline{k}_T)(2\pi) \tag{3.24}$$

If we want to select some particular region of wave number space, as we do when detecting plane wave signals, $g(\omega\ \underline{k})$ should be as narrow as possible However, just as in temporal filtering, this introduces an attendant sidelobe problem, and much of optimum array theory essentially involves determining the best trade-off of these two issues according to a statistical measure.

We have not introduced the most general type of spatial processing In much of optical theory lenses are considered as wave number filters that generate a reradiated field of the form

$$Y_{output}(\omega:\underline{k}) = g(\omega\ \underline{k})\ Y_{input}(\omega.\underline{k}) \tag{3 25}$$

which is completely parallel to temporal filtering. With the exception of some application to multiple beam outputs, we do not need to use this more general formulation for our applications On closer examination, it does, however, suggest some interesting possibilities for implementing our processors

3.3 FILTERING OF RANDOM PROCESSES

The next issue of concern is describing how random processes propagate through these apertures Here, the frequency wave number representation of the ambient noise field is particularly relevant We confine the discussion to those random fields which lend themselves to this description Using Eqs 2 12 and 3 21, we have

$$y(t\ \underline{z}) = \int\int\int\int dY(\omega\ \underline{k}) e^{j(\omega t - \underline{k}\cdot\underline{z})} \tag{3 26}$$

and

$$d\ K_o(\omega) = \int_{\underline{k}}\int\int\int g(\omega\ \underline{k})\ dY(\omega\ \underline{k}) \tag{3.27}$$

Our harmonic analysis led to the result that disjoint regions of the frequency wave number space had uncorrelated increments $dY(\omega\ \underline{k})$ The output spectrum is, therefore, given by[1]

$$S_{r_o}(\omega) = \int\int_{-\infty}^{\infty}\int \left| g(\omega:\underline{k}) \right|^2\ P(\omega:\underline{k})\ \frac{d\underline{k}}{(2\pi)^N} \tag{3 28}$$

This particular formula is extremely important in our subsequent analyses It is parallel to the input-output relation for temporal spectra

$$S_{output}(\omega) = |H(\omega)|^2\ S_{input}(\omega) \tag{3 29}$$

We integrate over all $\underline{k}$ space because our aperture acts as a weighted collimator of the ambient plane waves If we want to examine a particular region of frequency wave number space, e g , to make an estimate of $P_y(\omega\ \underline{k})$, the above formulae implies that we look at this region through an aperture weighting of $|g(\omega\ \underline{k})|^2$ Ideally, we would like to make this function as impulsive as possible The finite aperture limits our ability to do this We are again led to a trade off between sidelobe level—which causes the other regions of the space to interfere—and the beamwidth which compromises our resolution

---

[1] *The vector output, or multibeam, generalization of this is given by*

$$S_{r_o}(\omega) = \int \underline{g}(\omega\ \underline{k})\ P(\omega\ \underline{k})\ \underline{g}^{\dagger}(\omega\ \underline{k})\ \frac{d\underline{k}}{(2\pi)^N}$$

One can consider $|g(\omega \underline{k})|^2$ to be the power transform function for the aperture It would be convenient to define the aperture autocorrelation function as the inverse Fourier transform, or

$$R_G(\omega \underline{z}) = \int\cdot\int |g(\omega:\underline{k})|^2 e^{j\underline{k}\cdot\underline{z}} d\underline{k} \qquad (3\ 30)$$

When one accounts for difficulties with spatial impulse functions in inverse transforming $g(\omega \underline{k})$, it is not surprising that these are compounded when dealing with $|g(\omega \underline{k})|^2$ unless one is dealing with linear or planar geometries

3.4 SENSOR, OR RECEIVER, NOISE

Any real, or physical, receiving aperture cannot measure the incident signal field perfectly, as the observation operation is inherently noisy Sometimes this noise may be insignificant compared with other system noises, however, it does ultimately set limits on the performance of the receiving aperture and on any subsequent processing This sensor, or receiver noise typically may manifest itself in several different ways The electronics of the sensor elements and their associated preamplifiers, microseisms for seismic systems, or flow noise past the hydrophone for underwater acoustics are possible sources

In our discussion, this component of the noise process, denoted $w(t \underline{z})$ is modeled as being additive such that the ambient signal field plus the receiver, or sensor, noise is recorded at the sensor output The noise $w(t \underline{z})$ has temporal and spatial bandwidths that are much larger than any other processes of interest The essential aspect of the model is that the observation noise is uncorrelated among sensor locations For a continuous aperture, Ω, this implies that the space/time correlation function across the receiving aperture is given by

$$K_w(t,\tau \underline{z},\underline{\zeta}) = E[w(t \underline{z}) w^*(\tau \underline{\zeta})] = N_o \delta_o(t-\tau)\delta_\Omega(\underline{z}-\underline{\zeta}) \qquad (3\ 31)$$

The use of the operator $\delta_\Omega(\underline{z}-\underline{\zeta})$ deserves some comment The Ω subscript on the δ_Ω indicates that its sifting property as an identity operator is defined only across the extent of the aperture At first glance it would seem appropriate to model the white noise as being uncorrelated across all regions of the spatial domain Unfortunately, such a model can introduce fundamental difficulties, and divergent results for an otherwise realistic model are often obtained For example, this occurs in the filtering of two dimensional white noise with a linear array

For a discrete array, the covariance between elements is given by

$$K_w(t,\tau:\underline{z}_i,\underline{z}_j) = E[w(t.\underline{z}_i)\ w^*(\tau.\underline{z}_j)] = N_o \delta_o(t-\tau)\delta_{ij} \qquad (3\ 32)$$

where the i^{th} element is denoted by its location z_i (Often the spectral level N_o is denoted by an effective operating temperature T_{eff} such that one has

$$N_o = k_B T_{eff} \tag{3 33}$$

where k_B is the Boltzmann constant, $1\ 38 \times 10^{-23}$ watts/Hz-°K)

As pointed out above, this white noise component is present in virtually all physically motivated problems Sometimes it can be realistically neglected as other effects dominate the system performance From a theoretical aspect, however, one can demonstrate that many detection and estimation problems are singular, i e , they predict perfect performance if the white noise component is not present For example, in many of the array processing problems that we shall study, the gain produced by the array may become artificially large as the number or density, of the sensors is increased Essentially, results which are singular imply a perfect measurement of the ambient field and then a resulting cancellation proces or a very sensitive situation where very precise knowledge of the system parameters is required Therefore we consider a more detailed study of the role of the receiver, or sensor, noise in our analysis of array and apertures Unfortunately, the issues are not nearly as apparent as they are when one deals with temporal processes While duals of temporal process results can be used extensively, some aspects of spatial processing have no duals as they are inherently coupled to the array geometry

In this section, we present some issues regarding receiver noise We discuss the possibility of using frequency-wave number concepts and the problem of equating discrete and continuous array performance Finally, we discuss a conservation property which sets the minimum output level that the receiver noise can have

At first inspection one would agree that receiver, or sensor, noise can be modeled by using a flat frequency wave number spectrum analogous to that which is done for purely temporal processes. Intuitive as this approach may be, it is fundamentally incorrect, except in some very special, albeit important, situations The basic difficulty is that the noise is coupled to the geometry of the array To illustrate this, we examine two situations

Assume that one is using a line array which is operating in a two-dimensional environment The array is capable of discriminating, or filtering, wave numbers projected along the array. Consequently, if one uses a two-dimensional flat wave-number spectrum, i e , two-dimensional white noise, the noise power which propagate- through the filter along wave numbers with the same projection is infinite. Similarly, one can use a ring array as described by Eq 3.15 which has resolution in all directions Here the wave number response does not fall off rapidly enough as $|\underline{k}| \to \infty$, it behaves as $1/|\underline{k}|$ and the noise power propagating through the array to the filter output is likewise infinite, i e ,

$$N_o \iint d\underline{k}\ J_o{}^2\left(|\underline{k}-\underline{k}_T|_{xy} R_a\right) \to \infty \tag{3 34}$$

Thus one cannot routinely extend one's concept of temporal white noise in representing sensor noise This is unfortunate since it introduces some difficulty in applying frequency domain concepts to the design of aperture response weightings In some situations, particularly linear or rectangular arrays, one can consider the noise to have a spectrum which is flat with respect to the wave number as projected along the array surface Using this approach, one can proceed in the study of linear arrays more or less in parallel to a temporal domain analysis For more complicated arrays, e g , crossed arrays or ring arrays, one needs to be quite careful about the effects of this noise

In our study of arrays, we generate an aperture weighting that produces a beam pattern which is directed at a specified wave number, yet suppresses the background noise If this background noise is composed of just sensor, or receiver noise, the optimum aperture weighting to minimize the noise power in the beam output is to phase the array towards the target wave number and use a constant amplitude weighting. This is the spatial analog to matched filtering Verifying this result is quite direct If we wish to direct a beam at wave number $\underline{k}_T$, we require

$$g(\omega\ \underline{k}_T) = \int_{\Omega} G(\omega\ \underline{z}) e^{j\underline{k}_T \cdot \underline{z}}\, d\underline{z} = 1, \quad \forall\ \omega, \tag{3 35}$$

with the noise power response given by

$$S_{n_o}(\omega) = \int_{\Omega} d\underline{z}_1 \int_{\Omega} d\underline{z}_2\, G(\omega\ \underline{z}_1)\, G^*(\omega\ \underline{z}_2) N_o\, \delta_{\Omega}(\underline{z}_1 - \underline{z}_2)$$

$$= N_o \int_{\Omega} dz\, |G(\omega \cdot \underline{z}|^2 \tag{3.36}$$

Straightforward application of the calculus of variations minimizes Eq. 3.36 subject to the constraint of Eq 3 35 This yields

$$G(\omega\ \underline{z}) = \frac{1}{A_{\Omega}} e^{-j\underline{k}_T \cdot \underline{z}} \tag{3 37a}$$

where

$$A_{\Omega} = \int_{\Omega} d\underline{z}, \quad \text{the "area" of the array} \tag{3 37b}$$

and

$$S_{n_o}(\omega) = \frac{N_o(\omega)}{A_\Omega} \tag{3.37c}$$

If we alter the aperture response so that some other noise source can be combated we increase the effect of the white noise at the output of the beam It is when these effects reach equilibrium that we have one of the fundamental tradeoffs which one must make in determining the optimum aperture response

3.5 DISCRETE ARRAYS VERSUS CONTINUOUS APERTURES

We have chosen to pursue an analysis which models the aperture as a continuum In most physical systems, the sensor elements are discrete which leads to matrix-vector formulation We have gone to a continuous aperture formulation for the following reason

A discrete array is essentially a spatial sampler As such, the sampling aspects of the analysis, particularly the imbedding of the geometry in vector notation, often tend to cloud the more fundamental issues of the spatial processing Many arrays in current or proposed systems involve interelement spacings which are so small that one is well above the spatial Nyquist sampling frequency Here, a denser sampling of any coherent, or spatially bandlimited, part of the signal field is redundant In these situations, the continuous approach is more informative regarding the actual processing, and the performance of the physically discrete system is closely approximated by the continuous aperture. Remember here that, in contrast to temporal processes, one is always working with bandlimited signals that arise through propagation in the medium They are strictly bandlimited due to the fixed upper limit of $2\pi/\lambda$ for the maximum value of the wave number, or spatial frequency When one pursues a temporal analysis, the continuous representation is usually more natural, although the implementation may be done using a sampled system with digital filters This does not imply that we can neglect these questions It is simply our assertion that we feel many of the concepts of optimum processing are more transparent and can be approached more directly using a continuous analysis.

There are two issues which concern us in comparing discrete and continuous arrays First, if we have a beam pattern which we generate with a continuous model, we want to determine the interelement spacing necessary to produce approximately the same beam pattern by using a discrete array Second, we want to equate the effects of sensor, or receiver noise, for discrete and continuous arrays so that we can compare their performance in subsequent sections To solve both of these problems in general for an arbitrary array geometry is quite difficult Significant understanding can be obtained, however, by examining linear arrays

Let us assume that we have a linear array with an aperture weighting

$$G(\tau\ \underline{z}) \text{ for } \underline{z} = \ell\underline{a}_a, \quad |\ell| < L/2\,, \tag{3 38}$$

which produces a beam pattern $g(\omega\ \underline{k})$ If this array is sampled with a spacing ΔL and the resulting beam pattern analyzed, one obtains

$$g_s(\omega\ k) = \sum_{n=-\frac{L}{2\Delta L}}^{n=-\frac{L}{2\Delta L}} G_n(\omega) e^{-j\underline{k}\cdot\underline{a}_a \Delta L\, n} \tag{3 39a}$$

where

$$G_n(\omega) = G(\omega\ n\underline{a}_a \Delta L) \tag{3 39b}$$

$g(\omega\ \underline{k})$ and $g_s(\omega\ \underline{k})$ can be related via a direct parallel to the temporal sampling theorem This yields

$$g_s(\omega\ \underline{k}) = \frac{1}{\Delta L} \sum_{n=-\infty}^{\infty} g(\omega\ \underline{k} - \frac{2\pi n}{\Delta L}\ \underline{a}_a) \tag{3 40}$$

Consequently, we have the spectrum repeated at intervals of $(2\pi/\Delta L)\underline{a}_a$ Two effects are significant here If $g(\omega\ \underline{k})$ is significant for $\underline{k}$ outside the region $|\underline{k}\cdot\underline{a}_a| < \frac{\pi}{\Delta L}$ then distortion is created via aliasing a classical problem of temporal filters Thus, we should consider the factors that govern the spatial bandwidth of the arrays Conventionally, the minimum beamwidth measured in radians/m of an array of length L is on the order of $(2\pi/L)$, or $1/(L/\lambda)$ radians The implication for this minimum bandwidth is that at least two samples spaced at an interval of $\Delta L < L/2$ would suffice The difficulty here is that this response would be reproduced at intervals of $2\pi n/\Delta L$ or $2\pi/L$ which could introduce significant sidelobe issues With larger beamwidths more samples are required, but the sidelobes remain To alleviate this, one usually shifts these sidelobes out beyond the region of propagating signals, i e., beyond the wave number region in which other sources could enter In effect, one is controlling the beam pattern across the region $|k| < 2\pi/\lambda$, not simply across the main beam region Examination of the proof of the sampling theorem shows that this is more of the essence than just the simple prevention of aliasing The sampling required then is

$$\frac{2\pi}{\Delta L} > 2\left(\frac{2\pi}{\lambda}\right), \tag{3 41}$$

or

$$\Delta L < \lambda/2, \tag{3.42}$$

which is a classical result in array theory

Related to this issue is the theory of superdirective arrays, defined in the conventional sense to be considerably narrower than that indicated by classical theory with either discrete or continuous signals This is done at the expense of creating a large sidelobe structure outside the region where propagating signals can arise, i e , for $|k| > 2\pi/\lambda$. In this case significantly denser samplings will be required to approximate a continuous array and to prevent aliasing Alternatively, one could start from a discrete formulation directly, as is done in the Dolph-Techebychev [16] theory When more than one coordinate, or dimension, is introduced, a number of issues appear which do not have analogs as developed in the classical temporal theory.

The second issue that we wish to consider is the effect of sensor, or receiver, noise In particular, ideal sampling of such a noise field by a point element cannot be realized The question arises, then, of how we can compare the continuous white noise level of Eq 3.31, for an array, with finite extent and discrete white noise as expressed by Eq 3 32, for a finite aperture element array

The key to this analysis is to consider that a discrete element is small enough that any coherent part of the noise field is observed undistorted while the incoherent, or white part, is averaged over an effective element region Essentially, we have a spatial parallel of a finite time averager Let us consider an example relating the equivalence of a continuous linear array and a very densely spaced linear point array

We assume that the i^{th} element of the discrete linear array is located at location $z_n = (n\Delta L,0,0)$ and the interelement spacing is ΔL, as shown in Figure 3-4 By assumption, this is very small compared to any spatial correlations of the coherent parts of the observed field to the noise levels We consider that the output of the nth sensor is even by

$$r_n(t) = \frac{1}{\Delta L}\int_{z_{x_n}-\Delta L/2}^{z_{x_n}+\Delta L/2} y(t\,\tilde{\underline{z}})\, dz_x \tag{3 43a}$$

where

$$z_{x_n} = n\Delta L \tag{3 43b}$$

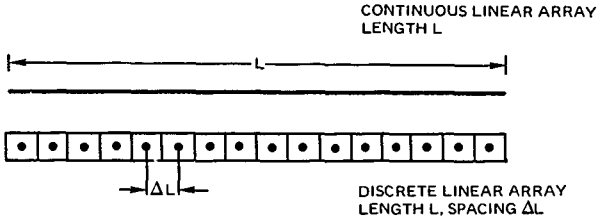

Figure 3-4. Continuous and discrete array

and

$$\underline{\tilde{z}} = (z_x, 0, 0) \tag{3 43c}$$

If we consider $y(t\ \underline{z})$ to be composed of a coherent part $s(t\ \underline{z})$ and spatial white noise $w(t\ \underline{z})$ with level N_{o_c}, we have

$$r_n(t) \simeq s(t, \underline{z}_n) + w_n(t) \text{ ,} \tag{3.44a}$$

where $s(t,\underline{z}_n)$ is the approximation for the coherent part of the signal and the sensor noise is

$$w_n(t) = \frac{1}{\Delta L} \int_{z_{x_n} - \Delta L/2}^{z_{x_n} + \Delta L/2} w(t;\underline{\tilde{z}})\, dz_x \tag{3 44b}$$

The cross covariance between elements of the $w_n(t)$ is given by

$$E[w_n(t) w_m(\tau)] = \frac{N_{o_c}}{\Delta L}\ \delta_{nm}\, \delta(t-\tau) = N_{o_d}\, \delta_{nm}\, \delta(t-\tau) \tag{3 45a}$$

where

$$N_{o_d} = \frac{N_{o_c}}{\Delta L} \text{ ,} \tag{3 45b}$$

i.e., the effective noise density for the discrete element is smoothed over the sensor extent, so that the larger the sensor face the smaller is the noise level. We finally point out that this noise is not isotropic as it is uncorrelated from sensor to sensor no matter how close they are

In discussing optimum array processing, we consider the comparison of discrete and continuous models in more detail This equivalence can be made more specific and the validity of some rather qualitative statements in replacing a discrete array by a continuous equivalent is somewhat surprising

3.6 KARHUNEN-LOEVE EXPANSIONS FOR SPACE/TIME PROCESSES

In the design of array processors which utilize the statistical properties of the ambient noise field, one often needs to visualize the signal, which is observed over a segment of time and across an aperture in terms of an orthonormal expansion This is particularly true for detection theory issues By using this expansion, one can design and specify the resulting performance of the array processor, which operates on a random field by applying classical detection and estimation methods to the generalized Fourier coefficients of the expansion of random variables. This procedure becomes particularly easy when the functions in the orthonormal expansion are chosen such that the Fourier coefficients are uncorrelated This is the essence of a Karhunen-Loeve representation [17] whose use is well established in random process theory. We discuss briefly some aspects of this representation The only issue which is somewhat peculiar to our problem is that we need to incorporate the spatial aspects, this generalization, however, is straightforward.

At this point, we are forced to make a somewhat artificial distinction between continuous apertues and discrete arrays With a continuous model we need an expansion of the processes over the product space created by the observation time and the receiving aperture, while with discrete array a more natural approach is to use an expansion for vector random processes where each component represents an individual sensor output. The issues in the development of a vector Karhunen-Loeve expansion are discussed by Van Trees [17] Since we pursue an analysis that treats the array as having a continuous aperture, we use the former expansion over the continuous space created by the observation time and the receiving aperture. Generally, it is quite easy to take the results and generate the parallel discrete array or vector formulation We emphasize that the expansion is done over a specific receiving aperture and observation time rather than over all space

We state, without proof, the following theorem (Ref 5, 6 and 17)[1]

Assume

1 that $y(t,z)$ is a space/time random process defined over a region which includes the interval $T_o \leq t \leq T_f$ and the spatial domain Ω; and

2 that $y(t,z)$ has finite means square value, i e , $y(t\ z) \quad \epsilon \quad \mathcal{L}_2$, or

$$E[|y(t,z)|^2] < \infty, \forall t, z \epsilon [T_o, T_f], \Omega$$

[1] *The essential issue in the proof is the validity of Mercers theorem where the expansion region is the space/time field rather than just a one-dimensional closed interval*

We can then represent $y(t\ \underline{z})$ in an orthogonal expansion with

$$\text{a)}\quad y(t\ \underline{z}) = \lim_{N\to\infty} \sum_{n=1}^{N} y_n \phi_n(t\ \underline{z}), \quad t \in [T_o, T_f], \quad \underline{z} \in \Omega, \tag{3.46a}$$

$$\text{where } y_n = \int_{T_o}^{T_f} dt \int_{\Omega} \phi_n^*(t\ \underline{z}) y(t, \underline{z}) d\underline{z} \qquad \text{(Generalized Fourier coefficient)} \tag{3.46b}$$

$$\text{b)}\quad \int_{T_o}^{T_f} dt \int_{\Omega} d\underline{z} \phi_n^*(t\ \underline{z}) \phi_m(t\ \underline{z})\, dt d\underline{z} = \delta_{nm} \qquad \text{(Orthogonal Basis functions)} \tag{3.47}$$

$$\text{c)}\quad E[y_n y_m^*] = \lambda_n \delta_{nm} \qquad \text{(Uncorrelated Coefficients)} \tag{3.48}$$

if, and only if, the Karhunen-Loeve integral equation

$$\lambda_n \phi_n(t\ \underline{z}) = \int_{T_o}^{T_f} d\tau \int_{\Omega} d\underline{\xi} K_y(t, \tau\ \underline{z}, \underline{\xi}) \phi_n(\tau, \underline{\xi}) \tag{3.49}$$

is satisfied. This is a very straightforward extension of the Karhunen-Loeve theorem for processes defined solely over a temporal domain or index set.

In general, the actual determination of the eigenvalues and eigenfunctions is difficult. For the case of processes defined over only a temporal domain, several basic methods have been developed for determining analytical solutions (see ref. 3 and references therein). Except for some special cases, one usually must resort to computational procedures to implement these methods. The extension of these methods to space time processes would require that (a) $P_y(\omega\ \underline{k})$ is a rational function of the components of k, (b) there is a partial differential equation, describing the generation of the process, i.e., a distributed system model, or (c) there is some very special property of the kernel which leads to an analytic result.

Even if one of these situations does exist, incorporating the geometry of the array poses some very fundamental problems The overall situation, then, is that direct implementation of this theorem is by no means a trivial task A similar situation exists for discrete arrays with many elements If there are a large number of significant eigenvalues in the expansion, this implementation rapidly becomes unmanageable with an array containing a large number of elements Consequently, in our approach and discussion, we use some relatively simple examples which can be approached analytically These highlight the major issues involved and lead to considerable insight into the behavior of more complex problems Fortunately, in many cases of practical interest, we can determine approximate solutions by "factoring" the temporal and spatial dependence. This leads to an analysis which is done in the temporal-frequency domain Consequently, for a narrow band situation we essentially have a complete analysis, whereas for a broadband situation we must consider the issue of integrating our result over the band of interest For temporal processes with stationary kernels and "long" observation intervals, we have a well-known result that the eigenfunctions become sines and cosines, or complex exponentials, and that the eigenvalues have the same distribution as the spectrum of the process This result allows us to "factor" the temporal issues out of the problem.[1] The essential step in this factoring is to assume that the solutions to the integral equation of Eq. 3.49 have the form

$$\phi_i(t:\underline{z}) = \frac{1}{\sqrt{T}} e^{jn\omega_o t} \Phi_m(n\omega_o \underline{z}), \tag{3 50}$$

where $\omega_o = 2\pi/T$ and we have replaced the single index i with the double index n,m (Since both are countable schemes, this is permissible) If we substitute this into Eq 3 49 we obtain

$$\lambda_m(n\omega_o \underline{z}) \frac{1}{\sqrt{T}} e^{jn\omega_o t} \Phi_m(n\omega_o \underline{z})$$

$$= \int_{-T/2}^{T/2} \int_{\Omega} K_y(t-\tau\ \underline{z},\underline{\zeta}) \frac{1}{\sqrt{T}} e^{jn\omega_o} \Phi_m(n\omega_o \underline{\zeta}) d\tau d\underline{\zeta}$$

$$= \int_{-T/2}^{T/2} \int_{\Omega} \left(\int_{-\infty}^{\infty} S_y(\omega:\underline{z},\underline{\zeta}) e^{j\omega(t-\tau)} \frac{d\omega}{2\pi} \right) \frac{1}{\sqrt{T}} e^{jn\omega_o \tau} \Phi_m(n\omega_o \underline{\zeta}) d\tau d\underline{\zeta}$$

[1] *The term "factor" is somewhat misleading since the temporal dependence is still imbedded in the spatial parameters e g , the magnitude of the wave number in our plane wave model*

$$= \int_{\Omega} \int_{-\infty}^{\infty} S_y(\omega\ \underline{z},\underline{\xi})\ \frac{e}{\sqrt{T}}^{\ j\omega t} \left[T\left(\frac{\sin\left([\omega - n\omega_o]\ \frac{T}{2}\right)}{(\omega - n\omega_o)\ \frac{T}{2}} \right) \right] \Phi_m(n\omega_o\ \underline{\xi}) d\underline{\xi}\ \frac{d\omega}{2\pi} \qquad (3\ 51)$$

for

$$-\frac{T}{2} \leqslant t \leqslant \frac{T}{2}\ ,\quad \underline{z} \in \Omega$$

The term in the braces of the last expression of Eq 3.51 approaches an impulse as T becomes large We, therefore, have

$$\lambda_m(n\omega_o\ \underline{z})\ \frac{1}{\sqrt{T}}\ e^{\ jn\omega_o t}\ \Phi_m(n\omega_o \cdot \underline{z}) \qquad (3\ 52)$$

$$= \frac{1}{\sqrt{T}} e^{\ jn\omega_o t} \int_{\Omega} S_y(n\omega_o : \underline{z},\underline{\xi})\ \Phi_m(n\omega_o\ \underline{\xi}) d\underline{\xi},\quad -\frac{T}{2} < t < \frac{T}{2},\ \underline{z} \in \Omega$$

The final result is that when dealing with temporally stationary random fields observed over a long time interval, we can obtain an approximate solution to the Karhunen-Loeve equation, as expressed by Eq. 3 49, by factoring the complex exponential temporal dependence and solving the equation

$$\lambda_m(n\omega_o)\ \Phi_m(n\omega_o : \underline{z}) = \int_{\Omega} S_y(n\omega_o\ \underline{z}\ \underline{\xi})\ \Phi_m(n\omega_o\ \underline{\xi}) d\underline{\xi},\quad \underline{z} \in \Omega \qquad (3\ 53a)$$

In this formulation we can solve for the spatial factor with the frequency of the complex exponential assuming the role of a parameter In the case of linear arrays, Eq 3 53 is identical in structure to the equation which needs to be solved in the Karhunen-Loeve expansion for temporal processes Consequently, the repertoire of methods that exist for solving this equation can be brought to bear here. For example, isotropic noise with its spectrum $S_{y_o}(\omega)$ sinc $[k_o\ |\Delta \underline{z}|]$ corresponds to the situation with bandlimited noise which has prolate spheroidial waveforms for its solution Unfortunately, the temporal situation, in which the spectrum is rational does not have direct application since it implies a wave number function of infinite extent Since all of our propagating signals have a bandlimited wave number spectrum at a given temporal frequency, such models can serve only as approximations Array geometries other than linear ones can be quite difficult to analyze and usually lead to copious use of the higher transcendential functions This is one of the reasons for

using relatively simple array geometries, for we can extract the fundamental concepts underlying the array processing operation without becoming enmeshed in a complicated analysis Even at this, however, we must develop some nontrivial spatial results for which there is no temporal parallel

In most of the problems of interest to us, the observed process r(t $\underline{z}$) is composed of two components one has a finite mean square value, the other is space/time white noise The first of these has a well defined Karhunen-Loeve expansion while the white noise does not However, across the aperture and observation interval we have for N_o times the identity operator

$$N_o\,\delta(t-\tau)\,\delta_\Omega(\underline{z}-\underline{\xi}) = N_o \sum_{n=1}^{\infty} \phi(t\ \underline{z})\,\phi(\tau\ \underline{\xi}), \quad -\frac{T}{2} < t, \tau < \frac{T}{2}, \quad \underline{z}, \underline{\xi} \in \Omega \tag{3 53b}$$

for any complete, orthonormal set Consequently, we can operationally use the result that white noise is "white" in any coordinate representation, in that it has eigenvalues of N_o when projected against any complete orthonormal representation Expanding a signal with an independent additive white noise component we have

$$K_r(t,\tau\ \underline{z},\underline{\xi}) = K_y(t,\tau\ \underline{z},\underline{\xi}) + N_o\,\delta(t-\tau)\,\delta_\Omega(\underline{z}-\underline{\xi})$$

$$= \sum_{m=1}^{\infty} (\lambda_m + N_o)\phi_m(t\ \underline{z})\,\phi_m(\tau\ \underline{\xi}), \quad -\frac{T}{2} < t, \quad \tau < \frac{T}{2}, \quad \underline{z}, \underline{\xi} \in \Omega \tag{3 53c}$$

so that the eigenfunctions remain as they are for y(t $\underline{z}$) alone, while the eigenvalues become

$$\lambda_m^r \Rightarrow \lambda_m^y + N_o$$

Henceforth, we suppress the r and y superscripts

Finally, we note in the case of what are termed "separable kernels" we can solve Eq 3 53a exactly The situation of interest to use here is that when the spectral covariance function is composed of directional noise components, i e.,

$$S_y(\omega\ \underline{z},\underline{\xi}) = \sum_{i=1}^{N}\sum_{j=1}^{N} S_{ij}(\omega) e^{j(\underline{k}_i\cdot\underline{z} - \underline{k}_j\cdot\underline{\xi})} \tag{3 54}$$

the solution is also composed of terms $e^{j\underline{k}_i\cdot\underline{z}}$ i e ,

$$\Phi_m(n\omega_o\,\underline{z}) = \sum_{k=1}^{N} C_{mk}(n\omega_o) e^{j\underline{k}_k\cdot\underline{z}}, \quad \underline{z}\in\Omega \tag{3 55}$$

Substituting this yields

$$\begin{aligned}
&\lambda_m(n\omega_o)\sum_{i=1}^{N} C_{mi}(n\omega_o)e^{j\underline{k}_i\cdot\underline{z}} \\
&= \int_{\Omega} d\underline{z}\sum_{i=1}^{N}\sum_{j=1}^{N} S_{ij}(n\omega_o)\, e^{j(\underline{k}_i\cdot\underline{z}-\underline{k}_j\cdot\underline{\zeta})}\sum_{\ell=1}^{N} C_{m\ell}(n\omega_o)e^{j\underline{k}_\ell\cdot\underline{\zeta}} \qquad (3\ 56a)\\
&= \sum_{i=1}^{N} e^{j\underline{k}_i\cdot\underline{z}}\sum_{j=1}^{N} S_{ij}(n\omega_o)\sum_{\ell=1}^{N} C_{m\ell}(n\omega_o) A_\Omega\, \mathrm{sinc}_\Omega[\underline{k}_j-\underline{k}_\ell],
\end{aligned}$$

where

$$\mathrm{sinc}_\Omega(\underline{k}) \triangleq \frac{\int_\Omega e^{j\underline{k}\cdot\underline{z}}\, d\underline{z}}{A_\Omega} \tag{3.56b}$$

The solution to this is given by

$$\left[\frac{\lambda_m(n\omega_o)}{A_\Omega}\underline{I} - [S(n\omega_o)]\ [\mathrm{sinc}_\Omega(\Delta\underline{k})]\right]\underline{C}_m(n\omega_o) = \underline{0} \tag{3 57a}$$

where

$$[S(n\omega_o)] \triangleq \begin{bmatrix} S_{11}(n\omega_o) & S_{12}(n\omega_o) & \cdots \\ S_{21}(n\omega_o) & S_{22}(n\omega_o) & \\ \vdots & & \ddots \end{bmatrix} \tag{3 57b}$$

$$[\mathrm{sinc}_{\Omega}(\Delta\underline{k})] \triangleq \begin{bmatrix} 1 & \mathrm{sinc}[\underline{k}_1-\underline{k}_2] & \cdots \\ \mathrm{sinc}_{\Omega}[\underline{k}_2-\underline{k}_1] & 1 & \\ \vdots & & \ddots \end{bmatrix} \tag{3 57c}$$

$$\underline{C}_m(n\omega_o) \triangleq \begin{bmatrix} C_{m1}(n\omega_o) \\ \vdots \\ \vdots \end{bmatrix} \tag{3 57d}$$

This is a homogeneous matrix equation which has N solutions at any given frequency $(n\omega_o)$ We will discuss the solution to it at various points where we encounter noise fields with directional components.

We now consider the application of the results to our fundamental problem of interest– the design and performance analysis of optimum processors

4. OPTIMUM ARRAY PROCESSING FOR PLANE WAVE SIGNALS

In the previous sections we have examined the representation of space/time random signals and the response of apertures during observation Until now, the two most important quantities were $P(\omega\ \underline{k})$, the distribution of a homogeneous space/time signal in temporal and spatial frequencies, and $g(\omega\ \underline{k})$, the response of an aperture to a plane wave signal with frequencies ω and $\underline{k}$ In the process of doing this we have now developed the concepts necessary for describing array methods

In the design of an array processor, the structure of the desired signal and the ambient and aperture noises all have a fundamental influence. The classical problem in array processing consists of finding the optimum beam pattern within the constraints of the array geometry for observing and/or detecting a plane wave signal with a wave number $\underline{k}_T$ Usually this is done in a somewhat intuitive manner Beamwidth and sidelobe level must be traded off and nulls are positioned, all under the influence of the constraints imposed by the array geometry and the noise field encountered. The methods of optimum array design essentially address the problem of

giving a rationale to this procedure in that the "optimum" processing method is specified for a given array and noise field. Naturally, we must make our definition of optimality precise, and the formulation of and solution for the "optimum" array processor is the topic of this chapter.

Like many problems in which linear processing, quadratic performance measure, and/or Gaussian statistics are introduced, this one is also quite robust in that the same solution can be arrived at via several different methods. We have chosen a formulation which emphasizes the linearity and quadratic aspects of the modeling. Various approaches have been unified for discrete arrays [18]

We focus upon processing for signals which are plane waves At the end of this section we comment on array processing for spatially spread signals, i e , the signal is composed of a possibly uncountable number of plane waves Despite their importance as a more realistic model for many problems and the numerous parallels to temporal random signal detection, the literature does not have many contributions on spatially spread signal detection. We shall subsequently discuss some aspects of these problems.

One of the important mathematical entities introduced here is the inverse kernel This is essentially the continuous analog to an inverse matrix and frequently appears in detection and estimation problems. Many of the operations appropriate for matrices have parallels in the continuous case. This function is important in our analyses in later chapters Therefore we emphasize its importance early. Van Trees offers a more detailed discussion of this function [3].

In this section we have a very concise formulation and solution for finding the optimum beam pattern, or array processor. This solution can be invoked to explain how large numbers of array processors operate, from superdirective arrays, to endfire gain, to null placement procedures, and to sidelobe level effects. It provides a unified approach to the design of beam patterns and array processing. One of the goals of our later chapters is to develop enough important examples so that the mathematics become more transparent and the underlying theory can be used in an intuitive and practical manner

4.1 OPTIMUM WAVE VECTOR RESPONSE FUNCTIONS AND MINIMUM VARIANCE ARRAY PROCESSES

Our mathematical formulation for determining the optimum beam pattern reflects our intuitive concept of how a good array processor should perform. We want to observe a plane wave signal, which we call the target, with temporal frequency ω and spatial wave number $\underline{k}_T$. To do this we want to direct a beam in this direction and obtain a response which has a minimum of interference caused by ambient and sensor noise We may want to determine the signal wave shape itself or we may simply want to measure its statistics

Mathematically, the operation of directing a beam is introduced by requiring that

$$g_o(\omega\ \underline{k}_T|\underline{k}_T) = \int_\Omega G_o(\omega\ z|\underline{k}_t)^{jk_T \cdot z}\, d\underline{z} = 1, \quad \forall\omega \qquad (4.1)^1$$

while minimizing the effects of the noise leads to the requirement that the output noise power

$$\sigma_o^2(\omega|\underline{k}_T) = S_o(\omega) = \int_\Omega \int_\Omega G_o(\omega.\underline{z}|\underline{k}_T) S_n(\omega\ \underline{z},\underline{\zeta}) G_o^*(\omega\cdot\underline{\zeta}|\underline{k}_T)\, d\underline{z}d\underline{\zeta} \qquad (4\ 2)$$

be a minimum Note that $\sigma_o^2(\omega|\underline{k}_T)$, the minimum noise, is a function of k_T and that $S_n(\omega.\underline{z},\underline{\zeta})$ is the temporal frequency spatial correlation function observed across the array aperture. The constraint of unity response is a convenience. We could require only a finite response; but the result is deterministic, so we could arbitrarily scale it back to unity.

If the wave number versus frequency for a plane wave signal is given by $\underline{k}_T(\omega)$, then requiring

$$g_o[\omega\ \underline{k}_T(\omega)|\underline{k}_T(\omega)] = 1, \quad \forall\omega \qquad (4\ 3)$$

will lead to an array processor which observes this signal undistorted This approach has been used to formulate the optimum distortionless filter for discrete arrays

We are presuming that $g(\omega.\underline{k}|\underline{k}_T)$ can be designed independently for all ω, i.e , the solution at ω_1 is not influenced by the solution at ω_2 The total broadband output noise for observing a signal is given by

$$\sigma_o^2 = \int_{-\infty}^{\infty} \sigma_o^2\left(\omega|\underline{k}_T(\omega)\right) \frac{d\omega}{2\pi} \qquad (4.4)$$

A pictorial representation of our formulation is indicated in Figure 4-1

The solution for the optimum beam pattern can be found by straightforward application of the calculus of variations where we impose the constraint using a Lagrange multiplier $\beta(\omega)$. For optimality we require that for all choices of $\delta G_o(\omega.\underline{z}|\underline{k}_T)$ that

---

[1] *We use the notation*

$$g(\omega\ k|k_T)$$

to represent a beam pattern in $\underline{k}$ for a beam "directed" at wave number $\underline{k}_T$, i.e ,

$$g(\omega\ k_T|k_T) = 1$$

$$0 = \frac{\partial}{\partial \epsilon} \left\{ \int_{\Omega} \int_{\Omega} \left[G_o(\omega, \underline{z} | \underline{k}_T) + \epsilon \delta G_o(\omega\ \underline{z} | \underline{k}_T) \right] \right.$$

$$\cdot S_n(\omega\ \underline{z}, \underline{\zeta}) \left[G_o^*(\omega\ \underline{\zeta} | \underline{k}_T) + \epsilon \delta G_o^*(\omega\ \underline{\zeta} | \underline{k}_T) \right] d\underline{z} d\underline{\zeta}$$

$$+ \beta(\omega) \int_{\Omega} \left[(G_o(\omega\ \underline{z} | \underline{k}_T) + \epsilon \delta G_o(\omega\ \underline{z} | k_T) \right] e^{j\underline{k}_t \cdot \underline{z}} \tag{4.5a}$$

$$\left. + (G_o^*(\omega : z | \underline{k}_T) + \epsilon \delta G_o^*(\omega\ \underline{z} | \underline{k}_T)) e^{-j\underline{k}_T \cdot \underline{z}} \right) d\underline{z} \Bigg\} \Bigg|_{\epsilon = 0}$$

or

$$0 = 2\mathrm{Re} \int_{\Omega} \delta G_o(\omega \cdot \underline{z} | \underline{k}_T \int_{\Omega} \left[S_n(\omega\ \underline{z}, \underline{\zeta}) G_o^*(\omega \cdot \underline{\zeta} | \underline{k}_T) + \beta(\omega) e^{j\underline{k}_T \cdot \underline{z}} d\underline{z} d\underline{\zeta} \right] \tag{4 5b}$$

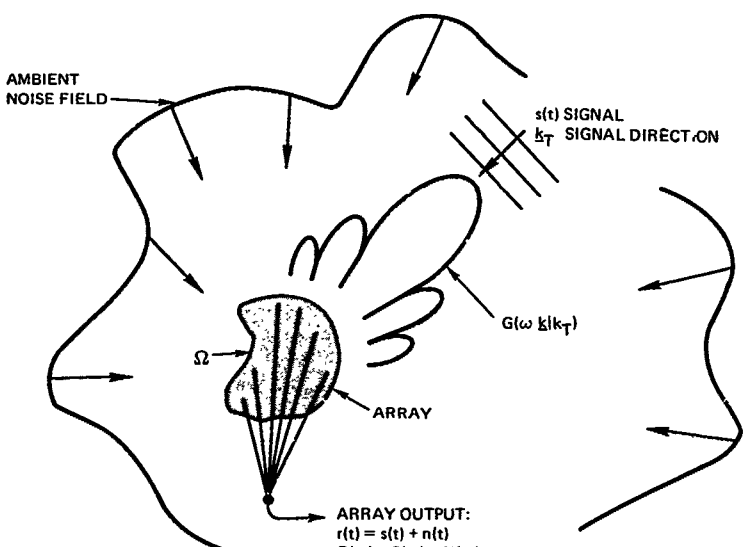

Figure 4-1. Pictorial representation of the design of the optimum beam pattern.

This implies that

$$\int_{\Omega} S_n(\omega:\underline{z},\underline{\zeta})\, G_o^*(\omega\, \underline{\zeta}|\underline{k}_T)d\underline{\zeta} = -\beta(\omega)e^{j\underline{k}_T^*\underline{z}}, \quad \underline{z} \in \Omega, \forall\omega \tag{4.6}$$

We first need to eliminate the Lagrangian multiplier $\beta(\omega)$. This can be done by applying the constraint of Eq 4.1, and we have

$$-\beta(\omega) = \int_{\Omega}\int_{\Omega} G_o(\omega\, \underline{z}|\underline{k}_T)S_n(\omega\, \underline{z},\underline{\zeta})G_o^*(\omega:\underline{\zeta}|\underline{k}_T)d\underline{z}d\underline{\zeta} \tag{4.7}$$

which implies that $\beta(\omega)$ is a real quantity

Substituting this into Eq. 4.6 yields the implicit solution for $G(\omega:\underline{z}|\underline{k}_T)$.

$$\frac{\int_{\Omega} S_n(\omega.\underline{z},\underline{\zeta})\, G_o^*(\omega:\underline{\zeta}|\underline{k}_T)d\underline{\zeta}}{\int_{\Omega}\int_{\Omega} G_o(\omega:\underline{z}'|\underline{k}_T)\, S_n(\omega:\underline{z}',\underline{\zeta}')\, G_o^*(\omega:\underline{\zeta}'|\underline{k}_T)d\underline{z}'\, d\underline{\zeta}'} = e^{j\underline{k}_T^*\underline{z}}, \quad \underline{z} \in \Omega, \forall\omega \tag{4.8}$$

Eq. 4.6 specifies the optimum beam pattern as the solution to an integral equation which appears often in solving temporal detection and estimation problems. Some reflection should indicate that we have a problem almost parallel to that of detecting a known signal in colored noise. We have a known signal structure, $e^{j\underline{k}_T^*\underline{z}}$, plus a background of spatial colored noise, $n(t:\underline{z})$. With the exception of a normalization constant, the integral equation for the optimum array weighting $G(\omega:\underline{z}|\underline{k}_T)$ and the optimum correlation detector are the same.

The solution for $G(\omega.\underline{z}|\underline{k}_T)$ can be found in a number of ways. First, we observe that we really want to solve

$$\int_{\Omega} S_n(\omega:\underline{z},\underline{\zeta})\, G_o^*(\omega:\underline{\zeta})d\underline{\zeta} = e^{j\underline{k}_T^*\underline{z}}, \quad \underline{z} \in \Omega, \forall\omega \tag{4.9}$$

and then scale the solution in amplitude to satisfy the constraint

We want to introduce the spatial generalization of the inverse kernel. The defining property of this function is specified by

$$\int_{\Omega} S_n(\omega;\underline{z},\underline{\zeta}')\ Q_n(\omega\ \underline{\zeta}',\underline{\zeta})d\underline{\zeta}' = \delta_{\Omega}(\underline{z}-\underline{\zeta}), \qquad \underline{z},\underline{\zeta} \in \Omega, \tag{4 10}$$

[1]

i e., the spatial functional analog of an inverse matrix. We also have

$$\int_{\Omega} Q_n(\omega;\underline{z},\underline{z}')\ S_n(\omega.\underline{z}',\underline{\zeta})\ d\underline{z}' = \delta_{\Omega}(\underline{z}-\underline{\zeta}), \qquad \underline{z}.\ \underline{\zeta}\epsilon\Omega \tag{4 11}$$

which corresponds to the result that right and left, or post and preinverses, of a matrix are identical. One of the important properties of the inverse kernel which we use relates to its expansion in terms of its spatial eigenvalues and eigenfunctions. Following the temporal theory [3] for example, we can expand both $S_n(\omega\ \underline{z},\underline{\zeta})$ and $Q_n(\omega;\underline{z},\underline{\zeta})$ in terms of the eigenvalues and eigenfunctions found in Section 3 6 in the discussion of Karhunen-Loeve expansions Mercer's theorem asserts that we have the expansions

$$S_n(\omega.\underline{z},\underline{\zeta}) = \sum_{m=1}^{\infty} \lambda_m(\omega)\Phi_m(\omega.\underline{z})\,\Phi_m^*(\omega\ \underline{\zeta}), \qquad \underline{z},\underline{\zeta} \in \Omega \tag{4.12a}$$

$$Q_n(\omega;\underline{z},\underline{\zeta}) = \sum_{m=1}^{\infty} \lambda_m^{-1}\ (\omega)\Phi_m(\omega;\underline{z})\,\Phi_m\ (\omega;\underline{\zeta}), \qquad \underline{z},\zeta \in \Omega \tag{4.12b}$$

where $\lambda_m(\omega)$ and $\Phi_m(\omega;\underline{z})$ are the solutions to Eq. 3 53a. In most cases n(t $\underline{z}$) is composed of a correlated, or finite mean square, component and a white one. For this we have

$$\lambda_m(\omega) = N_o + \lambda_m^{y}\ (\omega) \tag{4.12c}$$

where $\lambda_m^{y}\ (\omega)$ is the eigenvalue of the correlated component We then have

$$Q_n(\omega;\underline{z},\underline{\zeta}) = \sum_{m=1}^{\infty} (N_o + \lambda_m^{y}\ (\omega))^{-1}\ \Phi_m(\omega;\underline{z})\ \Phi_m(\omega.\underline{\zeta})$$

$$= \frac{1}{N_o}[\delta(t-\tau)\ \delta_{\Omega}(\underline{z}-\underline{\zeta}) - H(\omega;\underline{z},\underline{\zeta})], \qquad \underline{z},\underline{\zeta} \in \Omega \tag{4.12d}$$

---

[1] *The function $\delta_{\Omega}(\underline{z}-\underline{\zeta})$ is an impulse, or generalized, function which is defined only across the array or aperture Ω Consequently, no sifting property outside of this domain is implied. The same function was used in discussing sensor noise.*

where

$$H(\omega:\underline{z},\underline{\xi}) = \sum_{m=1}^{\infty} \frac{\lambda_m^y(\omega)}{N_o + \lambda_m^y(\omega)} \Phi(\omega:\underline{z})\Phi(\omega:\underline{\xi}), \quad \underline{z},\underline{\xi} \in \Omega \tag{4.12e}$$

All of these results with inverse kernels are complete duals to the temporal situation therefore we refer to ref. [3] by Van Trees for a more complete discussion

Returning to the explicit solution for $G(\omega:\underline{z}|\underline{k}_T)$ we conjugate Eq 4.9, employ the symmetry properties of $S_n(\omega:\underline{z},\underline{\xi})$ and then post multiply by $Q_n(\omega:\underline{z}',\underline{z})$ and integrate with respect to $\underline{\xi}$. Using Eq. 4.11 this yields

$$G_o(\omega:\underline{\xi}|k_T) = -\beta(\omega) \int_{\Omega} e^{-j\underline{k}_T\cdot\underline{z}} Q_n(\omega:\underline{z},\underline{\xi})\, d\underline{z}, \quad \underline{\xi} \in \Omega \tag{4.13}$$

Apply the constraint of Eq. 4.1 and we have

$$-\beta(\omega) = \left(\int_{\Omega}\int_{\Omega} e^{-j\underline{k}_T\cdot\underline{z}'} Q_n(\omega:\underline{z}',\underline{\xi}')\, e^{j\underline{k}_T\cdot\underline{\xi}'}\, d\underline{z}'\, d\underline{\xi}' \right)^{-1}, \tag{4.14}$$

and the final solution for $G_o(\omega:\underline{\xi}|\underline{k}_T)$ is

$$G_o(\omega:\underline{\xi}|\underline{k}_T) = \frac{\int_{\Omega} e^{-j\underline{k}_T\cdot\underline{z}} Q_n(\omega:\underline{z},\underline{\xi})\, d\underline{z}}{\int_{\Omega}\int_{\Omega} e^{-j\underline{k}_T\cdot\underline{z}'} Q_n(\omega:\underline{z}',\underline{\xi}')\, e^{j\underline{k}_T\cdot\underline{\xi}'}\, d\underline{z}'\, d\underline{\xi}'}, \quad q \in \Omega \tag{4.15}$$

The optimum beam pattern is given by

$$g_o(\omega:\underline{k}|\underline{k}_T) = \frac{\int_{\Omega}\int_{\Omega} e^{-j\underline{k}_T\cdot\underline{z}} Q_n(\omega:\underline{z},\underline{\xi})\, e^{j\underline{k}\cdot\underline{\xi}}\, d\underline{z}\, d\underline{\xi}}{\int_{\Omega}\int_{\Omega} e^{-j\underline{k}_T\cdot\underline{z}'} Q_n(\omega:\underline{z}',\underline{\xi}')\, e^{j\underline{k}_T\cdot\underline{\xi}'}\, d\underline{z}'\, d\underline{\xi}'} \tag{4.16}$$

Note that $g_o(\omega:\underline{k}_T|\underline{k}_T)$ is unity This last equation is particularly important in our subsequent analyses where we use it in contrast to some of the more conventional beam patterns discussed earlier Equations 4 15 and 4.16 constitute the solution for the optimum array weighting and the optimum beam pattern. The fundamental issue in determining a solution is finding $Q_n(\omega\ \underline{z},\underline{\xi})$. In general this is a difficult problem Fortunately, for the examples of interest we can determine the inverse kernel.

The only remaining issue is to find an expression for the output noise power $\sigma_o^2(\omega|\underline{k}_T)$ of the optimum beam pattern We simply substitute our solution into Eq 4 2 Using the properties of the inverse kernel we obtain

$$\sigma_o^2\ (\omega\,|\underline{k}_T) = \left[\int_{\Omega}\int_{\Omega} e^{-j\underline{k}_T\cdot\underline{z}} Q_n(\omega\ \underline{z},\underline{\xi}) e^{j\underline{k}\cdot\underline{\xi}}\, d\underline{z}\, d\underline{\xi}\right]^{-1} \qquad (4\ 17)$$

We should contrast this to the output of an arbitrary beam pattern

$$\sigma^2(\omega|\ \underline{k}_T) = \left[\int_{\Omega}\int_{\Omega} G(\omega:\underline{z}\,|\underline{k}_T)\ S_n(\omega:\underline{z},\underline{\xi})\ G^*(\omega:\underline{\xi}\,|\underline{k}_T)\ d\underline{z}\ d\underline{\xi}\right] \qquad (4\ 18)$$

The term $\sigma_o^2\ (\underline{\omega}\,|\underline{k}_T)$ is the minimum value that $\sigma^2(\omega\,|\underline{k}_T)$ can obtain over all choices of $G(\omega:\underline{z}\,|\underline{k}_T)$.

4.2 HIGH RESOLUTION ESTIMATES OF THE FREQUENCY WAVE NUMBER FUNCTION P(ω:k)

One of the most difficult aspects in applying techniques which utilize the process statistics is determining the actual statistics themselves There are a number of ways to do this, and a large number involve measuring sample covariances of the observed signals In array processing work, this is typically done as a function of frequency. At each of the array locations, a data segment is first transformed and then used as in the calculation of the estimate of the covariance, i e., we have

$$\hat{S}(\omega:\underline{z},\underline{\xi}) = \frac{1}{N}\sum_{n=1}^{N} R_n(\omega:\underline{z})\ R_n^*(\omega\ \underline{\xi}) \qquad (4\ 19a)$$

where

$$R_n(\omega;\underline{z}) = \int_{nT\Rightarrow\Delta T}^{(n+1)T\Rightarrow\Delta T} r(t\ z)\, e^{-j\omega t}\, dt \qquad (4\ 19b)$$

The important point is that one obtains $\hat{S}(\omega\ \underline{z},\underline{\zeta})$ only across the aperture, or array The problem now is to convert this into an estimate $\hat{P}(\omega\ \underline{k})$ Since the aperture is always finite we can not simply transform the estimate $\hat{S}(\omega\ \underline{z},\underline{\zeta})$ and obtain $\hat{P}(\omega\ \underline{k})$, no matter how accurate our covariance estimate is. This has led in the temporal theory to window trade offs and the indirect, or Blackman-Tukey, spectral estimation procedures [19] Several authors have brought optimum array processing to bear, and it has even had its impact on the estimation of purely temporal processes [18, 20-22]

We observe that if we were to measure the noise power originating from direction $\underline{k}_T$ we would direct a beam in that direction and try to suppress all other contributions of the noise field as best that we could This is just what the optimum beam pattern does Now if we measure the output noise power, a truly ideal beam pattern would yield only the noise power stemming from direction $\underline{k}_T$, since it responds to signals only with that wave number. The high resolution method simply asserts that $\sigma_0^2(\omega|\underline{k}_T)$ is the best we can do in this respect, and it represents the power in the signal field with wave vector $\underline{k}_t$ with the remainder of it suppressed in an optimal manner, i e., it is an estimate of $P_n(\omega\ \underline{k}_T)$ Consequently, to find this high resolution estimate, $\hat{P}_n(\omega\cdot\underline{k}_T)$ we find $\hat{Q}_n(\omega\cdot\underline{z},\underline{\zeta})$ from the sample covariance and compute $\hat{P}(\omega\ \underline{k}_T)$ as

$$\hat{P}_n(\omega\ \underline{k}_T) = \left[\int_{\Omega}\int_{\Omega} -j\underline{k}_T\cdot\underline{z}\ \hat{Q}_n(\omega\cdot\underline{z},\underline{\zeta}) e^{\ j\underline{k}_T\cdot\underline{\zeta}}\ d\underline{z}\ d\underline{\zeta}\right]^{-1} \qquad (4\ 20)$$

In essence, this procedure makes all the optimum trade offs in selecting the best estimate for finding $\hat{P}(\omega\ \underline{k}_T)$ Consequently, in relating our subsequent work to using $\hat{P}(\omega;\underline{k})$ for high resolution estimates for $P(\omega\ \underline{k})$ we should examine how close $\sigma_0^2\ (\omega\ \underline{k}_T)$ corresponds to $P(\omega.k_T)$.

One of the less satisfying aspects of using this high resolution measurement method is the difficulty in analyzing its estimation accuracy This contrasts to the classical procedures where the effects of aperture extent and shadings employed can be analyzed in terms of confidence intervals. The nonlinearity introduced by the inversion operation for $\hat{Q}_n(\omega\ \underline{z},\underline{\zeta})$ leads to complicated analyses.

4.3 FREQUENCY WAVE NUMBER ANALYSIS FOR OPTIMUM WAVE NUMBER RESPONSES

Before discussing specific geometries, we reexamine briefly our analysis of optimum beam patterns in terms of a frequency-wave number representation for the signals From Eq 4.2 we want to minimize the output noise power subject to the unity response in the direction of

the target If we have a noise field consisting of a propagating component plus sensor noise, we have

$$S_n(\omega:\underline{z},\underline{\zeta}) = \int_{-\infty}^{\infty}\cdots\int_{-\infty}^{\infty} P_n(\omega:\underline{k})e^{j\underline{k}\cdot(\underline{z}-\underline{\zeta})}\frac{d\underline{k}}{(2\pi)^N} + N_o\delta_\Omega(\underline{z}-\underline{\zeta}) \qquad (4\ 21)$$

We substitute this into Eq. 4 2 and obtain

$$\sigma_o^2(\omega|k_T) = \int\cdots\int_{-\infty}^{\infty} |g_o(\omega\cdot\underline{k}|\underline{k}_T)|^2 P_n(\omega.\underline{k})\frac{d\underline{k}}{(2\pi)^N}$$

$$+ N_o\int_\Omega |G_o(\omega:\underline{z}|\underline{k}_T)|^2\ d\underline{z} \qquad (4\ 22a)$$

subject to the constraint

$$g_o(\omega:\underline{k}_T|\underline{k}_T) = 1 \qquad (4.22b)$$

When we interpret the design of optimum beam patterns in the frequency wave number domain, we can observe that we want to minimize the overlap of the frequency wave number function and the beam patterns and the integral of the magnitude squared of the weighting function across the aperture subject to the target constraint. Generally, minimizing the two terms in Eq. 4.22a involves a trade off. Because of the constraints of the array geometry, minimizing the first term introduces high sidelobe levels. Since we have

$$\int_\Omega |G(\omega\ \underline{z}|\underline{k}_T)|^2\ dz \geq \frac{|g(\omega.\underline{k}\,|\underline{k}_T)|^2}{A_\Omega}, \qquad (4\ 23)^1$$

sidelobes which are in excess of unity increase the second term using this inequality. Generally, any increase in the sidelobe level increases the contribution of the aperture, or sensor noise, to the output noise level. As a result these two effects must be traded off until the optimum compromise for minimizing the total output noise level is obtained.

---

[1] *It would be very useful if we could use a general form of Parseval's equality, i.e ,*

$$\int_\Omega |G(\omega\ \underline{z})|^2 d\underline{z} = \iiint |g(\omega.\underline{k})|^2\frac{d\underline{k}}{(2\pi)^N}$$

Unfortunately, the integral on the right fails to converge in many cases

4.4 BEAM PATTERNS FOR SPATIALLY SPREAD SIGNALS

In many physical situations, the signals which are the object of the optimum array processing, or beamformer, are not true plane waves in that their frequency wave number function is not impulsive This may occur in a multipath environment in which local spreading is due to scattering, and gross spreading is due to separate travel paths Figure 4-2 illustrates a possible propagation situation leading to a spatially spread signal situation The most evident effect observable at the receiver is that the magnitude of the signal covari .e decays as a function of the separation of array location

We model the signal as a general space-time process s(t $\underline{z}$) with a spectral covariance $S_s(\omega:\underline{z},\underline{\zeta})$. In the special case of a plane wave structure, we have

$$S_s(\omega\ \underline{z},\underline{\zeta}) = S_o(\omega)e^{j\underline{k}_T^*(\underline{z}-\underline{\zeta})} \tag{4 24}$$

with an impulsive frequency wave number function In many situations concerning spatially spread signals, the frequency wave number function occupies a narrowband about $\underline{k}_T$. The principal difference in analyzing spatially spread signals involves their representation across the receiving aperture In the plane wave situation, the statistical representation in terms of a Karhunen-Loeve expansion is one dimensional, i.e , only one eigenfunction is required in the representation. In the spatially spread situation, more than one eigenfunction is required For example, with gross multipath spreading we need at least one eigenfunction per path, while with local scattering there is an upper bound, which is determined by the area of the array and extent of the spreading, on the number of eigenfunctions required to represent effectively the signal across the aperture In most cases of interest the number required is small so that we have

$$s(t\cdot\underline{z}) = \sum_{n=-\infty}^{\infty} \frac{1}{\sqrt{T}} e^{jn\omega_o t} \sum_{m=1}^{M} s_m(n\omega_o)\Phi_m(n\omega_o\ \underline{z}), \qquad \begin{matrix} |t| < T/2 \\ z \in \Omega \\ \omega_o = \dfrac{2\pi}{T} \end{matrix} \tag{4 25a}$$

and

$$S_s(\omega\ \underline{z},\underline{\zeta}) = \sum_{m=1}^{M} \lambda_m(n\omega_o)\Phi_m(n\omega_o\ \underline{z})\ \Phi_m^*(n\omega_o\ \underline{\zeta}) \tag{4 25b}$$

with

$$E[s_m(n\omega_o)s^*_k(\ell\omega_o)] = \lambda_m(n\omega_o)\ \delta_{mk}\ \delta_{n\ell} \tag{4 25c}$$

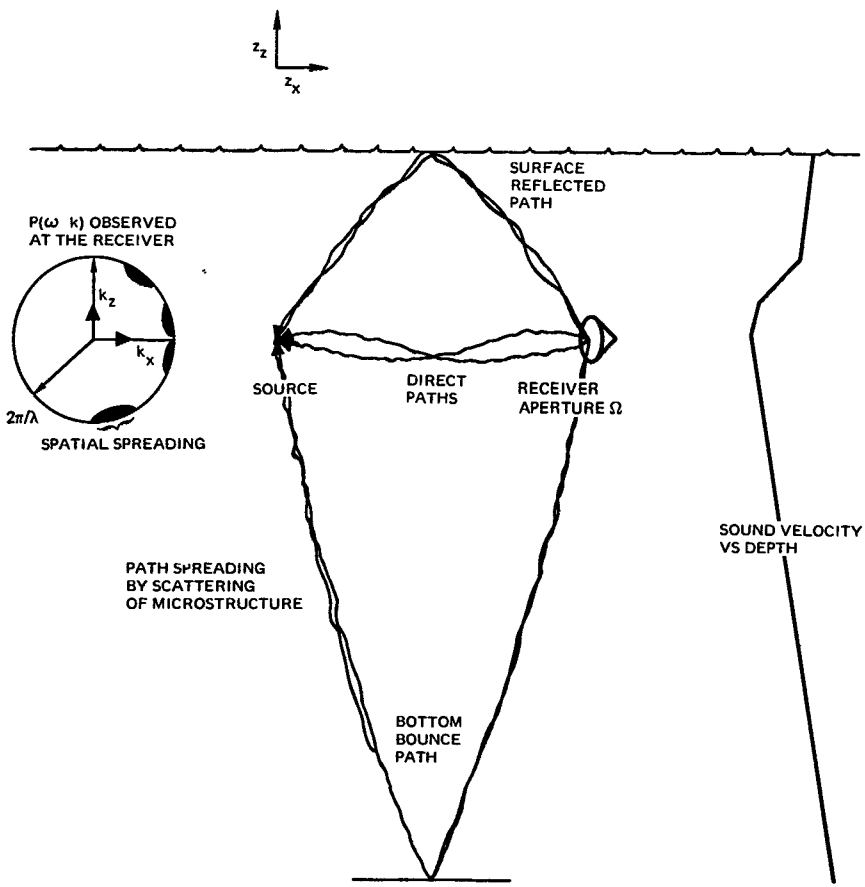

Figure 4-2. An example of spatial spreading due to global path structure and local scattering of thermal structure.

The structuring of the design of the optimum beam pattern is somewhat more subtle than that for a single plane wave in that we no longer want simply to direct a beam at a specific wave number. In our formulation, we generalize this concept by designing a set of beams, one for each of the M eigenfunctions in the spatial representation of the signal across the aperture For each of these beams we require that the response due to the ambient noise be a minimum under the constraint that there is an undistorted response to the eigenfunctions for all possible signals. Just as we noted earlier, we could alternatively formulate the optimization in terms of a detection theory problem with the resulting analysis leading to the same spatial structure that follows here

We have

$$\min_{G} \sigma_1^2(\omega) = \int_{\Omega}\int_{\Omega} G(\omega\ z|\phi_1)\, S_n(\omega\ \underline{z},\underline{\zeta})\, G(\omega\ z|\phi_1)\, d\underline{z}d\underline{\zeta} \tag{4 26a}$$

with

$$\int_{\Omega} G(\omega\ z|\phi_1) \sum_{m=1}^{M} s_m(\omega)\ \Phi_m(\omega\ \underline{z})\, d\underline{z} = s(\omega|\phi_1) \tag{4 26b}$$

for all

$$s(\omega|\phi_1)\Big|_{1=1}^{M}$$

The optimization procedure is quite similar to that which we did earlier so we just indicate the results. We define

$$\underline{\Phi}(\omega\ \underline{z}) = \begin{bmatrix} \Phi_1(\omega,\underline{z}) \\ \cdot \\ \cdot \\ \cdot \\ \Phi_M(\omega\ \underline{z}) \end{bmatrix}, \quad \underline{z} \in \Omega \tag{4.27a}$$

$$\underline{G}_o(\omega\cdot\underline{z}) = \begin{bmatrix} G_{1_o}\ G_o(\omega\ z|\phi_1) \\ \cdot \\ \cdot \\ \cdot \\ G_{M_o}\ G_o(\omega\ z|\phi_M) \end{bmatrix} \tag{4 27b}$$

$$\underline{\Lambda}(\omega) = \int_{\Omega}\int_{\Omega} \underline{\Phi}^{\dagger}(\omega\ \underline{z})\, Q_n(\omega\ \underline{z},\underline{\zeta})\underline{\Phi}(\omega:\underline{\zeta})\ d\underline{z}d\underline{\zeta} \tag{4 27c}$$

The optimum set of beam patterns are given by

$$\underline{G}_o(\omega:\underline{\zeta}) = \underline{\Lambda}^{-1}(\omega)\int_{\Omega} \underline{\Phi}^{\dagger}(\omega\ \underline{z})\ Q_n(\omega:\underline{z},\underline{\zeta})\ d\underline{z}, \quad \underline{\zeta} \in \Omega \tag{4 28a}$$

$$\underline{g}_o(\omega:\underline{k}) = \underline{\Lambda}^{-1}(\omega)\int_{\Omega} \underline{\Phi}(\omega\cdot\underline{z})\, Q_n(\omega.\underline{z},\underline{\zeta})e^{j\underline{k}\cdot\underline{\zeta}}\, d\underline{z}\ d\underline{\zeta} \tag{4 28b}$$

The mean square output level due to the signal component is given by

$$E\left[\int_{\Omega}|G_m(\omega:\underline{z})\ S(\omega\ \underline{z})\ dz|^2\right] = \lambda_m(\omega) \tag{4 29a}$$

while the output due to the noise components are given in matrix form by

$$\underline{\sigma}_o^2\ (\omega) = E\left[\left(\int_{\Omega} \underline{G}_o(\omega\ z)\, N(\omega\ \underline{z})\ dz\right)\left(\int_{\Omega} G_o(\omega\ \underline{\zeta})\, N(\omega:\underline{\zeta})\ d\underline{\zeta}\right)^{\dagger}\right]$$

$$= \left[\frac{\Lambda_{ij}(\omega)}{\Lambda_{ii}(\omega)\Lambda_{jj}(\omega)}\right] \tag{4.29b}$$

In summary, the signal components each pass through the filter undistorted, i e., they are unbiased. These components have a diagonal covariance matrix as given by Eq. 4.29a The noise components are correlated for each beam and their noise covariance is given by Eq. 4 29b Various means of combining the signal can be considered according to the criterion imposed. We consider this further in Section 8.

PART 3 - PROCESSING METHODS

5. LINEAR ARRAYS

The most important aperture is the linear, or line, array It is the simplest structure, yet the analysis of it yields many significant results which more complicated structures change only in detail, but not in substance. Much of the analysis of this array parallels that of temporal processes observed over a finite time duration Often this is a distinct advantage since only dual results need be developed This can also prove to be somewhat of a liability as several important aspects of the analysis of array processing do not appear until more complicated geometries are introduced. For our purposes we consider conventional and optimum array patterns when operating in different types of noise fields Then we consider some general feature of the processing, such as wave number analysis, superdirectivity, and null placement where we use the linear array as a discussion vehicle

As introduced in Section 3, the receiving aperture consists of a line of length L, centered at the origin (for convenience only), and oriented with a tangent vector in the direction specified by the unit vector $\underline{a}_a$.

$$\Omega = \left\{ \underline{z} = \ell \underline{a}_a, \ |\ell| \leq L/2 \right\} \tag{5.1}$$

as illustrated in Figure 5-1.

The beam pattern of the conventional array directed in wave number direction $\underline{k}_T$ is found to be (see Eq. 3.9)

$$g(\omega, \underline{k}) = \frac{1}{L} \int_{-L/2}^{L/2} e^{j(\underline{k}-\underline{k}_T)\cdot \underline{a}_a \ell} \, d\ell = \text{sinc}\left[(\underline{k}-\underline{k}_T)\cdot \underline{a}_a \frac{L}{2} \right] \tag{5.2}$$

When we apply a triangular shading of the form

$$g(\ell) = \frac{1}{L} \left[1 - \frac{2|\ell|}{L} \right], \ |\ell| < L/2 \tag{5.3}$$

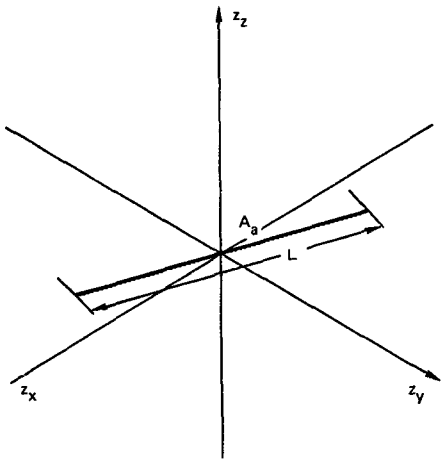

Figure 5-1. Linear array of length L, orientation $\underline{a}_a$

we obtain a beam pattern, or wave number response, of the form (see Eq 3 12)

$$g(\omega \cdot \underline{k}) = \text{sinc}^2 \left[(\underline{k} - \underline{k}_T) \cdot \underline{a}_a \frac{L}{4} \right] \tag{5 4}$$

Both of these are standard array patterns. Others can be developed, for example, the split array illustrated in Figure 3-3 We are primarily interested in optimum array patterns and their performance $\sigma_0^2(\omega\ \underline{k}_T)$ for various noise fields We contrast these optimum patterns and performance with those obtained conventionally to determine how they operate in obtaining their improved performance We also compare the performance to determine whether the additional effort in optional processing is worth while

5.1 LINEAR ARRAYS AND A SINGLE DIRECTIONAL NOISE SOURCE

The simplest nontrivial problem which one can analyze for an optimum processor is the linear array combatting a directional noise field as shown in Figure 5-2. This problem, in spite of its apparent simplicity, yields a surprising number of useful results and an insight into the general aspects of optimum array processing.

We have a directional noise source of power level $S_{n_c}(\omega)$ located at $\underline{k}_n = (\omega/c)\ \underline{a}_n = (2\pi/\lambda)\underline{a}_n$. Consequently, the colored component of the noise is a plane wave

$$n_c(t\ \underline{z}) = n_0\left(t - \frac{\underline{z} \cdot \underline{a}_n}{c}\right) \tag{5 5}$$

From our earlier analysis in Section 2, the temporal frequency spatial covariance function of this component is given by

$$S_{n_c}(\omega,\underline{z},\underline{\zeta}) = S_{n_o}(\omega)e^{j\underline{k}_n\cdot(\underline{z}-\underline{\zeta})} \tag{5.6}$$

while the corresponding frequency wave number function is given by

$$P_{n_c}(\omega\ \underline{k}) = S_{n_o}(\omega)\ \ \delta(\underline{k}-\underline{k}_n) \tag{5.7}$$

We also assume that a white noise component due to sensor noise is present In light of our earlier comments regarding this class of noise process, we have

$$S_w(\omega,\underline{z},\underline{\zeta}) = N_o\ \delta_\Omega\ (\underline{z}-\underline{\zeta}) \tag{5.8}$$

The total noise field is specified by

$$S_n(\omega\ \underline{z},\underline{\zeta}) = S_{n_o}(\omega)e^{j\underline{k}_n\cdot(\underline{z}-\underline{\zeta})} + N_o\ \delta_\Omega\ (\underline{z}-\underline{\zeta}) \tag{5.9}$$

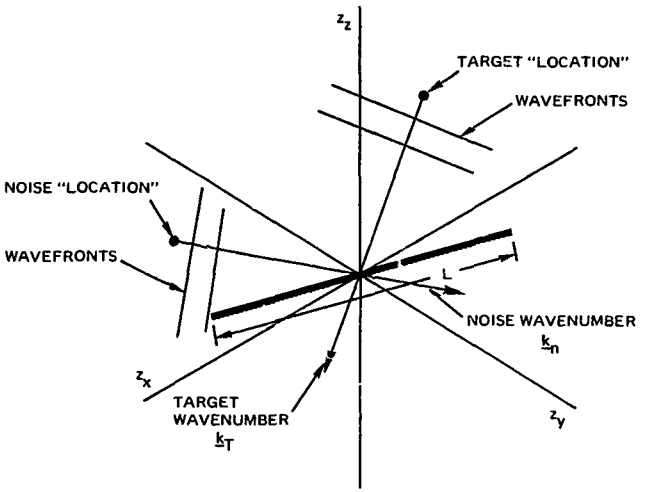

Figure 5-2. Linear array with directional noise source

We are interested in determining the optimum processor and its performance for detecting a signal at $\underline{k}_T$. The first step in designing this optimal processor is to find the inverse kernel. For directional sources this is particularly simple because the discrete spatial frequencies of the noise lead to a separable kernel with a finite number of eigenfunctions. The Karhunen-Loeve integral equation is given by

$$\int_{-L/2}^{L/2} S_{n_o}(\omega) e^{j\underline{k}_n \cdot \underline{a}_a(\ell_1 - \ell_2)} \phi(\ell_2) = \lambda \phi(\ell_1), \quad |\ell_1| \leq L/2 \tag{5.10}$$

The single non-trivial solution is

$$\Phi(\omega : \underline{z}) = \frac{1}{\sqrt{L}} e^{j\underline{k}_n \cdot \underline{z}}, \quad \left\{ \underline{z} = \ell \underline{a}_a, \ |\ell| < \frac{L}{2} \right\} = \Omega \tag{5.11a}$$

$$\lambda = L S_{n_o}(\omega) \tag{5.11b}$$

The inverse kernel is therefore given by

$$\begin{aligned} Q_n(\omega \ \underline{z}, \underline{\xi}) &= \frac{1}{N_o} [\delta_\Omega (\underline{z} - \underline{\xi}) - H(\omega \ \underline{z}, \underline{\xi})] \\ &= \frac{1}{N_o} \left[\delta_\Omega(\underline{z} - \underline{\xi}) - \frac{L S_{n_o}(\omega)}{L S_{n_o}(\omega) + N_o} \frac{e}{L} e^{j\underline{k}_n \cdot (\underline{z} - \underline{\xi})} \right], \quad \underline{z}, \underline{\xi} \in \Omega \end{aligned} \tag{5.12}$$

From Eq. 4.1 we have that the aperture pattern, or weighting, is given by

$$G(\omega \ \underline{z} | \underline{k}_T$$

$$= \frac{\displaystyle\int_{-L/2}^{L/2} d\ell_2 \frac{1}{N_o} \left[\delta_\Omega(\ell - \ell_2) - \frac{L S_{n_o}(\omega)}{L S_{n_o}(\omega) + N_o} \frac{e}{L} e^{j\underline{k}_n \cdot \underline{a}_a(\ell_1 - \ell_2)} \right] e^{j\underline{k}_T \cdot \underline{a}_a \ell_2}}{\displaystyle\int_{-L/2}^{L/2} d\ell_1 \int_{-L/2}^{L/2} d\ell_2 \, e^{-j\underline{k}_T \cdot \underline{a}_a} \frac{1}{N_o} \left[\delta_\Omega(\ell_1 - \ell_2) - \frac{L S_{n_o}(\omega)}{L S_{n_o}(\omega) + N_o} \frac{e}{L} e^{j\underline{k}_n \cdot \underline{a}_a(\ell_1 - \ell_2)} \right] e^{j\underline{k}_T \cdot \underline{a}_a \ell_2}} \tag{5.13}$$

$$= \frac{e^{-j\underline{k}_T\cdot\underline{a}_a\ell} - \dfrac{L\,S_{n_o}(\omega)}{L\,S_{n_o}(\omega)+N_o}\,\mathrm{sinc}\left[(k_n-\underline{k}_T)\cdot\underline{a}_a\dfrac{L}{2}\right]e^{-j\underline{k}_n\cdot\underline{a}_a\ell}}{L\left[1-\left(\dfrac{L\,S_{n_o}(\omega)}{L\,S_{n_o}(\omega)+N_o}\,\mathrm{sinc}^2\left[(\underline{k}_n-\underline{k}_T)\cdot\underline{a}_a\dfrac{L}{2}\right]\right)\right]},\ \underline{z}\in\Omega,\ \left\{\Omega=\ell\underline{a}_a,\ell\le\frac{L}{2}\right\}$$

Simularly, the beam pattern can be found using Eq 4 12 This yields

$g(\omega.\underline{k}|\underline{k}_T)$

$$= \frac{\mathrm{sinc}\left[(\underline{k}-\underline{k}_T)\cdot\underline{a}_a\dfrac{L}{2}\right] - \dfrac{L\,S_{n_o}(\omega)}{L\,S_{n_o}(\omega)+N_o}\,\mathrm{sinc}\left[(\underline{k}_n-\underline{k}_T)\cdot\underline{a}_a\dfrac{L}{2}\right]\mathrm{sinc}\left[(\underline{k}-\underline{k}_n)\cdot\underline{a}_a\dfrac{L}{2}\right]}{1-\dfrac{L\,S_{n_o}(\omega)}{L\,S_{n_o}(\omega)+N_o}\,\mathrm{sinc}^2\left[(\underline{k}_n-\underline{k}_T)\cdot\underline{a}_a\dfrac{L}{2}\right]} \qquad (5\ 14)$$

The operation of the optimum array can be interpreted as a null placement operation which depends upon the relative strengths of the directional and white noise If

$$\frac{L\,S_{n_o}(\omega)}{N_o} << 1$$

then

$$g(\omega\ \underline{k}|\ \underline{k}_T) = \mathrm{sinc}\left[(\underline{k}-\underline{k}_T)\cdot\underline{a}_a\frac{L}{2}\right] \qquad (5\ 15)$$

This is the conventional beam pattern which has a uniform weighting and is optimal when only white noise is present. Conversely when

$$\frac{L\,S_{n_o}(\omega)}{N_o} >> 1$$

then

$$g(\omega.\underline{k}|\ \underline{k}_T) \simeq \frac{\mathrm{sinc}\left[(\underline{k}-\underline{k}_T)\cdot\underline{a}_a\dfrac{L}{2}\right] - \mathrm{sinc}\left[(\underline{k}_n-\underline{k}_T)\cdot\underline{a}_a\dfrac{L}{2}\right]\mathrm{sinc}\left[(\underline{k}-\underline{k}_n)\cdot\underline{a}_a\dfrac{L}{2}\right]}{1-\mathrm{sinc}^2\left[(\underline{k}_n-\underline{k}_T)\cdot\underline{a}_a\dfrac{L}{2}\right]} \qquad (5\ 16)$$

In the direction of noise source, this beam pattern has the response level

$$g(\omega\, \underline{k}_n | \underline{k}_T) \simeq 0, \tag{5 17}$$

that is, a null is placed there Placing this null is done at the expense of increasing the output noise due to the white noise component Specifically, in this situation the white noise is increased by a factor of approximately

$$1\Big/\left(1 - \mathrm{sinc}^2 \left[(\underline{k}_n - \underline{k}_T)\cdot \underline{a}_a \frac{L}{2}\right]\right)^2$$

over the minimum level obtained with a uniformly weighted array If the noise and target are widely separated, i e ,

$$(\underline{k}_n - \underline{k}_T)\cdot \underline{a}_a \frac{L}{2} >> 2\pi \tag{5.18}$$

the null placement has no effect However, if

$$(\underline{k}_n - \underline{k}_T)\cdot \underline{a}_a \frac{L}{2} \simeq 0, \tag{5 19}$$

then the white noise response level is increased by a factor of approximately

$$\left[\frac{1}{3}(\underline{k}_n - \underline{k}_T)\cdot \underline{a}_a \frac{L}{2}\right]^{-4}$$

which is a very dramatic increase. Consequently, in designing array weightings with the target and noise close together, one follows a null placement procedure up to the point that response due to the white noise becomes dominant.

Figure 5-3 illustrates a situation in which the directional noise is dominant At separations of 30° the beam pattern resembles that of a uniformly weighted array. At 10° and 3° the pattern has very strong nulls near the noise term Finally, at 1° the null can no longer be maintained for the white noise has become the dominant consideration due to the large sidelobes appearing in maintaining the null Note that in the optimum beam pattern response, the peak does not fall right at the target location when the noise direction is close to that of the target Effectively, it is displaced over to facilitate placing the null. We shall return to this in subsequent discussions. The performance or noise power output $\sigma_o^2(\omega|\underline{k}_T)$ for this array and noise field can be found using Eqs 4 17 and 5.12. We have

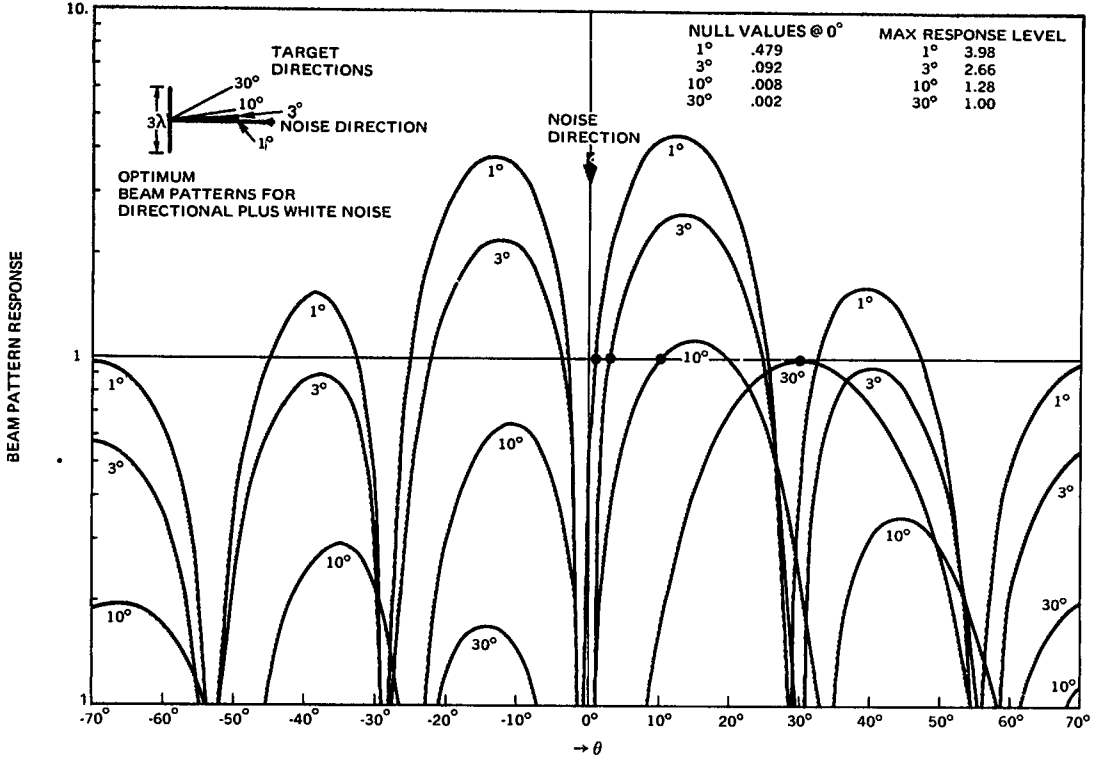

Figure 5-3. Optimum array beam pattern for a directional plus white noise environment $\frac{L\,S_{no}(\omega)}{N_o} = 120$

$$\sigma_o^2(\omega|\underline{k}_T) = \left\{ \frac{1}{N_o} \left[L - \frac{L^2 S_{n_o}(\omega)}{L\, S_{n_o}(\omega) + N_o} \operatorname{sinc}^2 \left[(\underline{k}_n - \underline{k}_T)\cdot \underline{a}_a \frac{L}{2} \right] \right] \right\}^{-1}$$

$$= \left\{ \frac{L}{N_o} \left[\frac{1 + \frac{L\, S_{n_o}(\omega)}{N_o} \left[(1 - \operatorname{sinc}^2 \left((\underline{k}_n - \underline{k}_T)\cdot \underline{a}_a \frac{L}{2} \right) \right]}{1 + \frac{L\, S_{n_o}(\omega)}{N_o}} \right] \right\}^{-1} \quad (5\ 20)$$

We see that all spatial aspects of the problem are incorporated in the parameter

$$\rho \triangleq \operatorname{sinc} \left[(\underline{k}_n - \underline{k}_T)\cdot \underline{a}_a \frac{L}{2} \right] \quad (5\ 21)$$

while the strength of the interfering noise appears in the ratio

$$\frac{L\, S_{n_o}(\omega)}{N_o}$$

In Figure 5-4 we have plotted the output noise power $\sigma_o^2(\omega|\underline{k}_T)$ versus ρ relative to a reference level of N_o/L

In interpreting this figure we first note that when the target and noise are widely separated, i.e., $\rho \cong 0$

$$\sigma_o^2(\omega|\underline{k}_T) = \frac{N_o}{L} \quad (5.22)$$

while when they are coincident, i.e., $\rho \simeq 1$

$$\sigma_o^2(\omega|\underline{k}_n) = \frac{N_o}{L} \Bigg/ \left(1 + \frac{L\, S_{n_o}(\omega)}{N_o} \right)^+ \quad (5\ 23)$$

In terms of the performance using optimum array design, the most important parameter is the resolution, that is, how close to the directional noise source a target can be before the noise power increases significantly. Alternatively, when using "high resolution" methods for noise field measurements, one wants to know the resolution of these methods

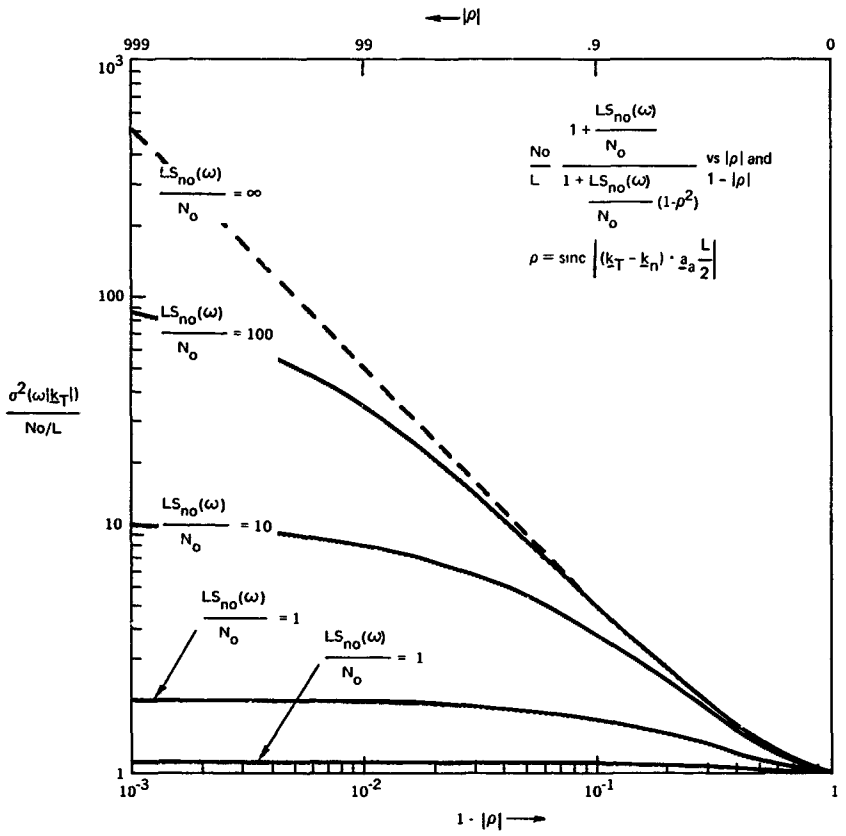

Figure 5-4 Optimum array performance vs $|\rho|$ and $1 - |\rho|$ (in units of N_o/L)

Since the spatial aspects are incorporated in the parameter ρ, the resolution is determined by this parameter. However, the value of ρ at which the interference becomes significant is dependent upon the parameter $L\,S_{n_o}(\omega)/N_o$, as stronger interference degrades the performance faster.

For discussion purposes let us define the value of ρ which leads to a 3dB performance loss by ρ_{3dB} or a 3dB increase above the background white noise. We have

$$\frac{1+\left(\frac{L\,S_{n_o}(\omega)}{N_o}\right)}{\left\{1+\frac{L\,S_{n_o}(\omega)}{N_o}\left(1-\rho^2_{3dB}\right)\right\}}=2 \tag{5 24a}$$

or

$$\rho_{3dB}=\sqrt{\frac{1}{2}\left(\frac{1+\frac{L\,S_{n_o}(\omega)}{N_o}}{\frac{L\,S_{n_o}(\omega)}{N_o}}\right)} \tag{5 24b}$$

This value ranges from one, as a 3dB reduction never occurs for noises with a level less than $(L/N_o)^{-1}$, to $1/\sqrt{2}$ for strong interference Consequently, even for strong interference one always can obtain a performance with 3dB of the limiting white noise level providing the spatial geometry yields a ρ less than $1/\sqrt{2}$. Equivalently, the resolution can be defined by

$$\text{sinc}\ (\underline{k}_T-\underline{k}_n)\cdot\underline{a}_a\frac{L}{2} \quad > 1/\sqrt{2} \tag{5.25a}$$

The response to a directional signal will be less than 3dB above background outside of this region. Solving this yields

$$(\underline{k}_T-\underline{k}_n)\cdot\underline{a}_a\frac{L}{2} \quad < 1.39 \tag{5 25b}$$

For broadside geometries

$$2\left|\cos\left(\frac{\pi}{2}-\frac{\theta_s}{2}\right)\right| \leq \frac{2.78}{2\pi(L/\lambda)}=\frac{444}{L_\lambda} \tag{5 26a}$$

or

$$\theta_s = 2 \sin^{-1} \left(\frac{.222}{L_\lambda} \right) \text{ rad}, \tag{5 26b}$$

where L_λ is the length of the array in wavelengths. Figure 5-5 illustrates a typical broadside array configuration for directional noise and target.

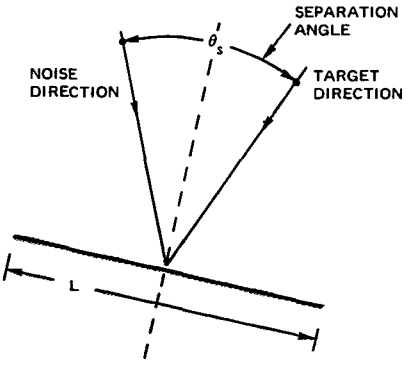

Figure 5-5. Broadside array configuration for directional noise and target

For an array larger than one half a wavelength, or $L_\lambda > 1/2$, we have

$$\theta_s \simeq \frac{.444}{L_\lambda} \text{ rad} = \frac{25.4^\circ}{L_\lambda} \tag{5.27}$$

This should be the "critical" separation angle for a linear array using "high resolution" methods in the broadside case. (Note that we assumed no other sources to be present in the noise field)

As the array is "beamed" off broadside, the effective resolution becomes smaller. Let us consider the endfire situation as represented in Figure 5-6. Here we have

$$\cos \theta_s - 1 = \frac{2.78}{2\pi L/\lambda} = \frac{.444}{L_\lambda} \tag{5.28a}$$

or

$$\theta_s = 2 \left(\sin^{-1} \frac{.222}{L_\lambda} \right)^{1/2} \text{rad} \tag{5 28b}$$

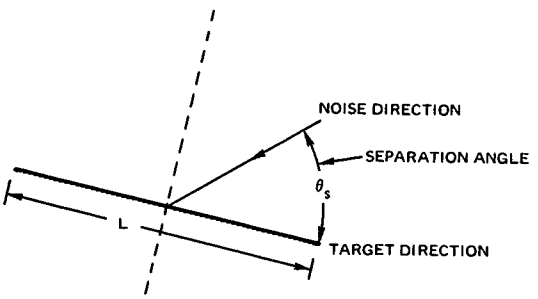

Figure 5-6. Endfire array configuration for directional noise and target.

For large arrays with $L_\lambda > 1$ this becomes

$$\theta_s \simeq .942/\sqrt{L_\lambda} \text{ rad} = 53.6°/\sqrt{L_\lambda} \tag{5 29}$$

Observe that the effective resolution of an array changes from L_λ^{-1} dependence at broadside to one of $L_\lambda^{-1/2}$ for an endfire configuration

Before illustrating the performance of the optimum beam pattern, we discuss the performance of some suboptimum beam patterns. In this context, we consider two commonly used array shadings, uniform, or conventional, and triangular; and then we contrast their performance to that of the optimal array processor just analyzed.

For a target with wave number $\underline{k}_T$, the conventional or uniformly weighted, linear array has a weighting

$$G_c(\omega \cdot \ell) = \frac{1}{L} \; e^{-j\underline{k}_T \cdot \underline{a}_a \ell}, \quad |\ell| > \frac{L}{2} \tag{5.30}$$

As discussed earlier in Section 3, this weighting produces a beam pattern

$$g_c(\omega : \underline{k}) = \text{sinc} \left[(\underline{k} - \underline{k}_T) \cdot \underline{a}_a \frac{L}{2} \right] = \rho \tag{5 31}$$

The mean square noise output, or the performance for a single directional signal and white noise environment follows directly from Eq 4 18. We have

$$\sigma_c^2(\omega | \underline{k}_T) = S_{n_o}(\omega) \, \text{sinc}^2 \left[(\underline{k}_n - \underline{k}_T) \cdot \underline{a}_a \frac{L}{2} \right] + \frac{N_o}{L}$$

$$= \frac{N_o}{L}\left\{\frac{L\,S_{n_o}(\omega)}{N_o}\ \text{sinc}^2\left[(\underline{k}_n-\underline{k}_T)\cdot\underline{a}_a\frac{L}{2}\right]+1\right\} \qquad (5\ 32)$$

A triangular shaded linear array directed to a target at wave number $\underline{k}_T$ has a weighting

$$G_T(\omega\ \underline{z}) = \frac{2}{L}\left[1-\frac{2}{L}\ |\ell|\right]e^{-j\underline{k}_T\cdot\underline{a}_a\ell}, \quad |\ell| < \frac{L}{2} \qquad (5\ 33)$$

A similar analysis shows that the beam pattern generated is given by

$$g_T(\omega\ \underline{k}) = \text{sinc}^2\left[(\underline{k}-\underline{k}_T)\cdot\underline{a}_a\frac{L}{4}\right] \qquad (5\ 34)$$

while the mean square noise output, or the performance, versus this noise field is

$$\sigma_T^2(\omega|\underline{k}_T) = S_{n_o}(\omega)\ \text{sinc}^4\left[(\underline{k}_n-\underline{k}_T)\cdot\underline{a}_a\frac{L}{4}\right]+\frac{4}{3}\left(\frac{N_o}{L}\right)$$

$$= \frac{N_o}{L}\left\{\frac{L\,S_{n_o}(\omega)}{N_o}\ \text{sinc}^4\left[(\underline{k}_n-\underline{k}_T)\cdot\underline{a}_a\frac{L}{4}\right]+\frac{4}{3}\right\} \qquad (5\ 35)$$

In Figures 5-7 through 5-9 we have plotted the performance, or noise output for the optimum, uniform, and triangular weighted arrays for various ratios of the directional signal power to background white noise level We see that the optimum array weighting combines the desirable features of both the uniform and triangular arrays Its enhanced performance is particularly significant when the ratio of directional to white background noise is high In this situation optimum design of the array weighting is worthwhile providing the results are not unduly sensitive to the model assumptions

The next observation concerns the sidelobe structure of the noise power response versus $\underline{k}_T$. When the directional noise is high, i.e., $L\,S_{n_o}(\omega)/N_o >> 1$, then the sidelobe level of $\sigma_c^2(\omega|\underline{k}_T)$ for a uniformly weighted array goes as $[2/(2n+1)\,\pi]^2$, or from 13 dB down, while $\sigma_T^2(\omega|\underline{k}_T)$ for a triangular weighted array goes as $[2/(2n+1)\pi]^4$, or from 26 dB down

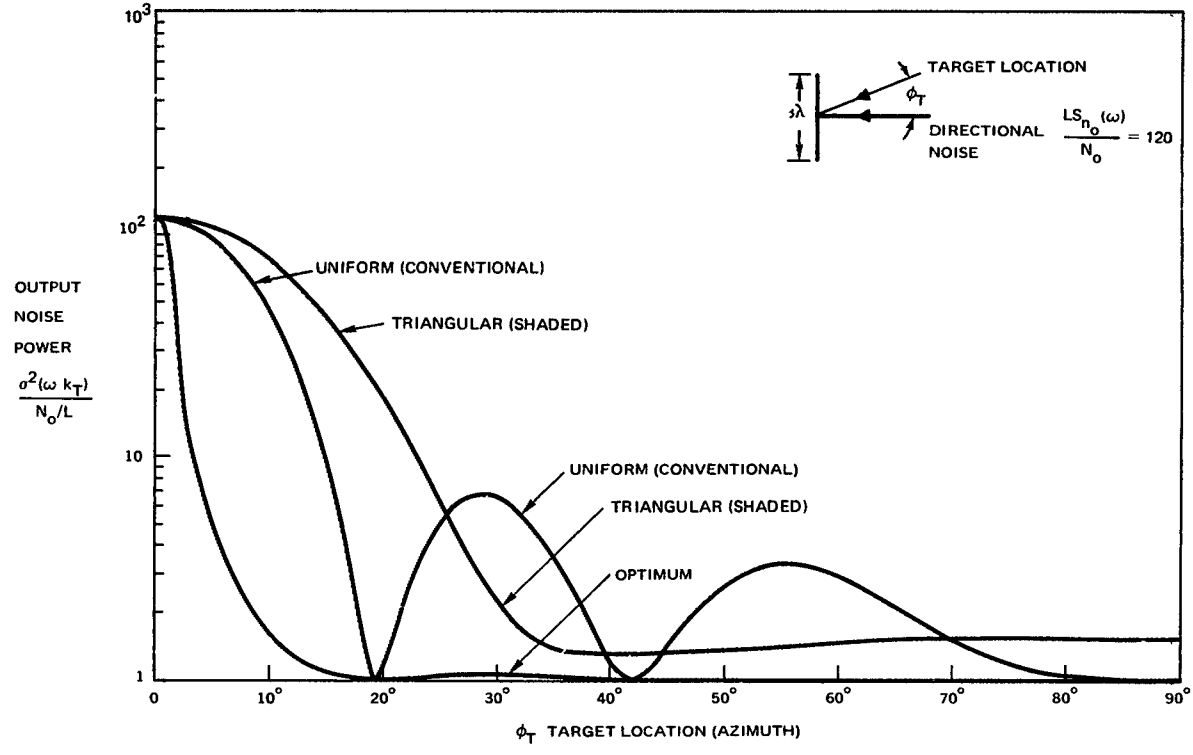

Figure 5-7. Performance of optimum, uniform, and triangular linear arrays vs target position for $LS_{n_o}(\omega)/N_o = 120$.

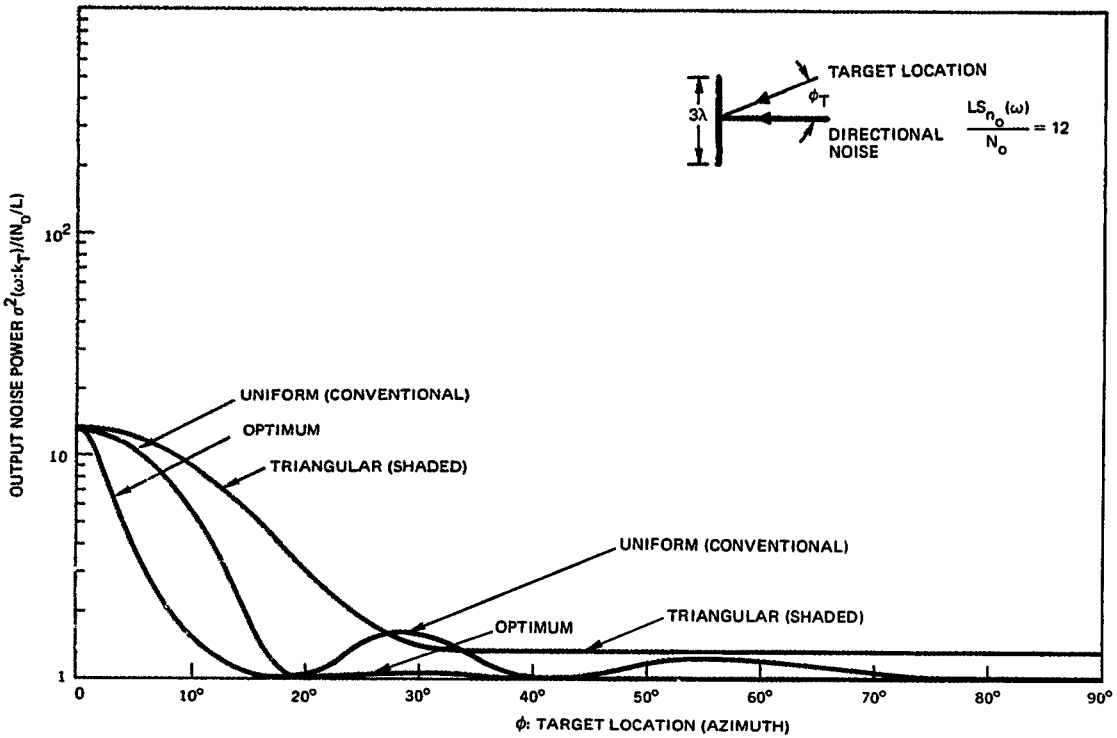

Figure 5-8. Performance of optimum, uniform, and triangular linear arrays vs target position for $LS_{n_o}(\omega)/N_o = 12$.

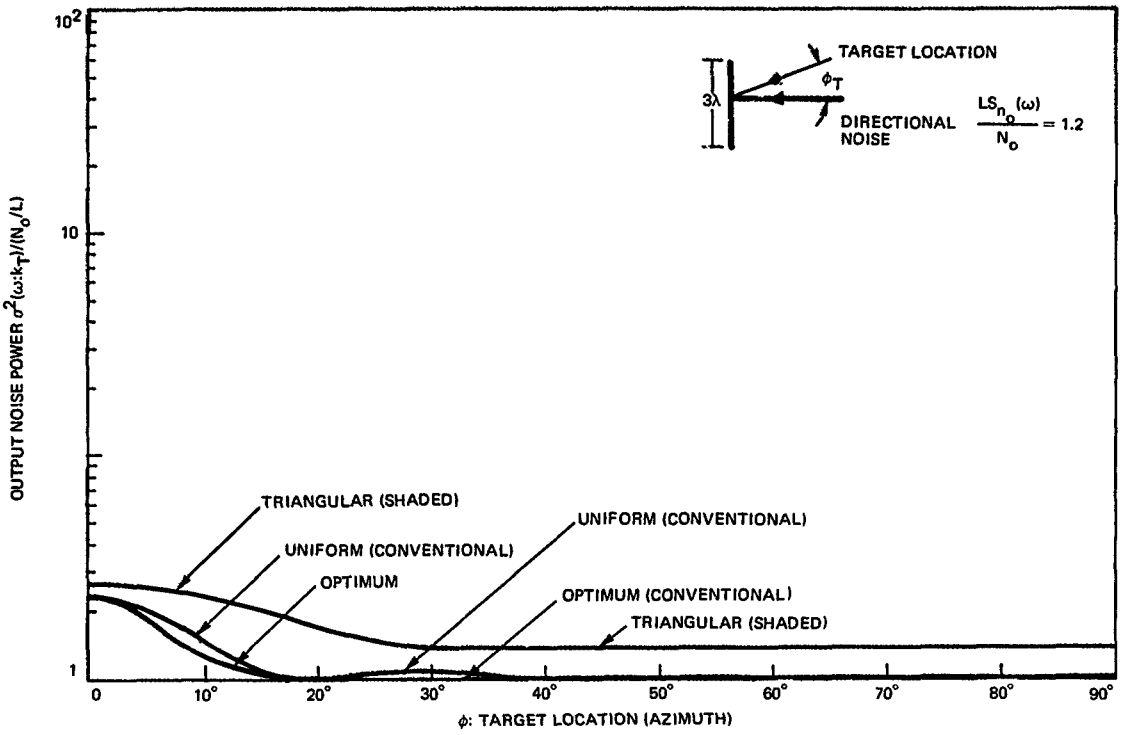

Figure 5-9. Performance of optimum, uniform, and triangular linear arrays vs target position for $LS_{n_o}(\omega)/N_o = 1.2$.

With the optimum array weighting, Eq. 5.20 implies that the maximum sidelobe level of $\sigma_c^2(\omega|k_T)$ goes as

$$\left\{ \frac{L\, S_{n_o}(\omega)}{N_o} \qquad \left(1 - \left[\frac{2}{(2n+1)\pi}\right]^2\right)\right\}^{-1}$$

or

$$1.05/\left(\frac{L\, S_{n_o}(\omega)}{N_o}\right)^{-1}$$

This indicates that the sidelobe level is inversely dependent upon the directional noise. For example, in Figure 5-7 the sidelobe level is down approximately 21 dB. Naturally, there is a premium to pay for this. As we have previously discussed, the optimum array shading is a null placement operation in the situation of strong directional noise. Unfortunately, this becomes a very sensitive situation requiring precise knowledge of the direction of the noise which is typically not available in an experimental situation. This sensitivity to direction is quite evident when one examines the beam pattern As indicated in Figure 5-3 the beam pattern has a very high sidelobe structure such that a small amount of error between the actual noise direction and the null location would lead to a very high response to this noise.

5.2 LINEAR ARRAYS WITH TWO-DIRECTIONAL NOISE SOURCES

The optimum array achieves an enhanced processing gain by effectively displacing its beam pattern to null the noise If the target is located between two noise sources this procedure is not viable, for one would have a strong response to the directional source due to sidelobes on the other side of the beam In these situations, optimum processing can still improve the array performance although, depending upon the geometry, not as much as in the single noise source. A particular example of two-directional noise source field, as shown in Figure 5-10, introduces important issues in the limited "high resolution" mapping methods and superdirectivity We consider the issue of determining when two noise sources are resoluable, or, from an optimum beam pattern viewpoint, we determine if we can create a beam that can observe a signal located between two noise sources This problem is a very special case since we can obtain closed-form expressions for a noise field composed of an arbitrary number of sources Insight, however, is lost in the matrix manipulations which are necessary. Moreover, this problem is simple enough that we can obtain considerable physical insight by carrying out a detailed analysis If we assume that the noise sources have the same temporal spectra, then we have a spectral covariance function of the form

$$S_{n_o}(\omega:\underline{k},\underline{\xi}) = \frac{S_{n_o}(\omega)}{2} \left\{ e^{-j\underline{k}_1\cdot(\underline{z}-\underline{\xi})} + e^{-j\underline{k}_2\cdot(\underline{z}-\underline{\xi})} \right\} \tag{5 36}$$

Substituting this into the spatial Karhunen-Loeve Eq 3.53, we can obtain a matrix equation since the kernel is separable, i.e , it contains a finite number of nonzero eigenvalues For a linear array of length L, oriented with array tangent $\underline{a}_a$, we obtain the eigenvalues and eigenfunctions

$$\lambda_1 = L \frac{S_{n_o}(\omega)}{2} (1 + \rho(\underline{k}_1-\underline{k}_2)) \tag{5.37a}$$

$$\Phi_1(\ell) = \frac{\psi_1(\ell) + \psi_2(\ell)}{(2[1 + \rho(\underline{k}_1-\underline{k}_2)])^{1/2}}, \quad |\ell| \leq L/2 \tag{5.37b}$$

$$\lambda_2 = L \frac{S_{n_o}(\omega)}{2} (1 - \rho(\underline{k}_1-\underline{k}_2)) \tag{5.37c}$$

$$\Phi_2(\ell) = \frac{\psi_1(\ell) - \psi_2(\ell)}{(2[1 - \rho(\underline{k}_1-\underline{k}_2)])^{1/2}}, \quad |\ell| \leq L/2 \tag{5 37d}$$

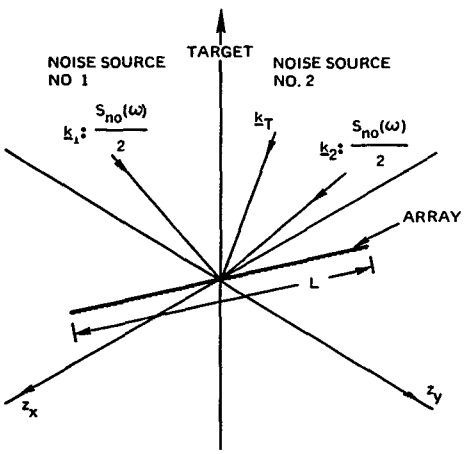

Figure 5-10. Geometry for two directional noise source field.

where

$$\rho(\underline{k}) = \text{sinc}\left(\underline{k}\cdot\underline{a}_a \frac{L}{2}\right) \tag{5.37e}$$

$$\psi_i(\ell) = \frac{e^{j\underline{k}_i\cdot\underline{a}_a\ell}}{\sqrt{L}}, \quad |\ell| \leq L/2 \tag{5.37f}$$

We observe two features characteristic of the eigenvalues and eigenfunctions of a directional noise field. The eigenfunctions consist of a linear combination of the functions $e^{j\underline{k}_i\cdot\underline{z}}$ while the eigenvalues are determined by how similar these functions are across the aperture. In this example, if the signals are orthogonal, i.e., $\rho(\underline{k}_2-\underline{k}_1) = 0$, then the eigenvalues are equal and reflect the noise power of $\frac{L}{2} S_{n_o}(\omega)$ from the individual directions. If they are very similar, i.e., $\rho(\underline{k}_2-\underline{k}_1) \simeq 1$, then there is one dominant eigenvalue of $L\, S_{n_o}(\omega)$ which represents the situation that almost all the noise power originates in a direction which is the average of the two source locations.

We can determine the optimum beam pattern and its output noise power using these expressions and assuming that sensor noise with level N_o is present. Since the total noise power is also the term that normalizes the beam pattern we determine it first We have after some manipulation

$$\sigma_o^2(\omega|\underline{k}_T)=\left[\int_\Omega\int_\Omega e^{-j\underline{k}_T\cdot\underline{z}}Q(\omega\,\underline{z},\underline{\zeta})e^{j\underline{k}_T\cdot\underline{\zeta}}\,d\underline{z}\,d\underline{\zeta}\right]^{-1} \tag{5 38}$$

$$=\frac{N_o}{L}\left[1-\frac{1}{2}\frac{\beta}{(1+\beta[1+\rho(\underline{k}_1-\underline{k}_2)])}(\rho(\underline{k}_1-\underline{k}_T)+\rho(\underline{k}_2-\underline{k}_T))^2\right.$$

$$\left.-\frac{1}{2}\frac{\beta}{(1+\beta[1-\rho(\underline{k}_1-\underline{k}_2)])}(\rho(\underline{k}_1-\underline{k}_T)-\rho(\underline{k}_2-\underline{k}_T))^2\right]^{-1}$$

and

$$g(\omega:\underline{k}|\underline{k}_T)=\left(\sigma_0^2(\omega|\underline{k}_T)\right)\frac{L}{N_o}\left\{\rho(\underline{k}-\underline{k}_T)\right. \tag{5.39}$$

$$-\frac{1}{2}\frac{\beta}{1+\beta[1+\rho(\underline{k}_1-\underline{k}_2)]}(\rho(\underline{k}-\underline{k}_1)+\rho(\underline{k}-\underline{k}_2))(\rho(\underline{k}_T-\underline{k}_1)+\rho(\underline{k}_T-\underline{k}_2))$$

$$\left.-\frac{1}{2}\frac{\beta}{1+\beta[1-\rho(\underline{k}_1-\underline{k}_2)]}(\rho(\underline{k}-\underline{k}_1)-\rho(\underline{k}-\underline{k}_2))(\rho(\underline{k}_T-\underline{k}_1)-\rho(\underline{k}_T-\underline{k}_2))\right\},$$

where

$$\beta=L\,S_{n_o}(\omega)/2N_o$$

While complicated, these expressions can be interpreted. If $\rho(k_1-k_2)\simeq 0$, then the beam pattern has nulls of approximately

$$\rho(\underline{k}_i-\underline{k}_T)=\frac{1}{1+\beta[(1-\rho^2(\underline{k}_1-\underline{k}_T)-\rho^2(\underline{k}_2-\underline{k}_T)]}$$

at each $\underline{k}_i$, i.e., stronger noise sources produce deeper nulls. If we have $\rho(\underline{k}_1-\underline{k}_2)\simeq 1$, the beam pattern and response resemble that for a single noise source.

In Figures 5-11 and 5-12, we have illustrated these results for an array and noise source geometry. We can observe that for 2° and 6° separations, the noise power output resembles that of a single source. Here $\rho(\underline{k}_1-\underline{k}_2)\simeq .99$ and .94 respectively. At 20° and 60° separations, the effects of the two noise sources are resolvable with each source producing a response approximately equal to β. If we examine the conventional beam pattern response in Figures 5-13 and 5-14, for comparison, we find much the same behavior for the peaks; however, the sidelobe level is very high and could easily be attributed to other sources of a lower power.

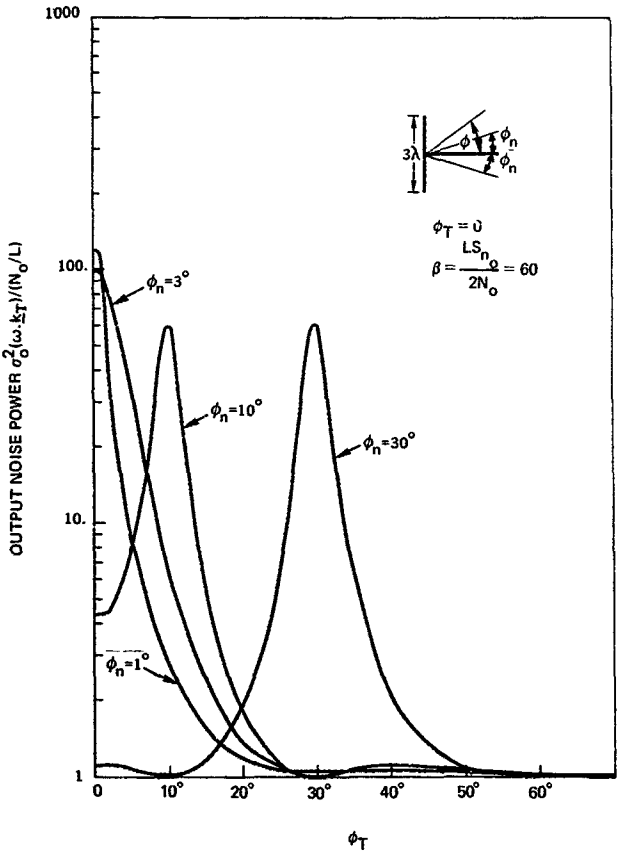

Figure 5-11. Optimum beam pattern noise power output for a two-directional noise source field.

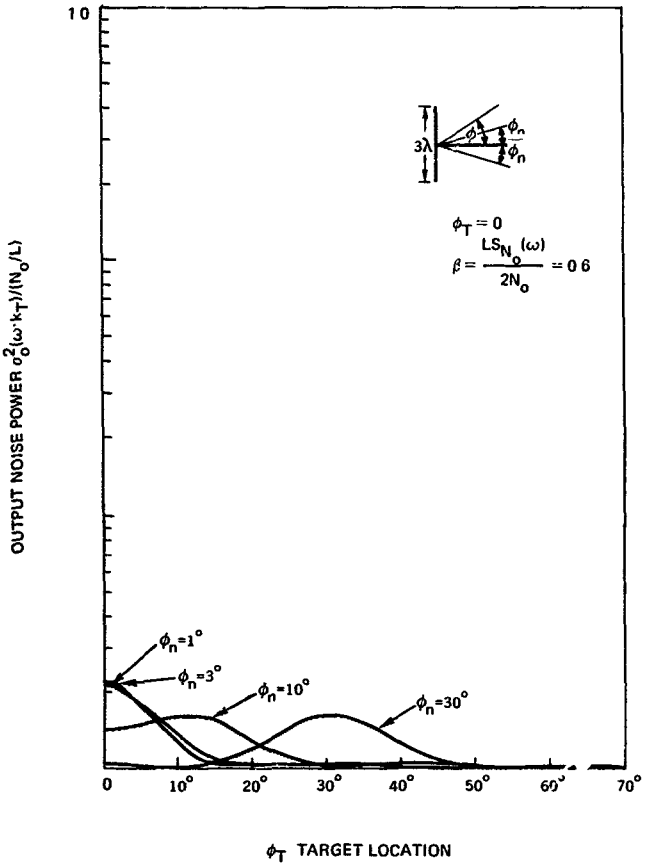

Figure 5-12 Optimum beam pattern noise power output for a two-directional noise source field.

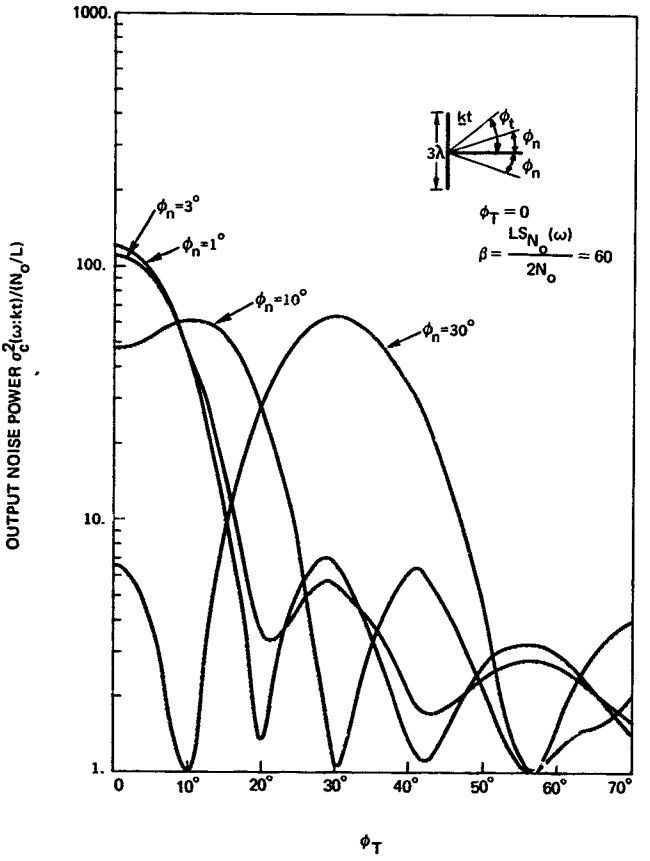

Figure 5-13. Conventional beam pattern noise power output for a two-directional noise source field.

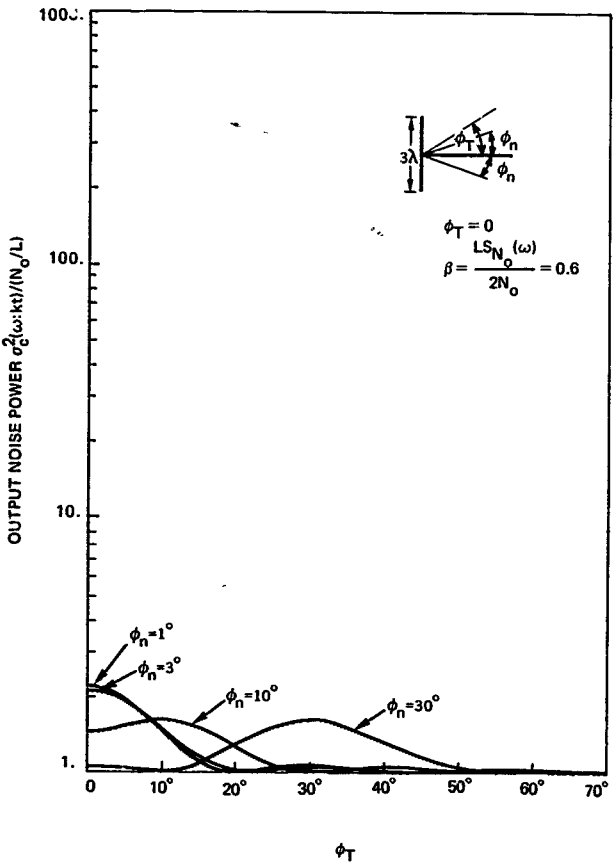

Figure 5-14. Conventional beam pattern noise power output for a two-directional noise source field.

The patterns illustrated in Figures 5-15 through 5-18 demonstrate how the output noise power is minimized. For a 2° separation the beam pattern differs substantially from the conventional one only when β=60 Even a minor reduction of the beam pattern in the noise directions is worthwhile when the directional noise level is high Note that a higher sidelobe level is introduced to accomplish this As the separation between the two noise sources increases, all the beam patterns differ from the conventional beam pattern The pattern for β=60 has very high sidelobe in excess of the main lobe for separations of 6° and 20° This behavior contrasts with that for a single source In that situation the closer the separation, the higher the sidelobe In this case, the beam pattern must minimize the effect of two sources, consequently, putting the target on the skirt of a main lobe is not a viable alternative At wide separations the large sidelobe disappears, and only the field with a very high noise source places a deep null in the noise direction In all cases we can see the gross behavior which governs the beam pattern for a directional noise field We try to place nulls in the direction of the noise sources while not disturbing the nulls at other noise sources and minimizing the total sidelobe level so as to reduce the effects of the sensor noise

We can interpret the output noise power in more detail by manipulating Eq 5.38 This also gives some insight into the optimum resolution of the two noise sources We can express $\sigma_o^2(\omega|\underline{k}_T)$ as

$$\sigma_o^2(\omega|\underline{k}_T) \tag{5.40}$$

$$= \frac{N_o}{L}\left[1 - \frac{\beta[(1+\beta)(\rho^2(\underline{k}_1-\underline{k}_T)+\rho^2(\underline{k}_2-\underline{k}_T)) - 2\beta\rho(\underline{k}_1-\underline{k}_2)\rho(\underline{k}_1-\underline{k}_T)\rho(\underline{k}_2-\underline{k}_T)]}{(\beta+1)^2-\beta^2\rho^2(\underline{k}_1-\underline{k}_2)}\right]^{-1}$$

The second component in the brackets represents an increase due to the directional noises, which is analogous to the term

$$\frac{\text{sinc}^2\left((\underline{k}_n-\underline{k}_T)\cdot\underline{a}_a\frac{L}{2}\right)L\,S_{n_o}(\omega)/N_o}{1+L\,S_{n_o}(\omega)/N_o}$$

for the single directional noise case (see Eq. 5 20). It is a quadratic function of the terms $\rho(\underline{k}_1-\underline{k}_T)$ and $\rho(\underline{k}_2-\underline{k}_T)$; consequently, the increase in output noise follows elliptic contours versus these parameters These ellipes have a major axis representing the geometry for maximum interference and a minor axis where it is a minimum. The major axis is specified by

$$\rho(\underline{k}_1-\underline{k}_T) = \rho(\underline{k}_2-\underline{k}_T) \tag{5.41a}$$

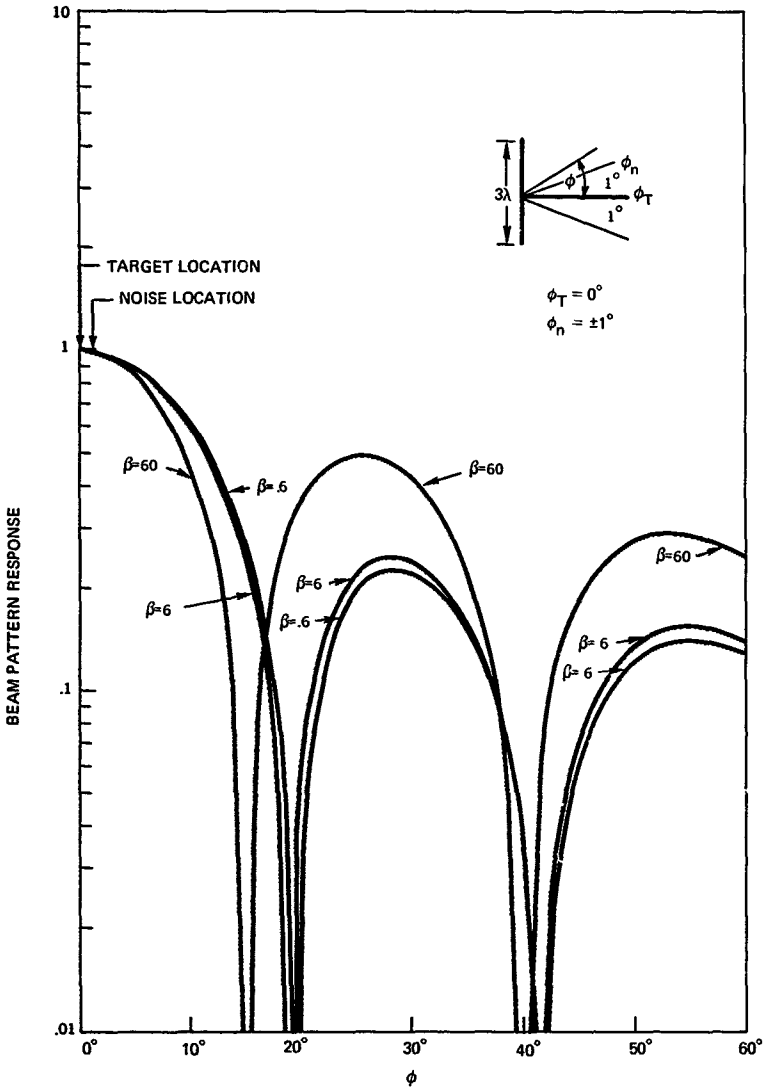

Figure 5-15. Optimum beam patterns for two-directional noise sources at θ=90°; ϕ_n=±1.0°; θ_T=90, ϕ_T=0°; and β=60.0, 6.0, 0.6.

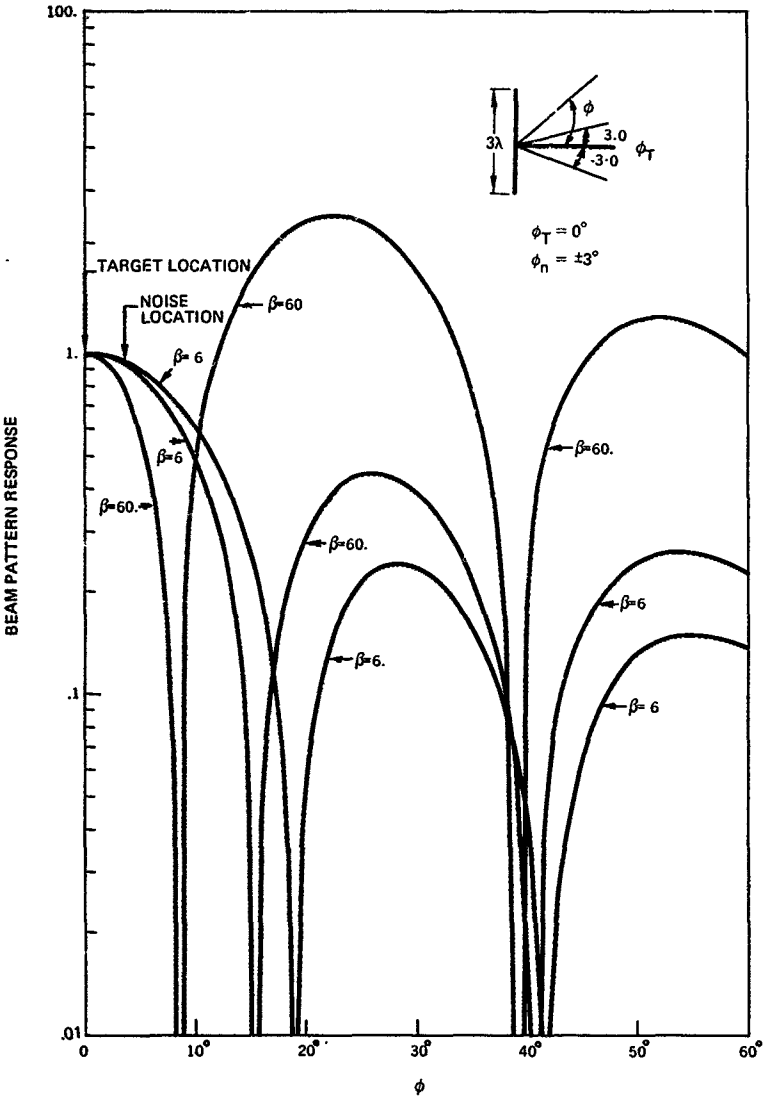

Figure 5-16. Optimum beam patterns for two-directional noise sources at θ=90°, ϕ_n=±3.0°; θ_T=90°, ϕ_T=0°; and β=60.0, 6.0, and 0.6.

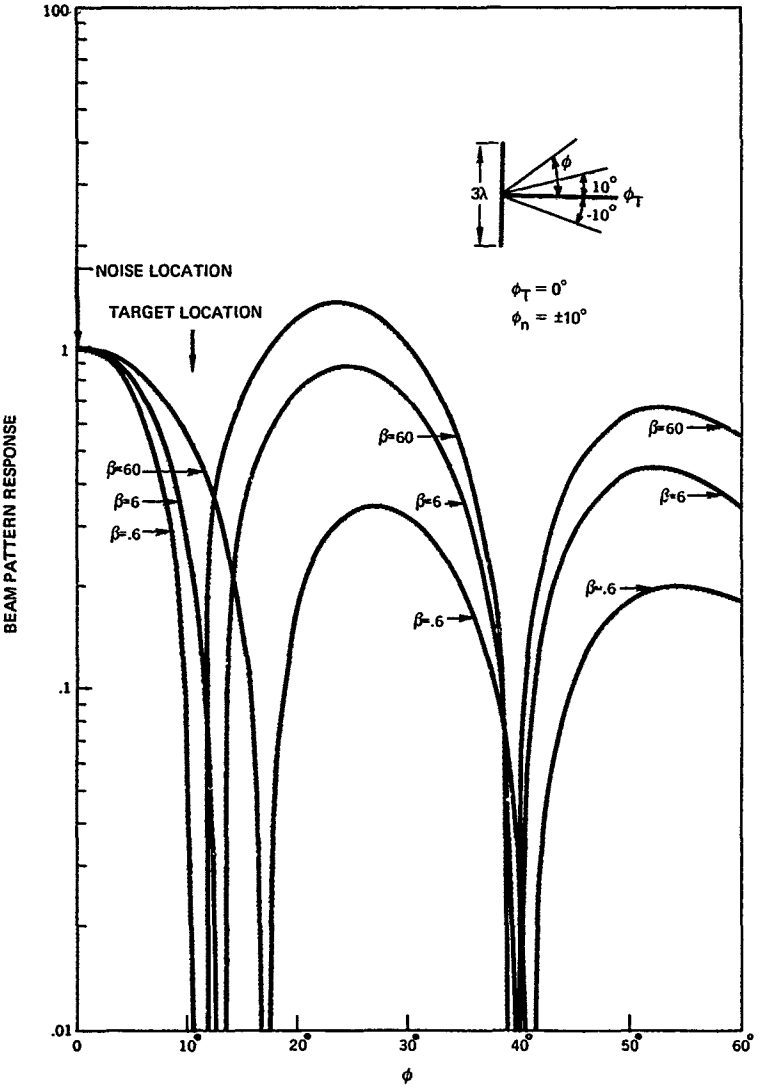

Figure 5-17. Optimum beam patterns for two-directional noise sources at θ=90°; ϕ_n=±10.0°; θ_T=90°; ϕ_T=0°; and SNR = β=60.0, 6.0, and 0.6.

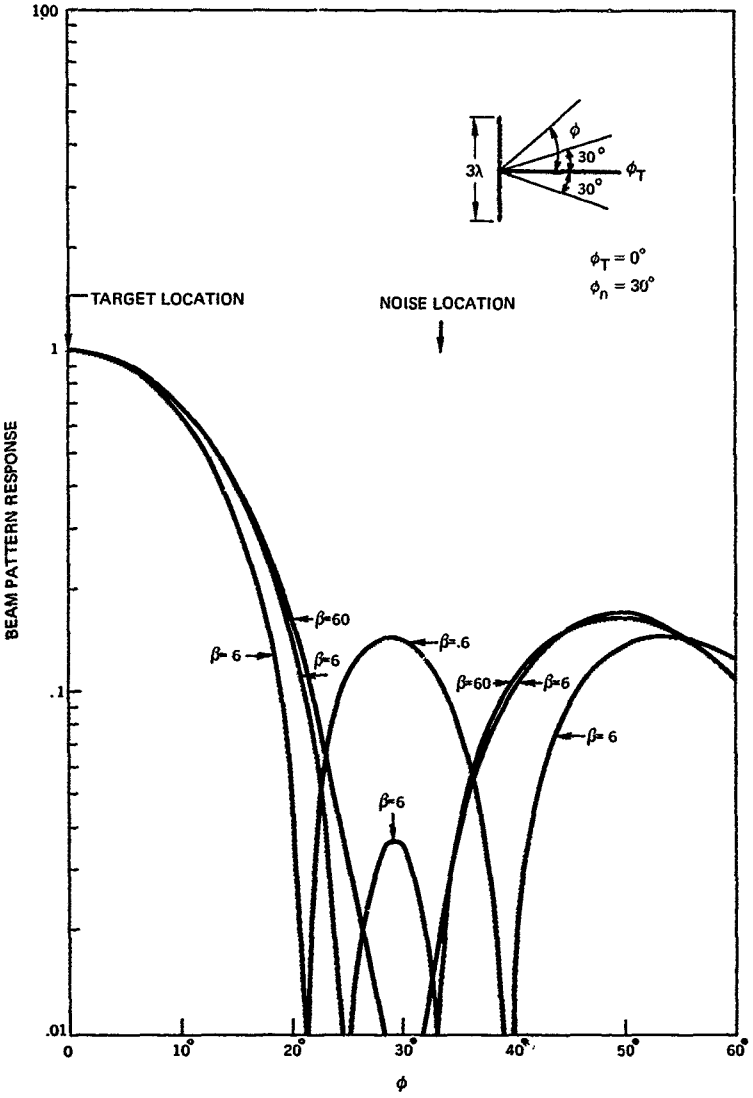

Figure 5-18. Optimum beam pattern for two-directional noise sources at θ=90°; ϕ_n=±30°; θ_T=90°; ϕ_T=0°; and β = 60.0, 6.0, and 0.6.

and the minor axis is

$$\rho(\underline{k}_1-\underline{k}_T) = -\rho(\underline{k}_2-\underline{k}_T) \tag{5.41b}$$

Since ρ is an even function of $\underline{k}$, the maximum noise interference occurs when

$$\underline{k}_1-\underline{k}_T = \underline{k}_2-\underline{k}_T \tag{5.42a}$$

or

$$\underline{k}_1-\underline{k}_T = -(\underline{k}_2-\underline{k}_T) \tag{5.42b}$$

The first occurs when the noise sources are close together and the target is identical to the case of a single directional noise source twice the level. In the second, the target is situated between the two noise sources, which is the geometry that we illustrated earlier.

We define the sources to be resolvable if

$$\sigma_o^2(\omega|\underline{k}_1) > \sigma_o^2\left(\omega|\frac{\underline{k}_1+\underline{k}_2}{2}\right) \tag{5.43}$$

In the geometry analyzed previously, this requires

$$1+\beta(1-\beta)\,\mathrm{sinc}^2(2\pi L_\lambda \sin\phi_n) > 2\mathrm{sinc}^2(\pi L_\lambda \sin\phi_n)$$
$$\cdot\,[1+\beta(1-\mathrm{sinc}(2\pi L_\lambda \sin\phi_n))] \tag{5.44}$$

In Figure 5-19 we have plotted the β required for resolving the two sources versus the separation angle between them for $L_\lambda = 3$ For example once they are closer than $\phi_n \simeq 3°$, a β of at least 600 is required.

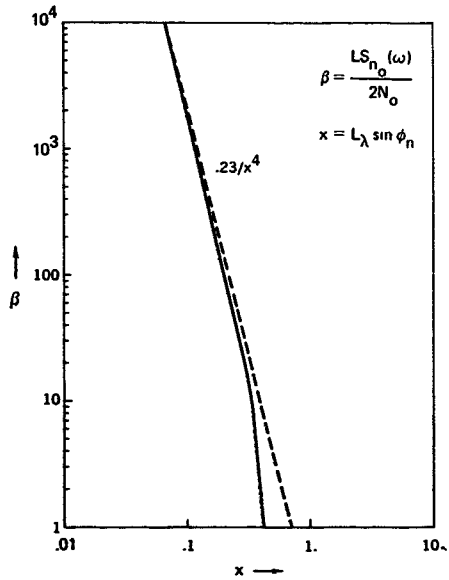

Figure 5-19. Required SNR for separating two-directional noise sources.

5.3 WAVE NUMBER ANALYSIS FOR LINEAR ARRAY

Before considering analyses for more noise fields, we examine a frequency wave number approach to optimal beam pattern design. We have found that the quantity $\sigma_o^2(\omega|\underline{k}_T)$ specified the noise power at the beamformer output. From Section 4.2 (Eqs. 4.22a, 4.22b), we minimize

$$\sigma_o^2(\omega|\underline{k}_T) = \int_{\infty}^{\infty}\cdots\int_{\infty}^{\infty}\frac{d\underline{k}}{(2\pi)^N}\,|g_o(\omega:\underline{k}\,|\underline{k}_T)|^2 P_n(\omega:\underline{k}) + N_o\int_{\Omega}|G_o(\omega:\underline{z}|\underline{k}_T)|^2 d\underline{z} \quad (5.45a)$$

with

$$g_o(\omega:\underline{k}_T|\underline{k}_T) = 1 \quad (5.45b)$$

For linear arrays we can obtain a particularly useful and intuitive approach using wave-number concepts. This was apparently used first by Woodward [23] and later extended for analyzing superdirective arrays by Francia [24].

Let us define $G_{\underline{\ell}}(\omega:\underline{\ell})$ to be a weighting across the array and

$$k_a = \underline{k} \cdot \underline{a}_a \tag{5 46}$$

We have for the beam pattern

$$g(\omega:\underline{k}) = \int_{-L/2}^{L/2} G_{\underline{\ell}}(\omega:\underline{\ell}) e^{j\underline{k}\cdot\underline{a}_a \underline{\ell}} \, d\underline{\ell} = g_{\underline{\ell}}(\omega:k_a) , \tag{5 47}$$

where $g_{\underline{\ell}}$ is the Fourier transform with respect to the spatial variable of $G_{\underline{\ell}}$. Consequently, only the projection of $\underline{k}_a = \underline{k} \cdot \underline{a}_a$ is relevant in determining the beam pattern output. This is illustrated in Figure 5-20.

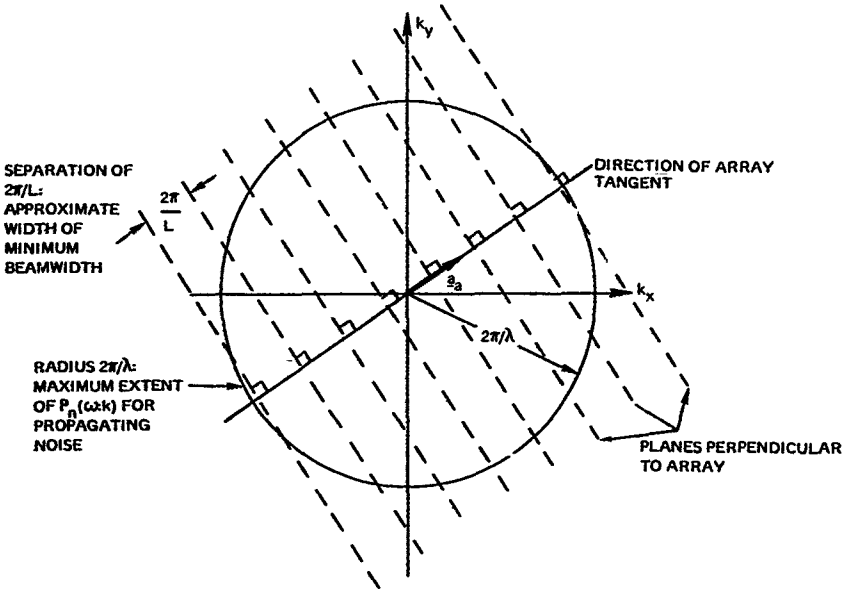

Figure 5-20. Planes of constant response for a linear array with orientation $\underline{a}_a$ and length L.

We now consider the component of the output due to sensor noise With this linear geometry we can develop a spatial dual to Parseval's theorem and represent it in the wave number domain We have

$$N_o \int_{\Omega} |G(\omega \cdot \underline{z})|^2 \, d\underline{z} = N_o \int_{-L/2}^{L/2} |G_{\underline{\ell}}(\omega \, \hat{\ell})|^2 \, d\ell = N_o \int_{-\infty}^{\infty} |g_{\underline{\ell}}(\omega . k_a)|^2 \frac{dk_a}{2\pi} \tag{5 48}$$

Applied to the optimum filter, we obtain

$$\sigma_o^2(\omega : \underline{k}_T) = \int_{-\infty}^{\infty} \cdot \int_{-\infty}^{\infty} \frac{d\underline{k}}{(2\pi)^N} |g_o(\omega \, \underline{k} \, | \underline{k}_T)|^2 P_n(\omega : \underline{k}) + N_o \int_{-\infty}^{\infty} |g_{\underline{\ell}_o}(\omega \, k_a)|^2 \frac{dk_a}{2\pi} \tag{5.49}$$

We can determine the output noise power by an integration over the sphere or disk of radius $2\pi/\lambda$ and an integration over k_a. The most important consideration is that if we tailor the sidelobe structure to minimize the first component, we increase the second component due to the white noise. If we have only sensor noise present, we know from Section 4 that the optimum beam pattern is

$$g(\omega : \underline{k} \, | \underline{k}_T) = \text{sinc} \left[(\underline{k} - \underline{k}_T) \cdot \underline{a}_a \frac{L}{2} \right] \tag{5.50}$$

This can be represented as indicated in Figure 5-21. The target has a wave number whose magnitude is $2\pi/\lambda$ and the beam pattern generates a main lobe of width 2 x $2\pi/L$.

We first examine what happens when we have a directional noise of level $S_{n_o}(\omega)$ and wave number $\underline{k}_n$ as illustrated in Figure 5-1. We want to minimize $\sigma_o^2(\omega : \underline{k}_T)$ which is given by

$$\sigma_o^2(\omega : \underline{k}_T) = S_{n_o}(\omega) | g_o(\omega : \underline{k}_n \cdot \underline{a}_a)|^2 + \frac{N_o}{2\pi} \int_{-\infty}^{\infty} | g_o(\omega : k_a)|^2 dk_a \tag{5.51}$$

We have a trade-off to make; we want to make the array response as small as possible in the response direction of the noise source, which can be done by null placement methods, for

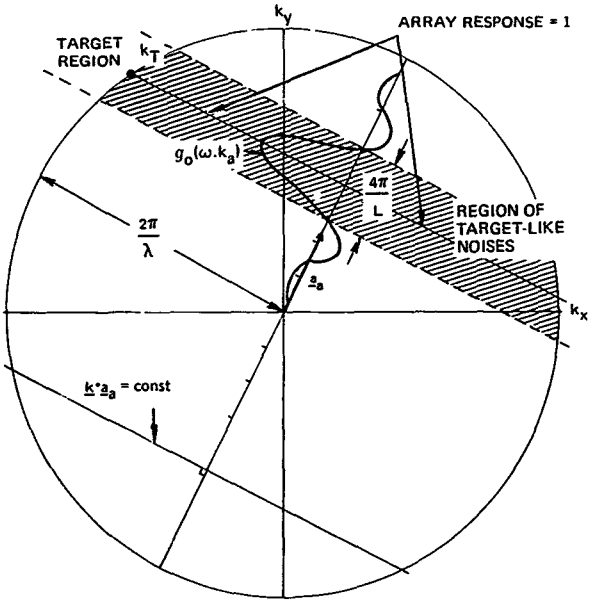

Figure 5-21. Optimum beam pattern with only sensor noise present.

this one would cancel the response in the noise direction with a beam of opposite sign. We cannot do this, however, in an arbitrary manner. Since array has finite length, we cannot realize an arbitrary $g(\omega:\underline{k})$. The sampling theorem says that on the average we can specify one sampled value per distance of $2\pi/L$ independent of the other samples and still realize the function with a finite length array. When we specify these points as $g\left(\omega.n\frac{2\pi}{L}\right)$, we can determine any intermediate values by the interpolation formula associated with the sampling theorem, i.e.,

$$g(\omega:\underline{k}|\underline{k}_T) = \sum_{n=-\infty}^{\infty} g\left(\omega:n\frac{2\pi}{L}\right) \operatorname{sinc}\left[(\underline{k}-\underline{k}_T)^*\underline{a}_a - n\frac{2\pi}{L}\right] \tag{5.52}$$

with

$$g(\omega:\underline{k}_T|\underline{k}_T) = 1$$

If we want to place a null in this beam pattern we must adjust the values $g\left(\omega\ n\frac{2\pi}{L}\right)$ To place a null for a single noise source, two situations can occur When the noise source is outside the main beam region the null can be placed by adjusting the $g\left(\omega\ n\frac{2\pi}{L}\right)$ nearest it so as to cancel the main beam response Only a modest value of $g\left(\omega\ n\frac{2\pi}{L}\right)$ is needed, since the main beam response is quite low Consequently, the added side lobe response is small If the noise source is inside the main beam, one must cancel a very large main beam response value. This requires a large value of the adjacent $g(\omega\ n)$ and as a result very large sidelobes are introduced. Both of these situations are illustrated in Figure 5-22. The amount of additional sidelobe response is the value expressed in Eq. 5.51 in terms of the effects background noise introduced. When noise single source is near the target, the response function appears to be displaced. The amount of displacement is governed by the ratio of directional to white noise and the proximity between the target and directional noise source This is the dominant effect with a single directional noise source

When several directional noise sources are present, the situation becomes more complicated. In adjusting the coefficients $g\left(\omega:n\frac{2\pi}{L}\right)$ we must consider not only the sidelobe level but also the mutual interference created by placing the various nulls If the sources are widely separated relative to the resolution of the array, the interference is minimal If they are not, we must determine the exact trade offs using our optimum array design procedures

For wave number fields which are not directional, the intuitive appeal of Eq. 5 51 is still useful Basically we attempt to minimize the overlap of the beam pattern and the wave number function for the noise field without undue effects from sensor noise As we will subsequently discuss, this minimization of the overlap can often be exploited in a manner unique to spatial processing. Essentially, for propagating signals, the maximum wave number for a given ω is ω/c, or $2\pi/\lambda$, and all propagating noise could be eliminated if the sidelobes were confined to a region

$$|k_a| > 2\pi/\lambda$$

In principle this can be done, however, it requires extremely large sidelobes for k_a outside this region. Since the output due to sensor noise still is affected in this region, the response becomes extremely noisy.

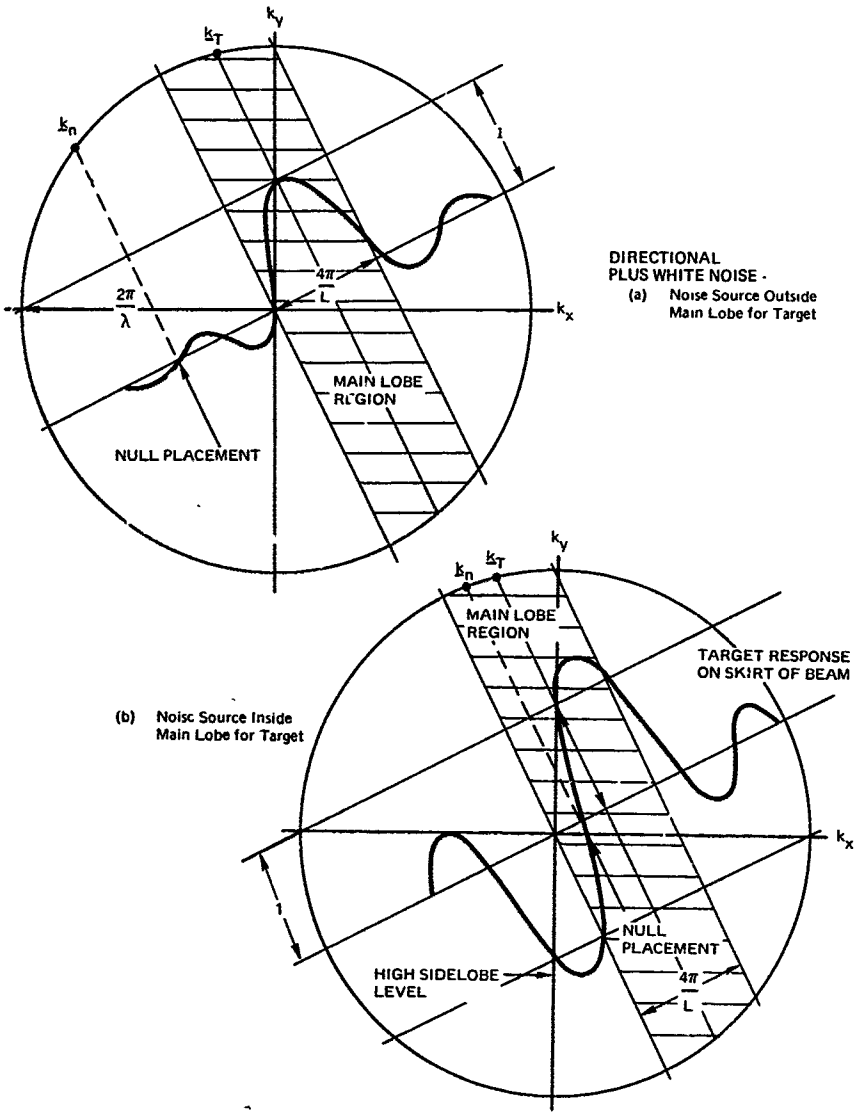

Figure 5-22. Null placement effects for optimum beam pattern design using frequency wave number methods.

5.4 LINEAR ARRAYS IN ISOTROPIC (OR OMNIDIRECTIONAL) NOISE

A common model for ambient noise of deep ocean noise is the isotropic noise field distribution discussed in Section 2.2. The spectral covariance function for the model is

$$S_n(\omega\ \Delta\underline{z}) = S_{n_o}(\omega)\ \text{sinc}\left(\frac{\omega}{c}|\Delta\underline{z}|\right) \tag{5 53}$$

Many beam patterns are designed, and the figures of merit attached to their performance are discussed in terms of their effectiveness in combatting this particular noise Unfortunately as we will see, using this noise field alone can be misleading for it is closely related to super-directivity and singularity issues it In this section, we briefly discuss how such noise fields can be incorporated in optimum array design by using results established in communication theory and electromagnetics. We also apply our frequency-wave-number analysis to discuss endfire gain in linear arrays. This same analysis extends to the nonuniform distributions of noise which we discussed in Section 2.2.

We consider the noise field to be composed of an isotropic and a white noise component such that

$$S_n(\omega:\Delta\underline{z}) = S_{n_o}(\omega)\ \text{sinc}\left(\frac{\omega}{c}|\Delta\underline{z}|\right) + N_o\,\delta_\Omega(\Delta\underline{z}) \tag{5.54}$$

The frequency wave number function in three-dimensional space for isotropic noise consists of a sphere of impulses; however, when one integrates all those parts of the sphere which have the same wave number projection $\underline{k}\cdot\underline{a}_a$, a rectangular function of $\underline{k}\cdot\underline{a}$ results. Alternatively, the one-dimensional transform of Eq. 5.54 with respect to the spatial frequency as observed by the array, i.e., k_a, yields the distribution as shown in Figure 5-23.[1]

For a linear array, the integral equation that specifies the optimum array weighting (see Eq. 4.6) is

$$\int_{-L/2}^{L/2} S_{n_o}(\omega)\ \text{sinc}\left(\frac{\omega}{c}|\ell_1-\ell_1|\right) G_o(\omega:\ell_2|\underline{k}_T)\,d\ell_2 + N_o\,G_o(\omega:\ell_1|\underline{k}_T)$$

$$= \beta(\omega)\,e^{j\underline{k}_T\cdot\underline{a}_a\ell_1}, \quad |\ell_1| < L \tag{5.55}$$

$$P_{k_a}(\omega:k_a) = \int_{\infty}^{\infty}\left[S_{n_o}(\omega)\ \text{sinc}\left(\frac{2\pi}{\lambda}\ell\right) + N_o\delta(\ell)\right]e^{jk_a\ell}\,d\ell,$$

---

[1] *Note that the linear array allows introducing the sensor noise in terms of an effective wave number k_a*

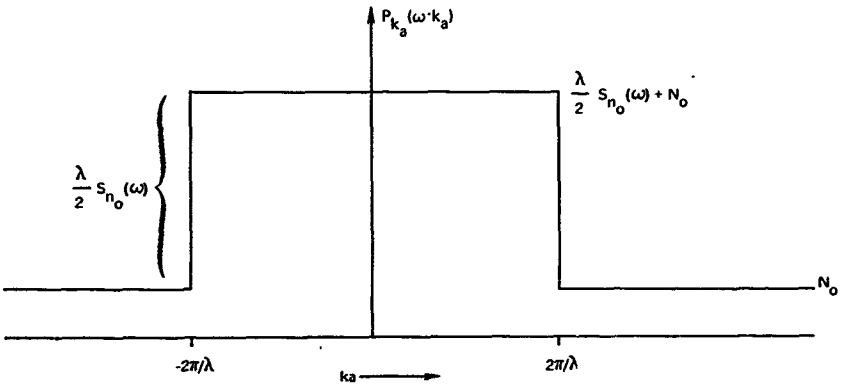

Figure 5-23. Distribution of noise power versus k_a, the effective wave number across the array.

where $\beta(\omega)$ is a normalizing constant for unity gain at $\underline{k}=\underline{k}_T$. The solution of this integral equation can be expressed in terms of the spatial eigenvalues and eigenfunctions of the homogeneous integral equation associated with the temporal frequency-spatial covariance of the isotropic noise. For this particular kernel, the prolate spheriodal wave functions specify the basis for the solutions. When one maps the parameters of the prolate spheroidal wave functions to the array design problem considered here, there are $2L_\lambda + 1$ significant eigenvalues. As an indication of this behavior, Figure 5-24 illustrates the six most significant eigenvalues as a function of array length L. For $2L_\lambda > 1$ the eigenfunctions resemble sinusoids where the spatial frequency separations is $\frac{1}{L}$.

If we denote the eigenvalues as $\gamma_n(\omega)$ and the eigenfunctions as $\Phi_n(\omega:\ell)$, the optimum array beam pattern is, using Eqs. 4.12d and 4.15,

$$g_o(\omega:\underline{k}|\,\underline{k}_T) = \sigma_o^2(\omega|\,\underline{k}_T)\cdot$$

$$\cdot\left[\sum_{n=1}^{\infty}\int_{-L/2}^{L/2} e^{-j\underline{k}\cdot\underline{a}_a\ell_1}\phi_n(\omega.\ell_1)d\ell_1\int_{-L/2}^{L/2}\phi_n^*(\omega:\ell_2)e^{j\underline{k}_T\cdot\underline{a}_a\ell_2}d\ell_2\Big/\left(\gamma_n(\omega)+N_o\right)\right], \tag{5.56a}$$

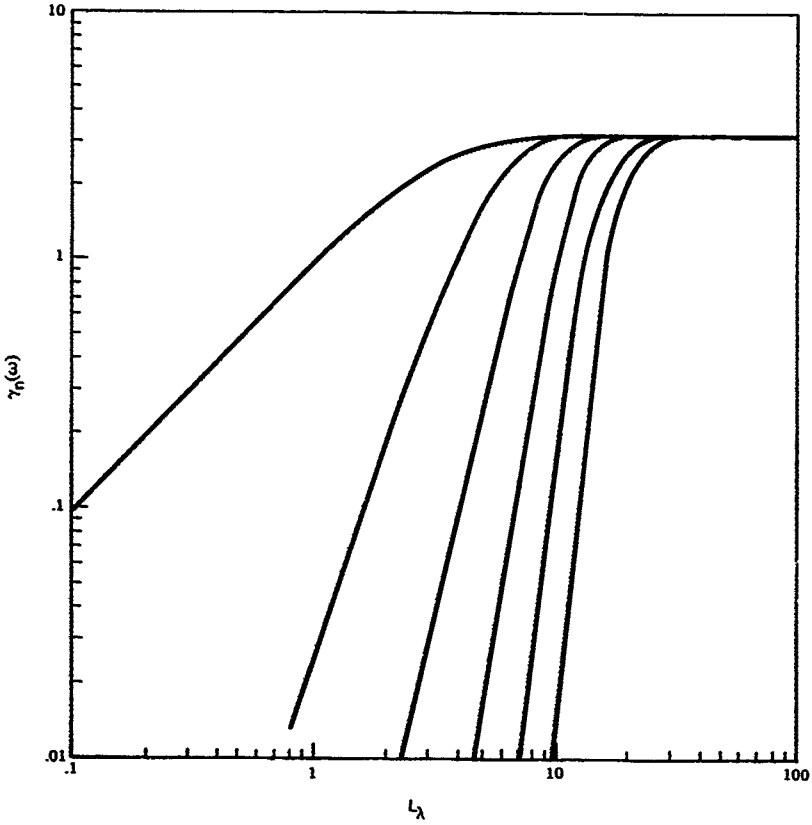

Figure 5-24. $\gamma_n(\omega)$ vs L_λ:m = 1, 2, . . . , 6 for isotropic noise (from Ref. 3)

where the performance as encompassed by the output noise power is

$$\sigma_o^2(\omega\,|k_T) = \left[\sum_{n=1}^{\infty} \int_{-L/2}^{L/2} \frac{\left| e^{-j\underline{k}_T\cdot\underline{a}_a \ell}\, \phi_n(\omega:\ell)d\ell \right|^2}{\gamma_n(\omega) + N_o}\right] \qquad (5\ 56b)$$

When the array length L_λ exceeds unity, the eigenfunctions approach a sinusoid harmonically related at a fundamental $2\pi/L$. Switching to a complex exponential representation for the sines and cosines we then have

$$\sigma_o^2(\omega\ \underline{k}_T) \simeq \left[L \sum_{n=-\infty}^{\infty} \frac{\operatorname{sinc}^2\left[\left(\underline{k}_T\cdot\underline{a}_a - \frac{2n\pi}{L}\right)\frac{L}{2}\right]}{\gamma_n(\omega) + N_o}\right]^{-1} = \frac{N_o}{L}\left[1 + L_\lambda P_{k_a}(\omega\ k_{T_a})\right] \qquad (5.57)$$

$$\simeq \begin{cases} \dfrac{N_o}{L}\left(1 + \dfrac{\lambda}{2}\dfrac{S_{n_o}(\omega)}{N_o}\right), & |\underline{k}_T\cdot\underline{a}_a| < 2\pi/\lambda \\ \dfrac{N_o}{L}\left(1 + \dfrac{\lambda}{4}\dfrac{S_{n_o}(\omega)}{N_o}\right), & |k_T\cdot\underline{a}_a| \simeq 2\pi/\lambda \text{ (endfire)} \\ \dfrac{N_o}{L}, & |\underline{k}_T\cdot\underline{a}_a| \text{ beyond region of propagating targets} \end{cases}$$

This represents the approximate performance of both the conventional and the optimum arrays. It is only in regions where the isotropic noise is dominant that the optimum array can achieve somewhat superior performance by displacing the main lobe into a region with $\underline{k}\cdot\underline{a}_a > \frac{2\pi}{\lambda}$, where only the white noise is present. This is an example of how a superdirective beam is formed.

In Figure 5-25 we have illustrated the performance found by solving Eq. 5.55. We have also indicated the results indicated by the approach discussed above for $L_\lambda > 1$. The arrays show a gradual decrease noise power output at endfire. This decrease can be interpreted as putting

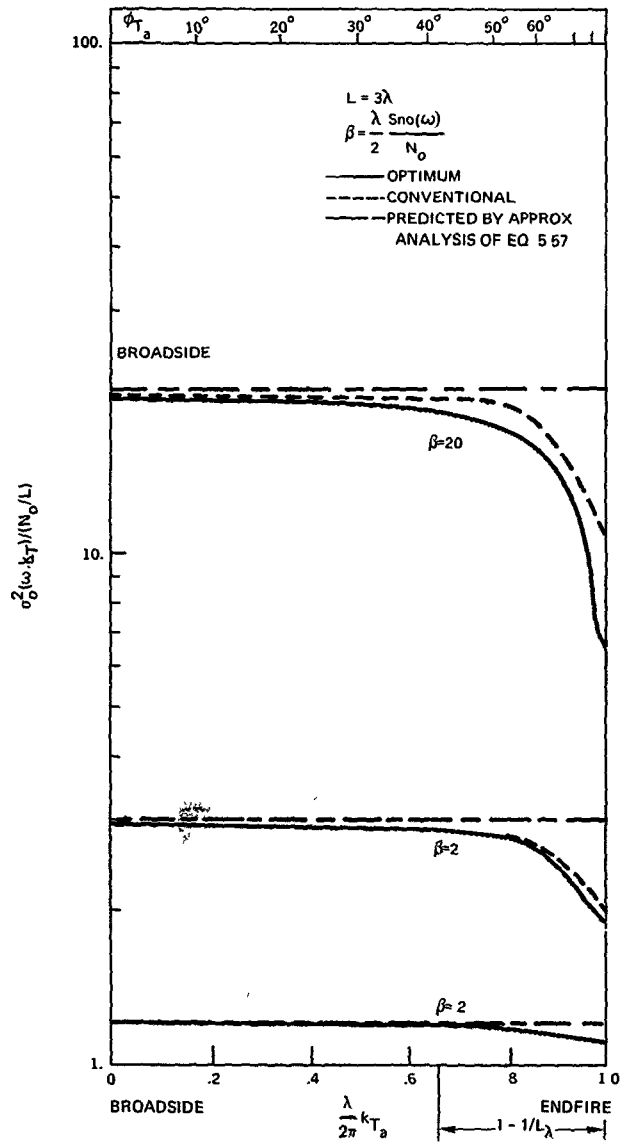

Figure 5-25. Output noise for a linear array (L_λ=3) operating in isotropic plus sensor noise.

the array wave number response in a region where the frequency wave number spectrum of the noise is lower The conventional array performs almost exactly as predicted by the large array approximation, while the optimum array displays an improved performance for the high isotropic noise case. This can be attributed to superdirective effects.

The presence of high endfire gains has been observed by several people, while the discussion by Vanderkulk [25] is best known, the first observation was by Schellkenoff [26] A report by Schulteiss [27] is notable because it has several sets of figures Its equivalent in signal design for temporal signals apparently has not been discussed.

If we examine Figures 5-26 and 5-27, the optimum beam patterns for operating in an isotropic noise environment, we observe that when the target is broadside the beam pattern has a conventional shape. In the case of very high isotropic noise, the beam is slightly displaced into a region of nonpropagating or sensor noise only. Again we observe that optimum processing offers substantial improvement when one can place part of the beam pattern in a wave number region where there is a lower noise level and yet satisfy the constraint of having a unity response in the target direction.

We can interpret high endfire gain for isotropic noise directly in terms of three-dimensional frequency wave number concepts. This interpretation also predicts the occurrence of similar behavior for other types of noise fields. In Figure 5-28 we have indicated the frequency wave number function of isotropic noise as distributed on a sphere of radius $2\pi/\lambda$. According to our intuitive wave number analysis, there is a strip of width $2 \times 2\pi/L$ representing the main lobe of the beam in the target direction. For broadside beams this strip intersects a ring-shaped region whose approximate area is $\frac{4\pi}{L} \times 2\pi \times \frac{2\pi}{\lambda}$, as indicated by target location on Figure 5-28 At endfire the region has a shape of a cap whose area is $\pi \left[\frac{2\pi}{\lambda}\sqrt{\frac{2\lambda}{L}}\right]^2$, as indicated by location B. The intersected area of the endfire region is half that of the broadside region. The gain can be additionally enhanced by displacing the lobes outside the sphere and increasing its gain. If the noise does not have the uniform distribution of isotropic noise, the intersected regions must be weighted appropriately. For example, if there is a high noise component normal to the array, the endfire performance will be enhanced. Such would be the case for a vertical array in a noise field such as that shown in Figure 2-8. Conversely, the high layer noise of Figure 2-4 would reduce endfire effects of the array performance. Some typical results for noise fields with nonuniform distributions are indicated in Figures 5-29 through 5-32.

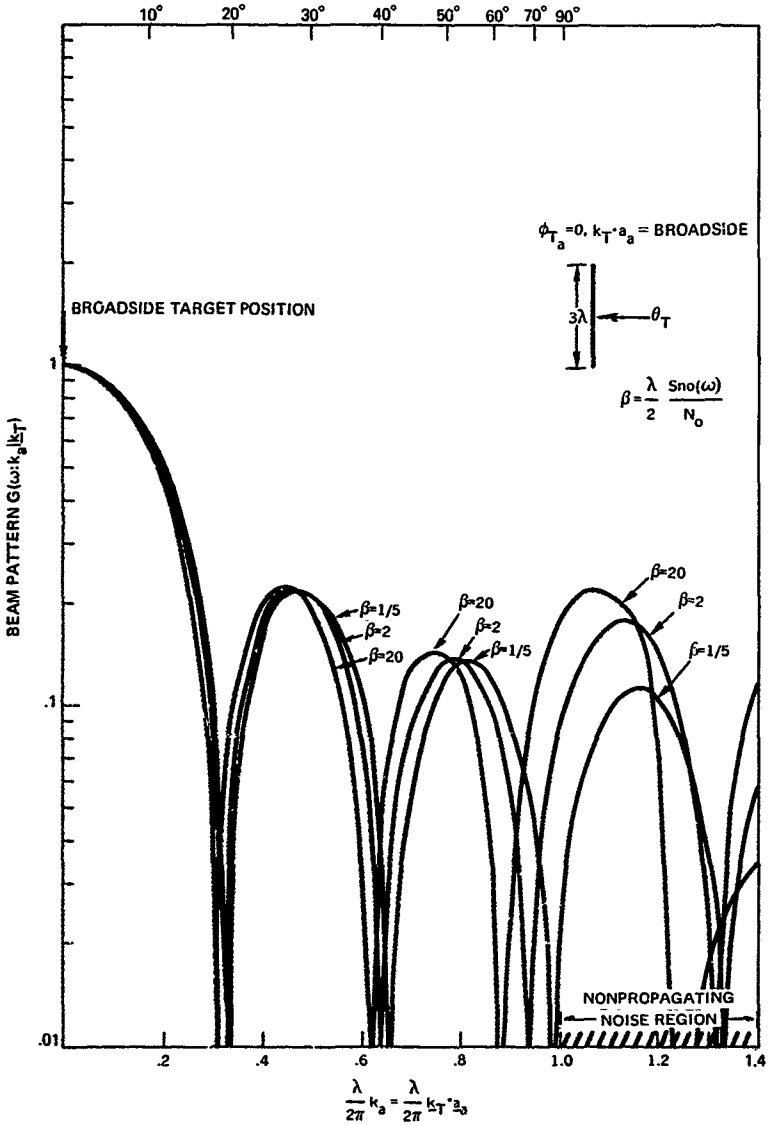

Figure 5-26 Beam pattern for a linear array operating in isotropic noise field, broadside target location

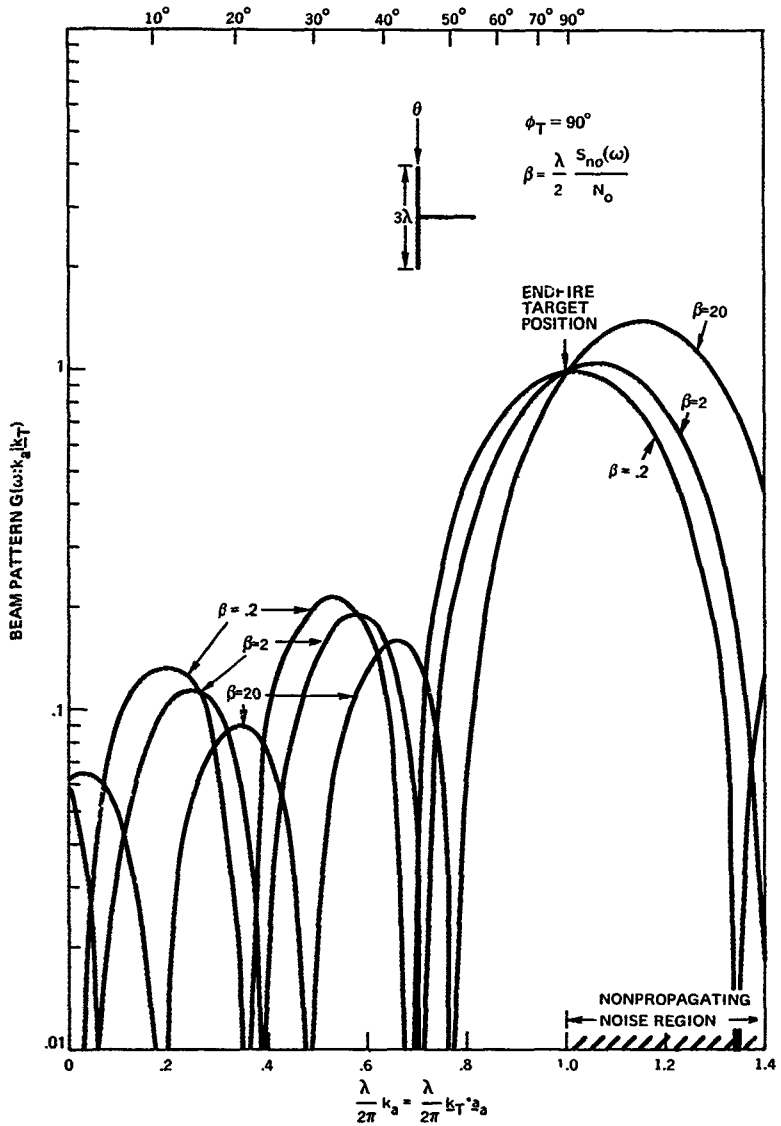

Figure 5-27. Optimum beam pattern for a linear array operating in isotropic noise.

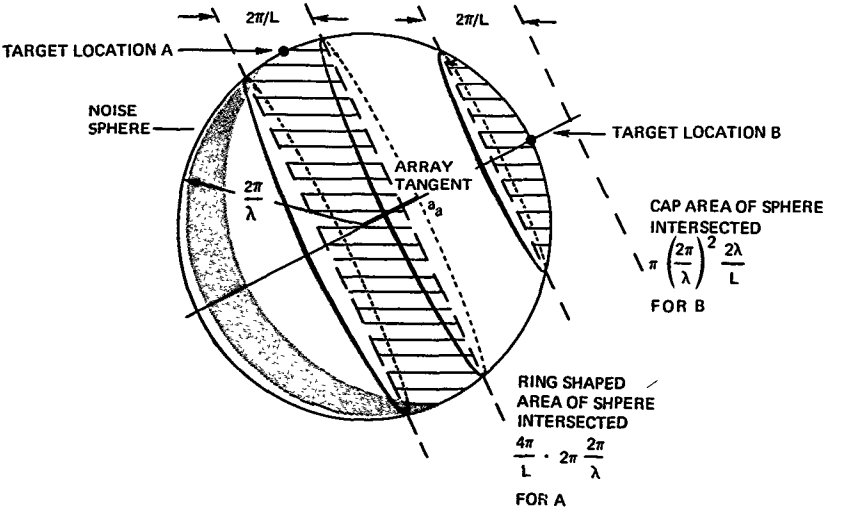

Figure 5-28. Approximate three-dimensional wave number analysis of endfire gain.

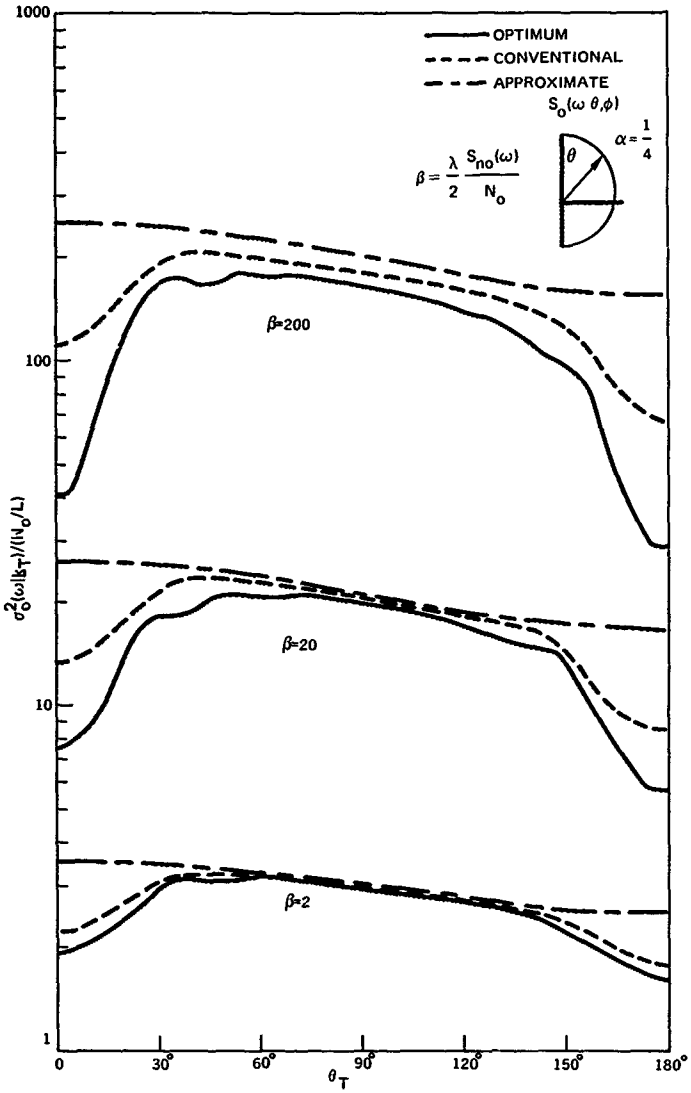

Figure 5-29. Output noise power for a 3λ vertical linear array in low-surface noise environment (see Figure 2-4)

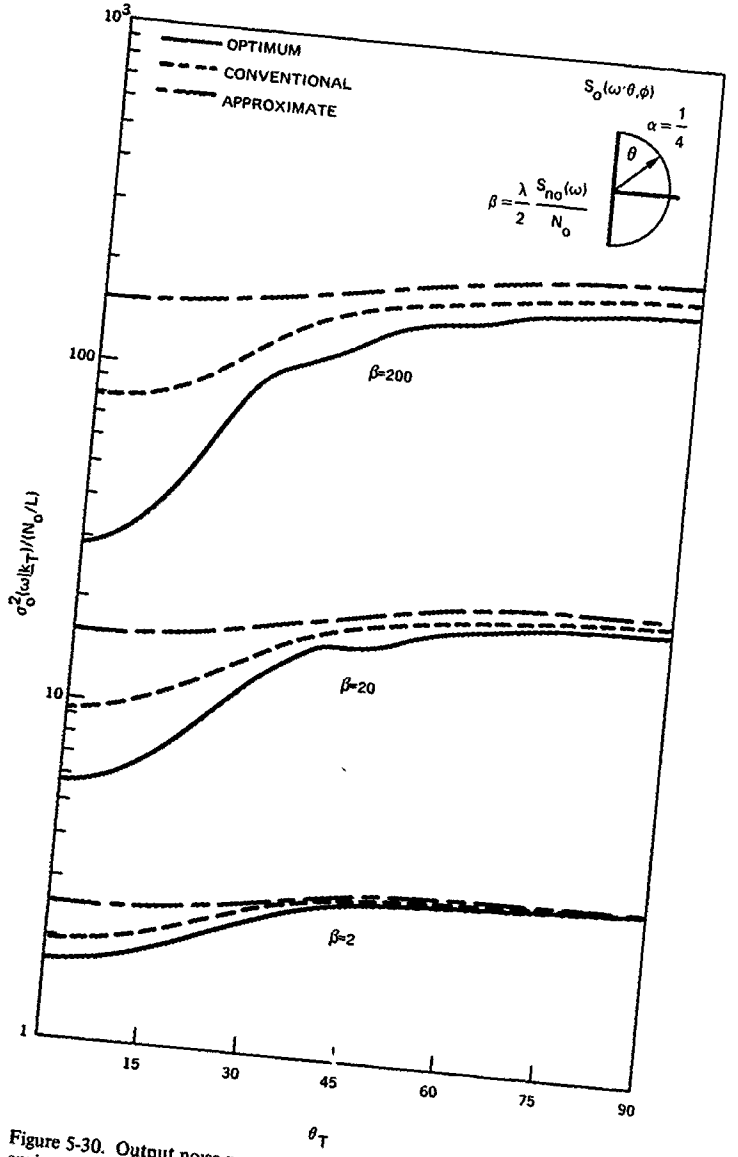

Figure 5-30. Output noise power for a 3λ vertical linear array in low-layer noise environment (see Figure 2-6)

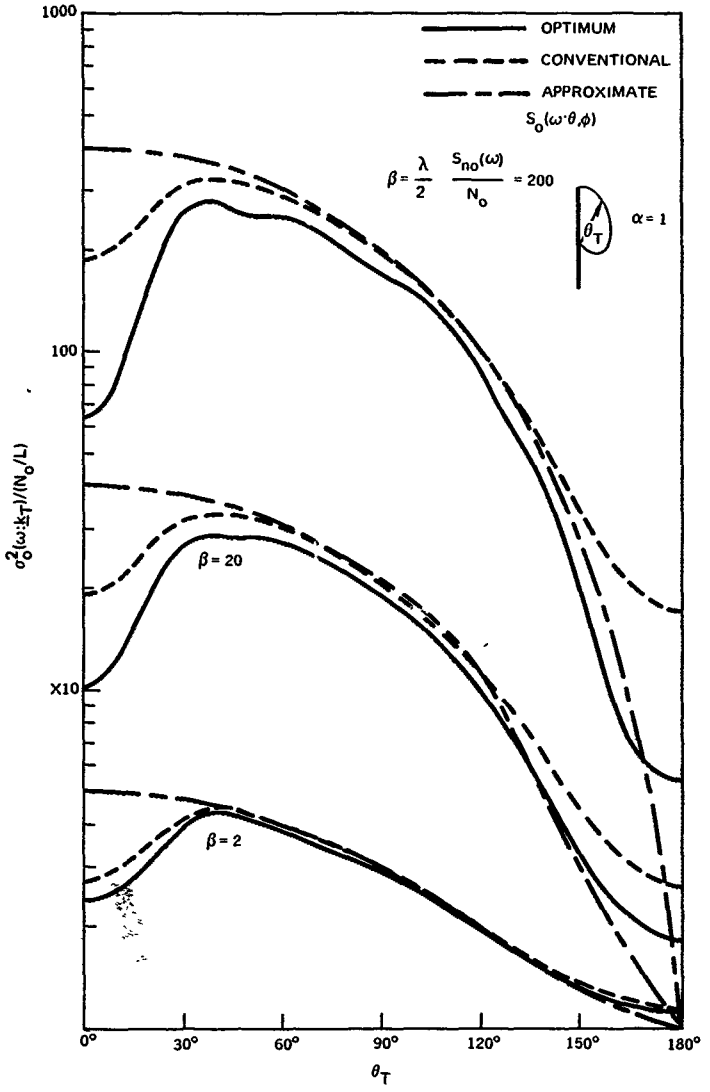

Figure 5-31. Output noise power for a 3λ vertical linear array in high-surface noise environment (see Figure 2-4).

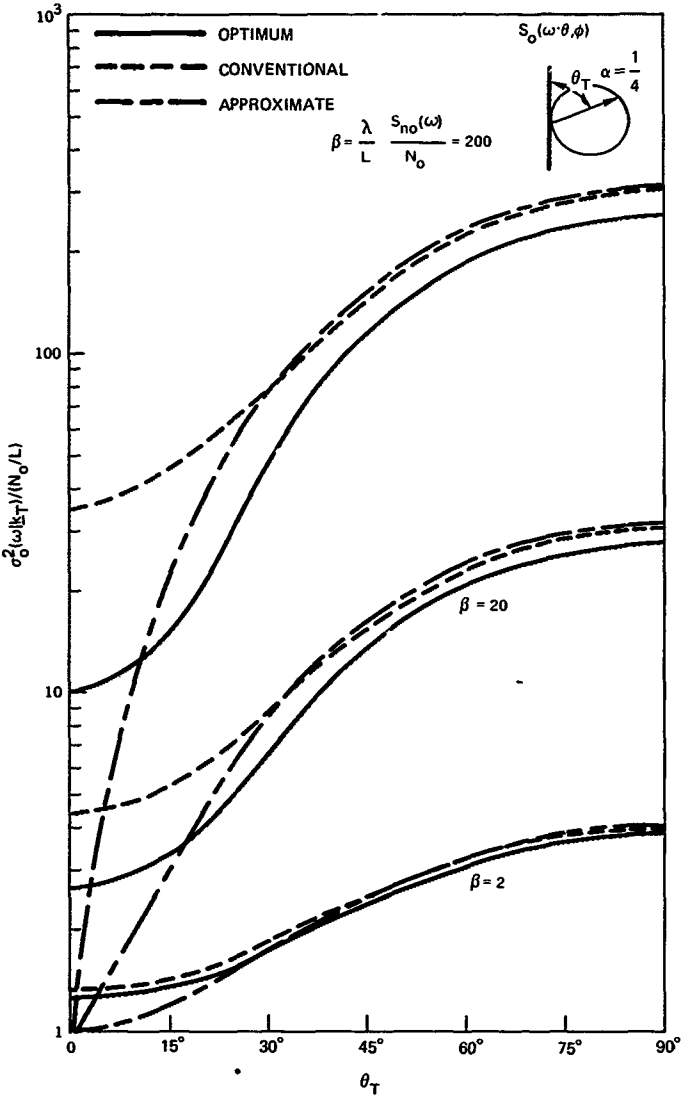

Figure 5-32 Output noise power for a 3λ vertical array in high-layer noise environment (see Figure 2-6)

5.5 SUPERDIRECTIVE LINEAR ARRAYS

Superdirective arrays have a long and rather interesting history The work on them has been motivated by the apparent ability to achieve very small beamwidths with finite length apertures. One of the first to recognize their existence and properties was Schelkunoff [26] in his algebraic theory of linear arrays They have also been extensively discussed in electromagnetics, where the problems inherent in their realization have been investigated Several synthesis procedures are related to superdirective arrays, in particular those of Pritchard [28] and some aspects of Dolph-Tchebychev arrays They are also intimately related to singular detection theory which in itself has seen a long period of development [3] Quantitative results are hard to come by, however, the general principles about superdirectivity and its relation to singular detection can be understood quite intuitively

For purposes of illustration we use a linear array, although there exist examples where other types of arrays, e g., circular, where similar approaches have been used If we have an array of length L oriented with an array tangent $\underline{a}_a$, its frequency wave number response, in principle, extends to all spatial frequencies If one considers the response to plane wave signals in a medium with finite propagation velocity, then the incident wave numbers, or spatial frequencies, are limited in magnitude to $|\underline{k}| < \frac{\omega}{c} = \frac{2\pi}{\lambda}$ The response outside this range is theoretically arbitrary. For a superdirective array, the wave-number response in this region is manipulated such that within the range $|\underline{k}| < \frac{2\pi}{\lambda}$ it has a very narrow beamwidth

We have pointed out the difficulty with this in a practical system, the narrow beamwidths are created by generating extremely large sidelobes in the region $|\underline{k}| > \frac{2\pi}{\lambda}$. If one investigates the beam pattern, or wave number response, by plotting it versus ϕ, these sidelobes never appear. Sensor noise, however, does not have a propagating structure but has an equivalent wideband wave number spectrum which can extend well beyond the limit on propagating limit of $|k| < 2\pi/\lambda$ Consequently, it enters through in these large sidelobes as we can see from the second term in Eq 5.51.

We can indicate some superdirective effects for a half wave length array by designing a beam which has half the width of a conventional pattern We use the procedure of Section 5.2 and let $N_o \to 0$, or $\beta \to \infty$. This yields

$$g(\omega, \underline{k}\,|\underline{k}_T) = C\left[\operatorname{sinc}\left[(\underline{k}-\underline{k}_T)\cdot\underline{a}_a\,\frac{L}{2}\right]\right.$$

$$\left.-\frac{2}{\pi}\left(\operatorname{sinc}\left[\left(\underline{k}-\underline{k}_T-\underline{a}_a\frac{\pi}{L}\right)\cdot\underline{a}_a\,\frac{L}{2}\right]+\operatorname{sinc}\left[\left(\underline{k}-\underline{k}_T+\underline{a}_a\,\frac{\pi}{L}\right)\cdot\underline{a}_a\,\frac{L}{2}\right]\right)\right], \tag{5 58a}$$

where $$C = \left(1 - \frac{8}{\pi^2}\right)^{-1} = 5.33 \qquad (5\ 58b)$$

and $$\sigma_o^2(\omega \mid \underline{k}_T) \Rightarrow c\,\frac{N_o}{L} \Rightarrow 0 \qquad (5\ 58c)$$

The beam pattern is indicated in Figure 5-33. The beam pattern is indeed narrower, but large sidelobes are created. These are outside the region of propagating noise, so that they would not be observed in a normal plot of response versus angle When it is plotted versus the wave number, however, they are very evident.

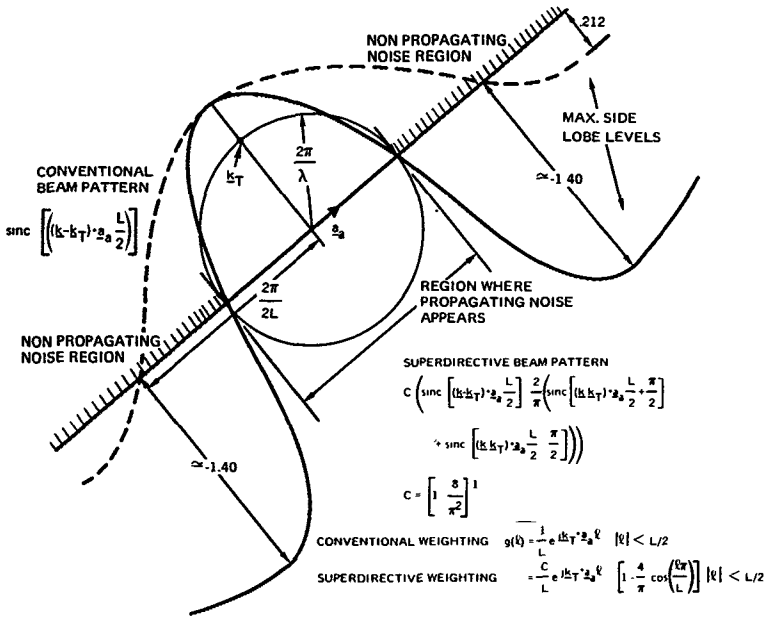

Figure 5-33. Example of a superdirective half wavelength array

If we compare the output noise level of the superdirective array to that of a conventional array, we find that the ratio of the ratio is

$$\frac{1 + 16/\pi^2}{1 - 8/\pi^2} \simeq 13.6$$

The superdirective array is much more sensitive to sensor noise

The optimum design of superdirective arrays is not, surprisingly, closely related to the optimum processing methods that we have been considering Also, this illustrates the connection between superdirectivity and problems in singular detection theory An ideal array would have a unity response.[1]

$$g_\ell(\omega \cdot k_a) = \begin{cases} \delta(k_a - T_a), & |k_a| \leq 2\pi/\lambda \\ g_s(\omega\ k_a), & |k_a| > 2\pi/\lambda \end{cases} \qquad (5\ 59)$$

For an array of length L we want the transform of this response to have the form

$$G_\ell(\omega\ \ell) = \begin{cases} \text{finite}, & |\ell| \leq L/2 \\ 0, & |\ell| > L/2 \end{cases} \qquad (5.60)$$

We have

$$G_\ell(\omega{:}\ell) = e^{-jk T_a \ell} + \int_{|k_a| > 2\pi/\lambda} g_s(\omega.k_a)\ e^{-jk_a \ell}\ \frac{dk_a}{2\pi} \qquad (5\ 61)$$

or

$$G_\ell(\omega{:}\ell) = e^{-jk T_a \ell} + G_\ell(\omega{:}\ell) * \left[\delta(\ell) - \frac{\lambda}{2}\ \text{sinc}\left(\frac{2\pi\ell}{\lambda}\right)\right]$$

This yields

$$\frac{\lambda}{2}\int_{-L/2}^{L/2} d\ell_2\ \text{sinc}\left[\frac{2\pi}{\lambda}\ (\ell_1 - \ell_2)\right] G_\ell(\omega\ \ell_2) = e^{-jk T_a \ell},$$

$$L/2 < \ell_1 < L/2 \qquad (5.62)$$

This is the integral equation which we would obtain if we posed the optimum detection problem of detecting a plane wave signal in the presence of isotropic noise alone, with no white noise present Such an integral equation is a Fredholm equation of the first kind, and the general solution has singularity functions appearing at the end points of the observation interval for

---

[1] *As noted earlier this value of unity near the target direction must yield a nonzero finite measure when integrated in a region "near" it*

temporal processes or at the aperture extremities for spatial processes One can specify a formal solution in terms of the solutions of the homogeneous equation—the prolate spheroidal wave functions; however the resulting series does not converge, in general, to well-defined functions

The essential points to be made regarding superdirective arrays are

1. They are primarily a mathematical issue since the effects of inter-element coupling and the sensitive adjustments required cannot be controlled precisely enough to implement them practically

2. Their sensitivity is closely coupled to singular detection and is of interest as a limiting situation when the white noise in a system becomes small

3. They are only effective across narrow frequency bands since the aperture phasing is coupled to the wavelength specification.

4 Their response should be determined for all wave numbers, not simply as a function of the incident bearing angle

6. OPTIMUM ARRAY PROCESSING FOR DIRECTIONAL NOISE FIELDS

Noise fields that consist of a finite number of directional sources plus a white component can be analyzed exactly. The final results require knowledge of $\text{sinc}_{\Omega}(k)$, the conventional wave number response of the array, the correlation, if any, among the noise sources, and a matrix inversion Since we have observed in Section 3.6 that directional noise field has a finite number of nonzero eigenvalues, we should be able to specify the solution in terms of a set on linear equations

The noise field has the temporal frequency spatial covariance function

$$S_n(\omega:\underline{z},\underline{\xi}) = \sum_{i=1}^{N}\sum_{j=1}^{N} e^{j\underline{k}_i\cdot\underline{z}} S_{ij}(\omega)\, e^{-j\underline{k}_j\cdot\underline{\xi}} + N_o\,\delta_{\Omega}(\underline{z}-\underline{\xi}), \qquad (6.1)$$

where $S_{ij}(\omega)$ represents the correlation among the various directional components Note that if we require the directional noise to form a homogeneous field, then homogeneity requires that plane waves with different wave numbers be uncorrelated. For convenience in the subsequent discussion, we define $[S(\omega)]$ to be the matrix whose elements are $S_{ij}(\omega)$. In addition, we define the propagation vector $e^{j\underline{k}_n\cdot\underline{z}}$ to be

$$\underline{e}^{j\underline{k}_n \cdot \underline{z}} = \begin{bmatrix} e^{j\underline{k}_1 \cdot \underline{z}} \\ \vdots \\ e^{j\underline{k}_i \cdot \underline{z}} \\ \vdots \\ e^{j\underline{k}_N \cdot \underline{z}} \end{bmatrix} , \tag{6.2}$$

where the $\underline{k}_i$ are the wave numbers for the various noise components. Consequently, we can express Eq. 6.2 as

$$S_n(\omega:\underline{z},\underline{\zeta}) = \underline{e}^{-j\underline{k}_n \cdot \underline{z}^\dagger} [S(\omega)] \, \underline{e}^{-j\underline{k}_n \cdot \underline{\zeta}} + N_o \, \delta_\Omega (\underline{z}-\underline{\zeta}) \tag{6.3}$$

To determine the wave number response and the output power, we must find the inverse kernel across the aperture Ω. We appeal to a functional analog of the following matrix inverions lemma

$$[\underline{u}^T \underline{v} + \underline{A}]^{-1} = \underline{A}^{-1} - \underline{A}^{-1}\underline{u}^T [\underline{I} + \underline{v}\underline{A}^{-1}\underline{u}^T]^{-1} \underline{v}\, \underline{A}^{-1} ,$$

where $\underline{A}$ is N X N, and $\underline{u}$ and $\underline{v}$ are M X N. We identify $\underline{A}$ as $N_o \, \delta_\Omega (\underline{z}-\underline{\zeta})$, while $\underline{u}$ and $\underline{v}$ are replaced by, respectively, $\underline{e}^{-j\underline{k}_n \cdot \underline{z}}$ and $[S(\omega)]\underline{e}^{-j\underline{k}_n \cdot \underline{\zeta}}$. The spaces of concern are Ω X Ω and Ω X R_N. We have for the inverse kernel

$$Q_n(\omega:\underline{z},\underline{\zeta}) = \frac{1}{N_o} \, \delta_\Omega (\underline{z}-\underline{\zeta})$$

$$- \frac{\underline{e}^{-j\underline{k}_n \cdot \underline{z}^\dagger}}{N_o} \left[I_N + A_\Omega \, \frac{[S(\omega)]}{N_o} \, [\rho_\Omega] \right]^{-1} \frac{[S(\omega)]}{N_o} \, e^{-j\underline{k}_n \cdot \underline{\zeta}} , \tag{6.4}$$

where we define

$$[\rho_\Omega] = \begin{bmatrix} 1 & \mathrm{sinc}_\Omega(\underline{k}_1-\underline{k}_2) & \mathrm{sinc}_\Omega(\underline{k}_1-\underline{k}_3) & \cdots \\ \mathrm{sinc}_\Omega(\underline{k}_2-\underline{k}_1) & 1 & & \\ \mathrm{sinc}_\Omega(\underline{k}_3-\underline{k}_1) & & & \\ \vdots & & & 1 \end{bmatrix} \tag{6.5}$$

(The term $[\rho_\Omega]$ is identical to the term $[\mathrm{sinc}_\Omega(\delta)]$ used in Eq 3 57c) This matrix reflects the mutual interference of the various noise sources as observed across the aperture

The output noise power as a function of the target direction follows from Eq. 4 17 as

$$\sigma_o^2(\omega\,|\underline{k}_T) = \frac{A_\Omega}{N_o} - \frac{A_\Omega \underline{\rho}_n^\dagger(\underline{k}_T)}{N_o}\ \underline{I}_N + A_\Omega \frac{[S(\omega)]}{N_o}\ [\rho_\Omega]^{-1} \frac{[S(\omega)]}{N_o}\ \underline{\rho}(\underline{k}_T)^{-1}, \tag{6 6a}$$

where

$$\underline{\rho}_N(\underline{k}) = \begin{bmatrix} \mathrm{sinc}_\Omega(\underline{k}-\underline{k}_1) \\ \mathrm{sinc}_\Omega(\underline{k}-\underline{k}_2) \\ \cdot \\ \cdot \\ \cdot \\ \mathrm{sinc}_\Omega(\underline{k}-\underline{k}_N) \end{bmatrix} \tag{6 6b}$$

This can be simplified considerably; the final expression is

$$\sigma_o^2(\omega\,|\underline{k}_T) = \frac{N_o}{A_\Omega}\ \left[1 - \mathrm{Tr}([\beta]\ \underline{\rho}(\underline{k}_T)\ \underline{\rho}^\dagger(\underline{k}_T)\ [I_N + [\beta]\ [\rho_\Omega]]^{-1})\right]^{-1}, \tag{6.7a}$$

where

$$[\beta] = \frac{A_\Omega[S(\omega)]}{N_o} \tag{6 7b}$$

This is the same form we had for the single noise source case. The limiting performance, or lowest noise level, is given by N_o/A_Ω, while any increase in the noise output level enters in the form of

$$\sigma_o^2(\omega\,|\underline{k}_T) = \frac{N_o/A_\Omega}{1-\alpha}, \tag{6 8a}$$

where

$$\alpha = \mathrm{Tr}\left([\beta]\ \underline{\rho}_N(\underline{k}_T)\ \underline{\rho}_N^T(\underline{k}_T)\ (I_N + [\beta]\ [\rho_\Omega])^{-1}\right), \tag{6.8b}$$

For a conventional wave vector response, we obtain

$$\sigma_c^2(\omega|\underline{k}_T) = \frac{N_o}{A_\Omega}\left\{1 + \mathrm{Tr}\left[[\beta]\ \underline{\rho}(\underline{k}_T)\ \underline{\rho}^T(\underline{k}_T)\right]\right\} \tag{6.9}$$

We can observe that the mutual interference is introduced via the term $[\rho_\Omega]$ in the optimum beam pattern output, whereas it is not included in the conventional processing

The optimum beam pattern follows directly from Eq. 6.4 using Eq 4 16 This yields

$$g(\omega:\underline{k}|\underline{k}_T) = \frac{\mathrm{sinc}_\Omega(\underline{k}-\underline{k}_T) - \mathrm{Tr}\left\{[\beta]\underline{\rho}_N(\underline{k}_T)\ \underline{\rho}_N^T(\underline{k})\ [I_N + [\beta]\ [\rho_\Omega]^{-1}\right\}}{1 - \mathrm{Tr}\left\{[\beta]\ \underline{\rho}_N(\underline{k}_T)\ \underline{\rho}_N^T(\underline{k}^T)\ [I_N + [\beta]\ [\rho_\Omega]^{-1}\right\}} \tag{6 10}$$

We have a conventional beam pattern and a term which introduces nulls in the direction of the various noise components.

We can completely analyze the optimum array performance for a source of arbitrary geometry operating in a directional noise field. Since we have introduced most of the intuitive concepts in our discussion of linear arrays, particularly null placement, we need not pursue this further. The major remaining issue is the effect of various array geometries

7. ARRAY GEOMETRIES IN HIGHER DIMENSIONS

The analysis of arrays with geometries that are more complex than linear generally becomes quite complicated. Since our primary consideration is the development of the major concepts that are involved in optimal array processing techniques, we have focused our attention upon linear arrays. The more tedious mathematical issues did not appear, yet we were able to analyze substantive examples illustrating the issues under consideration. In many respects, this is deceptively simple, in that added dimensions introduce unique problems and possibilities which have no direct temporal equivalent. This does not imply, however, that the introduction of more complex geometries changes the essential concepts we have developed Higher dimensional problems are sufficiently complicated such that any insights that can be drawn from simpler problems are valuable

In a discussion of optimum processing with more general array geometries, we cannot pursue as extensive an analysis as we did with linear arrays. There are simply too many combinations of array geometries and noise fields which rapidly reach a point of diminishing return once a few representative examples have been introduced We discuss some of the more

common geometries and then concentrate upon some representative examples of optimal processing and the limitations imposed upon it by various noise fields

To keep issues in perspective we point out that the only noise fields which can reasonably be analyzed are directional ones, and even these become quite complex for any more than two sources Exact analysis of fields with noise sources distributed in spatial wave number is impossible even for such a simple structure as isotropic noise The more complex geometries do not change these results. We have already done a complete analysis for the directional noise field and the only new issue is computing the $\text{sinc}_{\Omega}(\underline{k})$ function The exact analysis for distributed noise sources remains intractable, and we must still resort to approximate and/or asymptotic analysis

In the analysis of linear arrays we found that the important wave number was $\underline{k} \cdot \underline{a}_a$—the component of the wave number as projected upon the array tangent We are similarly concerned here with projections on a set of lines for crossed arrays, [illegible] for planar arrays. Just as for linear arrays, these projected wave numbers can be quit [illegible] calculating wave number responses

When dealing with white noise and frequency wave number issues one must be careful As before, we regard this class of noise as nonpropagating in origin and independent from point to point on the array This leads to a wave number representation which is flat where the array is capable of filtering and no definition for the entire wave number space is implied If the completely flat response for all wave number space is assumed, we are led to infinite noise power propagating through our spatial filters. This is not a very satisfactory model of a real array Essentially, we want the Parseval relation

$$N_o \int \cdot \int |g(\omega\ \underline{k}|^2 \frac{d\underline{k}}{(2\pi)^N} = N_o \int_{\Omega} G|(\omega\ z)|^2\ dz$$

In general this is <u>not</u> true, and only for those special cases in which we confine our integration to projected wave number components can we write relations of this form.

There are three situations of general interest in arrays with spatial extent of more than one direction · the target and any directional noise sources are near broadside, the target is broadside and significant components of the noise field propagate across the array, both the target and noise propagate across the array. Each introduces its particular set of considerations. Several typical cases are illustrated in Figure 7-1.

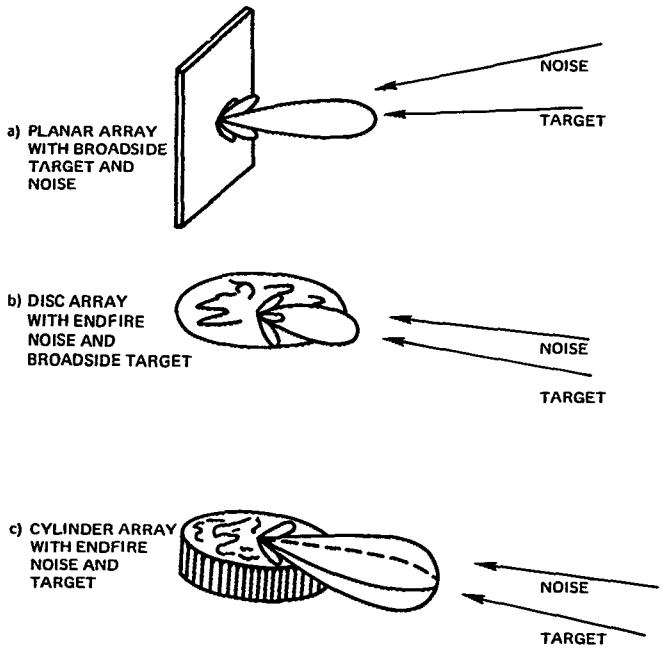

Figure 7-1. Typical array, target and noise geometries.

7.1 PLANAR ARRAYS

Planar arrays are the simplest two-dimensional array structures Our analysis of planar arrays is essentially the same as for linear arrays Figure 7-2 illustrates the array geometry under consideration, for convenience, we orient the array with a unit normal vector $\underline{a}_n$ and tangent vectors $\underline{a}_1$ and $\underline{a}_2$ (these are not necessarily orthogonal).

We can specify the array weighting pattern as a two-dimensional function

$$G(\omega:\underline{z}) = G(\omega.\ell_1\underline{a}_1, \ell_2\underline{a}_2), \quad |\ell_1| < \frac{L_1}{2}, |\ell_2| < \frac{L_2}{2} \tag{7.1}$$

We can attach all the common weightings or shadings as we did with the linear array for each coordinate ℓ_1 and ℓ_2, or we can specify more complex shadings with a function which need not factor. We consider some examples. For a target at $\underline{k}_T \cdot \underline{a}_1 = \underline{k}_T \cdot \underline{a}_2 = 0$ with conventional shading, $G(\omega\ \ell_1,\ell_2) = 1/L_1L_2$, or

$$g(\omega,\underline{k}) = \text{sinc}_{\Omega}(k) = \frac{1}{L_1 L_2} \int_{-L_1/2}^{L_1/2} \int_{-L_2/2}^{L_2/2} e^{j(\underline{k}\cdot\underline{a}_1 \ell_1 + \underline{k}\cdot\underline{a}_2 \ell_2}\, d\ell_1\, d\ell_2$$

$$= \text{sinc}\left(\underline{k}\cdot\underline{a}_1 \frac{L_1}{2}\right) \text{sinc}\left(\underline{k}\cdot\underline{a}_2 \frac{L_2}{2}\right) \tag{7.2}$$

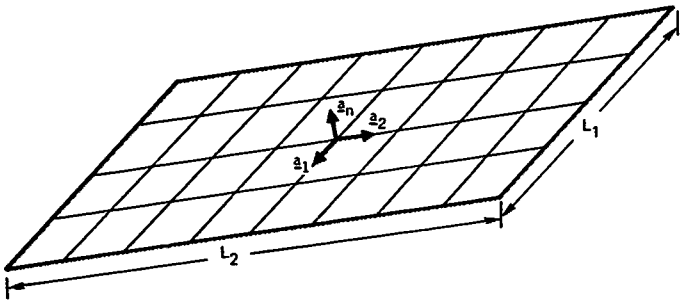

Figure 7-2. $L_1 \times L_2$ planar array with orientation $\underline{a}_1 \times \underline{a}_2 \propto \underline{a}_n$.

As we have seen, $\text{sinc}_{\Omega}(\underline{k})$ is important in our discussion of directional noise analyses and its form is sketched in Figure 7-3. Figure 7-4 is the beam pattern when the array response is presented in dimensionless units. If we examine the array pattern in Figure 7-3, we see that it has a resolution of $2\cdot(2\pi/L_1)$ in the $\underline{a}_1$ coordinate direction and $2\cdot(2\pi/L_2)$ in the $\underline{a}_2$ direction. The resolution cell has an area $(2\pi/L_1) \times (2\pi/L_2)$ in wave number space. The distribution of this area is determined by the orientation vectors $\underline{a}_1$ and $\underline{a}_2$.

A triangular shading in each direction produces a beam pattern of the form

$$g(\omega\ \underline{k}) = \text{sinc}^2\left(\underline{k}\cdot\underline{a}_1 \frac{L_1}{4}\right) \text{sinc}^2\left(\underline{k}\cdot\underline{a}_2 \frac{L_2}{4}\right) \tag{7.3}$$

We can also split the array such that

$$g(\omega\cdot\underline{k}) = \left\{F_1[(\underline{k}-\Delta\underline{k})\cdot\underline{a}_1] - F_1[-(\underline{k}+\Delta\underline{k})\cdot\underline{a}_1]\right\}$$
$$\cdot\left\{F_2[(\underline{k}-\Delta\underline{k})\cdot\underline{a}_2] - F_2[-(\underline{k}+\Delta\underline{k})\cdot\underline{a}_2]\right\}, \tag{7.4}$$

where F_1 and F_2 are the beam patterns on the array halves

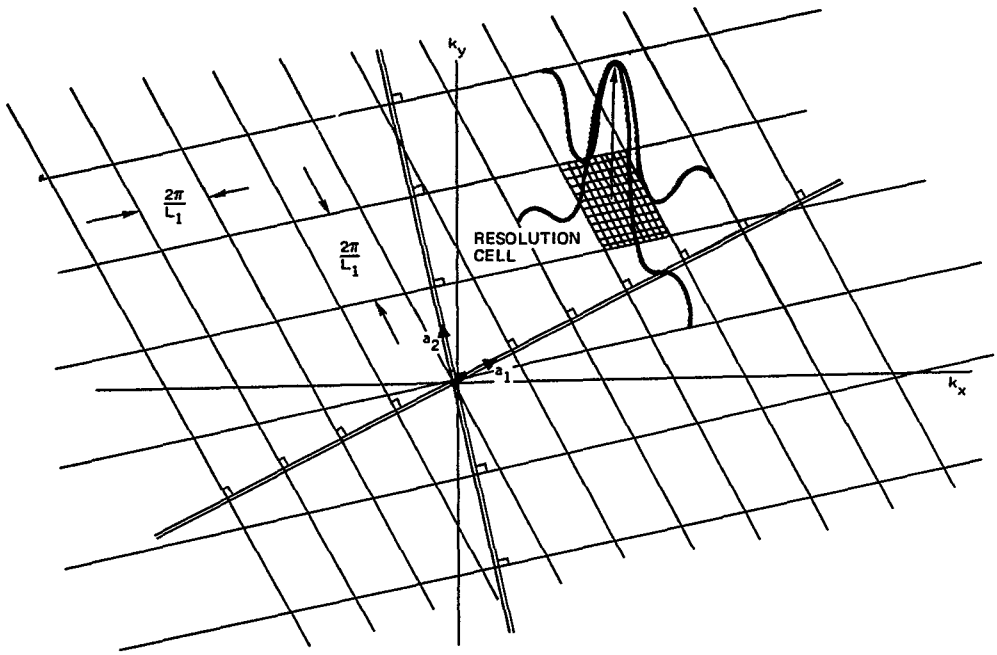

Figure 7-3. Wave number resolution of a planar array.

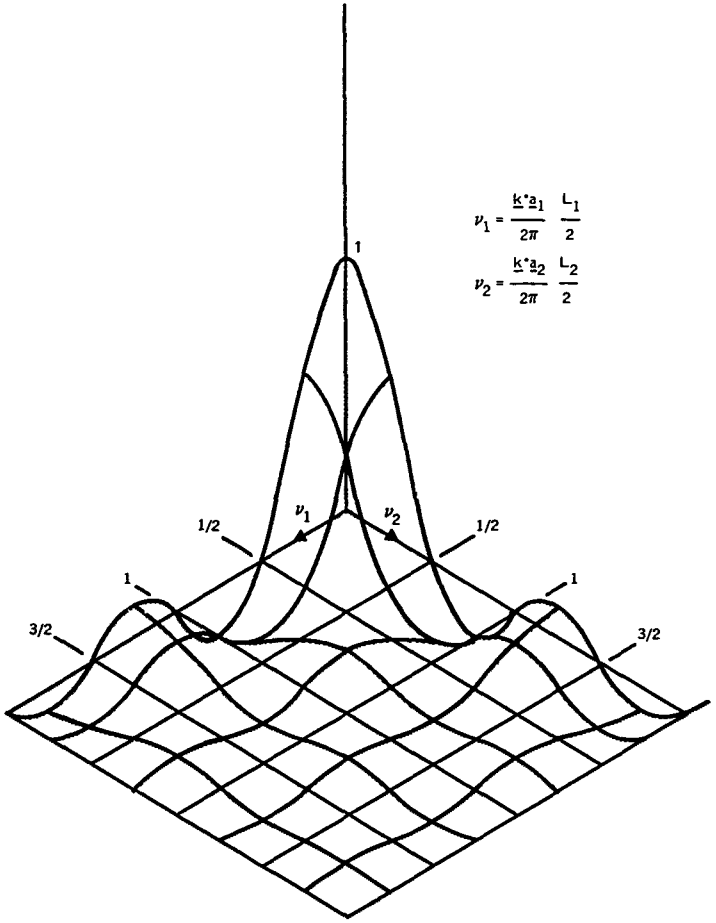

Figure 7-4. Beam pattern planar array sinc $(2\pi \nu_1)$ sinc $(2\pi \nu_2)$.

This beam pattern typically has a saddle point structure near the origin in wave number space where the cross defining the critical point locus of the saddle is along the vectors $\underline{a}_1$ and $\underline{a}_2$. We see that in this situation the generation of single beam is not a desirable processing method We need to generate two beam outputs, one for each coordinate direction in order to obtain our desired response for nulling at a particular point

The analysis for optimal processing in the presence of directional noise is substantially the same as for a linear array. The performance may be taken directly from Eq 6.8 as

$$\sigma_o^2(\omega\,|\,\underline{k}_T) = \frac{N_o}{L_1 L_2}\;\frac{1 + (L_1L_2/N_o)\,S_{n_o}(\omega)}{1 + (L_1L_2/N_o)\,S_{n_o}(\omega)\,(1-\mathrm{sinc}^2_\Omega(\underline{k}_T-\underline{k}_n))} \tag{7.5}$$

The beam pattern also follows directly from Eq. 6.10

$$g(\omega\ \underline{k}\,|\underline{k}_T) = \frac{\mathrm{sinc}_\Omega(\underline{k}-\underline{k}_T) - \mathrm{sinc}_\Omega(\underline{k}_T-\underline{k}_n)\,\mathrm{sinc}_\Omega(\underline{k}-\underline{k}_n)}{1 - \mathrm{sinc}^2_\Omega(\underline{k}_T-\underline{k}_n)} \tag{7.6}$$

In Figures 7-5 through 7-10 we indicate the performance for some typical noise geometries We observe the same effects that entered in our study of linear arrays Note the high sidelobe levels in the conventional versus the optimum processing The results when two directional sources are in the noise field are parallel to those for linear arrays.

For analyzing isotropic noise we encounter the same type of difficulties as in the linear case if we pursue an exact analysis. We can, however, pursue as approximate analysis. First, we need to find the asymptotic distribution of the eigenvalues for the isotropic noise kernel expanded over the aperture. The eigenfunctions will be spatial sinusoids. Asymptotically, the eigenvalues approach a skewed version of the two-dimensional wave number transform as the array extent increases. (We assume that the array is located in the (z_x, z_y) plane) We have from our previous results

$$P(\omega:\underline{k}) = \int_{-\infty}^{\infty}\int_{-\infty}^{\infty} S_{n_o}(\omega)\,\mathrm{sinc}\left[\frac{2\pi}{\lambda}\,|\underline{z}_a|\right]\,j\underline{k}\cdot\underline{z}_a\,dz_x dz_y$$

$$= \begin{cases} S_{n_o}(\omega)\;\dfrac{2}{\left(\dfrac{2\pi}{\lambda}\right)\sqrt{1-\left(\dfrac{\lambda|\underline{k}_a|}{2\pi}\right)^2}} & |\underline{k}_a| < \dfrac{2\pi}{\lambda} \\ 0 & |\underline{k}_a| > \dfrac{2\pi}{\lambda} \end{cases} \tag{7.7}$$

$$\underline{z}_a = z_x\underline{a}_x + z_y\underline{a}_y \qquad k_a = k_x\underline{a}_x + k_y\underline{a}_y$$

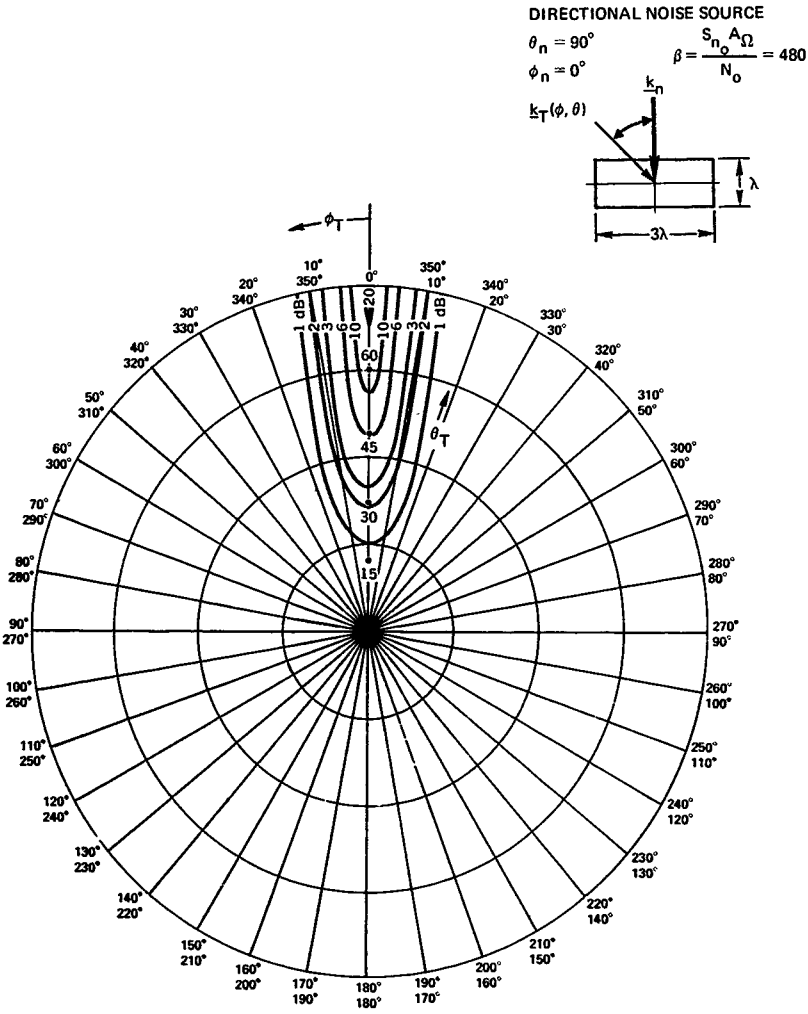

Figure 7-5. Contours (in dB) of noise power $\sigma_o^2(\omega:\underline{k}_T)$ relative to N_o/L_1L_2 for an endfire directional noise source optimum processing

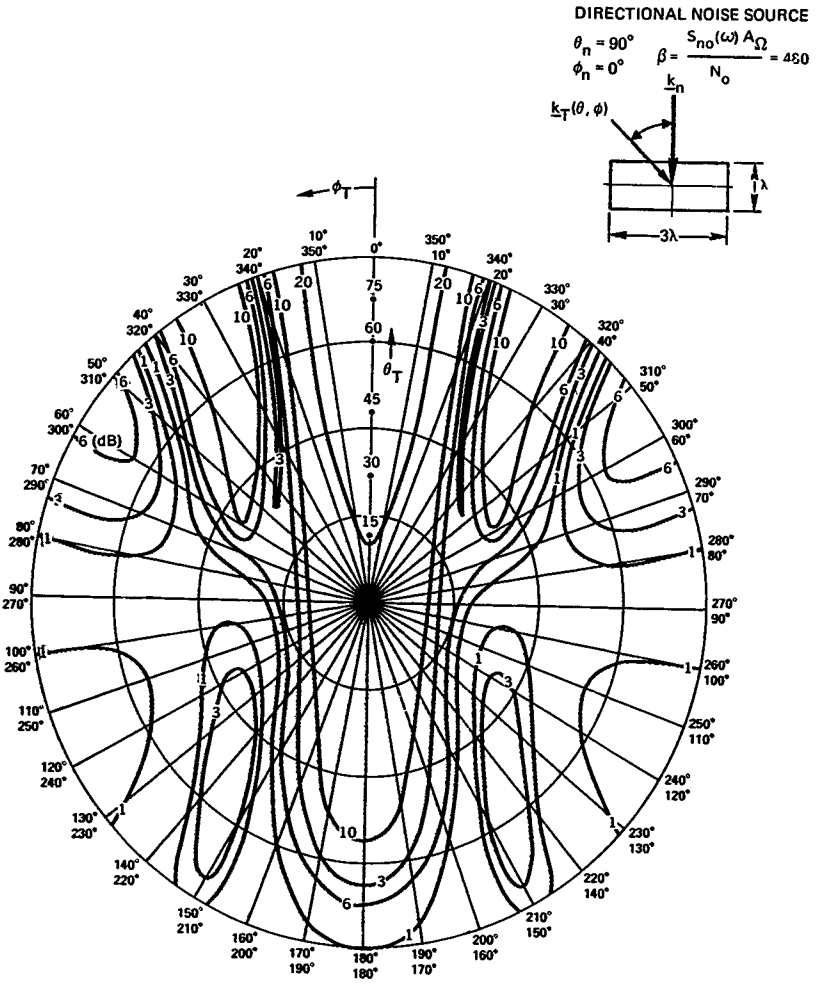

Figure 7-6. Contours (in dB) of noise power: $\sigma_o^2(\omega:\underline{k}_T)$ relative to N_o/L_1L_2 for endfire directional noise source conventional processing.

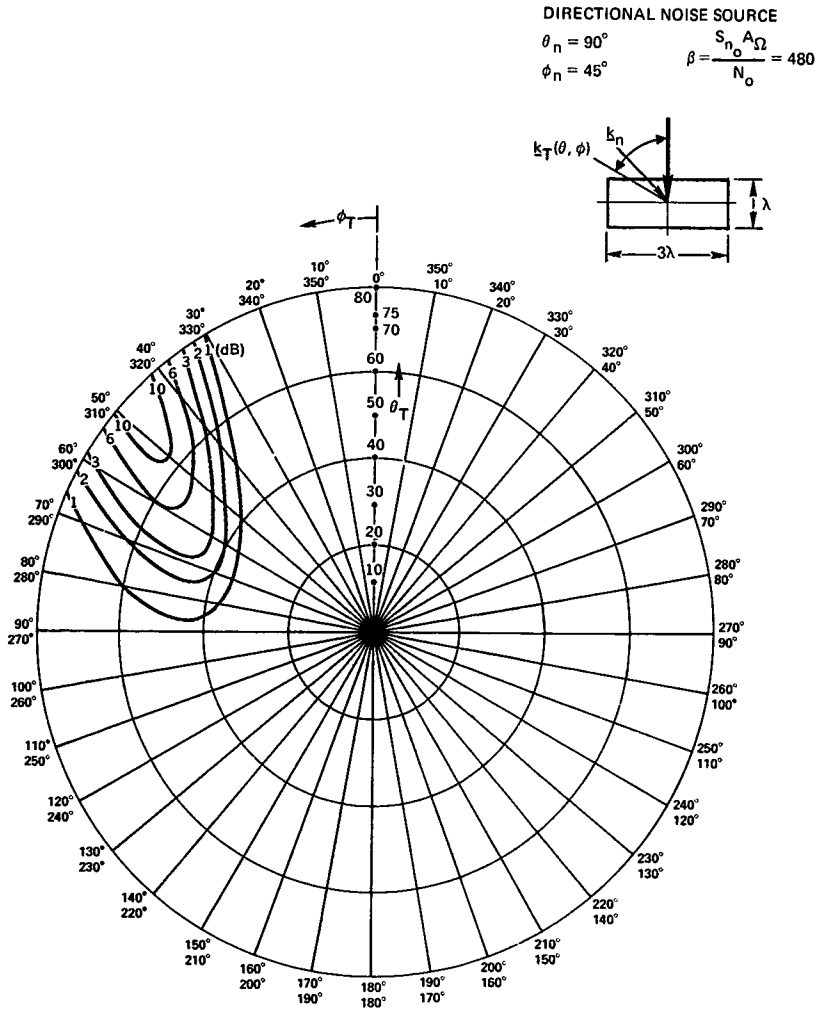

Figure 7-7. Contours (in dB) of noise power $\sigma_o^2(\omega\ \underline{k}_T)$ relative to N_o/L_1L_2 for an endfire directional noise source optimum processing

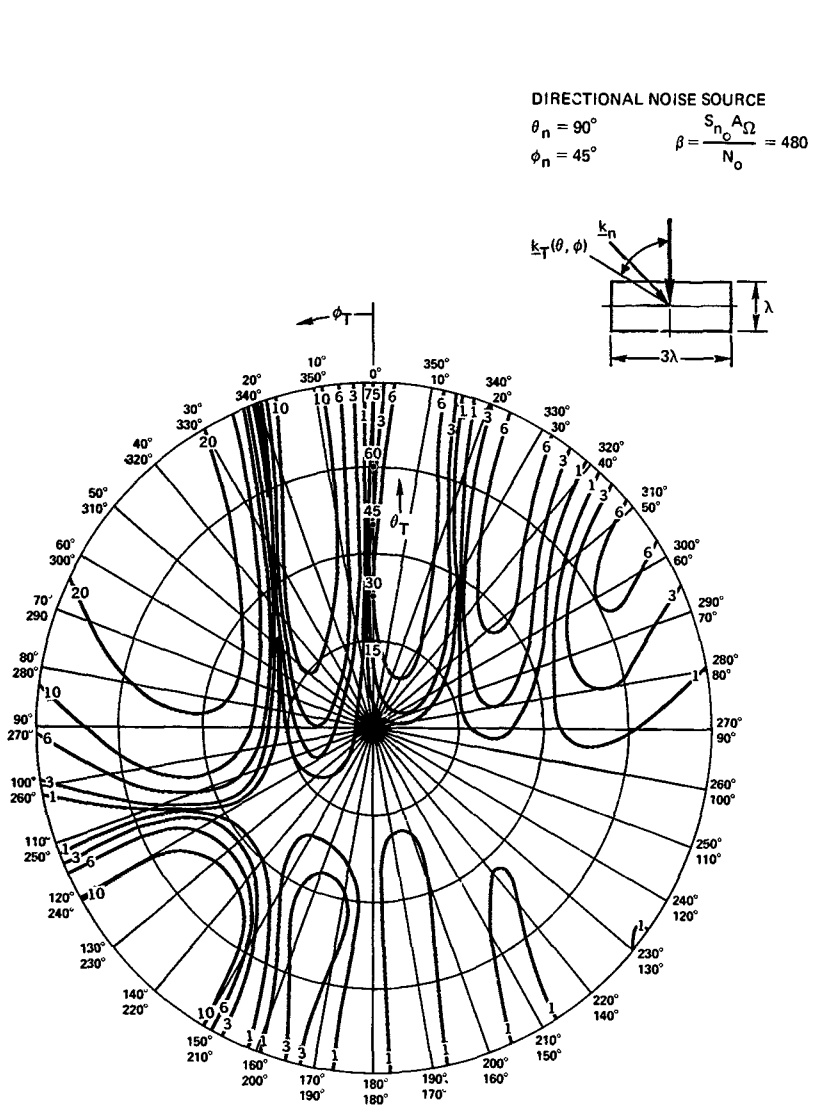

Figure 7-8 Contours (in dB) of noise power $\sigma_o^2(\omega\, \underline{k}_T)$ relative to N_o/L_1L_2 for an endfire directional noise source conventional processing

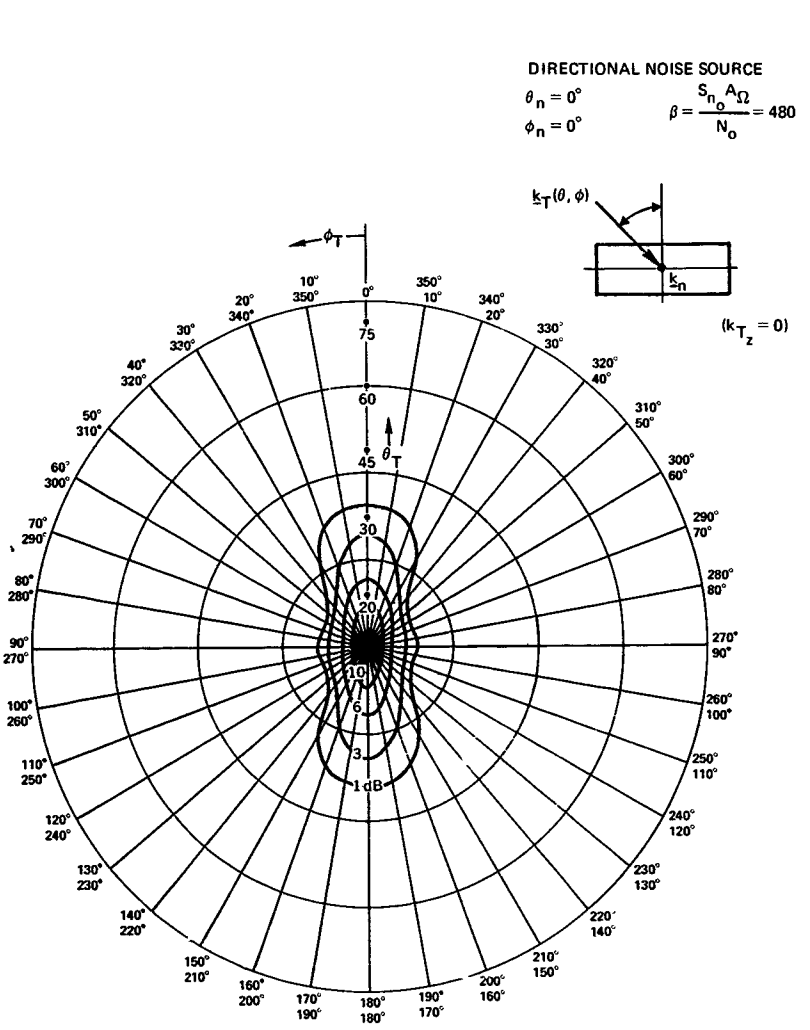

Figure 7-9 Contours (in dB) of noise power $\sigma_0^2(\omega, \underline{k}_T)$ relative to N_o/L_1L_2 for a broadside directional noise source optimum processing

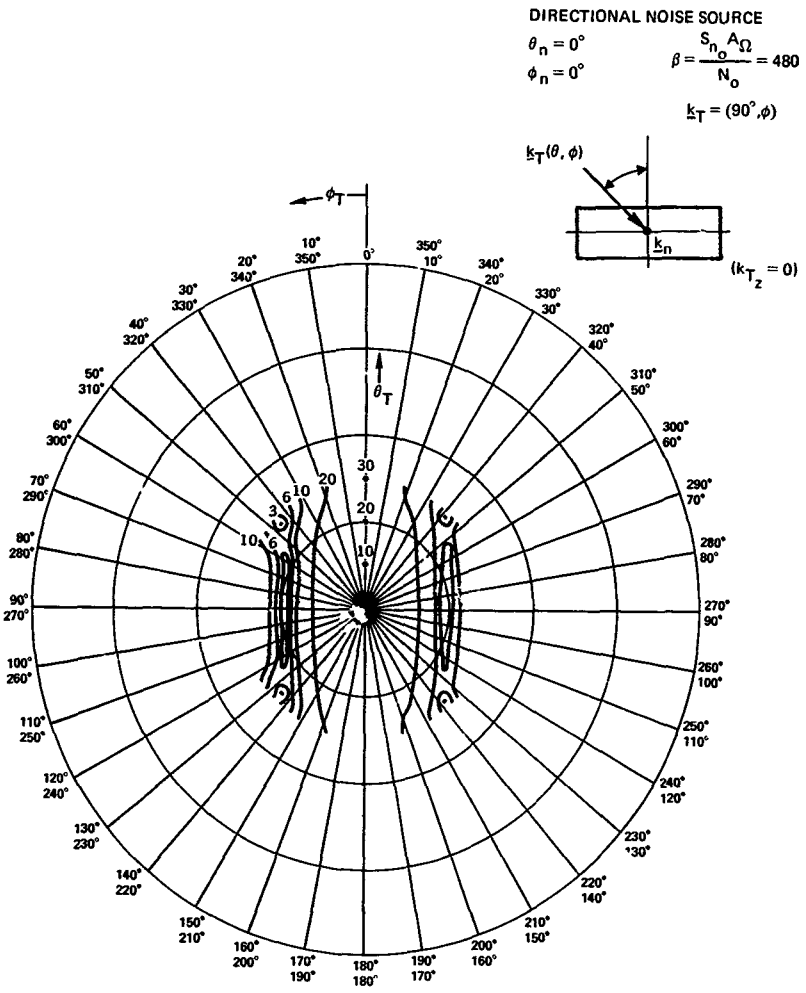

Figure 7-10 Contours (in dB) of noise power $\sigma_o^2(\omega:\underline{k}_T)$ relative to N_o/L_1L_2 for a broadside directional noise source optimum processing.

Computing the noise output as we go from broadside to endfire is more difficult for there is not a monotonic increase as is the case in the linear arrays If $L_{1\lambda} > 1$ and $L_{2\lambda} > 1$ the eigenfunctions will approach spatial sinusoids with an eigenfunction distribution given by the above two dimensional wave number function An approximation performance is

$$\sigma_o^2(\omega|\underline{k}_T) = \frac{1}{L_1 L_2} \quad (N_o + P(\omega\ \underline{k}_{T_a}) \tag{7 8}$$

$$\begin{cases} \dfrac{N_o}{L_1 L_2} \left[1 + \dfrac{\lambda^2}{2\pi} \dfrac{S_{n_o}(\omega)}{N_o} \left(1-\left(\dfrac{|k_{T_a}|\lambda}{2\pi}\right) 2\right)^{-1/2}\right], & |\underline{k}_T| < \dfrac{2\pi}{\lambda} \\ \dfrac{N_o}{L_1 L_2}, & |\underline{k}_T| > \dfrac{2\pi}{\lambda} \end{cases}$$

This diverges as k_{T_a} approaches endfire or $2\pi/\lambda$, so it is hard to predict the endfire performance It is easy to observe that our approximation can be refined with two considerations If we integrate over the finite beamwidth, we average over the integrable singularity in the wave number function In addition, at endfire half of the beam response is in the white noise region which has a lower noise level Consequently, we have that the output noise increases until we are beyond

$$|\underline{k}\text{-}\underline{k}\cdot\underline{a}_n| > \frac{2\pi}{\lambda} - \frac{2\pi}{2L} = \frac{2\pi}{\lambda}\left(1 - \frac{1}{2L_\lambda}\right)$$

at which point it levels off and then begins to decrease The optimum processing can increase these effects somewhat by appropriate showing of the beam Some representative performances are illustrated in Figures 7-11 and 7-12.

One can introduce various noise field geometries representing surface, bottom or layer noise. The results of our discussion on noise representation indicate how the two dimensional wave number function can be found, from which the approximate performance can be determined Alternatively, we can pursue an analysis in three dimensional wave number space with the noise field distributed on a sphere as we did in our discussion for linear arrays. We are led to the same results in either method.

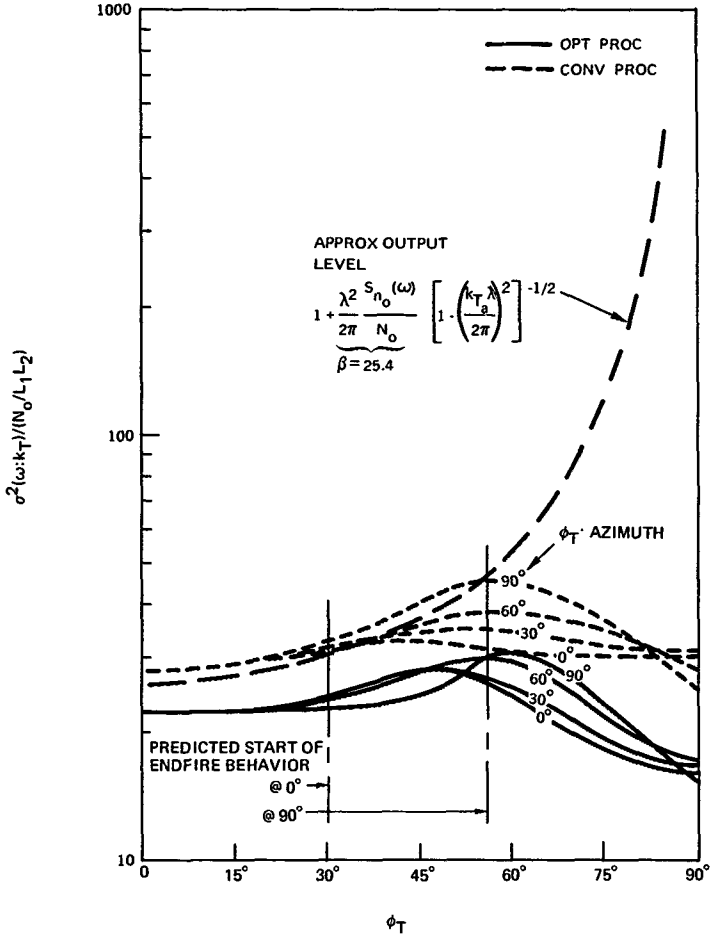

Figure 7-11. Planar array output noise level for an isotropic noise field

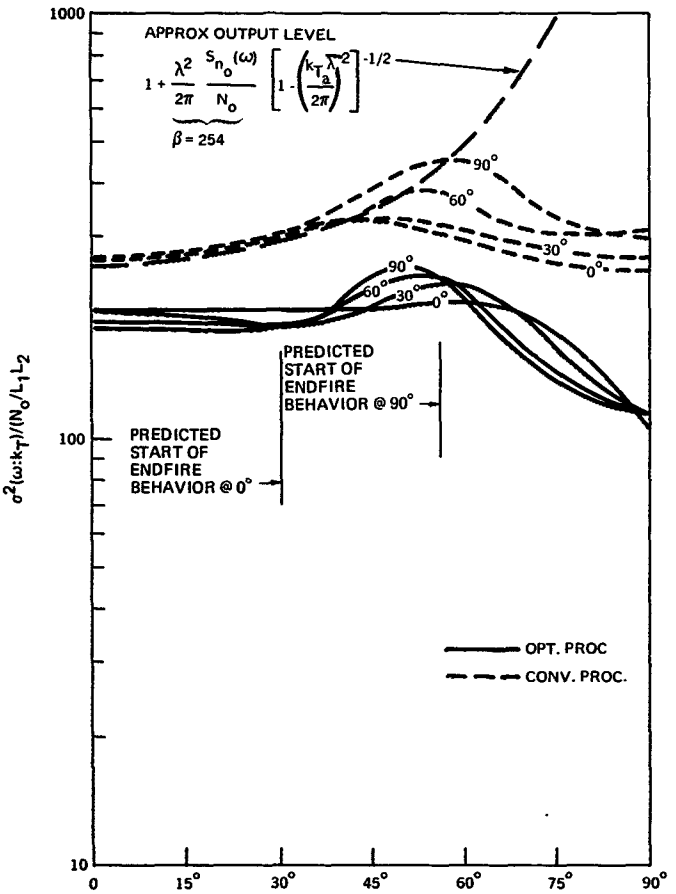

Figure 7-12. Planar array output noise level for an isotropic noise field.

7.2 CROSSED ARRAYS

The importance of crossed arrays lies in their capabilities of providing spatial information, or resolution, along two coordinates with fewer sensors than a planar array While in a planar array the number of sensors increases as $L_1 L_2$ of the crossed array sensors increases as $L_1 + L_2$ In most, but not all, cases crossed arrays perform virtually as well as their planar counterparts when their outputs are processed correctly. This is very significant in reducing computational demands

One of the most important facets of the analysis of crossed arrays is their tutorial value With a minimum of complexity, they introduce several significant concepts in the processing of array data. In particular, the importance of frequency wave number concepts as a means of obtaining approximate expressions for the system performance For our analysis we consider two noise fields – directional and isotropic.

We consider an array structure as illustrated in Figure 7-13. The class of beam patterns which we can generate is given by

$$g(\omega\ \underline{k}) = \int_{-L_1/2}^{L_1/2} G_1(\omega:\ell_1) e^{j\underline{k}\cdot\underline{a}_1\ell_1} d\ell_1 + \int_{-L_2/2}^{L_2/2} G_2(\omega:\ell_2) e^{j\underline{k}\cdot\underline{a}_2\ell_2} d\ell_2$$

$$= g_1(\omega.\underline{k}\cdot\underline{a}_1) + g_2(\omega:\underline{k}\cdot\underline{a}_2) \qquad (7.9)$$

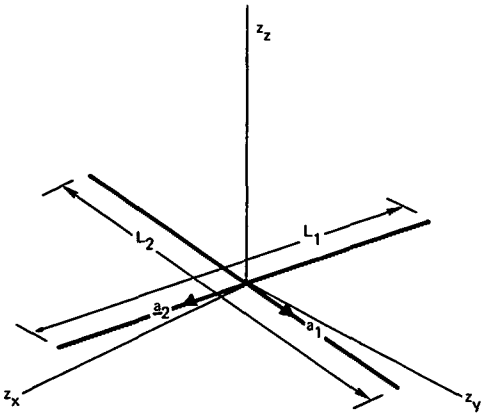

Figure 7-13. Crossed array–legs of length L_1,L_2, oriented in direction $\underline{a}_1$,$\underline{a}_2$, crossed at center of legs.

This is a much more restrictive form than that which we had for the planar array We cannot generate resolution cells, i e , regions where there is a main beam concentration and outside of which the beam is approximately zero With a crossed array we can generate only combinations of resolution strips In Figures 7-14 and 7-15 we have plotted the conventional beam pattern for a typical crossed array configuration This beam pattern is given by

$$g(\omega\ \underline{k}|\underline{k}_T) = \frac{L_1}{L_1+L_2}\ \text{sinc}\left[(\underline{k}-\underline{k}_T)\cdot\underline{a}_1\ \frac{L_1}{2}\right] + \frac{L_2}{L_1+L_2}\ \text{sinc}\left[(\underline{k}-\underline{k}_T)\cdot\underline{a}_2\ \frac{L_2}{2}\right] \tag{7 10}$$

Conventional beamforming can introduce ambiguity effects if a noise source appeared in one of the "sidelobe strips," one should weigh the use of the other line of the cross to a degree greater than that of the conventional weighting of L_1/L_1+L_2 Optimal processing achieves a substantial amount of its improved performance and sidelobe suppression by introducing this implicitly rather than by using esoteric beam patterns

We consider the analysis of a directional noise source of level $S_{n_o}(\omega)$. From our previous example, we can specify the performance and optimal beam pattern by inspection For the performance we have

$$\sigma_o^2(\omega\,|\underline{k}_T) = \left(\frac{A_\Omega}{N_o}\right)^{-1} \left[\frac{1 + \dfrac{A_\Omega S_{n_o}(\omega)}{N_o}\left(1 - \text{sinc}_\Omega^2(\underline{k}_n-\underline{k}_T)\right)}{1 + \dfrac{A_\Omega S_{n_o}(\omega)}{N_o}}\right]^{-1} \tag{7 11}$$

where

$$A_\Omega = L_1 + L_2$$

$$\text{sinc}_\Omega(\underline{k}) = \frac{L_1}{L_1+L_2}\ \text{sinc}\left(\underline{k}\cdot\underline{a}_1\ \frac{L_1}{2}\right) + \frac{L_2}{L_1+L_2}\ \text{sinc}\left(\underline{k}\cdot\underline{a}_2\ \frac{L_2}{2}\right)$$

This is plotted in Figures 7-16 through 7-18 At first inspection, it may appear that the above does not perform as well as a simple linear array when the noise appears in one of the sidelobe strips However, a comparison of this situation with the corresponding linear array yields

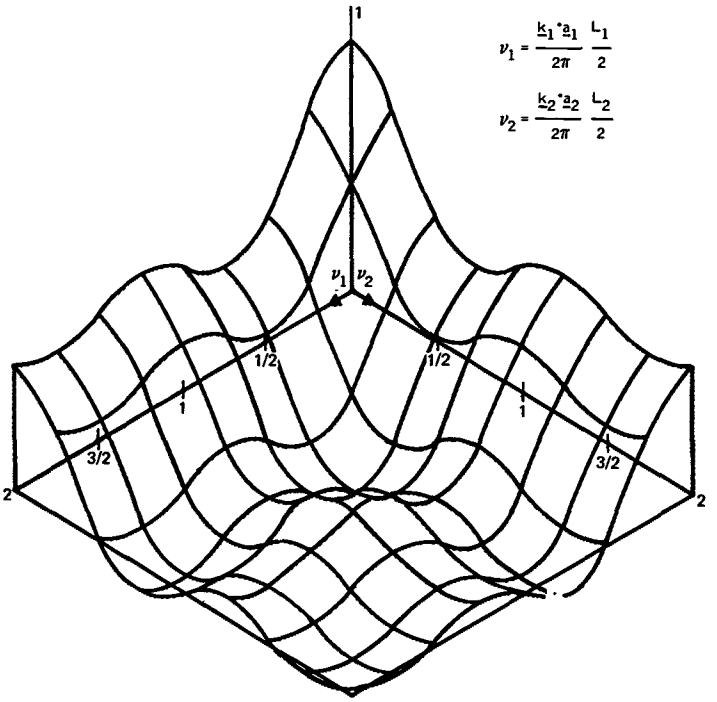

Figure 7-14 Beam pattern for crossed array, $\frac{1}{2}[\text{sinc}(2\pi\,\nu_1) + \text{sinc}(2\pi\,\nu_2)]$

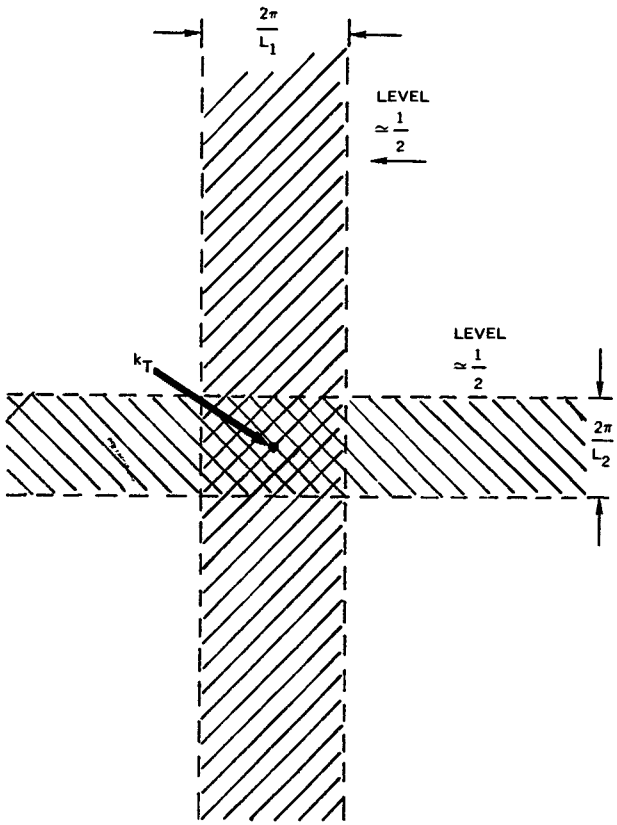

Figure 7-15 Region of significant sidelobe amplitude in the beam pattern of a crossed array.

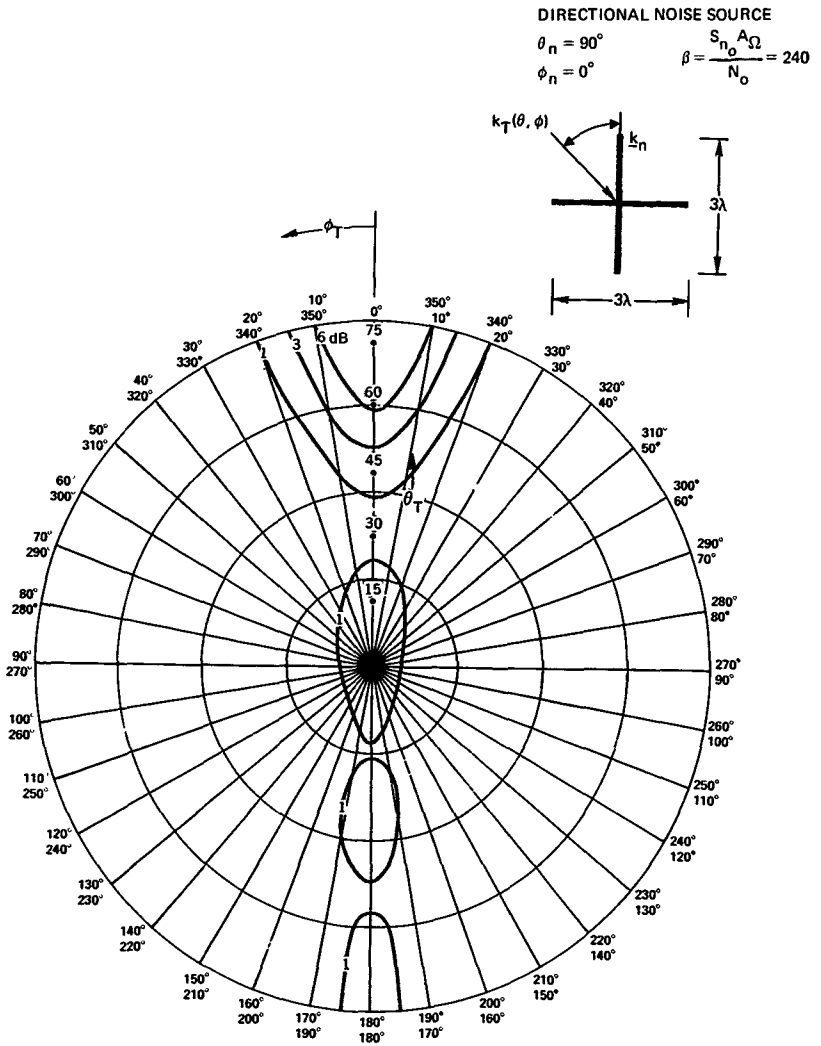

Figure 7-16 Contours (in dB) of constant noise power output, $\sigma_o^2(\omega|\underline{k}_T)$ relative to $N_o/(L_1+L_2)$ for a crossed array with endfire directional noise @ $\phi_n=0°$.

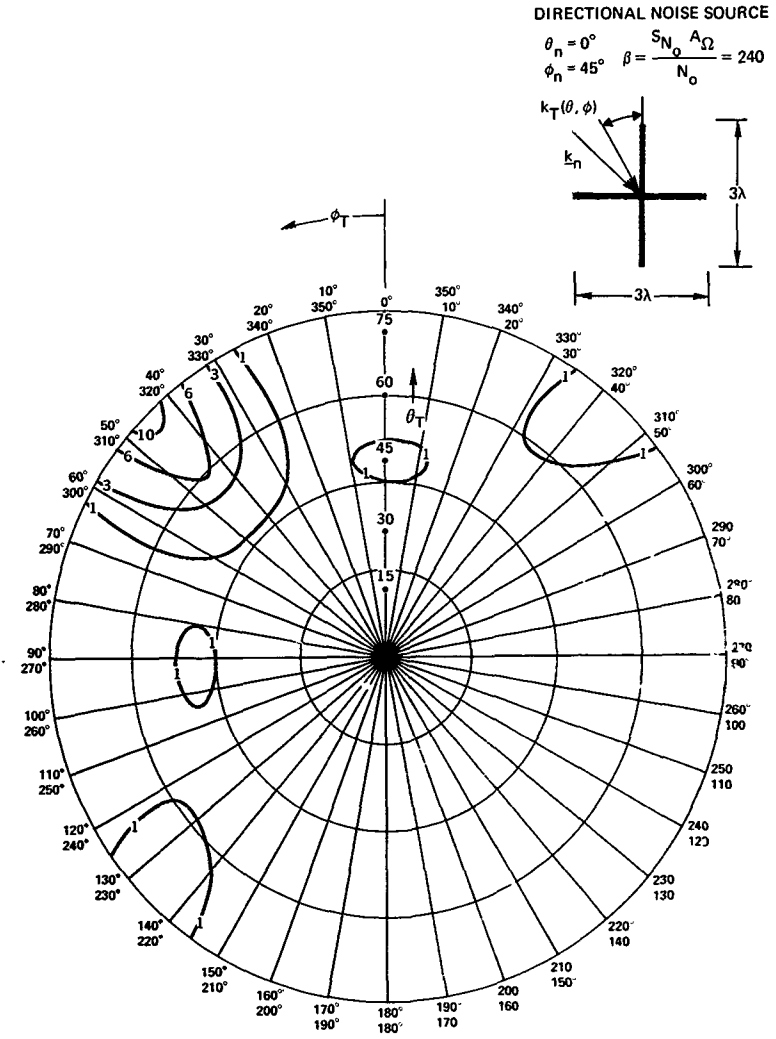

Figure 7-17 Contours (in dB) of constant noise power output, $\sigma_0^2(\omega|\underline{k}_T)$ relative to $N_o/(L_1+L_2)$ for a crossed array with end fire directional noise @ $\phi_n = 45°$

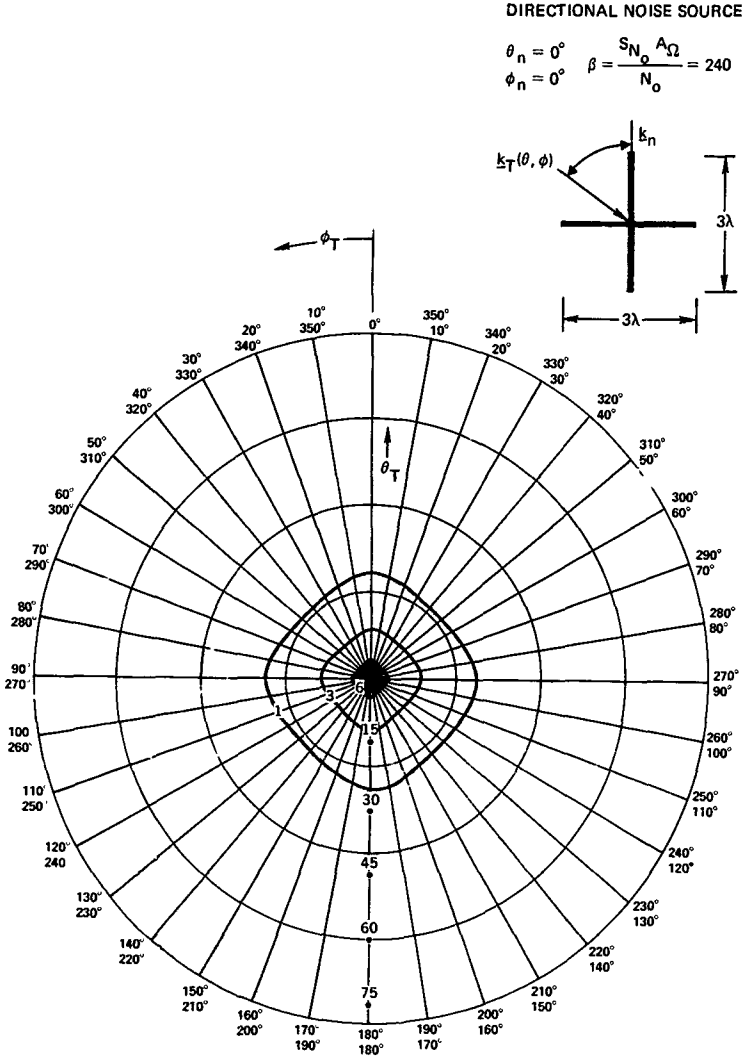

Figure 7-18 Contours (in dB) of constant noise power output σ_o^2 ($w|k_T$) relative to $N_o/(L_1+L_2)$ for a crossed array with endfire directional noise at broadside

$$\sigma_{o_x}^2(\underline{\omega}|k_{T_1}) =$$

$$\left(\left(\frac{A_\Omega}{N_o}\right)\left[\frac{1+\frac{A_\Omega S_{n_o}(\omega)}{N_o}\left(1-\left(\frac{L_1}{L_1+L_2}\,\mathrm{sinc}\left((\underline{k}_{T_1}-\underline{k}_n)\cdot\underline{a}_1\,\frac{L_1}{2}\right)+\frac{L_2}{L_1+L_2}\right)^2\right)}{1+\frac{A_\Omega S_{n_o}(\omega)}{N_o}}\right]\right)^{-1} \tag{7.12a}$$

with

$$(\underline{k}_{T_2}-\underline{k}_n)\cdot\underline{a}_2 = 0$$

for the crossed array, and

$$\sigma_{o_1}^2(\omega|\underline{k}_{T_1}) = \left(\left(\frac{L_1}{N_o}\right)\left[\frac{1+\frac{L_1 S_{n_o}(\omega)}{N_o}\left(1-\mathrm{sinc}^2\left((\underline{k}_{T_1}-\underline{k}_n)\cdot\underline{a}_1\,\frac{L_1}{2}\right)\right)}{1+\frac{L_1 S_{n_o}(\omega)}{N_o}}\right]\right)^{-1} \tag{7.12b}$$

for the linear array It is straightforward to demonstrate that the increase in noise output for $N_o \to 0$ is given by

$$\gamma = \left(1+\frac{L_2}{L_1}\right)\frac{1-\left(L_1\,\mathrm{sinc}\left[(\underline{k}_{T_1}-\underline{k}_n)\cdot\underline{a}_1\,\frac{L_1}{2}\right]+L_2\right)^2\Big/(L_1+L_2)^2}{1-\mathrm{sinc}^2\left[(\underline{k}_{T_1}-\underline{k}_n)\cdot\underline{a}_1\,\frac{L_1}{2}\right]} \tag{7.13}$$

The largest increase occurs when the noise appears in a null of the crossed array length with, i.e., it is the main beam of one length and the null of the other,

$$\left[1+\frac{L_2}{L_1}\right]\left[1+\frac{A_\Omega\, S_{n_o}(\omega)}{N_o}\left(\frac{1+2\dfrac{L_2}{L_1}}{\left(1+\dfrac{L_2}{L_1}\right)^2}\right)\right]\Bigg/\left[1+\frac{A_\Omega\, S_{n_o}(\omega)}{N_o}\right]$$

$$\cong \frac{1+2\dfrac{L_2}{L_1}}{1+\dfrac{L_2}{L_1}} \tag{7.14}$$

for $N_o \to 0$.

It is useful to demonstrate how the array obtains its increased performance. The optimum beam pattern is computed straightforward, and the next result is

$$g(\omega\cdot\underline{k}\,|\underline{k}_T) = \frac{\operatorname{sinc}_\Omega(\underline{k}-\underline{k}_T) - \dfrac{\dfrac{A_\Omega\, S_{n_o}(\omega)}{N_o}}{1+\dfrac{A_\Omega\, S_{n_o}(\omega)}{N_o}}\operatorname{sinc}_\Omega(\underline{k}_n-\underline{k}_T)\operatorname{sinc}(\underline{k}-\underline{k}_n)}{1-\dfrac{\dfrac{A_\Omega\, S_{n_o}(\omega)}{N_o}}{1+\dfrac{A_\Omega}{N_o}\, S_{n_o}(\omega)}\operatorname{sinc}^2_\Omega(\underline{k}_n-\underline{k}_T)} \tag{7.15}$$

We consider a situation $(\underline{k}_n-\underline{k}_T)\cdot\underline{a}_2 \simeq 0$ and $(\underline{k}_n-\underline{k}_T)\cdot\underline{a}_1 \frac{L_1}{2} > \pi$ The resulting beam pattern generated is illustrated in Figure 7-19 It simply has a null in the crossed array beam pattern

In the special case of a dominant directional noise source and $L_1=L_2$ we have

$$\frac{(L_1+L_2)\, S_{n_o}(\omega)}{N_o} \gg 1$$

$$\text{sinc}_\Omega\,(\underline{k}_T-\underline{k}_n) \simeq \frac{1}{2}$$

and

$$G_o(\omega:\underline{k}\,|\underline{k}_T) \simeq \frac{4}{3}\left(\text{sinc}_\Omega(\underline{k}-k_T) - \frac{1}{2}\,\text{sinc}_\Omega(\underline{k}-\underline{k}_n)\right) \tag{7.16}$$

This places a null at $\underline{k}=\underline{k}_n$ while maintaining unity response in the target direction A natural question which arises is why doesn't the array simply ignore that section along which there is no resolvability, i.e , assign a weighting of zero along that cross If this were done, we would have an array output noise of approximately N_o/L while if the optimum response is used, the output noise is 2 dB less, or $4/3\ N_o/2L_1$. Both weightings suppress the highly directional source by nulling it, however, in the optimum array a smaller amount of white noise enters through its reduced sidelobe level Only if the noise field has a strip of sources with $(\underline{k}_T-\underline{k}_n)\cdot\underline{a}_2 \cong 0$ does the beam pattern approach that of a linear array A representative beam pattern for a noise field approximating this class is illustrated in Figure 7-20 Note that there is effectively no resolution along k_y direction

For crossed arrays in directional noise fields the optimum patterns place nulls at the wave numbers of the directional noise sources, while simultaneously minimizing the mean square amplitude of sidelobes While the conventional array is designed independent of the noise field, the optimum patterns indicate an intuitively appealing design to exploit the structure of the noise fields encountered These optimum patterns are not too complicated and it is only when the noise and targets are close together that they become complicated, introducing the features we encountered earlier in the discussion of linear arrays

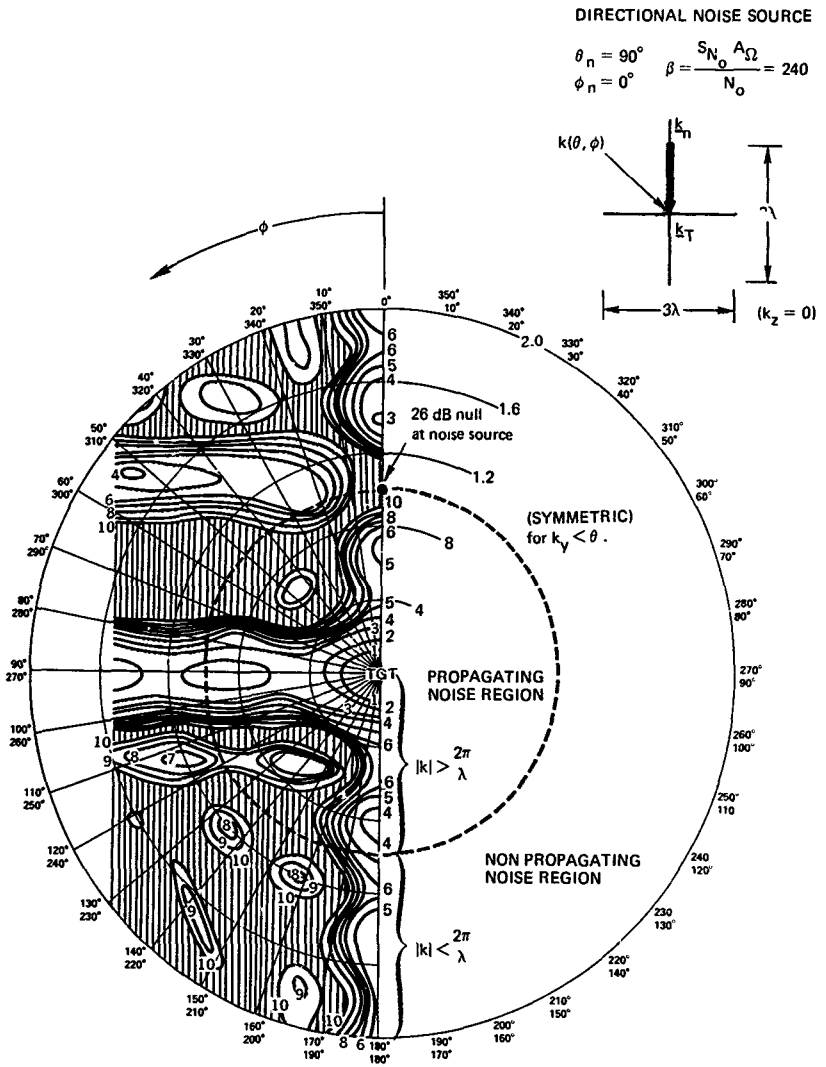

Figure 7-19 Optimum wave number response (in dB) for a crossed array with a) endfire noise and b) broadside target

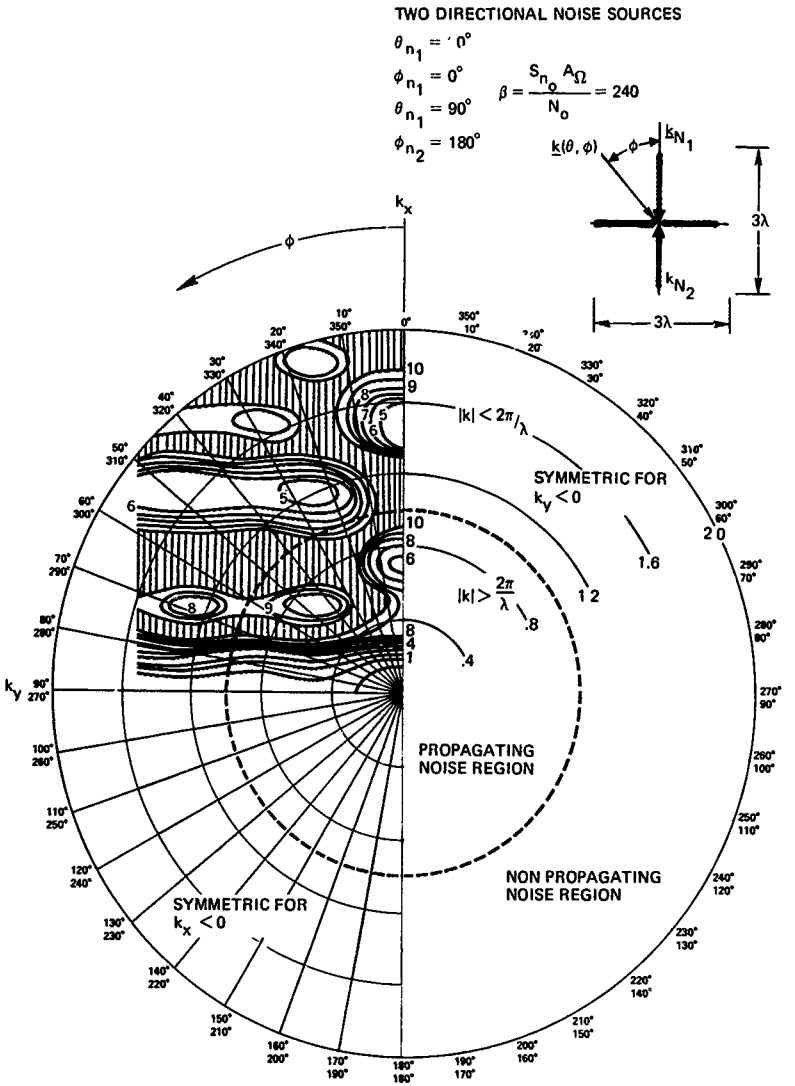

Figure 7-20. Optimum wave number response (in dB) for a crossed array with a) broadside target and b) two endfire noise sources; note lack of resolution along K_y axis

The design of crossed arrays for isotropic noise cannot be pursued analytically without considerable amount of mathematical detail The crossed geometry still reduces to the prolate spheroidal wave functions that we encountered in linear arrays We can, however, pursue an approximate analysis which encompasses the basic attributes of the processing

To analyze the performance of crossed arrays in noise fields which have a smoothly varying wave number function for $|\underline{k}| > 2\pi/\lambda$, we must isolate a set of temporal random processes which characterize the array outputs We can do this quite easily using wave number concepts Each leg of the array forms a set of orthogonal beam outputs $X_m(\omega)$ and $Y_n(\omega)$ at intervals of $2\pi/L_1$ in wave number space, as illustrated in Figure 7-21 For convenience, we subsequently assume the array crosses are perpendicular The spectra of each of the outputs $X_m(\omega)$ and $Y_n(\omega)$ is given approximately by

$$S_{x_m}(\omega) \simeq \frac{1}{L_1} \int_{-\frac{2\pi}{\lambda}\sqrt{1-\left(\frac{m}{L_1/\lambda}\right)^2}}^{\frac{2\pi}{\lambda}\sqrt{1-\left(\frac{m}{L_1/\lambda}\right)^2}} P_n(\omega\, m\frac{2\pi}{L_1}\underline{a}_1 + k_2\underline{a}_2)\frac{dk_2}{2\pi} + \frac{N_o}{L_1} \quad (7.17a)$$

$$S_{y_n}(\omega) = \frac{1}{L_2} \int_{-\frac{2\pi}{\lambda}\sqrt{1-\left(\frac{n}{L_1/\lambda}\right)^2}}^{\frac{2\pi}{\lambda}\sqrt{1-\left(\frac{m}{L_1/\lambda}\right)^2}} P_n\left(\omega\, k_1\underline{a}_1 + \frac{2\pi}{L_2}\underline{a}_2\right)\frac{dk_1}{2\pi} + \frac{N_o}{L_2} \quad (7.17b)$$

with

$$[|m|] < L_1/\lambda = L_1/\lambda$$

$$[|n|] < L_2/\lambda = L_2/\lambda$$

$$\underline{a}_1 \cdot \underline{a}_2 = 0$$

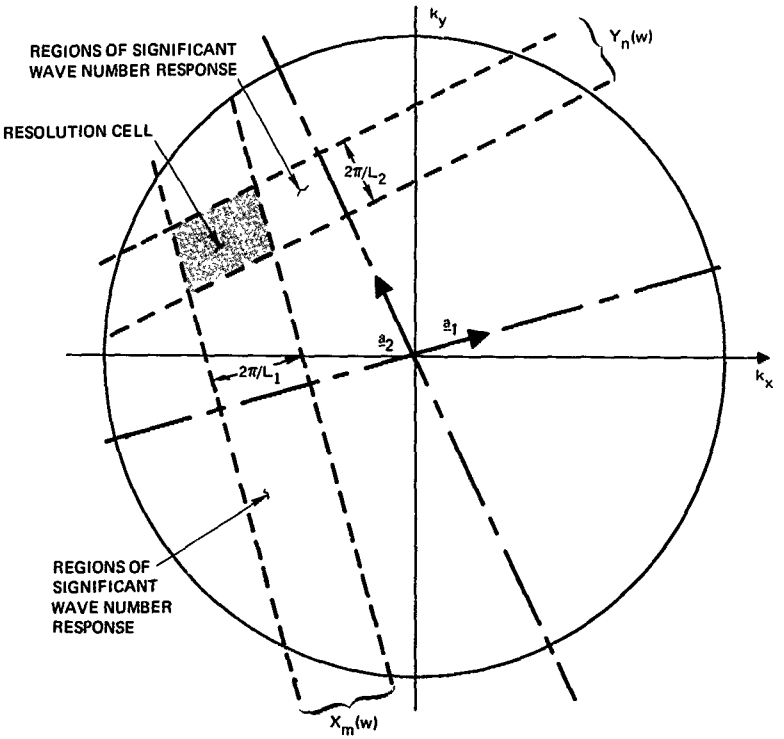

Figure 7-21. Wave number analysis for crossed array performance.

where $P_n(\omega \cdot \underline{k})$ is the two-dimensional wavenumber function Consequently, we have that there are $2(L_{1_\lambda} + L_{2_\lambda})$ random processes The random processes $x_{m_1}(t)$ and $x_{m_2}(t)$ are uncorrelated since the beams are orthogonal; however, $x_n(t)$ and $y_m(t)$ are correlated since the beams overlap at the crossing point We have for their cross spectral density

$$S_{x_n y_m}(\omega) = \frac{1}{L_1 L_2} P\left(\omega : m\frac{2\pi}{L_1}\underline{a}_1 + n\frac{2\pi}{L_2}\underline{a}_2\right) \tag{7 18}$$

so that as the array length L_1 and L_2 increase, the effect of the correlation decreases

Figure 7-21 Wave number filters for crossed array performance

If a target is located at or near the wave number location $m\frac{2\pi}{L_2}\underline{a}_1 + n\frac{2\pi}{L_2}\underline{a}_2$, the array forms a beam which has a combination of these random processes in its output The class of beams which are formed is, approximately, given by

$$g(\omega\ \underline{k}|\underline{k}_T) = \frac{\alpha L_1 \operatorname{sinc}\left[(\underline{k}-\underline{k}_T)\cdot\underline{a}_1\ \frac{L_1}{2}\right] + \beta L_2 \operatorname{sinc}\left[(\underline{k}-\underline{k}_T)\cdot\underline{a}_2\ \frac{L_2}{2}\right]}{\alpha L_1 + \beta L_2} \tag{7 19}$$

where α and β are adjusted to weight each array so as to minimize total noise output of the beam We have

$$\sigma_o^2(\omega|k_T)$$

$$\simeq \left(\frac{\alpha L_1}{\alpha L_1+\beta L_2}\right)^2 S_{x_m}(\omega) + \left(\frac{\beta L_2}{\alpha L_1+\beta L_2}\right)^2 S_{y_n}(\omega) + \frac{2L_1L_2\alpha\beta}{(\alpha L_1+\beta L_2)^2} S_{x_m y_n}(\omega) \tag{7.20}$$

Optimizing α and β yields

$$\frac{\alpha L_1}{\alpha L_1+\beta L_2} = \frac{S_{x_n}(\omega) - S_{x_m y_n}(\omega)}{S_{x_m}(\omega) + S_{y_n}(\omega) - 2S_{x_m y_n}(\omega)} \tag{7.21a}$$

$$\frac{\beta L_2}{\alpha L_1+\beta L_2} = \frac{S_{x_n}(\omega) - S_{x_m y_n}(\omega)}{S_{x_m}(\omega) + S_{y_n}(\omega) - 2S_{x_m y_n}(\omega)} \tag{7 21b}$$

This yields a performance of

$$\sigma_o^2(\omega\cdot\underline{k}_T) \simeq \frac{S_{x_m}(\omega)S_{y_n}(\omega) - S_{x_m y_n}^2(\omega)}{S_{x_m}(\omega) + S_{y_n}(\omega) - 2S_{x_n y_m}(\omega)} \tag{7.22}$$

where the various spectra are computed via Eq. 7.17 and 7 18

As an example, we consider the special case of three-dimensional isotropic noise of Example 2.2a with a crossed array. We have

$$S_{x_i}(\omega) = \begin{cases} \left(\frac{\lambda}{2}\, S_{n_o}(\omega) + N_o\right)/L_1, & |i| < \left[\frac{L_1}{\lambda}\right], \\ N_o/L_1, & |i| \geq \left[\frac{L_1}{\lambda}\right], \end{cases} \tag{7.23a}$$

$$S_{y_j}(\omega) = \begin{cases} \left(\frac{\lambda}{2}\, S_{n_o}(\omega) + N_o\right)/L_2, & |j| < \left[\frac{L_2}{\lambda}\right], \\ N_o/L_2, & |j| > \left[\frac{L_2}{\lambda}\right], \end{cases} \tag{7.23b}$$

$$S_{x_i y_j}(\omega) = \begin{cases} \lambda^2 S_{n_o}(\omega) \Big/ 2\pi L_1 L_2 \left(1 - \left(\frac{i\lambda}{L_1}\right)^2 - \left(\frac{j\lambda}{L_2}\right)^2\right)^{1/2}, \\ \left(\frac{i\lambda}{L_1}\right)^2 + \left(\frac{j\lambda}{L_2}\right)^2 < 1, \\ 0, \qquad \text{otherwise} \end{cases} \tag{7.23c}$$

Substituting this into Equation 7.22 we obtain for the special case of $L_1 = L_2$ with $\beta >> 1$

$$\sigma_o^2(\omega\, \underline{k}_T) \simeq \frac{N_o}{2L_1}\ (\beta)\ \left(\frac{1+\rho_o}{\pi/(L_1/\lambda)}\right) \tag{7.24}$$

where

$$\beta = \frac{\lambda S_{n_o}(\omega)}{2N_o}$$

$$\rho_o \simeq \left[1 - \left(\frac{i\lambda}{L_1}\right)^2 - \left(\frac{j\lambda}{L_2}\right)^2\right]^{1/2}$$

$$k_T \simeq \left(i\,\frac{2\pi}{L_1},\ j\,\frac{2\pi}{L_2}, 0\right)$$

The improvement over a simple linear array is

$$\frac{1}{2}\left(1+\frac{\rho_o}{\pi(L_1/\lambda)}\right)$$

We have assumed that $L_i/\lambda > 1$, otherwise, we would have need to consider superdirective effects immediately. In approximating the smoothness of $P(\omega\ k)$ we must have

$$\frac{\lambda}{L_i}\ \rho_o < \frac{\pi}{4}$$

or

$$\frac{\rho_o}{(\pi L/4\lambda)} < 1$$

If this is not satisfied, then the improvement becomes 1/2. Finally if

$$\left(\frac{i\lambda}{L_1}\right)^2 + \left(\frac{j\lambda}{L_2}\right)^2 > 1 - \frac{\lambda}{2L_i}$$

then we should be careful of superdirective effects. In summary, Figure 7-22 represents an example of a superdirective beam pattern when $\underline{k}_T = \frac{2\pi}{\lambda}, 0, 0$, while plots for $\sigma_o^2(\omega|\underline{k}_T)$ may be found in Figure 7-23. Observe that in Figure 7-23 at $\phi_T = 0°$ it is easier to place beam pattern volume outside $|k| > 2\pi/\lambda$ than it is at $\phi_T = 45°$, therefore the endfire affects are more significant

We can also use the above analysis to derive approximate expressions for the spatial eigenvalues and eigenfunctions of the crossed array when operating in a noise field whose frequency wave number function varies slowly over the resolution width maximum $(L/\lambda)^{-1}$ of the array. The results are indicative of what is obtained in the analysis of higher dimensional geometries. We emphasize that our analysis is approximate. It combines a classical temporal analysis with the features of the crossed array. To determine the eigenvalues and eigenfunctions we observe that at the frequency ω the random variables $x_i(\omega)$ and $y_j(\omega)$ lead to a spectral covariance matrix of the form

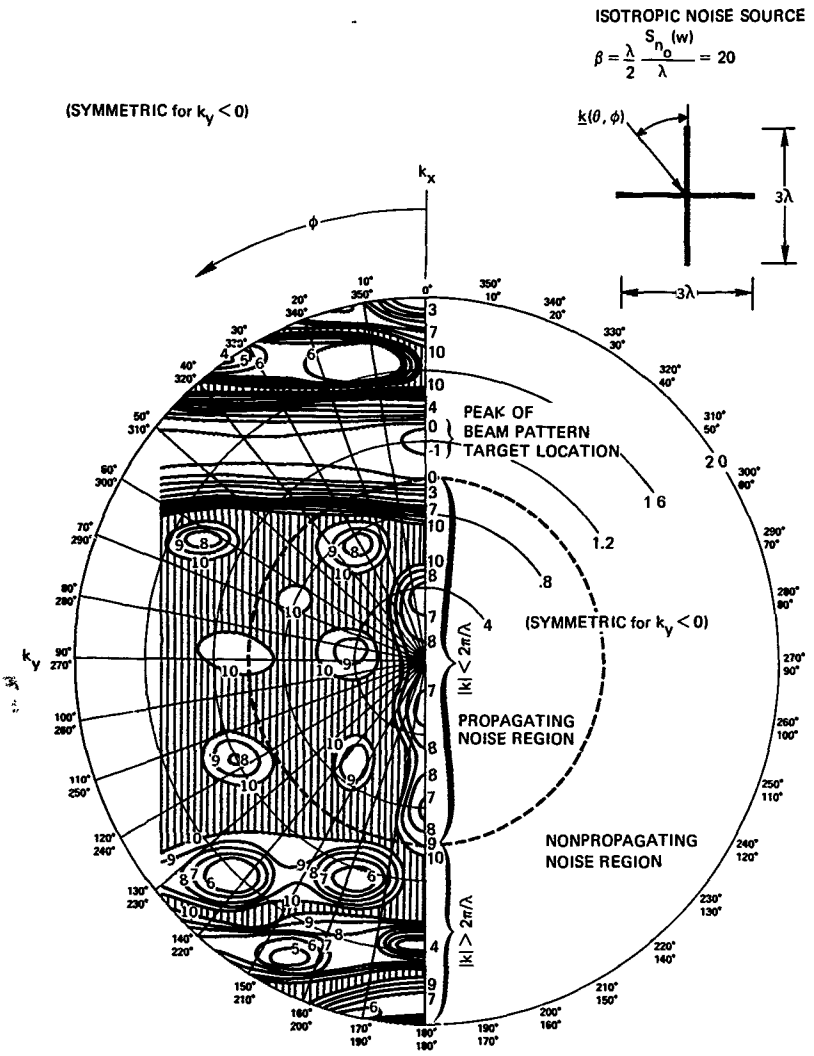

Figure 7-22 Optimum beam pattern for a crossed array with a) isotropic noise and b) endfire target

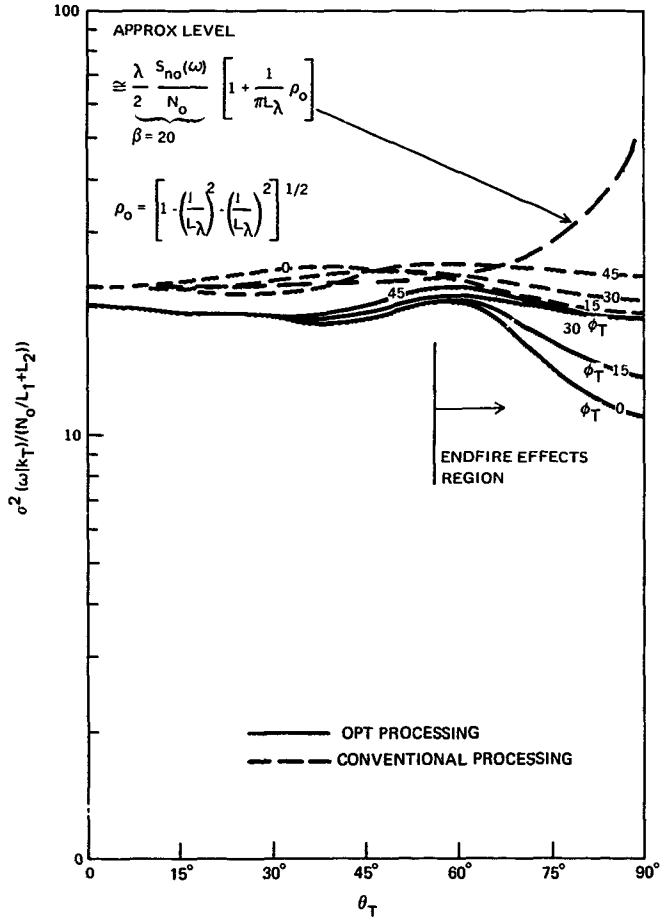

Figure 7-23 Noise power output relative to reference N_o/L_1+L_2 for a crossed array in isotropic noise.

$$[S(\omega)] = \begin{bmatrix} S_{x_{-N}}(\omega) & & 0 & & S_{x_i y_j}(\omega) \\ & \ddots & & & \\ 0 & & S_{x_N}(\omega) & & \\ \hline & & & S_{y_{-M}}(\omega) & 0 \\ S^*_{x_i y_j}(\omega) & & & \ddots & \\ & & & 0 & S_{y_M}(\omega) \end{bmatrix} \tag{7.25}$$

where $N = L_1/\lambda$, $M = L_2/\lambda$ and the elements $S_{x_i}(\omega)$ are computed as indicated in our previous discussion. The generation of a set of random variables which have a diagonal covariance matrix is a classical orthogonalization problem in matrix algebra [3]. One needs to solve for the eigenvalues and eigenvectors of the homogeneous equation

$$\left[[S(\omega)] - \lambda_k(\omega)\,\underline{1}\right]\,\Phi_k(\omega) = \underline{0} \tag{7.26}$$

The eigenvalues of the process at frequency ω are given by the set $\left\{\lambda_k(\omega)\,\middle|\,{k=2(N+M+1) \atop k=1}\right\}$

The spatial eigenfunctions can be expressed in terms of the elements of the eigenvectors. If we separate them such that the first $2N + 1$ components are associated with the x or L_1 leg, while the remaining $2M + 1$ are with the y or L_2 leg, we have

$$\underline{\phi}_k(\omega) = \begin{bmatrix} C^x_{k,-N}(\omega) \\ \vdots \\ C^x_{k,N}(\omega) \\ \vdots \\ C^y_{k,-M}(\omega) \\ \vdots \\ C^y_{k,M}(\omega) \end{bmatrix} \tag{7.27a}$$

and the eigenfunction $\phi_k(\omega\ \underline{z})$ associated with $\lambda_k(\omega)$ is

$$\phi_k(\omega.\underline{z}) = \begin{cases} \alpha \sum_{i=-N}^{N} C^{x}_{k,i}(\omega)\, e^{j(2\pi/L_1)\ell \underline{a}_1 \cdot \underline{z}} & \left\{\underline{z} = \ell \underline{a}_1 \quad |\ell| < L_1/2\right\} \\ \alpha \sum_{i=-M}^{M} C^{y}_{k,i}(\omega)\, e^{j(2\pi/L_2)\ell \underline{a}_2 \cdot \underline{z}} & \left\{\underline{z} = \ell \underline{a}_2 \quad |\ell| < L_2/2\right\} \end{cases} \tag{7 27b}$$

where α is a normalization constant Note that the basic approach is to isolate a set of random variables from which we could reconstruct the observed signal and then to apply an orthogonalization procedure.

We have assumed that our array is crossed at the center of each leg This simplified many of our results since there was no relative phasing between the center of each leg We now briefly consider the situation in which the center is separated. We assume a geometry as illustrated in Figure 7-24. The class of beam patterns which can be generated is given by

$$g(\omega:\underline{k}) = g_1(\omega:\underline{k}\cdot\underline{a}_1)\ e^{j\underline{k}\cdot\underline{R}_1} + g_2(\omega\cdot\underline{k}\cdot\underline{a}_2)\, e^{j\underline{k}\cdot\underline{R}_2} \tag{7 28a}$$

where

$$g_1(\omega:k_1) = \int_{-L_{1/2}}^{L_{1/2}} G_1(\omega\ \ell_1)\ e^{jk_1\ell_1}\, d\ell_1 \tag{7 28b}$$

$$g_2(\omega:\underline{k}_2) = \int_{-L_{2/2}}^{L_{2/2}} G_2(\omega\ \ell_1)\ e^{jk_2\ell_2}\, d\ell_2 \tag{7.28c}$$

with, respectively, $G_1(\omega\ \ell_1)$ and $G_2(\omega\ \ell_2)$ as the weighting patterns for the first and second array legs.

In our analysis we are concerned with the interference relationship between the two legs. We have

$$|g(\omega\ \underline{k})|^2 = |g_1(\omega\ \underline{k}\cdot\underline{a}_1)|^2 + |g_2(\omega\ \underline{k}\cdot\underline{a}_2)|^2$$

$$+ 2\mathrm{Re}\left[e^{j\underline{k}\cdot(\underline{R}_1-\underline{R}_2)}\ g_1(\omega\ \underline{k}\cdot\underline{a}_1)\ g_2^*(\omega\ \underline{k}\cdot\underline{a}_2)\right] \tag{7.29}$$

For example, a conventional beam pattern with only a constant magnitude weighting and a phasing directed to $\underline{k}=\underline{0}$, i e , $\underline{k}_T=\underline{0}$, has a power response of

$$|g(\omega:\underline{k})|^2 = \alpha^2\mathrm{sinc}^2\left(\underline{k}\cdot\underline{a}_1\ \frac{L_1}{2}\right) + \beta^2\mathrm{sinc}^2\ |\underline{k}\cdot\underline{a}_2\ \frac{L_2}{2}\Bigg)$$

$$+ 2\alpha\beta\cos\left(\underline{k}\cdot(\underline{R}_1-\underline{R}_2)\right)\ \mathrm{sinc}\left(\underline{k}\cdot\underline{a}_1\frac{L_1}{2}\right)\ \mathrm{sinc}\left(\underline{k}\cdot\underline{a}_2\frac{L_2}{2}\right) \tag{7 30}$$

We see that the term

$$\cos\left[\underline{k}\cdot(\underline{R}_1-\underline{R}_2)\right]$$

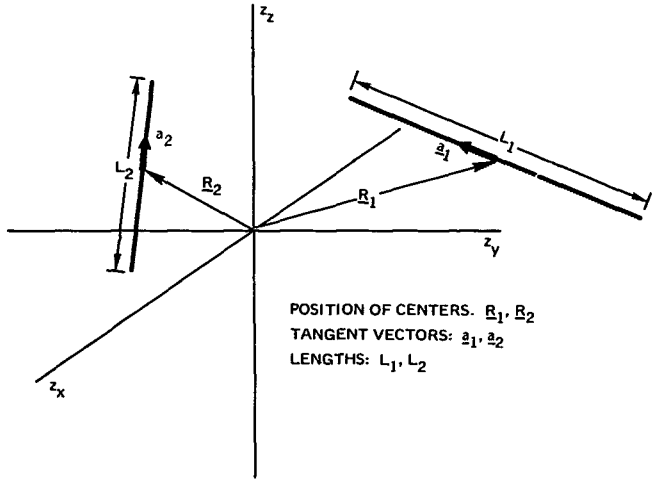

Figure 7-24 Geometry for two linear arrays with arbitrary centering

can alternatively cause the responses to interfer either constructively or destructively The crossed array with separated centers produces a larger array which leads to the narrower beam pattern ridges Since the array is not filled, i e , continuously connected, large sidelobes result giving the indicated interference pattern This is a general result when one is dealing with sparse arrays A typical situation is sketched in Figure 7-25 We can observe the general effects for the two types of noise fields that we have considered For directional noises the relevant term is the wave number difference between the target and the noise $\underline{k}_T - \underline{k}_n$ If this difference vector falls within one of the strips but not near the origin, we have essentially the same problem as discussed earlier The noise and target cannot be distinguished along that particular strip, i e , it is within a sidelobe strip so that the strip of the second resolves the two Our analysis would be substantially the same as before If, however, the difference vector is near the origin, we may be able to use the array separation to our advantage to achieve an enhanced resolution compared to that of the centered arrays, if the difference vector falls at a minimum of the interference pattern the separation can be significant This effect is clearly most pronounced when the noise difference vector is parallel to the array center separation vector One still has all the difficulties of ambiguous effects as we shall discuss for clustered arrays This effec. can not be used, however, if the two vectors are orthogonal, as indicated in Figure 7-26

The results for noise spectra with smooth frequency wave number functions are straightforward if there is no separation we have a power spectrum response

$$|g_1(\omega\, \underline{k}\cdot\underline{a}_1)|^2 + |g_2(\omega\, \underline{k}\cdot\underline{a}_2)|^2 + 2\mathrm{Re}\,[g_1(\omega\, \underline{k}\cdot\underline{a}_1)g_2^*(\omega\, \underline{k}\cdot\underline{a}_2)]$$

while if there is a separation we have

$$|g_1(\omega.\underline{k}\cdot\underline{a}_1)|^2 + |g_2(\omega\, \underline{k}\cdot\underline{a}_2)|^2 + 2\mathrm{Re}\left[e^{j\underline{k}\cdot(\underline{R}_1-\underline{R}_2)}\, g_1(\omega\, \underline{k}\cdot\underline{a}_1)g_2^*(\omega\, \underline{k}\cdot\underline{a}_2)\right]$$

If the space factor $e^{j\underline{k}\cdot(\underline{R}_1-\underline{R}_2)}$ reduces the overlap volume of the last term on the right, then there is a smaller amount of noise propagating through the array. This is generally the case Physically, with the greater separation, the noise field decorrelates Some typical optimum beam pattern responses for separated center arrays are shown in Figures 7-27 and 7-28 These should be compared to the original centered array results (See Figures 7-16 and 7-17.)

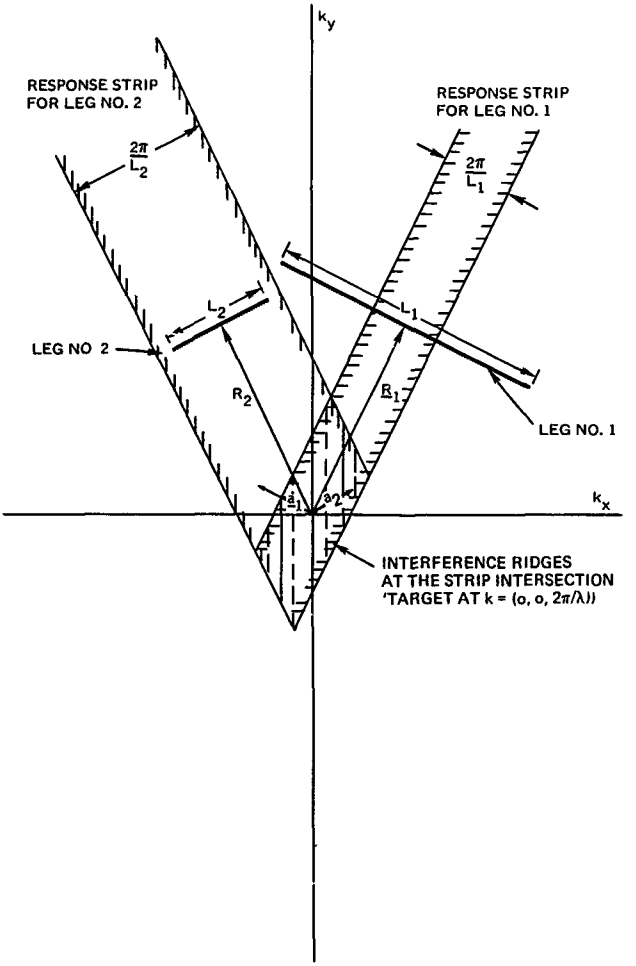

Figure 7-25. Conventional beam pattern for a crossed array with separated centers.

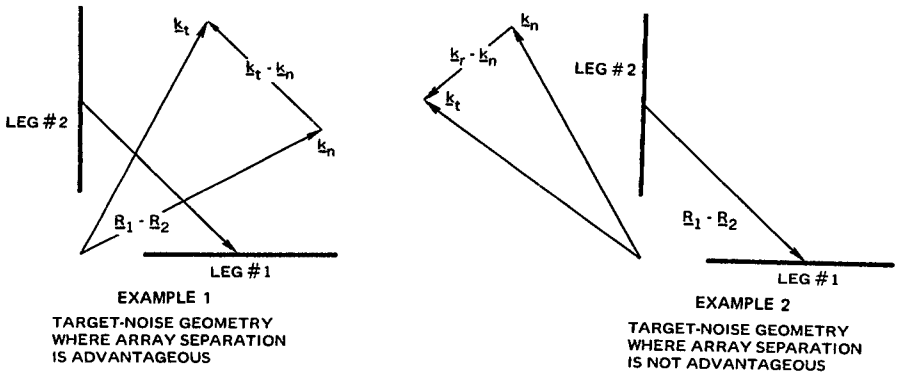

Figure 7-26. Target noise geometry with advantageous and nonadvantageous array separation

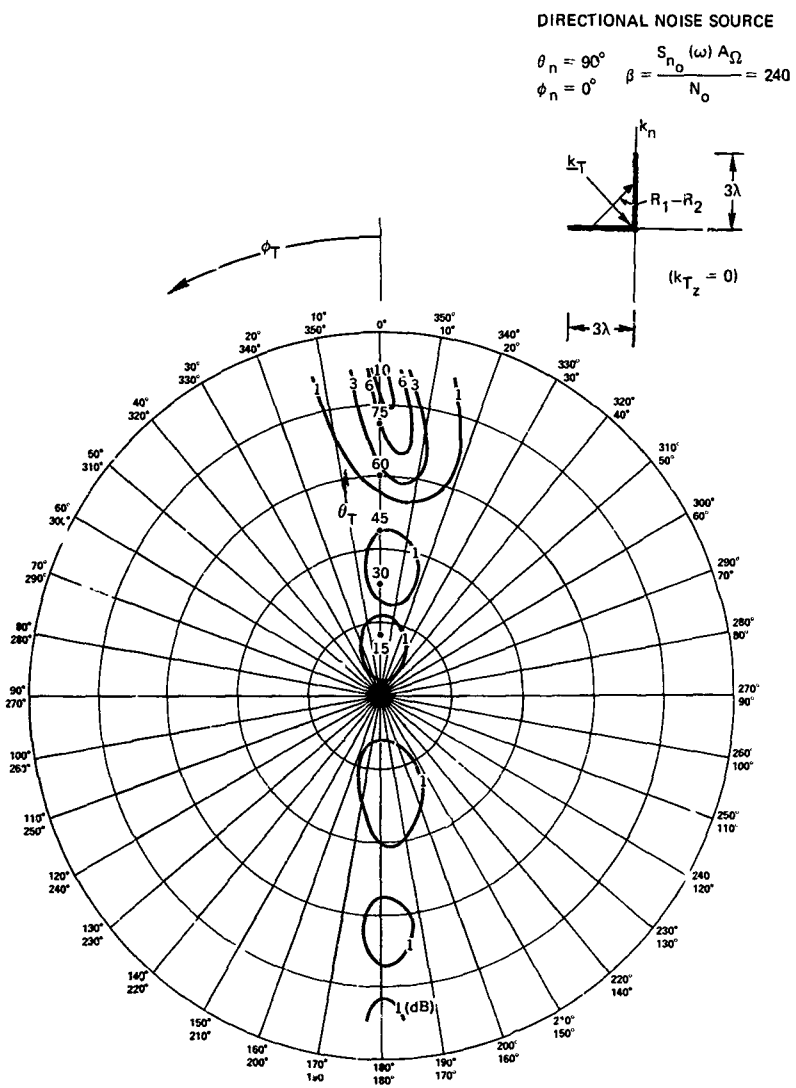

Figure 7-27 Contours (in dB) of constant noise power output, $\sigma_0^2(\omega|k_T)$ relative to N_o/L_1+L_2 for an offset center crossed array with endfire directional noise at $\phi_n = 0°$

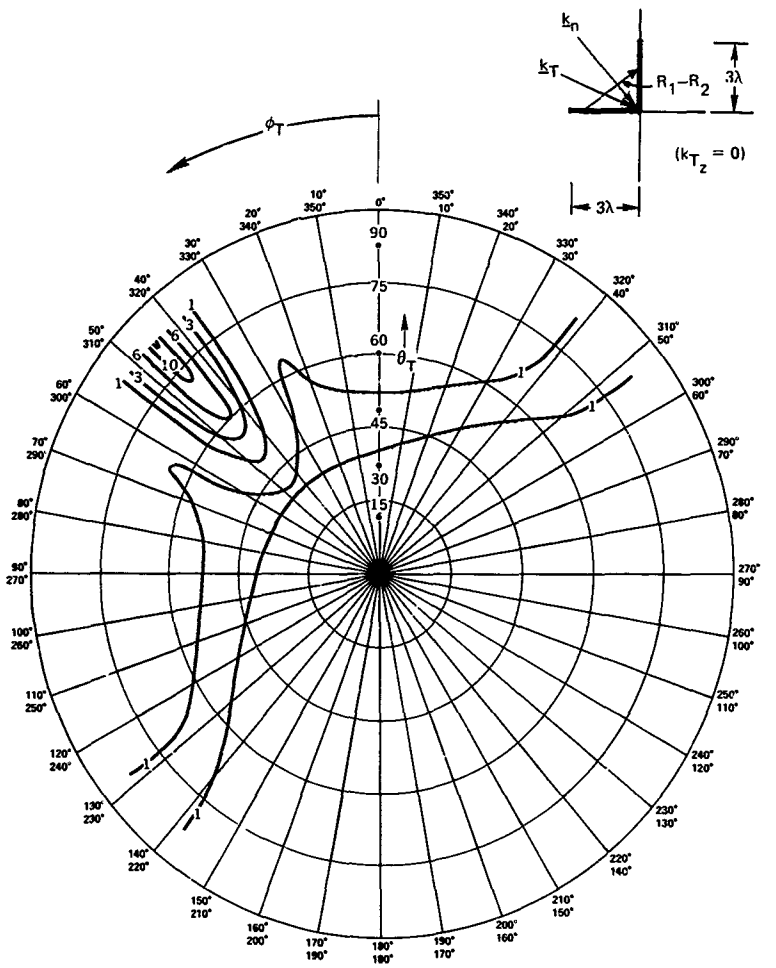

Figure 7-28. Contours (in dB) of constant noise power output, $\sigma_0^2(\omega|k_T)$ relative to N_o/L_1+L_2 for an offset center crossed array with endfire directional noise at $\phi_n = 45°$

7.3 CIRCULAR ARRAYS

The analysis of circular arrays is similar in principle to that of linear arrays, however, the transcendental functions appropriate for their analysis are not familiar to many Consequently, the salient features of circular array properties are often clouded due to the appearance of these functions Before discussing how the response patterns can be controlled to combat various noise fields, we examine the class of beam patterns that can be generated by typical circular array structures

Ring Arrays

A ring array is the simplest circular geometry, as indicated in Figure 7-29 For this array we have

$$g(\omega\ \underline{k}) = \int_0^{2\pi} G(\omega\ \phi)\, e^{j\underline{k}\cdot R\underline{a}_r(\phi)} R d\phi$$

$$= \int_0^{2\pi} G(\omega\cdot\phi)\, e^{jk_r R\cos(\phi-\phi_k)} R d\phi, \qquad (7\ 31a)$$

where

$$k_r = \sqrt{(\underline{k}\cdot\underline{a}_1)^2 + (\underline{k}\cdot\underline{a}_2)^2} \qquad (7.31b)$$

$$\phi_k = \tan^{-1}(\underline{k}\cdot\underline{a}_1, \underline{k}\cdot\underline{a}_2) \qquad (7.31c)$$

We expand $G(\omega\ \phi)$, the aperture weighting, in order to identify the structure of the beam pattern

$$G(\omega\ \phi) = \sum_{n=-\infty}^{\infty} G_n(\omega) e^{jn\phi} \qquad (7\ 32a)$$

where

$$G_n(\omega) = \frac{1}{2\pi}\int_0^{2\pi} g_n(\omega.\phi)\, e^{-jn\phi} d\phi \qquad (7\ 32b)$$

Substituting this into Eq 7 31a for $g(\omega\ \underline{k})$ yields

$$g(\omega.\underline{k}) = \sum_{n=-\infty}^{\infty} G_n(\omega) R \int_0^{2\pi} e^{j(k_r R \cos(\phi-\phi_k) + n\phi)} \, d\phi$$

$$= R \sum_{n=-\infty}^{\infty} G_n(\omega)\, e^{jn(\phi_k - \frac{\pi}{2})} \int_0^{2\pi} e^{j(k_r R \sin\phi' + n\phi')} \, d\phi'$$

$$= 2\pi R \sum_{n=-\infty}^{\infty} G_n(\omega)\, e^{jn\left(\phi_k - \frac{\pi}{2}\right)} J_n(k_r R) \qquad (7\,33)$$

We see, for example, that for a uniform weighting of $(2\pi R)^{-1}$ we have

$$g(\omega.\underline{k}) = J_0(k_r R),$$

which for a ring array plays a role similar to the $\mathrm{sinc}\left(k_a \frac{L}{2}\right)$ for linear arrays The functions $J_0(x)$ and sinc(x) are sketched in Figure 7-30. We point out that $J_0(x)$ has its first zero at 2 4 and a first sidelobe level of -.402 occurring at 3.8, as compared to π, and -.212 at 4 7 for sinc(x)

The effects of the higher order terms can be quite complex since they must be added in phase The weighting for each is $J_n(k_r R)$, and the first five members of the series are indicated in Figure 7-31. To illustrate the effects of the various terms we consider the n and -n terms in the series. We have

$$2\pi R\left(G_n(\omega) e^{jn(\phi_k - \pi/2)} J_n(k_r R) + G_{-n}(\omega) e^{-jn(\phi_k + \pi/2)} J_{-n}(k_r R)\right) =$$

$$2\pi R\, J_n(k_r R) \cdot 2R_e\left[G_n(\omega) e^{jn(\phi_k - \pi/2)}\right] \qquad (7\,34)$$

This produces a sinusoidal pattern versus ϕ_k. The total beam pattern consists of a complex linear combination of these terms The weightings have an amplitude dependence upon $k_r R$ determined by the term

$$J_n(k_r R)$$

Consequently, the important terms within the region of propagating signals are determined by the magnitude of $J_n(2\pi R/\lambda)$, which decreases for increasing n, the order of the Bessel function.

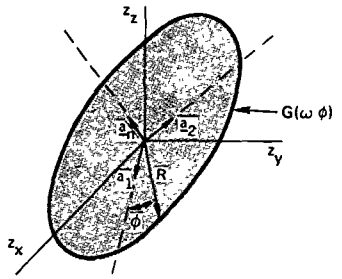

Figure 7-29. Ring array of radius R, normal orientation a_n.

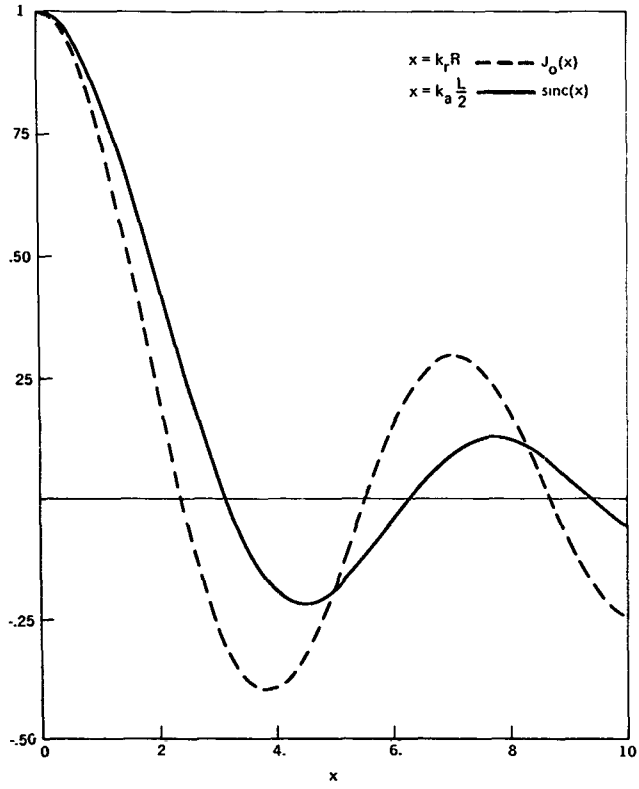

Figure 7-30 Comparison of $J_o(x)$ and sinc(x)

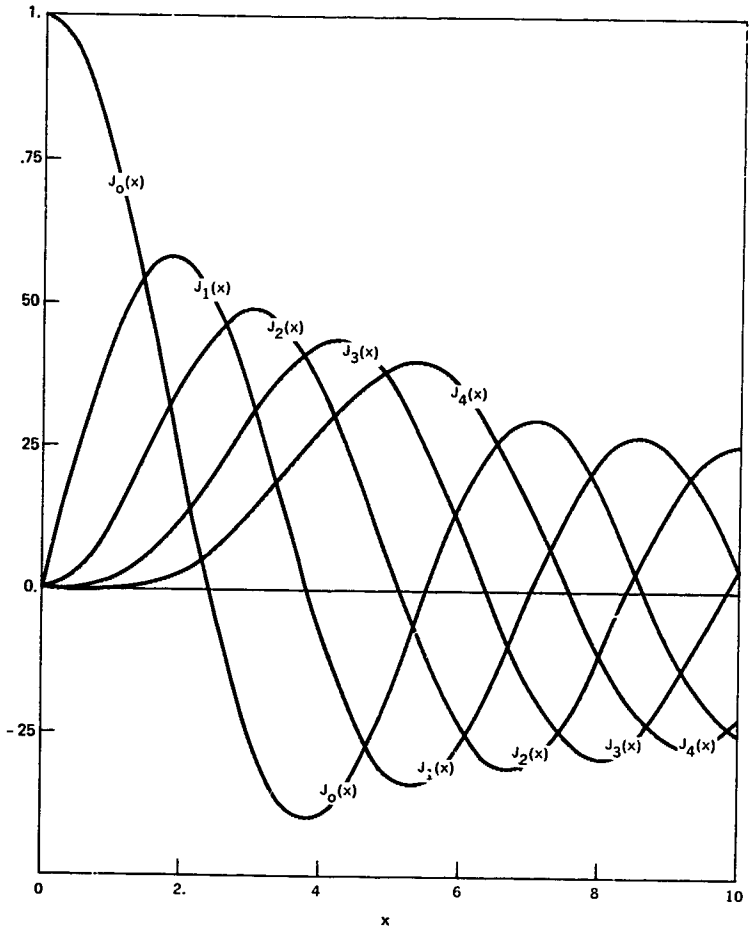

Figure 7-31 $J_0(x)$ through $J_4(x)$ vs x

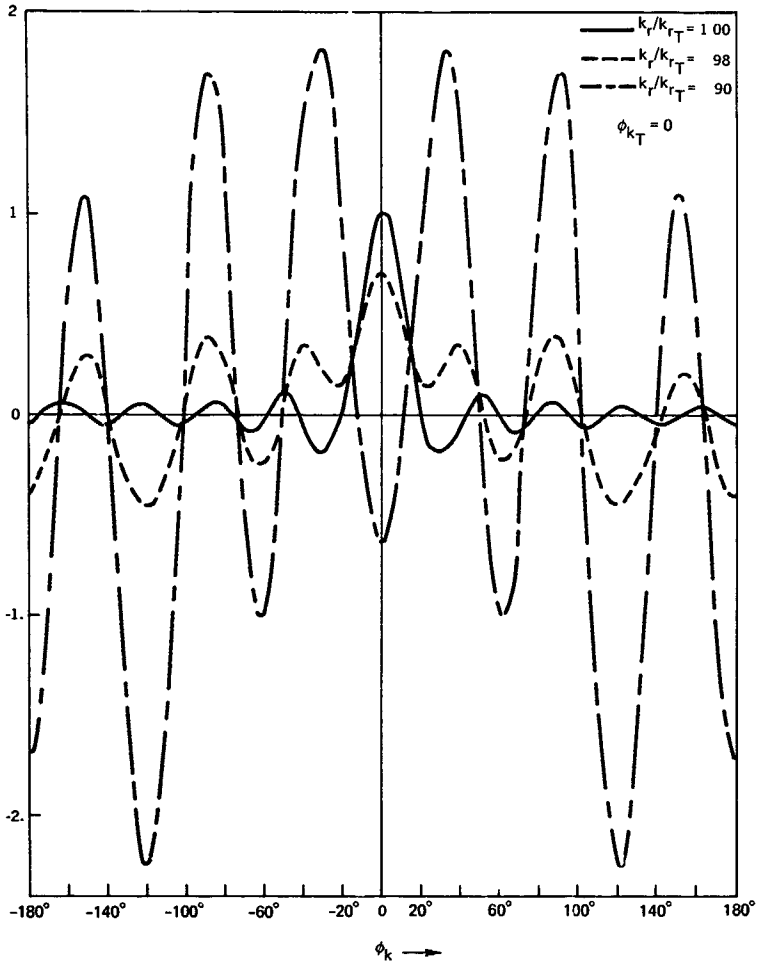

Figure 7-32. Effects of the change in wave number magnitude in the synthesis of a super-directive beam pattern for a circular array

One can intuitively see how superdirective effects can be produced at a specific k_{r_T} by choosing the coefficients needed to produce an impulsive function versus ϕ_k, i e , one can ignore the dependence upon the wave number magnitude. We have

$$2\pi R J_n(k_{r_T}R) e^{j\frac{n\pi}{2}} G_n(\omega) = e^{-jn\phi_{k_T}} \tag{7 35a}$$

so that

$$g(\omega\ k) \simeq \frac{1}{2N+1} \sum_{n=-N}^{N} \left(\frac{J_n(k_r R)}{J_n(k_{r_T}R)} \right) e^{-jn(\phi_k - \phi_{k_T})} \tag{7 35b}$$

which for $k_r = k_{r_T}$ approximates an impulse at ϕ_{k_T} As the value of k_r is changed the exact phasing necessary for the construction of the impulse altered which leads to extremely large sidelobe levels. If the white noise level is finite or there are signals propagating with a different wave number magnitude, this can introduce a serious degradation in performance. An illustration of these effects is given in Figure 7-32 We observe, consequently, that for any particular $\underline{k}_r$, we can achieve a superdirective beam pattern, however, we encounter a sensitivity problem in doing so In any finite element array, we cannot achieve the impulsive beam pattern; however, the basic arguments are similar. In reference 13, a detailed analysis of circular arrays with a finite number of elements has been done. Consideration was given to the effects of sensitivity

There are several useful relations dealing with integral representations, recurrences and series expansions for Bessel functions Reference 11 is one of the readily available sources which has tabulated many of them We can illustrate the use of several of them by considering an example where we phase the array to a wave number with finite $\underline{k}_T$.

For a signal with wave number $\underline{k}_T$ we need a phasing given by

$$\frac{1}{2\pi R} e^{-j\underline{k}\cdot\underline{r}_T} = \frac{1}{2\pi R} e^{-jk_{r_T}R\cos(\phi-\phi_{k_T})} = G(\omega,\phi), \tag{7.36}$$

where

$$k_{r_T} = [(\underline{k}_T\cdot\underline{a}_1)^2 + (\underline{k}_T\cdot\underline{a}_2)^2]^{1/2}$$

Substituting this into Eq 7 31 yields

$$g(\omega,\underline{k}) = J_o[(\underline{k}-\underline{k}_T)_r R]\,, \tag{7 37a}$$

where

$$(\underline{k}-\underline{k}_T)_r = [((\underline{k}-\underline{k}_T)\cdot\underline{a}_1)^2 + ((\underline{k}-\underline{k}_T)\cdot\underline{a}_2)^2]^{1/2} \tag{7 37b}$$

i e , we simply steer the array to $\underline{k}_T$ as expected For example, when both the target and wave number are in the same plane as the array with wave number magnitude of $2\pi/\lambda$, as illustrated in Figure 7-1b, we have

$$g(\omega\ \underline{k}) = J_o\left(\frac{4\pi R}{\lambda}\sin\left(\frac{\Delta\phi}{2}\right)\right) \tag{7 38}$$

where $\Delta\phi$ is the separation angle between the target wave number and h Naturally, there is no change as the target moves around at edge because of the circular symmetry

If we pursue the Fourier analysis, we arrive at the same result in a somewhat more circuitous manner The analysis is, however, illustrative of the use of the relations needed in the analysis of more complex problems We have

$$G_n(\omega) = \frac{1}{2\pi}\int_0^{2\pi} \frac{e^{-jk_{r_T}R\cos(\phi-\phi_{k_T})}}{2\pi R}\, e^{-jn\phi}\, d\phi$$

$$= \frac{1}{2\pi R}\, e^{-jn\left(\phi_{k_T}+\frac{\pi}{2}\right)} J_n(k_{r_T}R) \tag{7 39}$$

Substituting this into Eq. 7 33 yields

$$g(\omega\ \underline{k}) = \sum_{n=-\infty}^{\infty} e^{jn(\phi_k-\phi_{k_T})} J_n(k_{r_T}R)\, J_n(k_r R) \tag{7 40}$$

One now uses the relation [29, Eq 9.1 79]

$$J_n(W)e^{jn\beta} = \sum_{m=-\infty}^{\infty} J_{n+m}(u)\, J_m(v)e^{jm\alpha}$$

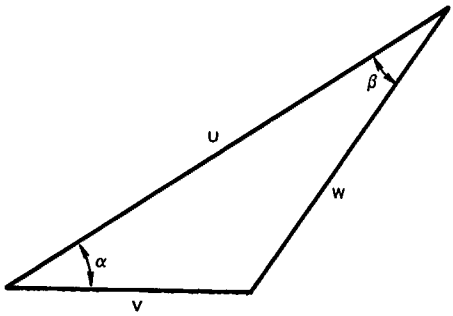

Figure 7-33. Relation of terms in equation 7 40

where the terms W,u,v, and α,β are geometrically related as indicated in Figure 7-33. This yields

$$g(\omega\ \underline{k}) = J_o\left[(\underline{k}-\underline{k}_T)_r R\right] \tag{7 41}$$

As pointed out above, this approach is not as direct, however, it does indicate the usefulness of one of the product theorems for Bessel functions. Generally, often complicated expressions can be simplified considerably by using these relationships or, more important, there is a more straightforward approach to the analysis

We now consider the effects of staving a circular array whose geometry is illustrated in Figure 7-34 We assume that the staving operation multiplies the shading $G(\omega\ \phi)$ by a gating function $G_{st}(\phi)$ as illustrated in Figure 7-35, where N is the number of staves, ϕ_s is their angular width, and ϕ_o is the origin The Fourier series associated with this function is given by

$$G_{st}(n) = e^{-j\phi_o}\sum_{m=0}^{N-1} e^{-j(2\pi mn/N)}\frac{1}{2\pi}\int_{-\phi_{s/2}}^{\phi_{s/2}} e^{-jm\phi}\,d\phi$$

$$= \begin{cases} 0, & n \neq Nk \\ \dfrac{e^{-jn\phi_o}}{2\pi}\, N\phi_w\ \mathrm{sinc}\ \dfrac{n\phi_s}{2}, & n = Nk \end{cases} \tag{7 42}$$

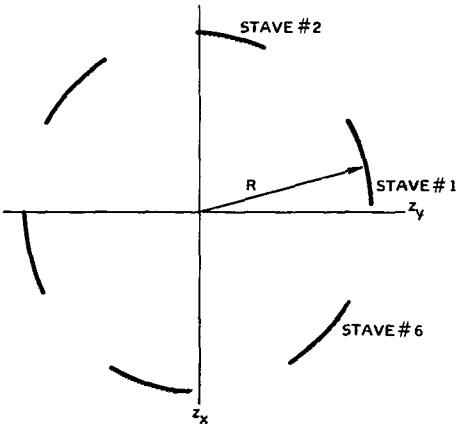

Figure 7-34. Circular array with six staves.

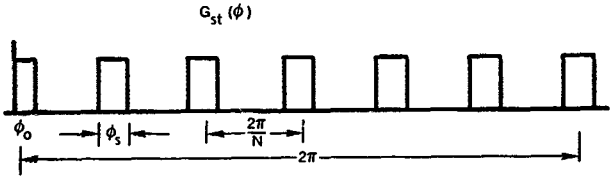

Figure 7-35 Gating function for representing staved arrays

The effect of the staving can be represented as a gating of the original pattern, i.e ,

$$G_S(\omega\ \phi) = G_{S_T}(\phi)\, G(\omega\ \phi) \tag{7.43}$$

Consequently, the coefficients $\{G_{st}(n)\}$ and $\{G(\omega\ n)\}$, which represent the Fourier series of the shading on the circle, must be convolved to obtain the final set of coefficients for the array If the weighting factor has significant harmonics greater than $\frac{N}{2}$, then the coefficients are aliased Generally this is not the case, the only effect of the staving is to cause the Fourier coefficients to be repeated at intervals of N The net beam pattern is then (assume $\phi_o = 0$)

$$g(\omega{:}k) = N\phi_w R \sum_{n=-\infty}^{\infty} \sum_{m=-\infty}^{\infty} G(\omega{:}m+n) e^{j(m+nN)\left(\phi_k + \frac{\pi}{2}\right)} J_{m+nN}(k_r R) \cdot \operatorname{sinc}\left(\frac{nN\phi_w}{2}\right) \tag{7.44}$$

which introduces the same type of grating structure that we observe for clustered linear arrays with a periodic repetition interval If a highly directional source can propagate through one of the ambiguous sidelobes we will experience deterioration in performance If not, we would not be bothered except for the increase in white noise due to the increased array area. The simplest example of these effects can be demonstrated when the array is conventionally steered. In this case, we have

$$G(\omega\ n) = \frac{1}{N\phi_S R}\ \delta_{n0} \tag{7.45}$$

the resulting pattern is given by

$$g(\omega\ k) = \sum_{n=-\infty}^{\infty} e^{jnN(\phi_k+\pi/2)} J_{nN}(k_r R) \operatorname{sinc}\ \frac{nN\phi_s}{2} \tag{7.46}$$

Exact statements regarding the number of significant sidelobes are difficult to make. The question becomes, for those values of n where $\operatorname{sinc}(nN\phi_s/2)$ is significant, i e , $n < 2\pi/\phi_s N$, how many functions $J_{nN}(k_r R)$ have maximum values in the wave number region of interest This question requires a rather lengthy examination of the behavior of Bessel functions.

In examining the design of optimum beam patterns for circular arrays we confine our detailed analysis to directional noise fields and to those which are isotropic in the plane containing the array The general concepts illustrated within the context of linear arrays are still applicable and are quite useful in analyzing more complicated noise field structures.

As with crossed arrays, we assume that there is sensor noise present This noise has a correlation given by

$$E[w(t\ \phi_1)w(\tau.\phi_2)] = N_o\delta(t-\tau)\delta(\phi_1-\phi_2) = N_o\delta(t-\tau)\delta_\Omega(\phi_1-\phi_2) \tag{7.47}$$

Note that the noise output generated by such a process is given by

$$\sigma_w^2(\omega) = N_o\int_0^{2\pi} |g(\omega\ \phi)|^2\ R d\phi \tag{7 48}$$

For a conventionally steered array, this yields

$$\sigma_w^2(\omega) = N_o\int_0^{2\pi} \left|\frac{e^{jk_{r_T}R\cos(\phi-\phi_T)}}{2\pi R}\right|^2 R d\phi = N_o/2\pi R = N_o/A_\Omega \tag{7.49}$$

Note that we cannot model the noise with a two-dimensional white noise spectrum of the form

$$E[w(t\ \underline{z})w(\tau\ \underline{\zeta})] = N_o\delta(t-\tau)\delta(\underline{z}-\underline{\zeta}) \tag{7 50a}$$

or

$$P_w(\omega\ \underline{k}) = N_o \tag{7 50b}$$

The reason for this is that although the circular array has resolution capabilities in all directions, its wave number response decays asymptotically only as $|\underline{k}|^{-1}$ When integrated across the entire two-dimensional wave vector domain, this decay is not sufficiently fast in the noise power output of the array so that any nonzero aperture weighting is necessarily infinite

In Section 6 we analyzed optimum beam pattern design for directional noise field with an arbitrary number of components and arrays of a general structure We can easily specialize these results for circular arrays. For example, for a single noise source we have

$$g(\omega,\underline{k}\ \underline{k}_T) = \frac{\left[J_o([\underline{k}-\underline{k}_{T_r}]R) - \frac{\frac{2\pi RS_n(\omega)}{N_o}}{1+\frac{2\pi RS_n(\omega)}{N_o}} J_o([\underline{k}_T-\underline{k}_n]_r R)\, J_o([\underline{k}-\underline{k}_n]_r R) \right]}{1-\frac{\frac{2\pi RS_n(\omega)}{N_o}}{1+\frac{2\pi RS_n(\omega)}{N_o}} J_o^2([\underline{k}_T-\underline{k}_n]_r R)} \qquad (7\ 51)$$

$$\sigma_o^2(\omega\cdot\underline{k}\,|\underline{k}_T) = \frac{N_o}{2\pi R}\left[\frac{1+\frac{2\pi RS_n(\omega)}{N_o}\left(1-J_o^2([\underline{k}_T-\underline{k}_n]_r R)\right)}{1+\frac{2\pi RS_n(\omega)}{N_o}} \right]^{-1} \qquad (7\ 52)$$

Since

$$J_o^2(x) \simeq 1-\frac{x^2}{2} \qquad |x| << 1$$

and

$$\mathrm{sinc}^2(x) \simeq 1-\frac{x^2}{3} \qquad |x| << 1,$$

a circular array has a 3/2 high resolution improvement over a linear array of comparable dimensions operating at broadside In Figures 7-36 and 7-37 typical noise power outputs for a circular array for directional noise fields incident normally and tangentially are indicated

For the circular array we can analyze the optimum processor for a noise field which has a two dimensional isotropic structure. Our representation of two-dimensional noise processes in Section 2 and some useful relations among Bessel functions are the key factors which produce a relatively simple result for the optimum beam pattern and its noise power output From Section 2, Eq. 2 70, we have

$$S_n(\omega\ |\underline{z}|) = \frac{1}{(2\pi)^2}\int_0^\infty \rho_o(\omega\ k_r) J_o(k_r|\underline{z}|)\, k_r dk_r = \frac{1}{2\pi}\, f_o(\omega\ |\underline{z}|) \qquad (7.53)$$

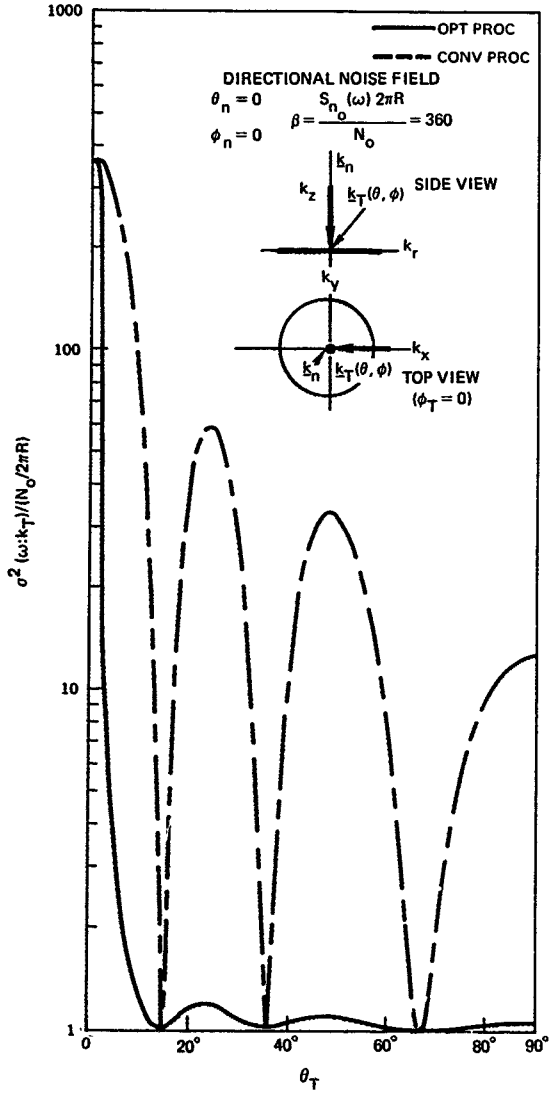

Figure 7-36. Output noise for a ring array with broadside directional noise.

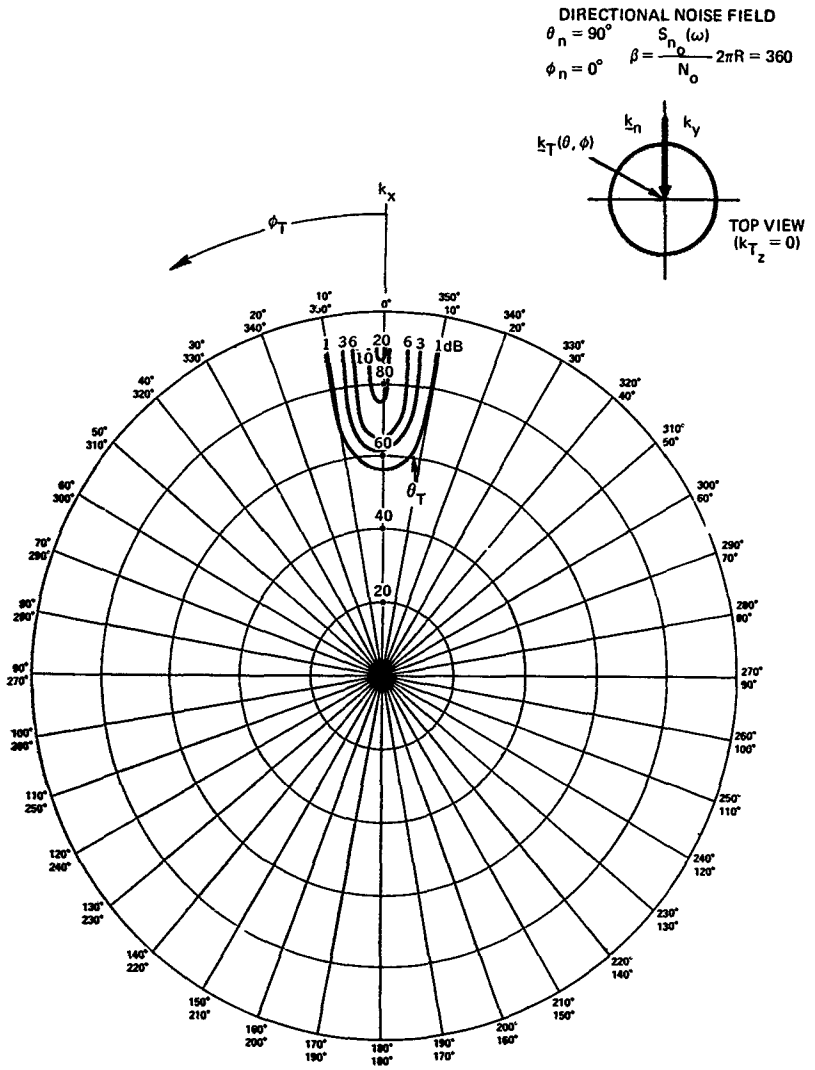

Figure 7-37. $\sigma_o^2(\omega:k_T)$: noise power output relative to $N_o/2\pi R$ for a directional noise source at endfire with a ring array.

for the structure of an isotropic two dimensional noise field From Section 4, Eq 4 9, we want to solve the integral equation

$$\int_{\Omega} S_n(\omega: |\underline{z} - \underline{\zeta}|)\, G(\omega \cdot \underline{\zeta}) d\underline{\zeta} + N_0 G(\omega\, \underline{z}) = \lambda(\omega) e^{j\underline{k}_T \cdot \underline{z}} \quad \underline{z} \in \Omega, \tag{7 54}$$

where $\lambda(\omega)$ is chosen such that the beam pattern has unity response in the target direction. For the circular array geometry this becomes

$$\int_0^{2\pi} S_n\left(\omega: \left|2R \sin\left(\frac{\phi_1 - \phi_2}{2}\right)\right|\right) G(\omega.\phi_2)\, R d\phi_2 + N_0 G(\omega \cdot \phi_1)$$

$$= \lambda(\omega) e^{jk_{T_r} R \cos(\phi - \phi_T)}, \qquad 0 \leq \phi_1 < 2\pi \tag{7 55}$$

The spatial eigenfunctions for this array and noise field are of the form $e^{jn\phi}$[1]. This suggests using an eigenfunction approach, which for this case is simply a Fourier series expansion of $G(\omega\ \phi)$, i e., we expand $G(\omega\ \phi)$ in the form

$$G(\omega.\phi) = \sum_{n=-\infty}^{\infty} G_n(\omega) e^{jn\phi} \tag{7.56}$$

For the left hand side of Equation 7.55 we have

$$\int_0^{2\pi} S_n\left(\omega: \left|2R \sin\left(\frac{\phi_1 - \phi_2}{2}\right)\right|\right) \sum_{n=-\infty}^{\infty} G_n(\omega) e^{jn\phi_2} R d\phi_2 + N_0 \sum_{n=-\infty}^{\infty} G_n(\omega) e^{jn\phi_1}$$

$$= \sum_{n=-\infty}^{\infty} G_n(\omega) \left[\int_0^{2\pi} S_n\left(\omega: \left|2R \sin\left(\frac{\phi}{2}\right)\right|\right) e^{-jn\phi} R d\phi + N_0\right] e^{jn\phi_1} \tag{7 57}$$

For the right hand side of Eq 7 55 we use the Bessel function expansion from Ref 25

---

[1] *This is the continuous analog of Gaarder's observation for the eigenvectors for discrete arrays [13]*

$$e^{jZ\cos\phi} = \sum_{n=-\infty}^{\infty} J_n(Z)e^{jn(\phi+\pi/2)} \tag{7.58}$$

From this we obtain

$$\lambda(\omega)e^{-jk_{T_r}R\cos(\phi-\phi_T)} = \lambda(\omega)\sum_{n=-\infty}^{\infty} J_n(k_{T_r}R)e^{jn(\pi/2-\phi_T)}e^{jn\phi}1 \tag{7.59}$$

We match Fourier coefficients to solve for $G_n(\omega)$, or

$$G(\omega:\phi) = \lambda(\omega)\sum_{n=-\infty}^{\infty} \frac{J_n(k_{T_r}R)\,e^{jn(\pi/2-\phi_T)}}{\int_0^{2\pi} S_n\left(\omega:|2R\sin\left(\frac{\phi}{2}\right)|\right)e^{-jn\phi}Rd\phi + N_o}\, e^{jn\phi}, \tag{7.60}$$

where $\lambda(\omega)$ is a normalization factor. The term in the denominator can be simplified appreciably by use of the wave number representation of Eq. 7.53. Substituting for $S_n\left(\omega:|2R\sin\left(\frac{\phi}{2}\right)|\right)$ yields

$$\int_0^{2\pi} S_n(\omega:|2R\sin\left(\frac{\phi}{2}\right)|\,e^{-jn\phi}Rd\phi = \frac{1}{(2\pi)^2}\int_0^{\infty}\int_0^{2\pi}\rho_o(\omega:k_r)J_o(k_r2R\sin\left(\frac{\phi}{2}\right))\,k_rRe^{-jn\phi}\,d\phi$$

(7.61)

Again one of the Bessel function relationships is useful. We have

$$\frac{1}{2\pi}\int_0^{2\pi} J_o\left(2Z\sin\left(\frac{\phi}{2}\right)\right)\,e^{jn\phi}\,d\phi = J_n^2(Z); \tag{7.62}$$

therefore,

$$\int_0^{2\pi} S_n\left(\omega:|2R\sin\left(\frac{\phi}{2}\right)|\right)e^{-jn\phi}Rd\phi = \frac{R}{2\pi}\int_0^{\infty}\rho_o(\omega:k_r)J_n^2(k_rR)k_rdk_r \tag{7.63}$$

In order to compute the output noise we need from Eq 4 15

$$\sigma^2(\omega\,|\underline{k}_T) = \left[\int_0^{2\pi} e^{-jk_{T_r}R\cos(\phi-\phi_T)}\, G(\omega:\phi)Rd\phi\right]^{-1} \tag{7.64}$$

Using the Fourier expansion of $G(\omega:\phi)$ and Eq 7.58 for the exponential we derive

$$\sigma^2(\omega\ k_T) = \left[2\pi R \sum_{n=-\infty}^{\infty} \left(\frac{J_n^2(k_{T_r}R)}{\frac{R}{2\pi}\int_0^{\infty} \rho_o(\omega:k_r)J_n^2(k_TR)k_r dk_r + N_o}\right)\right]^{-1} \text{ or} \tag{7.65a}$$

$$\sigma^2(\omega\ k_T) = \frac{N_o/2\pi R}{\left[\sum_{n=-\infty}^{\infty}\left(\frac{J_n^2(k_{T_r}R)}{\frac{N_oR}{2\pi}\int_0^{\infty}\rho_o(\omega:k_r)\,J_n^2(k_TR)k_r dk_r + 1}\right)\right]} \tag{7.65b}$$

A number of special cases can be considered at this point. For example, for a target normal to array, k_{T_r} is zero so we have

$$\sigma^2(\omega.\underline{k}_T) = \frac{N_o}{2\pi R}\left(\frac{2\pi}{N_oR}\int_0^{\infty}\rho_o(\omega:k_r)J_o^2(k_rR)k_r dk_r + 1\right) \tag{7 66}$$

i e., only the term n=0 is significant in the output noise power. For the case of ring noise, from Eq 2 79, we have

$$\rho_o(\omega:k_r) = \frac{2\pi}{k_r}\, S_o(\omega)u_o(k_r-k_o)$$

This produces an output power of

$$\sigma^2(\omega.\underline{k}_T) = \frac{N_o/2\pi R}{\left[\sum_{n=-\infty}^{\infty}\left(\frac{J_n^2(k_{T_r}R)}{N_oRS_o(\omega)\,J_n^2(k_oR) + 1}\right)\right]} \tag{7 67}$$

Most $\rho(\omega:k_r)$ of interest are zero for $k_r > 2\pi/\lambda$. Since $J_n(x) \to 0$ for $x < 2\pi/\lambda$ with n increasing, there are a finite number of terms which are significant This is analogous to linear arrays when there were $L/\lambda + 1$ significant eigenvalues Unfortunately, one must resort to numerical procedures to evaluate the expressions, just as in the linear array case Some typical situations are indicated in Figures 7-38 and 7-39 As the final topic in our analysis of circular array structures, we briefly consider some aspects of disc arrays The geometry of a disc array is the same as a circular, or ring, array except that the entire area is filled The beam pattern of a conventionally steered disc array can easily be found

$$g_c(\omega,\underline{k}|\underline{k}_T) = \frac{1}{A_\Omega}\int_\Omega e^{j(\underline{k}-\underline{k}_T)\cdot\underline{z}}dz$$

$$= \frac{1}{\pi R^2}\int_0^R\int_0^{2\pi} e^{j(\underline{k}-\underline{k}_T)_r\, r\cos(\phi-\phi_T)} rd\phi = \frac{2}{R^2}\int_0^R J_0((\underline{k}-\underline{k}_T)_r r)rdr$$

$$= \left(\frac{2J_1((\underline{k}-\underline{k}_T)_r R)}{(\underline{k}-\underline{k}_T)_r R}\right)^2 \qquad (7.68)$$

This is often termed an "Airy Disc" from its use in Fourier optics [30]. In Figure 7-40 we have compared the beam patterns of linear, circular, and disc arrays with the same length and/or diameters. We observe that $(2J_1(x)/x)^2$ has its first zero at x = 3.8 and a first sidelobe level of 0.0044 at x = 5.2. The behavior near the origin is

$$\frac{2J_1(x)^2}{1} \cong 1 - \frac{x^2}{4}, \quad |x| << 1 \qquad (7.69)$$

Consequently, its resolution is approximately the same as a ring array.

In analyzing the response to various noise fields we observe that directional fields are again a special case, as those results shown in Section 6, and that analytic results for isotropic fields are not tractable with the results taking the form of Bessel function series.

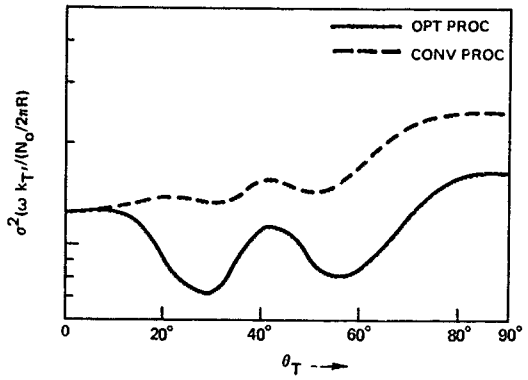

Figure 7-38. Optimum and conventional array noise power output relative to $N_o/2\pi R$ for isotropic noise with a ring array.

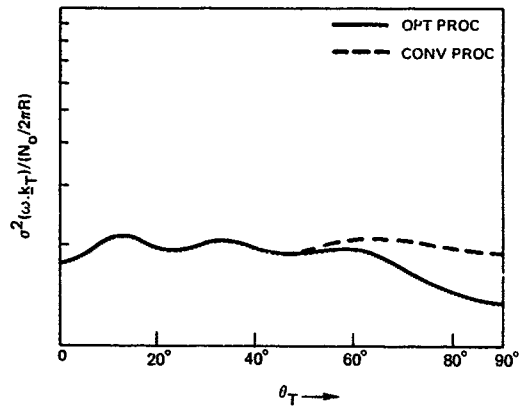

Figure 7-39. Optimum and conventional array noise power output relative to $N_o/2\pi R$ for ring noise with a ring array.

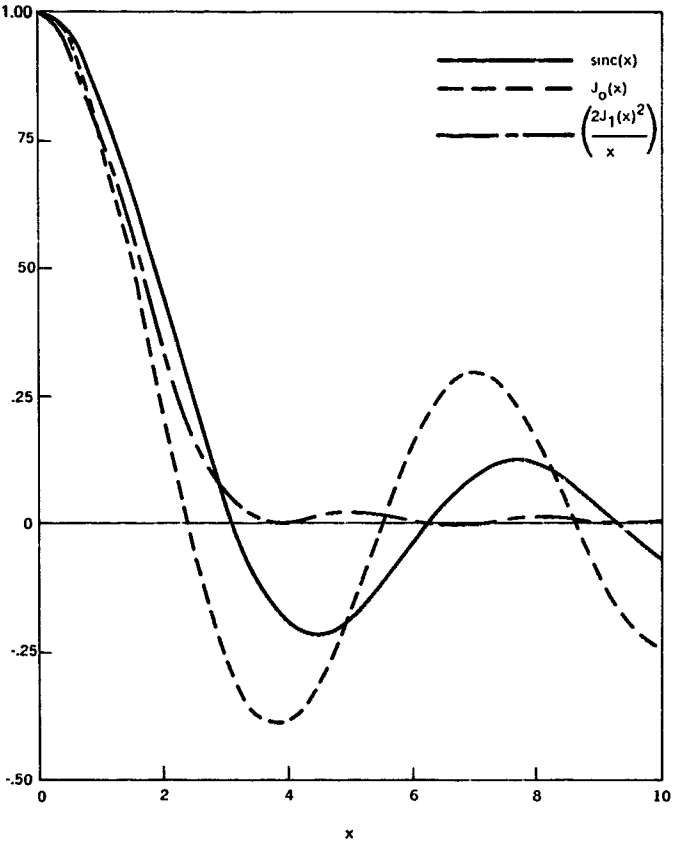

Figure 7-40. Array comparison of convention beam pattern, $\text{sinc}_\Omega(k)$, for

a) linear – $\text{sinc}\left(k\frac{L}{2}\right)$

b) ring – $J_0(kR)$, and

c) disc – $\left(\frac{2J_1(kR)}{kR}\right)^2$.

8. ARRAY PROCESSING SYSTEMS

In many situations one must consider systems composed of arrays, i e., an array of arrays. There are many practical reasons that lead one to this situation. For example, one often has a discrete set of sensors the apertures of which have a finite set of geometries, so that each sensor may have directional properties in itself. If the individual wave number responses are more or less omnidirectional for frequencies of interest and their separations are large, then the theory of discrete arrays is probably most appropriate. Typically, however, the sensors are not omnidirectional, the separations are modest, and we need to consider the system as a whole

The physical motivations for using clusters of arrays are that a complete coverage is either too expensive or impossible. Further economical motivation is that one may be forced simply by high data rates to "cluster" arrays because the sensor outputs can not be processed individually, particularly if real-time processing is important

Usually clustered array systems have a suboptimum performance so it is important to understand when the losses enter and to compare their performance to an optimized system In this section we consider the analysis of such systems and consider some representative examples. Figure 8-1 illustrates the general structure of the systems being considered.

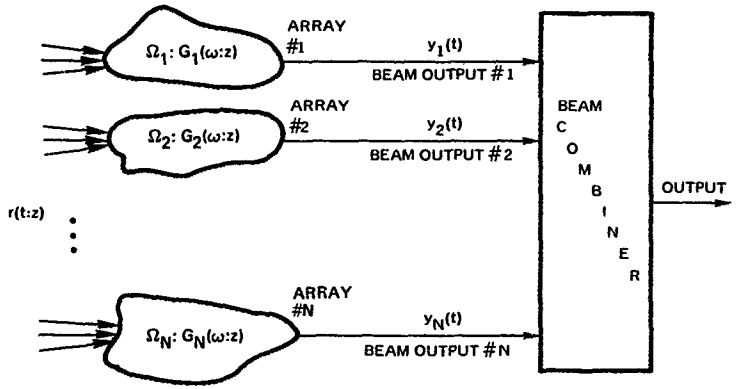

Figure 8-1. Clustered array structures.

Several possibilities and combinations exist in the design of these systems One can conventionally phase, or beamform, with or without shading each subarray, or one can generate an optimum beam as we have done throughout the text. In addition, one can perform direct delay and sum beamforming, or one can introduce the theory of an optimal discrete array to do

the beam-combining Consequently, there are four combinations of processing that we consider We have tabulated and commented upon these combinations in the following table

Processing combination for clustered arrays

Combinations of Beams

Individual Beams	*Conventional Combination*	*Optimum Combination*
Conventional Arrays	Conventional array theory of sonar texts	General area of application of discrete array theory
Optimum Arrays	Possible application for non-plane (distributed) wave targets	Least amount of performance loss for these suboptimum systems

There are also two considerations which commonly simplify the details of the analysis considerably First, each of the individual arrays has the same pattern, except for a phase offset due to the displacement of their centers, in the second arrays are regularly spaced

Since we have considered the synthesis of individual arrays, we concentrate upon the problem of combining them. We define the beam pattern of each array for a target of $\underline{k}_T$, as $G_i(\omega:\underline{k}\,|\underline{k}_T)$. The output of each array is given by

$$dY_i(\omega) = \iint G_i(\omega\ \underline{k}|\underline{k}_T)\ dR\,(\omega.\underline{k}) + dW_i(\omega) \tag{8.1}$$

Consequently, the spectral noise covariance matrix for the beams is

$$S_{n_{ij}}(\omega) = \iint G_i(\omega_i\underline{k}\ k_T)P_n(\omega,\underline{k})G_j^*(\omega:\underline{k}\,|\underline{k}_T)\ \frac{d\underline{\kappa}}{(2\pi)^N} + N_o\delta_{ij}\int_{\Omega_i}|G_i(\omega:\underline{z})|^2\ d\underline{z} \tag{8.2}$$

We constrain the individual array responses to satisfy

$$G_1(\omega:\underline{k}_T|\underline{k}_T) = 1\ ,$$

i.e., we have incorporated the steering delay in the individual arrays. There is no loss of generality here since the combiner can assign an arbitrary weighting to compensate for this.

The beam combiner calculates a weighted sum of the individual array outputs In suboptimum processing, the weights are preassigned and do not directly depend upon the noise spectral covariance

matrix of the individual array outputs. In optimum processing, these weights are optimized to achieve the minimum noise output power From discrete array theory this is given by [30, 31]

$$C_i(\omega) = \frac{\underline{E}[\omega|\underline{k}_T]^t\,[S_n(\omega)]^{-1}\,e^{jk_Tz_1}}{\underline{E}[\omega|\underline{k}_T]^t\,[S_n(\omega)]^{-1}\,\underline{E}(\omega|\underline{k}_T)} \tag{8.3}$$

where

$$\underline{E}[\omega|\underline{k}_T] = \left[e^{-j\underline{k}_Tz_1}, \quad , e^{-j\underline{k}_Tz_n}\right]^\dagger$$

and $\underline{z}_1$ is the location of the center of the Nth array

In either the optimum or conventional case

$$dY_o(\omega) = \sum_{i=1}^{N} C_i(\omega)\, dY_i(\omega), \tag{8.4a}$$

where we impose the constraint of unity response in the target direction,

$$\sum_{i=1}^{N} C_i(\omega)\, G_i(\omega:\underline{\kappa},\underline{k}_T) = \sum_{i=1}^{N} C_i(\omega) = 1 \tag{8.4b}$$

The beam pattern for the total system is

$$g(\omega.\underline{\ell}|\underline{\ell}_T) = \sum_{i=1}^{M} C_i(\omega)\;\; g_i(\omega\;\underline{\ell}|\underline{k}_T) \tag{8.5}$$

and the performance can be expressed as the inverse of the noise output power, or

$$\sigma^2(\omega|\underline{k}_T) = \left(\sum_{i=1}^{N}\sum_{j=1}^{N} C_i(\omega)\, S_{n_{ij}}(\omega)\, C_j^{*}(\omega)\right) \tag{8 6}$$

For the optimum array configuration this becomes

$$\sigma_o^2(\omega|\underline{k}_T) = \left(E[\omega|\underline{k}_T]^t\,[S_n(\omega)]^{-1}\,\underline{E}[\omega|\underline{k}_T]\right)^{-1} \tag{8 7}$$

which is identical to that derived for discrete element arrays This is as far as one can go with a general formulation for an arbitrary collection of beams

To proceed a step further, we require that the individual arrays have a common aperture weighting except for a linear phasing for its arising from their location, or

$$g_i(\omega\cdot\underline{\kappa}|\underline{k}_T) = g_{com}(\omega\ \underline{\kappa}|k_T)e^{j(\underline{k}-\underline{k}_T)\cdot\underline{z}_1} \tag{8 8}$$

Here we have assumed that each array is centered at z_1 and there exists the possibility of only steering the individual beams, i.e., the weighting is constant but one adds a linear phase shift to account for each array location

$$S_{n_{ij}}(\omega) = \iint g_{com}(\omega\ \underline{\kappa}|\underline{k}_T)|^2\,P(\omega\ \underline{\kappa})e^{j(\underline{k}-\underline{k}_T)\cdot(\underline{z}_i-\underline{z}_j)}\frac{d\underline{k}}{(2\pi)^N}$$

$$+\ N_o\,\delta_{ij}\int_{\Omega_{com}}|G(\omega.z)|^2\,dz \tag{8.9a}$$

$$g_o(\omega\underline{\kappa}\cdot\underline{k}_T) = g_{com}(\omega\ \underline{\kappa}|\underline{k}_T)\sum_{i=1}^{N}C_i(\omega)e^{j(\underline{k}-\underline{k}_T)\cdot\underline{z}_1}$$

$$= g(\omega\ \underline{k}|\underline{k}_T)\,g_{comb}(\underline{k}-\underline{k}_T) \tag{8.9b}$$

where Ω_{com} is the aperture of the common array

$$G_{comb}(\underline{k}) = \sum_{i=1}^{N}C_i(\omega)\,e^{j\underline{k}\cdot\underline{z}_1} \tag{8 9c}$$

Consequently, we find that the final beam pattern can be expressed as a product of the beam pattern for the individual arrays and a beam factor for the combination of them as distributed in space. Note that the $C_i(\omega)$ can be designed either conventionally or in an optimum fashion.

The performance is expressed in basically the same form as above with somewhat minor simplifications.

$$\sigma^2(\omega\,|k_T) = \sum_{i=1}^{N}\sum_{j=1}^{N} C_i(\omega) S_{n_{ij}}(\omega)\, C_j(\omega) \tag{8.10}$$

$$= \iint |g_{com}(\omega.\underline{k}\,|\underline{k}_T)|^2\, |G_{comb}(\underline{k}\text{-}\underline{k}_T)|^2\, \frac{d\underline{k}}{(2\pi)^N} + \sum C_i(\omega)|^2 \iint_{\Omega} |G_{com}(\omega\, \underline{z})|^2\, dz$$

When the combination beam is designed in an optimum manner, we obtain

$$\sigma_o^2(\omega\,|\underline{k}_T) = \left(\sum_{i=1}^{N}\sum_{j=1}^{N} e^{-j\underline{k}_T \cdot \underline{z}_i} [S_{n_{ij}}(\omega)]^{-1} e^{j\underline{k}_T \cdot \underline{z}_i} \right)^{-1}$$

$$= (\underline{E}^T(\omega|\underline{k}_T)\, [S_n(\omega)]^{-1}\, \underline{E}(\omega|\underline{k}_T))^{-1} \tag{8.11}$$

Essentially, we are examining the covariance for a noise field which has passed through the wave-number filter $g(\omega:\underline{k}\,|\underline{k}_T)$. There is an extensive literature on the theory of optimum discrete arrays. Sometimes the relative spacing between the clusters is so small that the continuous array theory is a more convenient analysis tool as, for example, when the individual array responses are omnidirectional and their separations quite close In other cases the spacing is wide and the continuous theory is no longer appropriate for analyzing the design and operation of the beam combiner Essentially, one should say that the element spacing is sparse

The analysis of sparse arrays is quite difficult and the dominant concern is the sidelobe structure of the beam. There are two special cases, however, which can be analyzed. Fortunately, they are of practical interest and are indicative of the general results encountered. In the first of these we have the clusters spaced at regular intervals in a lattice, whereas in the second the individual arrays are spaced at regular intervals on rings. The analysis of lattice

transforms has been studied extensively in spectrographic methods for the analysis of crystal structures. In the single dimensioned distributions, the theory of sampled data systems and Z transform methods are quite useful. The analysis of ring structures is more complex and it is easy to become mixed in a maze of the Bessel functions which appear. Fortunately, there are some reasonable simple examples which indicate the basic theory involved

A complete discussion of lattice array would take us too far astray at this point In particular, a large literature exists dealing with optimum processing for discrete arrays. Most of it does not convey the intuitive insight that we have obtained for continuous arrays We consider line clusters which have a distribution of the form and which are conventionally combined

We have assumed an even number of elements The modification for an odd number with a cluster located at the origin is straightforward. Substituting into Equation 8.9c yields

$$g_{comb}(\underline{k}) = \sum_{n=-N/2}^{N/2-1} C_n(\omega)\, e^{j(\underline{k}\cdot\underline{\alpha}_a)[(2n+1)/2]L} \tag{8.12}$$

This is in a form that is useful for defining a term which puts our analysis in the context of Z transforms. One identifies $Z(\underline{k})$ as

$$Z(\underline{k}) = e^{j\underline{k}\cdot\underline{a}_a L} \tag{8.13}$$

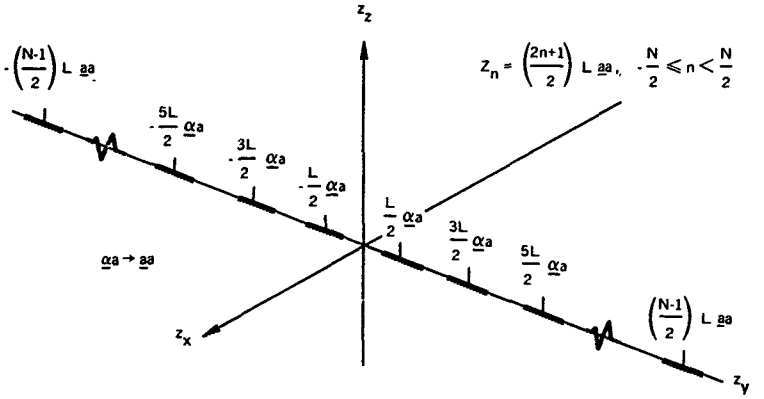

Figure 8-2. Clustered line array.

This leads to the expression

$$G_{comb}(k) = e^{-j\underline{k}\cdot\underline{\alpha}_a(N-1/2)L} \sum_{n=0}^{N-1} C_{n-\frac{N}{2}}(\omega)\, e^{j\underline{k}\cdot\underline{a}_a L\, n}$$

$$= Z(\underline{k})^{-(N-1/2)} \sum_{n=0}^{N-1} C_{n-\frac{N}{2}}(\omega)\, Z(\underline{k})^{n} \qquad (8.14)$$

Tables of these have been extensively tabulated in conjunction with the use in digital filtering methods. It is also the basic formulation used by Schelkunoff in his studies of linear arrays.

First we note that Z repeats itself as a function of $\underline{k}$. We have

$$Z(\underline{k}) = Z\left(\underline{k} + n\,\frac{2\pi}{L}\,\underline{\alpha}_a\right) = Z\left(\underline{k} + n\,\frac{2\pi}{\lambda}\,\frac{\lambda}{L}\,\underline{a}_a\right) \qquad (8.15)$$

Consequently, if $L/2\lambda$ is greater than unity then the beam pattern repeats itself within the region of $|k| < \frac{2\pi}{\lambda}$ or where propagating noise appears, i e., there is an ambituity in the beam pattern. We examine the consequences of this in subsequent discussions. Basically, the array is undersampled at this point.

In order to make our discussion more concrete we consider an example; let

$$C_n(\omega) = \frac{1}{N} \tag{8 16}$$

We then have

$$G_{comb}(\underline{k}) = (Z(k))^{-(N-1/2)} \sum_{n=0}^{N-1} \frac{1}{N} Z(k)^n$$

$$= \frac{Z(k)^{-(N-1/2)}}{N} \frac{1 - Z(k)^N}{1 - Z(k)} = \frac{1}{N} \frac{Z(\underline{k})^{N/2} - Z(\underline{k})^{-N/2}}{Z(\underline{k})^{1/2} - Z(\underline{k})^{-1/2}} \tag{8.17}$$

$$= \text{sinc}\left[(k \cdot \alpha_a) N \frac{L}{2}\right] \Big/ \text{sinc}\left[(k \cdot \alpha_a) \frac{L}{2}\right]$$

This is the space factor for a linear array weighting of the individual outputs, as illustrated in Figure 8-3. The main lobe of the pattern array factor has a width of $\frac{2\pi}{NL}$, i.e., it is still determined by the total array length. However, there exists the possibility of ambiguous effects due to the sidelobe at $2\pi/L$. If this is outside $2\pi/\lambda$, then only white noise enters through this side lobe To consider the effect in more detail, let the individual arrays be phased conventionally and assume that their length is

$$L_o = \frac{L}{K} \tag{8.18}$$

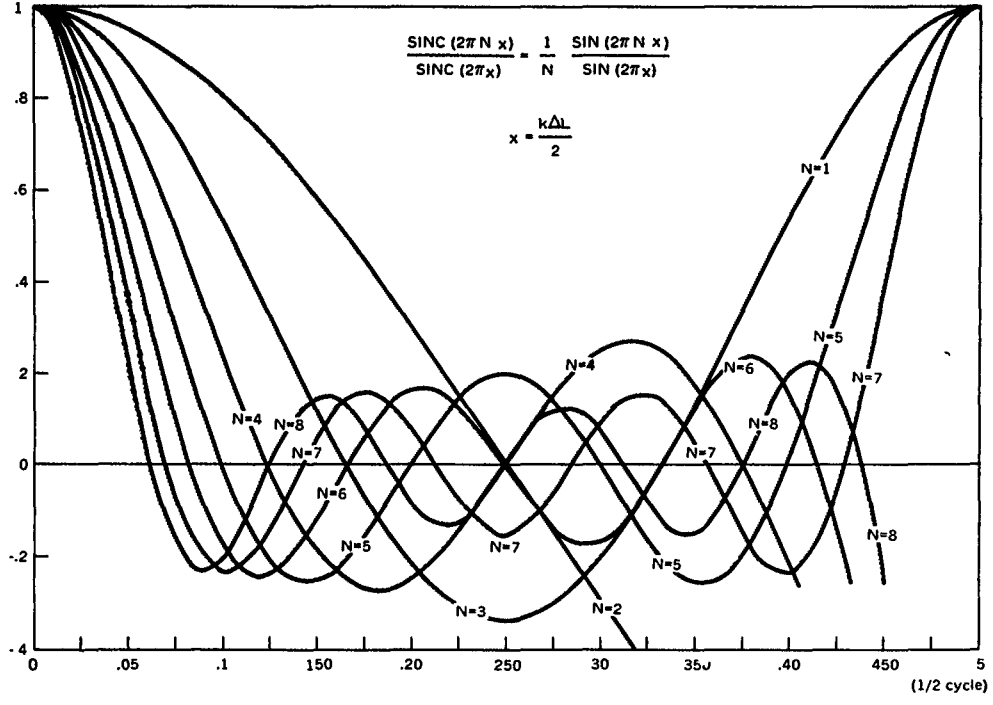

Figure 8-3. Space factor, or grating lobe structure for clustered arrays

In Figure 8-4 we have sketched the product $G(\omega.\underline{k}|\underline{k}_T)\, G_{comb}(\underline{k}\text{-}\underline{k}_T)$ which assumes the target is broadside such that $\underline{k}_T \cdot \underline{\alpha}_a = 0$. We make a comparison for this case N = 4 There are 2k-1 side lobes of level

$$\operatorname{sinc}\left(\frac{n\pi}{K}\right) \qquad n = \pm 1, \ldots, \pm k$$

One consequently obtains a main lobe of width $2(\pi/NL)$ The effect of the sparse sampling is to introduce these side lobes If the background noise is over regions which are significant, then one has a performance deterioration due to the sparse sampling. For example, a directional noise sourse could enter through one of them. If the noise is uniform, or $L_\lambda < 1/2$ with small elements, then the array is not sparse and one does not observe a reduction in performance.

While we have chosen a uniform weighting of the individual array outputs, one can use any type of weighting desired. Tables of Z transforms are useful in this respect. For the more common shadings one observes a spreading of the width $2(\pi/NL)$ and a reduction of the minor side lobe levels between the beams.

The modification for the situation in which each array is designed optimally is straightforward. One still observes a modulation of the main beam by the space factor However, the more important issue concerns combining the beams optimally, which is the basic issue in the design of discrete arrays.

The design of optimum discrete sparsely spaced discrete arrays is, in general, best done by computational methods as analytical results are quite tedious to obtain. There is, however, one example which does not involve a great deal of tedium and illustrates some of the issues which appear in the design of sparse arrays. As one might expect, the noise field consists of directional signal plus a white component. We assume that the noise has a wave number $\underline{k}_n$ and a level $S_{n_o}(\omega)$ and that the white component has level N_o. From Equation 8.2 we have

$$S_{n_{ij}}(\omega)\int G_{com}(\omega:\underline{k}|\underline{k}_T|^2\, P(\omega,k)e^{j\underline{k}(\underline{z}_i-\underline{z}_j)}\, \frac{dk}{2\pi} + N_o \int_{L/2}^{L/2} |G_{com}(\omega:\ell|\underline{k}_T)^2\, d\ell$$

$$+ S_{n_o}(\omega)|G_{com}(\omega.\underline{k}|\underline{k}_n)|^2\, e^{j\underline{k}_n(\underline{z}_i-\underline{z}_i)} = N_o \int |G_{com}(\omega:\underline{k}_a|\underline{k}_T)|^2\, \frac{dk_a}{(2\pi)^N} \quad (8.19)$$

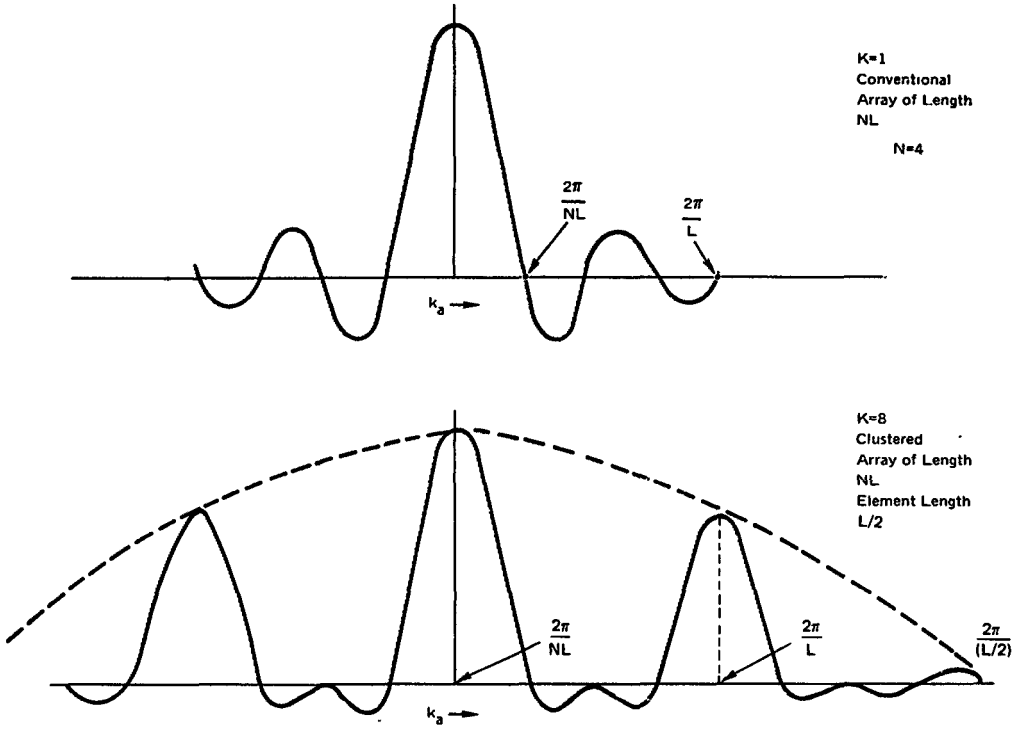

Figure 8-4. Comparison of clustered array and conventional array of the same length.

We define

$$\alpha = N_o \int |G_{com}(\omega\ \underline{k}|\underline{k}_T)|^2\ \frac{dk}{2\pi} \tag{8 20a}$$

$$\beta = S_{n_o}(\omega)\ |\ G_{com}(\omega\ \underline{k}_n|\underline{k}_T)|^2 \tag{8 20b}$$

the matrix whose elements are defined above can be represented as

$$[S] = \alpha \underline{I}_N + \beta \begin{bmatrix} e^{j\underline{k}_n \cdot \underline{z}_1} \\ \cdot \\ \cdot \\ \cdot \\ e^{j\underline{k}_n \cdot \underline{z}_N} \end{bmatrix} \begin{bmatrix} e^{j\underline{k}_n \cdot \underline{z}_1} \\ \cdot \\ \cdot \\ \cdot \\ e^{j\underline{k}_n \cdot \underline{z}_N} \end{bmatrix}^{\dagger} \tag{8.21}$$

The inverse of the matrix can be found using the inversion formula of Section 4

$$[S]^{-1} = \frac{1}{\alpha} \left\{ \underline{I}_N - \frac{\beta}{\alpha\left(1 + \frac{BN}{\alpha}\right)} \begin{bmatrix} e^{j\underline{k}_n \cdot \underline{z}_1} \\ \cdot \\ \cdot \\ \cdot \\ e^{j\underline{k}_n \cdot \underline{z}_N} \end{bmatrix} \begin{bmatrix} e^{j\underline{k}_n \cdot \underline{z}_1} \\ \cdot \\ \cdot \\ \cdot \\ e^{j\underline{k}_n \cdot \underline{z}_N} \end{bmatrix}^{\dagger} \right\} \tag{8.22}$$

The optimum noise power output then becomes

$$\sigma_o^2(\omega|\underline{k}_T) = \left(\frac{N}{\alpha} \left| 1 - \frac{\beta N/\alpha}{1+\beta N/\alpha} \sum_{i=1}^{N} \frac{e^{j(\underline{k}_T - \underline{k}_n)\cdot \underline{z}_i}}{N} \right|^2 \right)^{-1} \tag{8.23}$$

We observe that the space factor for a uniformly weighted summing of the individual array output enters the calculations. The same comments regarding closed form expressions for lattice space arrays and the use of Z transform theory enter here.

If we consider the same linear regularly spaced distribution discussed above with individual arrays of extent L_o, we have

$$\alpha = \frac{N_o}{2L_o} \tag{8 24a}$$

$$\beta = S_{n_o}(\omega)\,\mathrm{sinc}^2\left((\underline{k}_n - \underline{k}_T)\cdot\underline{\alpha}_a\,\frac{L_o}{2}\right) \tag{8 24b}$$

$$G_{comb}(\underline{k}) = \left|\sum_{n=1}^{N}\frac{1}{N}\,\epsilon^{j\underline{k}\,\underline{z}_n}\right|^2 = \frac{\mathrm{sinc}\left[\underline{k}\cdot\underline{\alpha}_a N\,\frac{L}{2}\right]}{\mathrm{sinc}\left[\underline{k}\cdot\underline{\alpha}_a\,\frac{L}{2}\right]} \tag{8.24c}$$

$$\sigma_o^2(\omega\,|\underline{k}_T) = \frac{L_o N}{N_o}\left\{\frac{1+\left(\frac{L_o N}{N_o}\right)S_{n_o}(\omega)\,\mathrm{sinc}^2\left(\Delta\underline{k}\cdot\underline{\alpha}_a\,\frac{L}{2}\right)\left(1-\frac{\mathrm{sinc}^2\left(\Delta k\cdot\underline{\alpha}_a N\,\frac{L}{2}\right)}{\mathrm{sinc}^2\left(\Delta\underline{k}\cdot\underline{\alpha}_a\,\frac{L}{2}\right)}\right)}{1+\left(\frac{L_o N}{N_o}\right)S_{n_o}(\omega)\,\mathrm{sinc}^2\left(\Delta\underline{k}\cdot\underline{\alpha}_a\,\frac{L}{2}\right)}\right\} \tag{8.24d}$$

where

$$\Delta\underline{k} = \underline{k}_T - \underline{k}_n \tag{8.24e}$$

This is very similar to the results that we obtained for a continuous array of length L_oN. In Equation 8.24 we need only identify the directional noise level as β and the array length as L_oN. The important term is the space factor which is identified as ρ. This causes deterioration in the performance at wave number intervals of

$$(\underline{k}_T - \underline{k}_n)\underline{\alpha}_a\,\frac{L}{2} = \pi, \tag{8 25}$$

i.e., when the target and noise are separated by wave number components of $2\pi/L$ as projected upon the array. At these points, the performance becomes

$$\sigma_o^2(\omega\,|\underline{k}_T) = \frac{L_o N}{N_o}\left\{1+\frac{L_o N}{N_o}\,S_{n_o}(\omega)\,\mathrm{sinc}^2\,\frac{n\pi}{K}\right\}^{-1} \tag{8.26}$$

for

$$L_o = \frac{L}{K} \qquad n = \pm 1, \ldots, \pm k-1$$

Consequently, if $L_\lambda > 1$, spatial aliasing enters and degrades the performance The only way to combat this is for the individual arrays to have enough resolution to eliminate these effects. In Figure 8-5, we have sketched the performance for some representative values of the parameters.

This concludes our discussion on clustered arrays The principle effects are space factors and spatial aliasing If these effects are not significant, then clustering represents a possible processing method which has distinct computational advantages, especially for optimum processing. We have confined our attention to linear combinations. While the clustering is suboptimum for spatially coherent signals, it may become a superior method if the signals are not plane waves. Here quadratic operations upon the clusters may become desirable.

PREFORMED BEAMS

One of the most time consuming aspects of processing array data for changing noise fields is in calculating and forming the spatial, or beamforming, operations One method of reducing the amount of computation is to preform the beams and operate solely upon the beam outputs. For arrays which can spatially sample the ambient field on the lattice distribution of points, the computational advantages are even more attractive since fast Fourier transform methods can be introduced in order to form the multiple beam outputs.

Consider an array processing system as illustrated in Figure 8-6. In general, one has

$$y_i(t) = \int_\Omega \int_{-\infty}^{\infty} r(\tau:\underline{\xi})\, g_i(t-\tau:\underline{\xi})\, d\underline{\xi} d\tau \tag{8.27}$$

The combiner performs a linear combination upon the beam outputs so as to direct a sum beam in the target direction $\underline{k}_T$, with

$$\sum_{i=1}^{N} C_i(\omega:\underline{k}_T)\, g_i(\omega:\underline{k}_T) = 1 \quad \forall\omega \tag{8.28}$$

For conventional processing the beam spacing is quite close in wave numbers, so that the individual beam outputs are simply scanned to look in the respective direction. There are two areas where more general combinations of beams are useful: in null placement methods, which are closely related to the synthesis of optimum pattern for directional noises, and in the approximate synthesis of patterns in general. As the two are closely related, we consider them simultaneously.

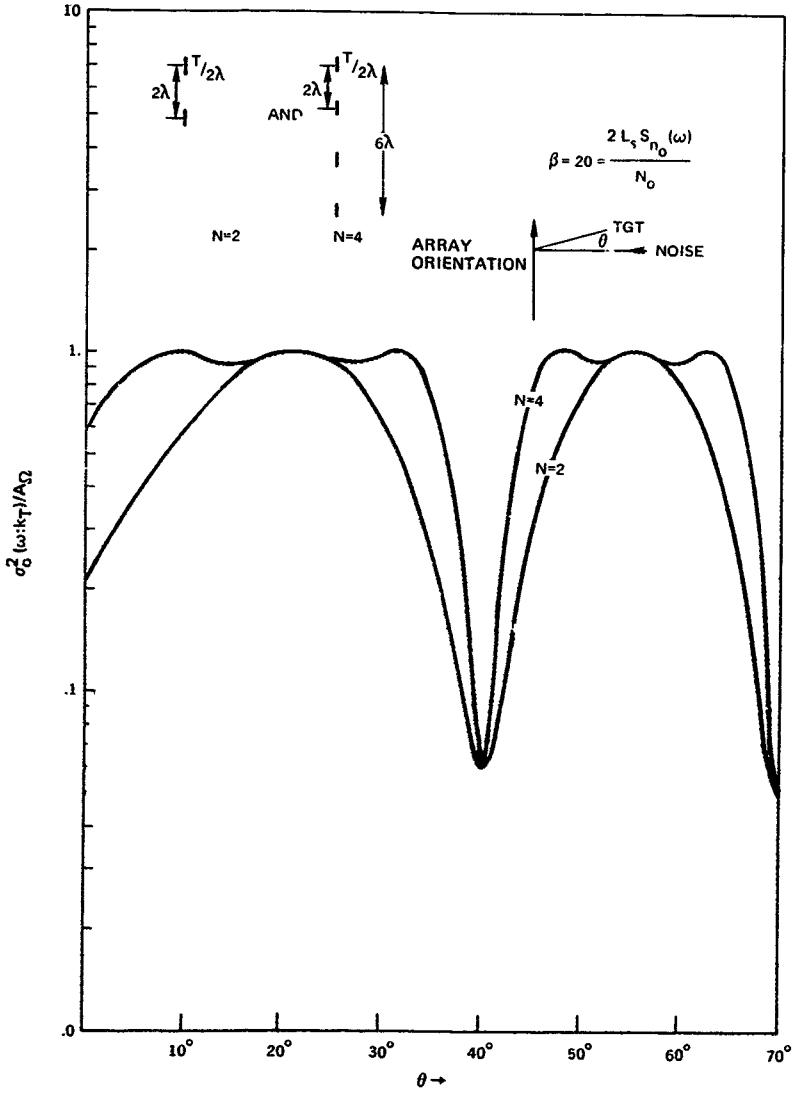

Figure 8-5. Optimum array output power relative to A_Ω for clustered arrays in directional plus white noise (normalized).

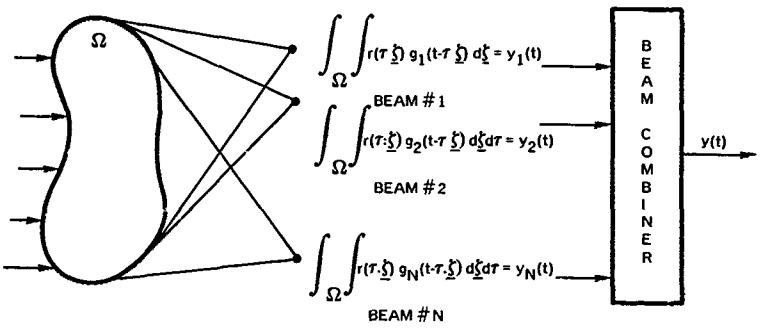

Figure 8-6 Preformed beam processing.

The basic issue is the selection of a set of coefficients $\left\{C_i(\omega:\underline{k}_T)\right\}\Big|_{i=1}^{N}$

$$g(\omega:\underline{k}\,|\,\underline{k}_T) = \sum_{i=1}^{N} C_i(\omega:\underline{k}_T)\, g_i(\omega:\underline{k}) \tag{8.29a}$$

or

$$G(\omega:\underline{z}\,|\,\underline{k}_T) = \sum_{i=1}^{N} C_i(\omega:\underline{k}_T)\, G_i(\omega:\underline{z}) \tag{8.29b}$$

such that

$$\sigma^2(\omega:\underline{k}_T) = \iint \left|g(\omega:\underline{k}\,|\,\underline{k}_T)\right|^2 P(\omega:k)\, \frac{d\underline{k}}{(2\pi)^N} + N_o \int_\Omega \left|G(\omega:\underline{z}\,|\,k_T)\right|^2 d\underline{z} \tag{8.30}$$

is minimized subject to the constraint of 8.28.[1] This becomes

$$\sigma^2(\omega:\underline{k}_T) = \sum_{i=1}^{N}\sum_{j=1}^{N} C_i(\omega:\underline{k}_T) C_i^*(\omega:\underline{k}_T) \iint P_n(\omega:\underline{k})\, g_i(\omega:k) g_j^*(\omega:\underline{k})\, \frac{d\underline{k}}{(2\pi)^N} + N_o \int_\Omega G_i(\omega:\underline{z})\, G_i^*(\omega:\underline{z})\, d\underline{z} \tag{8.31a}$$

[1] *We are temporarily suppressing the $|k_T$ conditional*

and

$$\sum_{i=1}^{N} C_i(\omega:\underline{k}_T)\, g_i(\omega\cdot\underline{k}_T) = 1 \tag{8.31b}$$

To optimize the choice of the coefficients $\left\{C_i(\omega.\underline{k}_T)\right\}\Big|_{i=1}^{N}$ we differentiate incorporating the constraint by Lagrange multipliers. By differentiating the performance with the constraint introduced we have for the k^{th} coefficient

$$2\sum_{j=1}^{N} S_{ij}(\omega)\, C_j^*(\omega) + \lambda g_i(\omega:\underline{k}_T) = 0, \tag{8.32a}$$

where the elements of the matrix $[S_{ij}(\omega)]$ are

$$S_{ij}(\omega) = \iint P_n(\omega:\underline{k}) g_i(\omega:\underline{k}) g_j^*(\omega:\underline{k}) + N_o \int_{\Omega} G_i(\omega.\underline{z}) G_j^*(\omega.\underline{z})\, dz \tag{8 32b}$$

The optimal choice of $\left\{C_j^*(\omega.\underline{k}_T)\right\}\Big|_{i=1}^{N}$ is then

$$C_j^*(\omega\cdot\underline{k}_T) = -\frac{\lambda}{2}\sum_{i=1}^{N} [S(\omega)]^{-1}_{ji} g_i(\omega:\underline{k}_T) \tag{8.33}$$

In order to determine the Lagrangian multiplier λ we impose the constraint equation to obtain

$$1 = -\frac{\lambda}{2}\sum_{i=1}^{N}\sum_{j=1}^{N} [S(\omega)]^{-1}_{ji} g_i(\omega:\underline{k}_T) g_j(\omega:\underline{k}_T) = -\frac{\lambda}{2}\, T_r([S(\omega)]\rho_G(\omega\ k_T)), \tag{8 34a}$$

where

$$\rho_g(\omega:\underline{k}_T) = \begin{bmatrix} |g_1(\omega:\underline{k}_T)|^2 & g_1(\omega\ \underline{k}_T)g_2^*(\omega:\underline{k}_T) \\ g_2(\omega\ \underline{k}_T)g_1^*(\omega:\underline{k}_T) & |g_2(\omega\cdot\underline{k}_T)|^2 \\ & g_1(\omega:\underline{k}_T)g_j^*(\omega\ \underline{k}_T) \end{bmatrix} \quad (8.34b)$$

As a result, we have

$$C_j(\omega\ \underline{k}_T) = \frac{\sum_{i=1}^{N} g_i^*(\omega:\underline{k}_T)\ [S(\omega)]^{-1}_{ij}}{Tr\left[\rho_g(\omega:\underline{k}_T)\ [S(\omega)]^{-1}\right]} \quad (8\ 35)$$

The system performance is given by

$$\sigma^2(\omega:\underline{k}_T) = \left(T_r\left\{\rho_g(\omega:\underline{k}_T)\ [S(\omega)]^{-1}\right\}\right)^{-1} \quad (8.36)$$

Several special cases are of interest here For directional noise fields with a white background component, the matrix [S(ω)] is evaluated easily

$$S_{ij}(\omega) = \sum_{m=1}^{M} S_m(\omega) g_i(\omega:\underline{k}_m) g_j^*(\omega\cdot\underline{k}_m) + N_o \int_{\Omega} G_i(\omega:\underline{z}) G_j^*(\omega:\underline{z})\, dz \quad (8.37)$$

This is further simplified if

$$g_m(\omega:\underline{k}_T) = 0 \quad m = 2,M$$

i.e., all but one of the preformed beams have nulls in the target direction. The performance becomes

$$\sigma^2(\omega\cdot\underline{k}_T) = [S(\omega)]^{-1}_{11}$$

with a total beam pattern of the form

$$g(\omega:\underline{k}) = \left(g_1^*(\omega:\underline{k}_T) \sum_{i=1}^{N} [S(\omega)]^{-1}_{1j}\, g_j(\omega:k)\ \ ([S(\omega)]^{-1}_{11})\right)^{-1} \quad (8.38)$$

This is shown to represent an optimum null placement technique

As an example of this, we consider the following Assume that we have an array of length L and that there are noise sources of level $S_{n_o}(\omega)/2$ located symmetrically at broadside, $k_n = \pm \frac{2\pi}{\lambda}\cos(\theta)$, plus the background noise. Because of the symmetry of the situation we generate preformed beams of the form

$$G_o(\omega:\ell) = \frac{1}{L} \quad |\ell| < L/2 \tag{8.39a}$$

$$G_1(\omega\ \ell) = \frac{2}{L}\cos\left(\frac{12\pi\ell}{L}\right) \quad \ell < L/2 \tag{8 39b}$$

for

$$i = 1,M-1$$

so that

$$g_o(\omega:\underline{k}) = \mathrm{sinc}\left(\underline{k}\cdot\underline{\alpha}_a \frac{L}{2}\right) \tag{8 40a}$$

$$g_1(\omega:\underline{k}) = \mathrm{sinc}\left[\underline{k}\cdot\underline{\alpha}_a \frac{L}{2} - \pi\right] \tag{8 40b}$$

$$+ \mathrm{sinc}\left[\underline{k}\cdot\underline{\alpha}_a \frac{L}{2} + \pi\right]$$

We have then

$$S_{oo}(\omega) = S_{n_o}(\omega)\,\mathrm{sinc}^2(\pi L_\lambda \cos\theta_n) + \frac{N_o}{L}, \tag{8.41a}$$

$$S_{oi}(\omega) = S_{io}(\omega) = S_{n_o}(\omega)\,\mathrm{sinc}^2(\pi L_\lambda \cos\theta_n) \times [\mathrm{sinc}(\pi L_\lambda \cos\theta_n - i\pi)$$

$$+ \mathrm{sinc}(\pi L_\lambda \cos\theta_n + i\pi)], \tag{8 41b}$$

for i = 1,M-1,

$$S_{ij}(\omega) = S_{n_o}(\omega)\,(\mathrm{sinc}(\pi L_\lambda \cos\theta_n - i\pi) + \mathrm{sinc}(\pi L_\lambda \cos\theta_n + i\pi))$$

$$\times\,[\mathrm{sinc}(\pi L_\lambda \cos\theta_n + j\pi) + \mathrm{sinc}(\pi L_\lambda \cos\theta_n - j\pi)] + \frac{N_o}{L}\,\delta_{ij},$$

for $i,j = 1,M-1$ (8.41c)

and

$$[S(\omega)]^{-1}$$

$$= \frac{L}{N_o}\left\{ I - \frac{LS_{n_o}(\omega)}{N_o}\left[\mathrm{sinc}^2(\pi L_\lambda \cos\theta_n) + \sum_{i=1}^{M-1}(\mathrm{sinc}(\pi L_\lambda \cos\theta_n - i\pi) + \mathrm{sinc}(\pi L_\lambda \cos\theta_n + i\pi))^2\right]^{-1}\right.$$

$$\left.\times \begin{bmatrix} \mathrm{sinc}(\pi L_\lambda \cos\theta_n) \\ \mathrm{sinc}(\pi L_\lambda \cos\theta_n - \pi) \\ + \mathrm{sinc}(\pi L_\lambda \cos\theta_n + \pi) \\ \vdots \\ \mathrm{sinc}(\pi L_\lambda \cos\theta_n - (M-1)\pi) \\ + \mathrm{sinc}(\pi L_\lambda \cos\theta_n + (M-1)\pi) \end{bmatrix} \begin{bmatrix} \mathrm{sinc}(\pi L_\lambda \cos\theta_n) \\ \mathrm{sinc}(\pi L_\lambda \cos\theta_n - \pi) \\ + \mathrm{sinc}(\pi L_\lambda \cos\theta_n + \pi) \\ \vdots \\ \mathrm{sinc}(\pi L_\lambda \cos\theta_n - (M-1)\pi) \\ + \mathrm{sinc}(\pi L_\lambda \cos\theta_n + (M-1)\pi) \end{bmatrix} \right\} \quad (8.42)$$

The only beam which is nonzero at broadside is the 0th one; consequently we are interested in $[S]^{-1}_{11}$, or

$$[S(\omega)]^{-1}_{11} = \frac{L}{N_o}\left\{ \frac{1 + \left((LS_{n_o}(\omega)/N_o) \sum_{i=1}^{M-1} \mathrm{sinc}(\pi L_\lambda \cos\theta_n - i\pi) + \mathrm{sinc}(\pi L_\lambda \cos\theta_n + i\pi) \right)^2}{1 + (LS_{n_o}/N_o)\left(\mathrm{sinc}^2(2\pi L_\lambda \cos\theta_n)\right) + \sum_{i=1}^{M-1}\left[\mathrm{sinc}(\pi L_\lambda \cos\theta_n - i\pi) + \mathrm{sinc}(2\pi L_\lambda \cos\theta_n + i\pi)^2\right]} \right\}$$

(8.43)

We see that the term

$$\frac{LS_{n_o}(\omega)}{N_o} \sum_{i=1}^{M-1} \text{sinc}(\pi L_\lambda \cos\theta_n - i\pi) + \text{sinc}(\pi L_\lambda \cos\theta_n + i\pi)^2$$

determines how fast we can approach the white noise performance This term, however, represents the amount of noise energy that can be cancelled by the off-target beams One can also generate a general expression for the beam pattern.

It is more illustrative, however, to consider an example

$$L_\lambda = 1 \tag{8.44a}$$

$$\cos\theta_n = \frac{1}{2} \tag{8.44b}$$

$$M = 2 \tag{8.44c}$$

Then we have

$$\text{sinc}(\pi L_\lambda \cos\theta_n) = \frac{2}{\pi} \tag{8.45a}$$

and

$$\text{sinc}(\pi L_\lambda \cos\theta_n - \pi) + \text{sinc}(\pi L_\lambda \cos\theta_n + \pi) = \frac{4}{3\pi} \tag{8.45b}$$

$$[S(\omega)]^{-1} = \frac{L}{N_o} \frac{\begin{bmatrix} 1+\frac{4}{9}\gamma & -\frac{2}{3}\gamma \\ -\frac{2}{3}\gamma & 1+\gamma \end{bmatrix}}{1+\frac{13}{9}\gamma} \tag{8.45c}$$

where

$$\gamma = \frac{LS_{n_o}(\omega)}{N_o} \left(\frac{2}{\pi}\right)^2 \tag{8.45d}$$

The beam pattern follows as

$$g(\omega:\underline{k}\,|\underline{k}_T) = \frac{1}{1+\frac{4}{9}\gamma}\left\{(1+\frac{4}{9}\gamma)\,\mathrm{sinc}\;\underline{k}\cdot\underline{\alpha}_a\frac{L}{2}\right.$$

$$\left.-\frac{2}{3}\gamma\,(\mathrm{sinc}\;\underline{k}\cdot\underline{\alpha}_a\frac{L}{2}+\pi)+\mathrm{sinc}\;\underline{k}\cdot\underline{\alpha}_a\frac{L}{2}-\pi)\right\} \quad (8\,46)$$

We see that when γ is small we have a conventional beam; however, as the directional noises become strong we approach

$$(\omega:k\,|k_T) \simeq \mathrm{sinc}\left(\underline{k}\cdot\underline{\alpha}_a\frac{L}{2}\right)-\frac{3}{2}\left[\mathrm{sinc}\left(\underline{k}\cdot\underline{\alpha}_a\frac{L}{2}+\pi\right)+\mathrm{sinc}\left(\underline{k}\cdot\underline{\alpha}_a\frac{L}{2}-\pi\right)\right], \qquad (8.47)$$

which places a null on the direction of the noise $k=\frac{2\pi}{\lambda}\cos\theta_n=\frac{\pi}{\lambda}$. However, as we have seen in our discussion of superdirective array, it introduces severe side lobes at other wave numbers with all the attendent shortcomings of this result. The performance is given by

$$\sigma^2(\omega:\underline{k}\,|\underline{k}_T) = \frac{N_o}{L}\left(\frac{1+\frac{13}{9}\gamma}{1+\frac{4}{9}\gamma}\right) \qquad (8\,48)$$

When γ is small, we are limited by the white noise level performance of $\frac{L}{N_o}$. When γ is large the performance approaches

$$\frac{13}{4}\,\frac{N_o}{L},$$

i.e., we are willing to accept 13/4 increase from the white noise in order to cancel the directional noise sources. This represents the additional energy that enters through the large side lobes in the beam.

There is another case which is worthwhile to examine. Assume that each of the beams are distributed about a wave number $\underline{k}_i$ and that the beam outputs are uncorrelated, i.e.,

$$S_{ij}(\omega) = S_i(\omega)\delta_{ij}$$

Such a situation could appear with orthogonal aperture weightings and a frequency wave number spectrum which varies slowly, so that we have

$$S_{ij}(\omega) = (P(\omega:k_i) + N_o) / \Omega_A \, \delta_{ij}$$

i.e., each beam has a power level proportional to the frequency wave number spectrum at its nominal center of its distribution. The optimum processor is now an optimal diversity ratio combiner with the weighting determined by the signal-to-noise ratio in that beam.

REFERENCES

1. A. Papoulis, *Probability, Random Variables and Stochastic Processes*, McGraw-Hill, New York, 1965.
2. W. Davenport and W. Root, *Random Signals and Noise*, McGraw-Hill, New York, 1958.
3. H. L Van Trees, Detection, Estimation and Modulation Theory Pt 1 J. Wiley and Sons, New York, 1969.
4. J. Doob, *Stochastic Processes*, J. Wiley and Sons, New York, 1953.
5. A. Yaglom, "Some Classes of Random Fields m in Dimensional Space, Related to Stationary Random Process," Theory of Probability and Its Applications, November 3, 1957, p. 273
6. A Yaglom, *An Introduction to the Theory of Stationary Random Functions*, Prentice Hall, Englewood, N.J , 1960.
7. A. Papoulis, *The Fourier Integral and Its Application*, (Appendix 2)
8. H. W. Marsh, Jr., "Correlation in Wave Fields," in U.S. Navy Underwater Sound Laboratory for period ending 31 March 1950 pp. 63-68, also, B Gron and C. Sherman, "Spatial Correlation for Various Noise Models," Journal of the Acoustical Society of America, Vol. 34, No. 11, November 1962.
9. J. Stratton, *Electromagnetic Theory*, McGraw-Hill, 1941.
10. M. Abramowitz and I. Stegun, *Handbook of Mathematical Functions*, Dover Publications, 1965.
11. M. Abramowitz and I. Stegun, *ibid*
12. J. Berg, "Three Dimensional Filtering with an Array of Seismometers," *Geophysics* Vol. 29, No. 5, October 1964, pp. 693-713.
13. N. Gaarder "The Design of Point Detector Arrays," Pt. II, "*IEEE Transactions on Information Theory*," Vol. IT-12, No 2, April 1966.
14. J. Capon "High Resolution Frequency Wave Number Estimation," *Proc. of the IEEE*, Vol. 51, No. 8, August 1969.
15. A. Erdelyi, et al, Bateman Manuscript Project, California Inst of Tech., (3 Vols), McGraw Hill, New York, 1954.
16. C. Dolph, Proc. Inst. of Radio Engineers, 34, 335-348 (1946); also; R Pritchard, "Optimum Directivity of Linear Point Arrays, Journal of the Acoustical Society of America," Vol. 25, No. 5, September 1953.
17. H. L. Van Trees, *Detection Estimation and Modulation Theory*, Pt. 3, J. Wiley and Sons, New York, 1971
18. H. L. Van Trees, "Optimum Array Processing," 1966 Hawaii Symposium
19. R. Blackman and J. Tukey, *The Measurement of Power Spectra*, Dover Publications, 1959.
20. F. Bryn, "Optimum Processing of Three Dimensional Arrays Operating on Gaussian Signals and Noise, *The Journal of the Acoustical Society of America* Vol. 34, No. 3, March 1962.
21. D. Middleton and H Groginsky, "Detection of Random Acoustic Signals with Distributed Elements Optimum Receiver Structures for Normal Signal and Noise Fields, *Journal of the Acoustical Society of America*, paper 15 3 of the Acoustical Society Symposium of 1964.
22. F. Schweppe, "Sensor Array Data Processing for Multiple Signal Sources," *IEEE Trans. on Information Theory*, Vol. IT-4, No 2, 1968, pp. 294-305.
23. P. M. Woodward and J. D. Lawson, "The Theoretical Precision with Which an Arbitrary Radiation Pattern May Be Obtained with a Source of Finite Size," *Journal of the I.E E* , Vol. 95, pp 363-370, 1948.

24. G. Toraldo di Francia, "Directivity, Super-Gain and Information Electromagnetic Wave Theory Symposium"
25 W. Vanderkulk, "Optimum Processing for Acoustic Arrays," Journal of Brit IEE, October 1963.
26. S. A. Schelkunoff, "A Mathematical Theory of Linear Arrays," Bell System Technical Journal.
27. P. Schulteiss, "SUBIC Reports"
28. R. Pritchard, "Optimum Directivity of Linear Point Arrays, Journal of the Acoustical Society of America, Vol. 25, No. 5, September 1963.
29. Abramowitz and Stegun, *ibid*
30. R. Goodman, *Fourier Optics,* McGraw-Hill, 1969.
31. D. Childers and I Reed, "On the Theory of Continuous Array Processing," I.E.E.E. Transactions on Aerospace and Navigational Electronics, June 1965.